2000

Electronic Control of Torque Ripple in Brushless Motors

Kocybik, Peter Franz

http://hdl.handle.net/10026.1/2643

http://dx.doi.org/10.24382/3693
University of Plymouth

Electronic Control of Torque Ripple in Brushless Motors

by

Peter Franz Kocybik

A thesis submitted to the University of Plymouth in partial fulfilment for the degree of

Doctor of Philosophy

School of Electronic, Communication and Electrical Engineering

Faculty of Technology

In collaboration with

Automotive Motion Technology Ltd

July 2000

Peter Franz Kocybik

Electronic Control of Torque Ripple in Brushless Motors

Abstract

Brushless motors are increasingly popular because of their high power density, torque to inertia ratio and high efficiency. However an operational characteristic is the occurrence of torque ripple at low speeds. For demanding direct drive applications like machine tools, robot arms or aerospace applications it is necessary to reduce the level of torque ripple.

This thesis presents an in depth investigation into the production and nature of torque ripple in brushless machines. Different torque ripple reduction strategies are evaluated and one reduction strategy using Park's transform as a tool is identified as the promising strategy. The unified machine theory is checked to clarify the theory behind Park's transform; in particular assumptions made and general validity of the theory. This torque ripple reduction strategy based on Park's transform is extended to include the effect of armature reaction. A novel adaptive torque ripple reduction algorithm is designed. The ineffectiveness of the conventional approach is demonstrated. Further a novel torque ripple reduction strategy using direct measurements of the torque ripple is suggested, reducing implementation time and allowing higher accuracies for torque ripple reduction. Extensive measurements from the experimental system show the validity of the novel torque ripple reduction strategies. The experimental results allow derivation of a formula for all load

situations. This formula makes it possible to further increase the reduction accuracy and enables improved real time implementation of the torque ripple reduction algorithm.

The work presented here makes a substantial contribution towards understanding the nature of torque ripple in brushless motors and solving the associated problems. The novel reduction strategies form the basis for the development of intelligent dynamometers for motor test beds. Further the torque ripple reduction method presented here can be used to overcome manufacturing imperfections in brushless machines thus removing the cost for precise manufacturing tools. Future designs of controllers can "build" their own correction formula during set-up runs, providing a motor specific torque ripple correction.

Table of Contents

List of Figures

x

List of Tables

Acknowledgement

Author's Declaration

At no time during the registration for the degree of Doctor of Philosophy has the author been registered for any other University degree.

This studied was financed with the aid of a studentship from the Higher Education Funding Council and was carried out in collaboration with Automotive Motion Technology Ltd, Andover. The collaboration was in the form of hardware support and regular visits for progress meetings.

Relevant scientific seminars, conferences and exhibitions were regularly attended.

A paper was presented at the Power Conversion and Intelligent Motion conference, PCIM, 1997 in Nuremberg.

Signed

Date   26/7/2000

Chapter 1   Introduction

1.1 Motion Systems

Modern motion systems comprise three principal components; the motor, the drive and the control. The motor is the essential component of every motion system converting electrical into mechanical energy. The drive provides the power management to the motor. The control unit serves to supervise the drive.

When electrical motors were first utilised they were directly interfaced to the supply system. This made for ease of use but restricted their capabilities. Most applications were straight forward, relatively slow, highly repetitive processes. Motors had to be reliable and simple to use. To use motors for more demanding applications it became necessary to invent additional mechanical and electrical devices to extend their capabilities. This included devices to facilitate start up and braking for instance. Often these devices were cumbersome and not very reliable to use.

New applications demanded higher motor capabilities such as assembly processes requiring different speeds and quicker response times. To meet these higher requirements drives were developed. Drives allow the operation of motors at different speeds and load levels by adjusting voltage and current levels. A well-matched matched drive system makes it possible to use a motor up to its electrical and mechanical limits. Older drive systems were very limited in their capabilities and only allowed fairly simple operations to

be performed. However during the last 20 years power electronics has evolved a great deal [1], [2] and [3]. Drives have a much faster response these days and will accommodate much higher power levels.

The improvements in drive technology made it necessary to use control systems to supervise the drive [4]. Whereas a simple passive rectifier could convert an ac into a dc voltage to supply a fixed speed dc motor, an active power converter will drive a dc motor at variable speeds. However the active power control usually requires some form of control. As capabilities of and demands on drives increased demands on control grew in parallel. From simple analogue to extremely sophisticated digital or combined analogue and digital control systems there exists a wide range of control systems in use with specific drive systems.

Although some motors are still operated without drive and control systems there is an increasing trend to use more and more sophisticated drive and control systems to facilitate higher user demands. It is not a simple matter of choosing the right motor for a particular application, it is the overall system performance, which counts. Only a well-matched and fine tuned motion system will achieve the highest possible performance. Therefore it becomes more important to design good interfaces between the individual components of a motion system. Increasingly drive and control components will be integrated with the motor to form a compact motion system.

Figure 1.1 shows a motion system with its components. It illustrates the interface connections between the components and shows possible feedback loops between them.

Control signals   Supply current

Control   **Drive**   **Motor**

Current and/or voltage feedback

Position and/or speed feedback
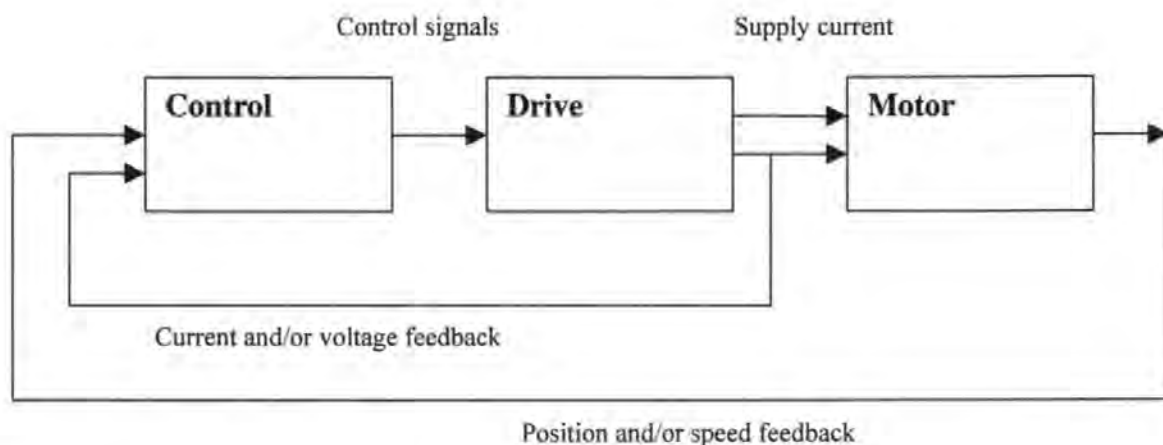
Figure 1.1 Motion system and its components

In the following section the individual components of a motion system: motor, drive and control will be looked at in more detail.

1.2 Different Motor Types

Many different varieties of motors exist including special design motors for particular applications. The more important motors are described in [5], [6] and [7]. In the following the main motor types will be briefly looked at.

The dc motor is probably the best known motor type. It is operated using dc voltages and dc currents. Stator and rotor carry windings, which are both excited using dc current. One of them constitutes the excitation field and the other one the torque producing field. Alternatively permanent magnets can be used on the stator replacing the stator winding and providing the excitation field. Conventional dc motors are used in a variety of standard

applications usually running at fixed speed. They can be supplied either from a dc voltage source, e.g. battery, or from an ac supply, e.g. mains, using a rectifier. No sophisticated power management or control is required. DC motors can also be used as variable speed drives when powered by drives capable of varying supply voltage and current. These can then be used in applications where different speeds are required, e.g. modern production processes. DC motors are simple to use and to control; which makes them very popular. Speed can be varied by simply changing the supply voltage, and torque production can be adjusted by varying supply current. Both are straight forward linear relationships. However most dc motors are more expensive to manufacture than other motors because they have windings on both stator and rotor.

The induction motor is the most popular motor type in industry. About 80% of all industrially used motors are induction motors. Induction motors consist of a stator containing the windings and normally a laminated rotor containing a solid cage instead of windings, e.g. squirrel cage. These motors can be connected to an ac supply voltage, e.g. the 3 phase mains, to run at a fixed speed. This is a simple way of driving them and proves sufficient for many standard applications. For more demanding applications induction motors are used with inverters. Inverters allow variation of the supply frequency and voltage to the induction motor. Thus the induction motor becomes a variable speed drive. This is useful for production processes where different speeds are required. Inverters are off the shelf items, available from many manufacturers. They can be controlled using standard control strategies like PWM control. However the induction motor exhibits a few undesirable features when driven using standard control strategies. The start up torque is low and there are torque resonances in the lower frequency range. A considerable amount of research is directed towards addressing these problems and generally improving the

overall characteristics, like response times, of induction motor systems. Extremely sophisticated motor and drive models have been developed. The research is on going.

Brushless motors or so-called permanent magnet motors are relatively new motor types. All brushless motors have magnets, hence the name permanent magnet motors. These are normally mounted on the rotor. The stator contains the windings. The stator configuration may be similar to the induction motor. Brushless motors exhibit the same control features as traditional dc motors. The motor speed can be varied by changing the supply voltage, and the torque output can be manipulated by controlling the supply current. Both are described through linear relationships. However the rotor position needs to be known to drive the brushless motors. For this purpose feedback devices like Hall effect devices, encoders or resolvers are used. A considerable amount of research is directed towards replacing these feedback devices by indirect methods like measuring supply currents and voltages to determine rotor position. Some so-called sensorless brushless drive packages are already available. As the price of magnets has come down over the last 15 years brushless motors have become cheaper to manufacture and are now seen as the main contender to the induction motor. The main advantage being the simpler control principle compared to the induction motor. However it is clear from the fact that the rotor position needs to be known that all brushless motors require some form of control and associated power stage. It is not possible to simply run them from the mains. This means that they are more suited for more demanding applications where the extra cost for the power stage and the control is justified.

The switched reluctance motor is also a fairly new motor type. The stator contains the windings, whereas the rotor is a simple stack of metal laminations formed to provide

reluctance torque. This makes for a motor, which is easy to manufacture. However the control has the task of driving the motor in a way to ensure constant torque output. This requires sophisticated control mechanisms. Torque ripple and noise posed severe problems for manufacturers of switched reluctance motors up to a few years ago. Only recently have switched reluctance motors been used in higher volume products. Research to improve drive system characteristics is ongoing.

Besides the main motor types more specialised motors or motors for a more restricted range of applications exist. The best known of these is the stepper motor, which is often used for lower power positioning tasks. Other motors are hybrids between standard motor types.

From the above it can be concluded that the motor user faces a bewildering choice of motor types for most applications. Normally it is not very meaningful to compare one motor type to another. A well-designed motor will be comparable in terms of power to weight ratio and efficiency to most other well-designed motors of a different type. However from a scientific point of view there are considerable differences between the individual motor types. All motor types have inherent characteristics. Depending on the specific application these can be intolerable; forcing the choice of a different motor type to avoid them. The ideal motor doesn't exist. Later it will be seen how the design of a sophisticated control improves motor performance to overcome these problems.

This study considers in detail the brushless motor. The main reason being that brushless motors have become cheaper because the price of magnets has come down over the last 15 years. They are now more competitive and starting to take market share from induction

motors. Furthermore they are judged to be potentially very interesting for new application areas like hybrid cars, which use both combustion and electrical motors for traction purposes. Also a lot of research has been directed towards induction machines and switched reluctance machines. Progress there has been very fast over the last 5 years. Whereas in the area of brushless motors most research has been directed towards replacing the rotor feedback systems. The brushless motor has therefore been found to be both a promising motor type and interesting for further scientific examination. Hardware in the form of a suitable brushless motor was made available for this study by the supporting company.

It has been mentioned before that it is necessary to judge the whole motion system rather than the motor itself when a particular motion task needs solving. A sophisticated control strategy allows improvement of the operating characteristics of the motor and can extend its performance envelope.

In the following section the development and importance of drive and control systems will be emphasised. Drives and controls are described together as they form a unit and cannot be chosen independent from each other.

1.3 Trends in Drive and Control System Development

Traditionally many industrial processes utilise fixed speed machines. Induction motors for instance are switched directly on line (dol) and run up to near their synchronous speed at which they are then operated. This is a simple and reliable way to use electrical machines.

However this mode of operation does not allow for different working speeds. Therefore the use of gear boxes is required to achieve different running speeds. Gear boxes introduce additional mechanical components with the associated problems. They require maintenance, wear out and they might introduce undesired resonances into the system. But most importantly they contribute to system losses. Further, the fact that the motor is not always operated at optimum speed, also leads to higher energy consumption. As energy consumption is under close scrutiny due to recent legislation and higher environmental awareness it becomes necessary to search for more energy efficient ways of motor operation.

The second major disadvantage of fixed speed machines using gear boxes is their poor dynamic behaviour. Quick changes in production speeds are hard to accommodate. Many production processes require fast ramping up to full speed and numerous braking and reaccelerating cycles. Fixed speed machines are not ideally suited to this purpose.

Finally many other applications require a continuous speed variation. Again fixed speed machines are not able to provide this feature.

In conclusion it can be said that energy consumption, dynamic requirements and advanced application requirements necessitate the use of variable speed instead of fixed speed machines.

Recent developments are reviewed in [8], [9] and [10].

1.4 Variable Speed Drives and Controls

Most electrical machines can be used as variable speed machines if power electronics are used to supply the machine. Induction motors for instance can be operated at varying speeds if frequency converters are used for their supply.

There are three major motor types, which are normally used for variable speed applications [11], [12] and [13].

The first one is the conventional brushed dc motor. The major advantage here is the ease of speed control. As speed is directly proportional to applied voltage only a simple power electronics configuration is required. However the major disadvantage is the use of mechanical parts, that is brushes and commutators. This leads to mechanical wear and makes regular maintenance necessary, especially if a high number of speed changes occurs. Furthermore the occurrence of sparks at commutation instances makes the dc motor unsuitable for hazardous environments. Therefore there are considerable disadvantages in utilising the brushed dc motor for variable speed applications.

The second motor type is the induction motor. The induction motor is the most widely used motor type today. Its simple construction makes it cheap to manufacture. Because it is used in a wide variety of applications many motor engineers are familiar with it and prefer its use. The major drawback of the induction motor is the non-linear operating characteristic. Neither speed nor torque output can be controlled in a simple manner. Advanced control strategies like vector control need to be employed to make use of the motor potential. Furthermore torque ripple occurs at low speed which makes fairly sophisticated control approaches necessary to combat this problem. Recently highly refined motor models have

9

been developed which take into account a large number of motor parameters and operating conditions. These models demand high computing power in order to implement advanced control techniques. However it is very likely that the induction motor will continue to take a major share of the motor market.

The third motor topology considered here is the so-called brushless motor. This is the motor type chosen for the purpose of this project. This motor type has in the last few years emerged as a main competitor to the induction motor. As mentioned before the brushless motor needs a drive and the associated control to be operational. It is therefore only natural to utilise the variable speed capabilities of the brushless motor to justify the extra cost incurred by using the drive and the control. Chapter 2 will be looking at the operating principles of the brushless motor and list some application areas for its use as a variable speed machine.

In the following section the terminology used throughout this thesis will be defined.

1.5 Terminology

It is necessary to define a few technical terms as the use in the literature varies considerably.

First the terms motor and machine will be used interchangeably in the following. The reason being, that each electrical machine can be operated as a motor or a generator. Usually the brushless machine will be operated in motoring mode.

Secondly the term brushless machine itself requires clarification. Originally it applied to the so-called brushless dc motor which replaced the conventional brushed commutation through electronic commutation. Therefore the new machine was considered brushless as opposed to being brushed. However the induction motor for instance is of course also brushless.

The following is an attempt to define brushless machines.

Definition: **A brushless motor is a machine, which uses permanent magnets as the excitation source and commutates its phases electronically.**

All brushless machines use permanent magnets, they are therefore often called permanent magnet machines. However conventional dc motors can also employ permanent magnets, as can synchronous machines. It is therefore slightly ambiguous to call the brushless machine a permanent magnet machine. What makes it discernible from other permanent magnet machines is the fact that the commutation is done electronically. In the permanent magnet brushed dc motor the commutation is still done mechanically. In the permanent magnet synchronous motor the three-phase supply automatically generates the commutation.

If brushless machines are described, usually a particular type of brushless motor is implied. For example the so-called brushless dc motor, which is a machine with ideally rectangular back emfs or more realistically trapezoidal back emfs. This motor is normally supplied through rectangular current pulses. Here the closeness to the conventional brushed dc motor can be seen. The other machine type is the so-called brushless ac motor. It ideally exhibits a sinusoidal back emf waveform or more realistically a near sinusoidal back emf waveform. It will usually be supplied through sinusoidal phase currents. Sometimes these

machines are called permanent magnet synchronous motors as they can be analysed in exactly the same way as normal synchronous motors. However it should be remembered that, because electronic commutation takes place relative to rotor position, the motor is controlled in a way so to exhibit the control behaviour of the conventional brushed dc motor. That is to say the brushless ac motor also exhibits a linear relationship between supplied voltage and speed and between supplied current and resulting torque output. In this respect there is no difference between the brushless dc and the brushless ac motor.

Chapter 2 describes the operating principles of the brushless motor. Some principal application areas will be named. The underlying technological developments are described, which have made the brushless motor more competitive. The principle of torque production in the brushless motor and possible sources for torque ripple will be discussed.

Chapter 2   Brushless Motors

2.1   Operating Principles

Recently several books have been published describing brushless motors, both brushless dc and brushless ac motors [14] – [21]. Some of the illustrations in the following have been taken from these books.

The traditional brushed dc motor contains phase windings both on the stator and the rotor of the machine. The stator windings are normally supplied by a fixed dc current to produce the excitation field of a particular value. Alternatively permanent magnets can be used to provide a fixed excitation field. The rotor is then supplied by a dc current, which builds the torque producing field. The value of this current will be adjusted to produce the desired value of torque output. The commutation of the torque producing field on the rotor is done mechanically through brushes and commutators.

The induction motor usually only has windings on the stator whereas the rotor is formed as a laminated metal block containing a solid cage, i.e. squirrel cage. The ac supply current into the stator provides the excitation field on the stator, but it also provides the torque-producing field on the rotor via electromagnetic induction on the rotor. There are no mechanical connections between rotor and supply. The commutation is facilitated through the ac currents going into the stator windings. The level of torque can be adjusted by varying the magnitude and frequency of the supply currents. However this relationship is

13

non-linear. As mentioned before to operate the induction motor as a true variable speed machine some form of drive is necessary.

The brushless motor uses magnets on the rotor. These magnets set up the excitation field. No current is required to provide the excitation. This has the advantage that all the supply current to the brushless motor can be used for torque production as opposed to the dc motor and the induction motor. Therefore the user of brushless motors does not have to pay an excitation penalty. However the value of excitation is fixed and cannot be varied. Furthermore the excitation field cannot be switched off. This can prove hazardous when a fault on the motor or drive side occurs.

The number of magnets on the rotor can vary considerably from one brushless motor to another. They can best be regarded as magnet pole pairs, which implies that there is always an even number of magnets on the rotor: 2,4,6 and so forth. Typically the magnets set up a trapezoidal flux pattern with positive and negative polarity around the rotor circumference as depicted in figure 2.1. The actual shape of the flux pattern depends on the magnetisation of the magnets, the shaping of the magnet surface, the fact that the rotor can be skewed and a number of other design parameters. The motor designer will try to produce the optimum flux pattern for his particular task.
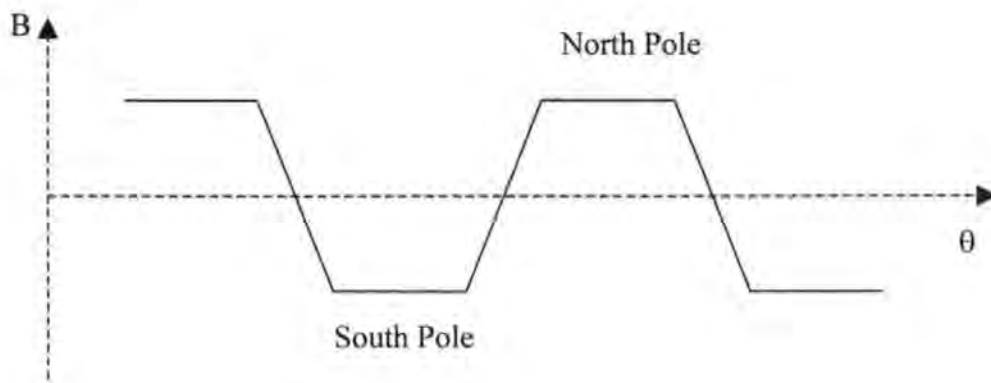
Figure 2.1 Magnet flux distribution in airgap with rotor position

The stator contains the windings. Its design can follow the traditional design of induction motor stators. However whereas most induction motors have 3 phases to interface to the supply system, the brushless motor is not restricted to 3 phases. Any number of phases from 2 phases upwards is possible, because the brushless motor is not directly connected to the 3 phase supply system but utilises a drive for its power supply. The motor phases are normally connected in star configuration to keep the number of connecting leads down.

Figure 2.2 shows a typical design for a brushless motor. The rotor contains 4 magnets, alternately arranged as north and south poles. The stator has 12 winding slots, which are filled with 3 phase windings. This represents a standard brushless motor configuration. However as mentioned before the number of magnets and slots is variable and a large variety of combinations is possible. Further figure 2.2 shows the more common configuration, where the rotor is on the inside of the machine and the stator on the outside. It is also possible to reverse the positions and to have the rotor on the outside and the stator on the inside. Potentially this design allows for higher torque densities.
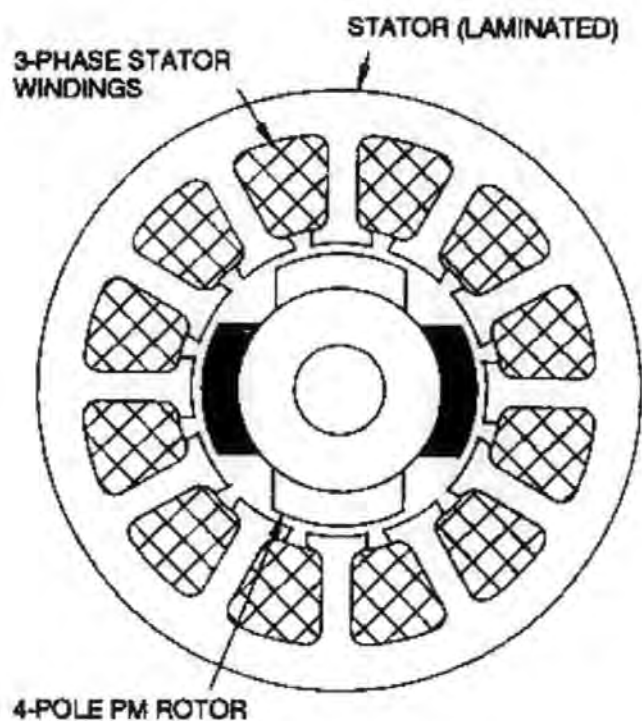
Figure 2.2 Sectional view of typical brushless motor from [18]

Although the brushless motor can have any number of phases, it is desirable to restrict the number of phases to keep the number of required power switches in the drive low. Therefore 2, 3 and 4 phase machines are the most popular ones. The additional advantage of using 3 phase machines is that standard inverters can be used, which interface to the 3-phase supply system and allow connection of 3 motor phases at the output of the inverter. This makes it possible to utilise inverters developed for induction motors.

The commutation in the brushless motor is achieved electronically. This is to say that the drive has to facilitate the commutation by switching the power devices corresponding to rotor position. In an ideal brushless dc motor the drive generates rectangular current pulses as long as the excitation field from the magnets aligns with a particular stator phase

16

winding. Then the next phase winding is excited as the rotor moves into alignment with the next phase. In reality it is not possible to generate ideal rectangular current pulses, but only trapezoidal current pulses. Depending on the number of rotor poles and stator phases different excitation patterns are employed. For an ideal brushless ac motor the drive has to produce ideal sinewave currents, which are offset by their phase angle. It is possible to achieve a good approximation to the ideal sinewave currents by utilising high bandwidth current control. The brushless ac motor is therefore more suitable for high precision control tasks than the brushless dc motor.

The commutation relies on signals from a feedback device. Usually either Hall effect devices, encoders or resolvers are employed for position sensing. Hall effect sensors are comparatively cheap, and are used for many brushless dc motors. Brushless ac motors normally utilise encoders or for higher resolutions resolvers. However the higher device cost is only justified if the control task is more demanding and cannot be full-filled using Hall effect transistors.

As mentioned earlier the fact that the brushless motor relies on a feedback device for its operation is a major drawback of the brushless motor. If the feedback device fails or transmits the wrong signals to the control it will not be possible to maintain normal operation.

It has been highlighted already that the brushless motor shows the same control characteristics as a conventional dc motor. This holds true for both brushless dc and brushless ac motor and also for combinations of these two types.

Firstly speed is proportional to the applied voltage and can therefore be varied in a linear manner by controlling the supply voltage to the motor as long as the voltage drop across the resistance is negligible.

$$\omega \propto V \quad (2.1)$$

Here ω represents the machine speed and V stands for the applied voltage.

Secondly torque output is proportional to applied input current. The torque can therefore also be varied in a linear fashion by controlling the input current(s) to the motor.

$$T \propto I \quad (2.2)$$

Here T represents the output torque of the machine and I the input current.

These equations are exactly the same as for the conventional dc motor. The two quantities speed and torque can be controlled independent of each other. Therefore it can be seen that the brushless motor exhibits the same simple control characteristic as the brushed dc motor. This is a distinct advantage compared to the induction motor.

In the following section a description of principal application areas for brushless motors is given.

2.2 Principal Application Areas

In order to understand why brushless motors are used in specific applications, it is useful to look at some inherent advantages of brushless motors.

Firstly well designed brushless motors exhibit a high power to volume ratio; especially if rare earth magnets are used for the excitation field. This results in a high power density. Brushless motors will therefore occupy less space than a conventional brushed dc motor or a induction motor; allowing for space savings and compact designs.

Secondly brushless motors also exhibit a high torque to inertia ratio. This improves the dynamic capabilities of the machine and makes it suitable for use in fast response systems. Finally the efficiency of brushless motors is comparably high due to the fact that magnets are used. This fact makes them ideally suited to realise the energy saving potential in modern applications.

A new and promising application area for brushless motors is the field of so called hybrid cars. Because of new legislation demanding lower or even zero pollution vehicles, electrical motors are used as traction motors in cars. Often a conventional combustion engine is combined with a brushless motor; creating a hybrid car. Brushless motors are used because of their high dynamics and high power density, allowing for weight savings. Brushless motors are also used in general traction applications like trains.

Another big application area is the aerospace industry. Traditional dc motors cannot be used because of their weight, the danger created by commutation sparks and the general wear of brushes and commutators. Brushless motors are comparatively light-weight and maintenance free.

Brushless motors are also used in high accuracy machine tooling applications. They offer precise and fast dynamic control, which is necessary in modern production processes.

Many other, specialised application areas exist. Principally it is always possible to utilise a brushless motor. Whether the brushless motor or a different motor type will be used is always a compromise between performance and price.

In the following the underlying technological developments are described which have led to the more wide spread use of brushless motors.

2.3 Recent Technological Developments

Brushless motors utilise permanent magnets as their excitation source. In the past the cost of permanent magnets was very high and it was difficult to manufacture them to preferred shapes and polarisation directions. Furthermore traditional motor manufacturers were not experienced in using magnets in production processes which led to handling and retaining problems. Therefore the brushless motor represented a niche market in the lower power range. Nowadays prices for permanent magnets have come down and are expected to fall in the future. Magnet characteristics have been improved which push brushless motors into higher power applications. Furthermore it is now possible to manufacture different magnet shapes and polarisations much cheaper than a few years ago. Manufacturers have also solved the practical issues in terms of handling magnets. All these developments have made and continue to make the brushless motor much more competitive opening up application areas, which have been out of reach previously [22].

Secondly there has been considerable progress in developing faster power switches, which facilitate higher currents and voltages and occupy less physical space [23]. Further these devices have been optimised to provide lower losses, both on-time and switching losses, [24] and [25]. These advances in power electronics make it possible to fit the drive directly onto the motor into the space, which previously has been occupied by the gear box for example. Further the cost of power electronic devices has come down considerably. Power electronics have been developed for a wide variety of applications and power devices are now readily available in mass production. All this has promoted the use of motors, which rely on power electronics for their operation, like brushless motors.

Thirdly the introduction of Digital Signal Processors (DSPs) into the market place about 15 years ago has provided the designer with high power real time computing capabilities. Mass production has lead to a decrease in prices; leading to a whole range of reasonably priced and well-tested devices available to implement digital control strategies. Therefore it is now possible to realise more demanding control strategies, which help to utilise the potential of brushless motors, [26] and [27].

In the following the principle of torque production in brushless motors is described.

2.4   Torque Production

For any motor topology torque production can be described through the interaction of two excitation sources. One of them associated with the stator and the other with the rotor of the machine. The two excitation sources can in general be represented by two coils

carrying electrical current. Using this model the following general equation for torque production in electrical machines can be given.

$$T = \frac{1}{2} * i_1^2 * \frac{dL_1}{d\theta} + \frac{1}{2} * i_2^2 * \frac{dL_2}{d\theta} + i_1 * i_2 * \frac{dL_{12}}{d\theta} \quad (2.3)$$

Here T represents the developed output torque of the machine. i_1 and i_2 represent the current through coils 1 and 2. L stands for the coil inductance, i.e. self-inductance and mutual inductance respectively, and θ denotes the rotational angle of the rotor.

The first term of equation 2.3 describes the production of torque if the self-inductance of coil 1 varies with rotor position. This is the so-called reluctance torque. Accordingly term two describes the production of torque with the variation of self-inductance for the second coil. Again this is a reluctance torque. Finally the third term gives torque produced through the variation of mutual inductance between coils 1 and 2. This is called mutual or alignment torque.

For the brushless motor one of the excitation sources will be replaced by permanent magnets. Therefore a new form for the general torque equation can be given which applies specifically to the brushless machine.

$$T = \frac{1}{2} * i^2 * \frac{dL}{d\theta} - \frac{1}{2} * \phi_m^2 * \frac{dR}{d\theta} + N * i * \frac{d\phi_m}{d\theta} \quad (2.4)$$

Again T represents the output torque of the machine. i is the current through the remaining coil. L represents the self-inductance of the coil. ϕ_m stands for the magnet flux. R denotes the magnetic path reluctance and N is the number of turns. Finally θ again stands for the rotational angle of the rotor.

22

Again the first term in equation 2.4 represents the torque production if the self-inductance of the coil changes with rotational position. Corresponding to the interpretation above this is called reluctance torque. The second term describes the production of torque due to the change of reluctance in the magnetic flux path. This is also a reluctance torque. Finally the third term considers the contribution of a change of flux linkage between the coil and the permanent magnet. This represents the alignment torque of the machine.

For the normal operation of a brushless motor the production of alignment torque is desired. Therefore the first term, which results from the change in coil self-inductance, is normally minimised by machine design. The marked exception is the brushless machine with buried magnets. This topology is occasionally used and produces a significant reluctance torque. In the following only the brushless machine with surface mount magnets is considered, as this is by far the most popular topology. Further the second term in equation 2.4 is also nulled. By design it is undertaken to minimise changes in reluctance to achieve a constant magnetic reluctance. This leaves only the third term to produce torque in a brushless motor. In conclusion it can be said that the torque production in the brushless machine is accomplished through the interaction of current and magnet flux. This electromagnetic interaction produces alignment torque depending on the rotor position.

In the following sources for the production of torque ripple are described.

2.5 Sources of Torque Ripple

Normally it is desirable for any machine to produce a constant output torque. No machine however produces ideal constant output torque. Torque ripple can be a particular problem of brushless motors. In conventional dc motor it is possible to use a high number of commutation elements to minimise the occurrence of torque ripple.

Torque ripples are undesirable because they excite mechanical resonances and introduce speed variations into the system. Therefore it is demanded that the alignment torque of the machine is constant and that no contribution through reluctance torque is made. However this can only be achieved in an ideal machine.

There are two main sources for torque ripple in brushless machines. One is the so-called cogging torque. The second one is the electromagnetic or energised torque ripple.

Cogging torque is produced through the alignment of permanent magnets and stator slots. The magnet flux seeks a minimum reluctance path, which is found when the edge of a magnet is aligned with a stator slot opening. Therefore the magnet path reluctance changes and undesired reluctance torque, owing to the second term in equation 2.4 is produced. The cogging torque occurs even when the machine is not energised, that is not supplied with phase currents. Cogging torque is therefore independent of current excitation in the machine. For low current loadings it represents the dominant torque ripple factor. An analytical description of cogging torque production is given in chapter 5.1.

The second main source for torque ripple production is the electromagnetic or energised torque ripple. This torque ripple contribution results from the mismatch between back emf

waveforms and phase currents. It can be described through the third term in equation 5.4. Practical winding arrangements and magnet designs make it impossible to achieve ideal machine characteristics. For a brushless ac motor ideal sinusoidal back emfs are required. For a brushless dc motor ideal rectangular back emfs are required. Any combination between the two is theoretically possible. In practise a real machine will exhibit a back emf waveform which is a combination of the two ideal cases. Therefore the motor will develop torque ripple on the alignment torque if the motor is supplied with ideal sinusoidal or rectangular currents respectively. In other words it is not possible to achieve constant alignment torque. In the following this torque ripple will be called energised torque ripple as the machine needs to be energised for this torque ripple to become visible. In the case of brushless dc motors this torque ripple is also called commutation ripple as it is not possible to supply the machine with ideal rectangular phase currents, even if the machine was to show ideal rectangular back emfs. This is due to the fact that the slope of the supplied currents will be limited by the phase inductance. Therefore ideal rectangular supply currents are not achievable. This torque ripple is of course also energised torque ripple. Energised torque ripple becomes the dominant factor for higher current loadings. A closer look at energised torque ripple will be taken in chapter 5.2.

Both cogging and energised torque ripple result from the non-ideal motor design. Other components of the motion system rather than the motor design itself will also result in torque ripple. For instance manufacturing tolerances will increase both the production of cogging and energised torque ripple. The drive system can introduce additional variations of the supply currents. A limited control bandwidth will also result in higher energised torque ripple. Further temperature shift and measurement inaccuracies in current transducers and position sensors will contribute additional torque ripple components. These

contributions can be significantly reduced if care is taken during the design of the overall control - drive - machine system.

Chapter 3 defines the direction of this examination and describes the expected gain of knowledge.

Chapter 3 Objectives

3.1   Structure of Thesis

Chapter 1 presented an introduction into the subject of motion systems. It highlighted the functionality of the system and described the individual system components. Further recent developments for both system components and motion systems as a whole have been emphasised. It became clear that a system component can be chosen from a wide choice of similar modules. The choice of the individual module will depend on the overall system and demands made on it. The interaction of the system components via well-defined interfaces is very important.

Chapter 2 described the brushless motor as a module for high performance systems. Its operating principles, application areas and advantages of the use of brushless motors were described. Chapter 2.4 dealt with the principles of torque production and chapter 2.5 already highlighted the main problem of brushless motors; the production of torque ripple. Because of its many advantages like high power to volume ratio, low inertia and high efficiency, the brushless motor is increasingly utilised for a variety of new applications. However if the brushless motor is fitted as a direct drive to replace conventional motor topologies, like the brushed dc motor, the torque ripple may become a significant problem. Often high precision operation for robot arms, machine tools or aerospace applications is required where torque ripple needs to be reduced to a minimal level.

27

This thesis will deal with the problem of torque production in brushless motors as a component of high performance systems.

Torque production will be dealt with from the motor point of view. Analytical descriptions of torque production will be presented based on different motor quantities. Equations and computer simulation will highlight the nature of torque production and its particular problems. Both cogging and energised torque ripple production will be dealt with in depth. Torque ripple production as a motor inherent problem will then be dealt with from a system's point of view. The interaction of control components, power components and motor component will be used to create a system with much reduced torque ripple. A literature search reveals different strategies for torque ripple minimisation in brushless motors. These concepts are evaluated and promising reduction strategies are described. A new adaptive torque ripple reduction strategy is presented to deal with the problem of load dependent torque ripple. Further a new improved torque ripple reduction strategy will be introduced to achieve higher accuracies and to facilitate ease of measurement. The experimental set up will be described; presenting both individual system components and the overall concept. Extensive experimental results are given and finally a formula describing these results is developed.

3.2   Objectives

It is envisaged to realise the following objectives throughout the course of this thesis.

The first objective is to establish an overview over the state of the art dealing with the problem of torque ripple. To achieve this objective an extensive literature review of recent papers is undertaken.

The second objective is to evaluate current concepts and to identify the most promising solutions. Based on these strategies new improved concepts need to be developed.

Thirdly the scope of current solutions needs to be extended towards the concept of load dependent reduction strategies.

Finally these new concepts need to be experimentally tested and their effectiveness and ease of application needs to be evaluated.

The following chapter presents an in depth literature review of current solutions for the torque ripple problem in brushless motors. Both design measures and system approaches will be highlighted. Advantages and limitations of current concepts will be discussed.

Chapter 4 Literature Review

4.1 General Review

In the following an attempt is undertaken to review the more recent literature (last ten years) regarding proposals to reduce torque ripple. Both energised torque ripple and cogging torque are considered. An extensive literature review has been undertaken. The results of this literature review show the diversity of approaches to the problem of torque ripple.

Hanselman [28] discusses modifications of the motor design. Hemati and Leu [29] present a theoretical model for the brushless motor to understand torque production. Renfrew and Karunadasa [30] use simulations to derive a suitable motor control scheme. Ha and Kang [31] use a linearised control concept. References [32] to [34] use some form of current control. Lee and Kwok [35] utilise a compensator mechanism. Dente and Esteves [36] propose a hysteresis control. In [37] different control concepts are compared and evaluated. References [38] to [40] describe different concepts of torque control. [41] to [43] introduce the concept of field orientation. In [44] some form of non-linear control is described. Le-Huy, Slimani and Viarouge [45] use a predictive approach to motor control. Pillay [46] and Renfrew and Al-Naamany [47] apply vector control to brushless machines. [48] describes a digital control concept. Rossi and Tonielli [49] utilise sliding mode control.

The remaining literature review discusses the most relevant papers in depth. It is organised in two parts. The first part (4.2) deals with design measures to reduce torque ripple. Here the motor design is taken as the natural starting point to minimise torque ripple production. Different concepts, their effectiveness and limitations are discussed. The second and longer part (4.3) reviews supply side measures. Here some form of control algorithm is implemented to control the supply currents and supply voltages in the drive. Different methods are compared. They are evaluated in terms of achieved accuracy and ease of implementation.

4.2   Design Measures to Reduce Torque Ripple

One possible starting point to address the problem of torque ripple is the motor design. If it is possible to modify the machine structure to cure the problem of torque ripple no further measures on the drive and control side would be necessary. This would provide an application independent solution to the torque ripple problem.

The design of the traditional dc motor ensures low torque ripple through the high number of commutation segments. For the brushless motor it is not desirable to increase the number of commutation points, as a higher number of commutation points requires a higher number of phases. This in turn leads to a higher commutation frequency, which makes the control more demanding, and a higher number of switching elements, which increases the system cost. Therefore it is necessary to utilise other design measures to improve the torque characteristic of the brushless motor.

Much work has been undertaken ever since the introduction of the brushless motor to overcome this inherent disadvantage of the brushless motor. The following is a review of

some of the more recent work done employing design measures to overcome the torque ripple problem.

Slemon and Ishikawa [50] address both the problem of cogging torque and the problem of commutation torque. It is shown that cogging torque can be reduced by an appropriate choice of the magnet width. This is an alternative to skewing either the slots or the magnets. Slemon and Ishikawa claim that by avoiding the skewing of slots or magnets an easier and cheaper manufacturing of the motor will be possible. The problem of commutation torque results from the fact that in trapezoidal motors the current rise time will be limited by the LR time constant of the motor. Therefore it is not possible to achieve ideal rectangular current pulses with indefinite slopes at the commutation points. A possible solution is a design manipulation, which results in a modified back emf waveform to match the implementable current pulses. The solution employed here is to shift one of the magnet pole pairs by half a slot pitch relative to the other pole pairs. This results in a significant reduction of torque ripple. Three disadvantages are apparent for this method. A complete reduction of torque ripple is not possible. The motor design requires intensive finite element studies (FE) to obtain design modifications. These modifications will be motor dependent. Finally considerable manufacturing effort is required to achieve shifting of the pole pair.

Nogarede and Lajoie-Mazenc [51] consider the problem of energised torque ripple. The problem of cogging torque doesn't exist for them as they are using a slotless motor. Cogging torque is caused by the alignment of permanent magnets and slots. The slotless motor therefore doesn't produce cogging torque. The penalty is a reduction in torque output for the same motor dimensions. The first design measure suggested is a particular

32

choice of magnet width to cancel certain torque harmonics. The disadvantage here is a reduction in average output torque. Secondly they propose to change the conductor distribution to reduce the existing torque ripple. Again a reduction in average torque output occurs. Thirdly it is suggested to increase the phase number. As discussed earlier this will result in a higher commutation frequency and a higher system cost because of the increased number of switching elements. Finally they suggest utilising a multi-star winding configuration to cancel certain torque harmonics. This is not very practical from the manufacturing point of view. In conclusion these design measures only allow the cancellation of certain torque ripple harmonics. Furthermore the manufacturing effort is considerably increased.

In a different publication by the same authors [52] a trapezoidal motor is considered. A skewed design is suggested to reduce cogging torque. This results in a significant reduction of cogging torque ripple at the expense of higher manufacturing requirements. Proposals for the reduction of energised torque again include the use of a higher phase number with the inherent disadvantages discussed earlier. Secondly it is suggested to utilise only a certain percentage of the slot area. This will result in a reduced output torque. Finally the splitting of a phase into two or more windings is tested. This however results in a higher switching frequency and adds considerably to the manufacturing cost. All these measures don't result in a complete elimination of torque ripple.

Kim, Sim and Won [53] regard the effect of skewing on cogging torque. They compare the skewing of stator and rotor. It is mathematically shown that both skewing actions result in the same reduction of cogging torque ripple. Although a substantial reduction of cogging

torque is achievable no complete reduction is possible. Again the additional manufacturing effort leads to increased cost. Furthermore the energised torque ripple is not catered for.

Kawashima and Mizuno [54] are exploring different ways to reduce the cogging torque ripple. Firstly the influence of stator tooth shapes is investigated. A considerable reduction of cogging torque ripple can be achieved through slight design changes to the tooth shape. The new design still represents a viable option for manufacturing. Secondly the magnets are considered. An optimised magnet width reduces cogging torque levels significantly. The magnetisation direction can be optimised. However this will increase the manufacturing costs. The magnet shape can as well be adapted. Again this leads to a more costly manufacturing process. All these design measures don't lead to a complete reduction of cogging torque. Furthermore it is necessary to employ intensive finite element modelling to arrive at optimised design values. It would be feasible to employ stator tooth shaping for cogging torque reduction as it doesn't result in a marked increase in manufacturing cost. However again only a partial reduction of cogging torque is achievable.

Murray [55] looks at the cogging torque. One design measure suggested is an increased airgap size. This acts similar to a slotless machine to reduce the cogging torque level. The clear disadvantage is the loss of output torque magnitude. Another design measure is the use of chamfered magnets. Unfortunately this results in a reduced plateau width for trapezoidal machines, which in turn increases the energised torque ripple because of the mismatch of back emf waveform and phase current. Two experimental machines are built to investigate the effect of proposed design measures. The first machine contains a high number of slots. Furthermore the number of slot is also odd. This helps to avoid some of

the alignment problems, which lead to high cogging torque levels. A marked reduction in cogging torque levels is achieved. For the second machine dummy slots are introduced to increase the number of slots without employing empty slots. Dummy slots are shallow slots without a winding, which only change the surface structure of the stator. Intensive finite element investigations are necessary to design these dummy slots. Again a reduction in cogging torque is achieved. The main disadvantage here is that the problem of the energised torque ripple is not addressed.

In conclusion it can be said that the use of design measures to reduce torque ripple in brushless machines carries several disadvantages. Firstly in depth investigations of the system using finite element methods are normally required. Secondly machine specific solutions are found. Thirdly it is extremely difficult to address the problem of energised torque ripple. Only the reduction of certain torque harmonics is possible. Finally the use of most design measures results in higher manufacturing costs and more complicated production processes. Therefore it can be concluded that design measures can only assist in solving the torque ripple problem without providing a complete solution. If cost and complexity considerations permit it would be possible to use a specific design measure to find partial solutions to the torque ripple problem. So it would be perfectly feasible to employ design measures to reduce or cancel cogging torque. However the problem of energised torque can not be sufficiently addressed. This leads to the conclusion that it is necessary to look at the supply side of the machine to arrive at constant torque output.

4.3 Supply Side Measures to Reduce Torque Ripple

Instead of modifying the motor design itself it is possible to implement some form of control on the supply side. This control will try to achieve suitable supply currents and supply voltages for the brushless motor. A whole variety of control concepts exists. They control different motor variables, require different forms of feedback and use different mathematical approaches. Some are suitable for fast, real-time control and some require considerable computational overhead.

In the following supply side measures are considered, which apply to brushless dc machines (trapezoidal machines), brushless ac machines (sinusoidal machines) or both motor topologies.

4.3.1 Current Profiling for Sinusoidal Machines

Benkhoris, Meibody, Caron and Le Doeuff [56] use a thyristor inverter to supply the motor currents. Therefore the only control variable available is the firing angle of the inverter. It is found that torque-pulsations are independent of speed. The theoretical reason for this will be discussed in chapter 5. Further a dependence on load is observed. Therefore it is suggested to vary the firing angle depending on the load level. The clear disadvantage with this primitive control system is the fact that flexible current profiling is not possible. As a result a substantial amount of torque ripple remains.

Cohen, Cohen, Berg and Petsch [57] suggest a digital control system. They discuss the offset problem of current transducers, which leads to wrong feedback values for the currents. An adaptive digital filter to correct for this is employed. Further a load torque-

controller and a velocity torque-controller are used. The load torque-controller serves to reduce torque ripple whereas the velocity torque-controller masks remaining torque variations. Unfortunately both control structures are not described. Further no simulation or experimental results are given. It is therefore not possible to evaluate the effectiveness of the described control system.

Matsui, Makino and Satoh [58] and [59] consider both cogging torque and harmonics of air gap flux, which lead to energised torque ripple. The d-q reference frame is used. This reference frame results from the conversion of the three stator phases (a, b and c) to a system with two rotor phases (d and q). The transformation and its validity will be discussed in detail in chapter 6. The authors assume that the flux distribution is nearly sinusoidal. Therefore harmonic components can be considered small and they conclude that it is therefore justified to use the transformation into the d-q system. Non-linearities and offsets of the current transducers are discussed. Again a digital filter is employed to cancel torque ripple resulting from this phenomenon. To reduce both cogging torque and energised torque a torque observer is designed. The main objective behind using the torque observer is to combat speed variations caused by torque fluctuations. The torque observer is implemented using a TMS32010 DSP from Texas Instruments. Current and position feedback are quantised using 12 bit A/D converters. A switching speed of 5 kHz for the inverter is achieved. Experimental results are presented. The main problem in using a torque observer is the time delay introduced by the observer and the achievable accuracy. Here an accuracy of 2.5 % of rated torque is realised. It seems to be extremely difficult to achieve higher accuracies and higher dynamic performance of the torque observer without increasing model complexity and calculation time significantly.

In follow up publications by the same authors [60] and [61] they expand on the proposed torque observer system. It is claimed that the torque observer leads to higher system robustness if load torque disturbances occur. Also an additional inertia identifier is realised to further increase system robustness. From the new publications it becomes clear that only flux harmonics up to the order 7 are taken into account, therefore neglecting part of the energised torque ripple. Further deviations between model parameters and actual system parameters will lead to some remaining error. Again only greater modelling efforts and increased computing efforts can lead to more satisfactory results.

Bogosyan, Goekasan, Guerleyen and Kutman [62] use the equivalent circuit model of the brushless motor. Here each phase is represented as a serial connection of a resistance, an inductance and the back emf. Mathematically this is expressed as follows:

$$v = R * i + \frac{d\Phi_m}{dt} \quad (4.1)$$

Here v represents the phase to star point voltage, R is phase resistance, i phase current and Φ_m stands for the flux. The flux is composed as follows:

$$\Phi_m = L * i + \Phi_{m,fd} \quad (4.2)$$

L denotes phase inductance, i phase current again and $\Phi_{m,fd}$ is the stator flux in one phase induced by the permanent magnets on the rotor.

This system describes the three stator phases (a, b and c). To allow for torque control the whole system is transformed into the d-q reference frame. No explanation is given why this transformation is mathematically and physically permitted. A reduction of the three phase-

currents a, b and c is achieved to the two phase-currents d and q. To implement torque control it is necessary to control these two currents. A rather complicated approach is chosen here as the so-called direct component of current (d component) is controlled to a constant value. This leads to an expression for the so-called quadrature current component (q component) so that the resulting torque output remains constant. The control algorithm for the torque control relies on knowledge of instantaneous flux linkages and inductance variations. The authors acknowledge that it will be quite difficult to obtain this knowledge for a practical machine. They therefore propose an adaptive torque control to cater for flux linkage variations. However no time constant and accuracy for the observer are quoted. The presented experimental results do not show a visible cancellation of torque ripple. Again it can be concluded that only substantial modelling effort and available computing power will result in the implementation of a fast and accurate torque observer, which in turn leads to a satisfactory torque control.

Low, Tseng, Lock and Lim [63] also use the equivalent model of the brushless motor in essentially the same form as before. They also employ the transformation into the d-q plane. Again it is not documented why it should be permissible to use this transformation. If the torque equation, for instance equation 2.4, is transformed to the d-q plane the following form is obtained neglecting the contributions through reluctance torque.

$$T = \frac{2}{3} * P * (\frac{d\Phi_d}{d\theta} * i_q - \frac{d\Phi_q}{d\theta} * i_d) \quad (4.3)$$

Here T represents the instantaneous torque output, P is the number of pole pairs, and Φ_d and Φ_q are the flux associated with phase d and phase q respectively, θ is the rotational angle. Finally i_d and i_q are the phase currents.

To implement the torque control it is necessary to control the currents in the d-q plane as can be seen from equation 4.3. No control over the flux linkages is available. If i_d is chosen to be zero equation 4.3 will take a simpler form.

$$T = K(\theta) * i_q \quad (4.4)$$

T again represents instantaneous output torque, $K(\theta)$ is the back emf constant depending on rotor position and i_q is the quadrature current.

As can be seen from equation 4.4 only current i_q remains to be controlled. Furthermore instead of using flux linkage the back emf waveform described by $K(\theta)$ can be used. The back emf waveform is obtainable from terminal measurements.

The task of the control algorithm is to increase and decrease i_d and i_q respectively to follow the reference currents. If the d-q system is back-transformed the three phase currents a, b and c result. The control system has to ensure that they are decreased and increased according to their reference values. As there are three control variables, which are the states of the six switching devices, it is possible to describe the system as a 3-bit control vector. The switching states of the three devices will depend on rotor position and reference values. Therefore current feedback and position feedback are required. Simulation results are given. The new torque control scheme is compared to an ordinary PWM current controller. A visible improvement in ripple torque reduction is achieved, however a certain residual ripple torque still remains.

In a further publication by the same authors [64] the previously described torque control is implemented on an experimental machine. A switching frequency of 10 kHz is realised. Again the experimental results show some remaining torque ripple. Additionally speed

40

control is realised. The speed control is tested for conventional PWM current control and for the proposed torque control. A visible improvement is achieved using the torque control, as expected.

In a different paper by Low [65] Park's transform is used. He assumes that the back emf distribution is sinusoidal. For machines with a uniform airgap i_q is controlled to be constant and i_d is controlled to be zero. For machines with a non-uniform airgap he proposes to control i_q still to be constant and to control i_d to be non-zero. The so-called electromechanical spring-stiffness coefficient is introduced to describe the torque production in brushless machines. This coefficient serves to derive reference values for i_d. Only simulation results are given. No experimental verification is presented. Apart from neglecting back emf harmonics the presented control structure appears to be quite complicated and requires high computational effort for realisation.

4.3.2 Current Profiling for Trapezoidal Machines

Kettleborough, Smith, Al-Hadithi and Vadher [66] consider a machine with trapezoidal back emf waveform. They assume that the abc-plane and dq-plane models of the brushless motor are not valid because the winding distribution is not sinusoidal. Instead they introduce a new model which simultaneously incorporates stator variables and rotor variables. The resulting model is very complex. Further it is doubtful whether it is permissible to incorporate stator and rotor quantities in one reference system. The model also requires knowledge of inductive properties and flux linkages with the associated problems as discussed previously. Of course the measurement accuracy will limit the overall model accuracy. Desired phase currents can be calculated from the model. However considerable computational effort is required to arrive at the new phase currents.

Simulation results show the effectiveness of the proposed scheme. The major drawbacks are the considerable modelling, motor testing and computing capabilities required for implementation of the suggested control scheme.

4.3.3 Current Profiling for Both Sinusoidal and Trapezoidal Machines

Hung and Ding [67] present a Fourier representation of torque ripple based on back emf and current harmonics. Halfwave symmetry is assumed for back emfs. A system of linear equations follows, which is under-determined. It is therefore necessary to introduce an additional constraint. Here power efficiency is used as an additional criteria. A Lagrange minimisation problem results, which can be solved by computer calculations. Even if the number of back emf harmonics is restricted, a still very cumber-some system needs solving. It is not possible to implement the solution in real time. Only simulation results are presented.

Cho, Bae, Chung and Youn [68] use a form of back emf estimation in their control algorithm. These estimated back emf values are then used to estimate the flux linkages of the machine. The flux linkages are in turn transformed into the d-q-representation. Here they are used to calculate i_d and i_q currents to cancel the torque harmonic of order six. Higher torque harmonics are neglected. Both the i_d and the i_q current component are controlled to be non-zero. Because of the stepped calculation approach a time delay is introduced, which leads to deviations from the desired torque output.

Karunadasa and Renfrew [69] derive an expression for torque from the MMF distribution caused by the supply currents and the magnet flux distribution caused by the permanent magnets. This expression is then examined in order to maximise the average torque output

and to minimise certain torque harmonics. Considerable computational efforts are required to find a convergent solution. Simulations of the drive - motor system are carried out. The results are compared for voltage vector control and hysteresis band control. Voltage vector control allows the selection of a vector for the switching states of the inverter as described before. Hysteresis band control tries to control the current within a chosen band around the desired reference currents. Control accuracy will depend on switching period for vector control and hysteresis band-width for hysteresis control. Here vector control is found to deliver better results for tracking the desired reference currents. Further the proposed current control schemes are tested on a practical machine. Only phase current measurements are obtained. Therefore it is not possible to judge the effectiveness of the proposed scheme in practise. However the theoretical approach only allows the reduction of selected torque harmonics. Further it requires considerable computational efforts to arrive at a convergent solution. Also accurate design data is necessary to calculate the expected torque output.

Cho, Bae, Chung and Youn [70] conduct their analysis in the d-q reference system without discussion of validity. They restrict their analysis to torque harmonics of order 6 and 12. Higher harmonics are neglected. The torque expression is split up to separately cancel the torque harmonics. i_d current is therefore not controlled to zero but used to cancel one particular torque harmonic. To take into account changing operating conditions, like temperature variations or armature reaction resulting from different current loadings, some form of parameter estimation is necessary. The authors employ a back emf estimation algorithm to take into account parameter changes. Experimental results are given which show cancellation of 6th and 12th order torque harmonics. Voltage vector control with a switching frequency of 10 kHz is employed. Because of the back emf estimation the

control algorithm proves to be very computational extensive. Further the theoretical approach is not very systematic and only allows cancellation of two torque harmonics.

Wavre [71] considers cogging and energised torque for an actuator in a demanding aerospace application. Cogging torque must be minimised so that it is possible to remove the actuator in case of power failure. Optimisation of air gap width, magnet thickness and shape, slot profile and number of slots is utilised to reduce cogging torque. The reduction meets the required standard in theory. However due to production inaccuracies like rotor eccentricities and varying magnet properties it will be extremely difficult to meet the set requirements in practice. Therefore a slotless, also called toothless, motor design is employed. Of course no cogging torque appears for the slotless machine as there is no alignment of stator slots and magnet edges. Losses and weight are compared for the slotted and the slotless machine. Iron and copper losses and weight are found to be higher for the slotless motor. This results in a performance reduction for same size motors. Further higher manufacturing efforts are necessary to produce the slotless machine. For the energised torque ripple a desired current profile is derived from relationships for the ideal back emf profiles, sinusoidal or rectangular back emf waveforms. The derived current waveforms are approximations, which are valid if the considered back emf waveform does not differ significantly from the ideal cases. Therefore the experimental results clearly show some remaining torque ripple resulting from higher harmonics in the back emf.

Favre and Jufer [72] first give a theoretical deduction of torque ripple based on MMF distribution and magnet flux distribution. This formula can be rewritten to express torque as a function of back emf harmonics and current harmonics. Each torque component is described as follows.

$$T_{ui}(t) = \pm\hat{T}_{ui} * \cos[(-u \pm i) * \omega * t \pm \varphi_i - \varphi_u] \quad (4.5)$$

with:

$$\hat{T}_{ui} = \frac{3}{2} * \frac{P}{\omega} * \hat{U}_u * \hat{I}_i \quad if \quad \frac{u+i}{3} \quad or \quad \frac{u-i}{3} \quad are \quad integer \quad (4.6)$$

$$\hat{T}_{ui} = 0 \qquad \cdot \quad otherwise \quad (4.7)$$

Here $T_{ui}(t)$ represents the individual torque component, $\hat{T}_{ui}$ is the amplitude of a particular torque component, u is the index for back emf harmonics, i is the index for current harmonics, ω represents the machine speed, t is time, φ_i is the phase angle of a particular current harmonic and φ_u is the phase angle of a particular back emf harmonic. Further P is again the number of pole pairs, $\hat{U}_u$ is the amplitude of a back emf harmonic and $\hat{I}_i$ is the amplitude of a current harmonic.

The summation of all torque harmonics with the same frequency $\lambda\omega$ gives the resulting torque harmonic for this particular frequency $T_\lambda(t)$. The total output torque is given through the summation of all torque harmonics. It can be written as:

$$T = \sum_\lambda T_\lambda(t) \quad (4.8)$$

Formula 4.5 can be interpreted as follows. Each current harmonic produces two torque components of a particular frequency through interaction with two back emf harmonics. The summation over all current harmonics gives the resulting torque harmonic of this frequency $T_\lambda(t)$. For the next torque harmonic another summation over all current harmonics will be necessary and so on.

45

To cancel torque ripple of a certain frequency it is possible to modify one current harmonic so that its contribution cancels the contributions made by all the other current harmonics. It is best to choose the current harmonic, which contributes most to the particular torque harmonic. To cancel another torque harmonic another current harmonic will be modified and so on till all undesired torque harmonics are cancelled. However modifying a second and further current harmonics will influence the first torque harmonic and result in the reappearance of torque ripple of the first frequency. It is therefore necessary to employ an iterative process to cancel all undesired torque harmonics. The cancellation of a discrete number of torque harmonics is possible. The same method is used for cogging torque suppression.

Simulation results are given which show the effectiveness of the proposed scheme. The main disadvantage of the proposed method is the extensive computational effort required for implementation of the scheme. It is certainly not possible to implement this form of control in real time. Further the approach is not very systematic, therefore not giving any insights into torque ripple management.

In a further publication by the same authors [73] the previously described work is extended. Here the modification of two current harmonics is employed to cancel torque ripple of a certain harmonic. The authors acknowledge that their approach could lead to an unlimited number of possible current waveforms. It is therefore necessary to find additional selection criteria to choose the optimal current waveforms. It is suggested to utilise the harmonic contents of the current waveforms or the expected copper losses as an additional criterion. A further modification of current waveforms is necessary to maintain the desired output torque level. The proposed control scheme is implemented on an experimental machine. However due to the small torque level and high torque harmonics it

is not possible to present measurements of instantaneous output torque. It is therefore not possible to judge the effectiveness of the proposed control scheme. In conclusion it can be said that the introduction of additional selection criteria increases the computational complexity. The fact, that an unlimited number of solutions is possible for the proposed scheme, suggests that most solutions will be suboptimal solutions. No systematic way is proposed to arrive at an optimal solution.

Further to the two previously discussed publications the same authors expand the existing system [74] to make the control scheme load dependent. An encoder is used for position feedback. A separate current control is implemented for each phase. The current references are stored in EPROMs. Cogging torque is countered through the first part of the current control, employing a constant current waveshape, as the amplitude of cogging torque remains constant with load changes. The level of energised torque changes dependent on load current. The amplitude of the second part of the current control is therefore adjusted accordingly. Dc offset of current sensors is taken into account to avoid additional errors. It is claimed that the remaining torque ripple lies between 1.3 % and 4 % of rated torque, increasing with load current. The authors state that a further reduction is not possible as the motor phases exhibit considerable asymmetry. The torque ripple suppression is in the order of one magnitude. It can therefore be concluded that the proposed control schemes works if pre-stored information is utilised. Use of a different test motor could document further torque ripple reductions.

Jouve and Bui [75] examine cogging torque and energised torque ripple for trapezoidal and sinusoidal machines. A good overview in form of a table listing different torque disturbances with amplitudes and frequencies is given. Cogging torque resulting from the

alignment of slots and magnet edges occurs even in the unenergised state of the machine. As this effect is not caused by the supply currents it follows, that the amplitude of cogging torque will remain constant. The frequency of cogging torque is the number of slots times the mechanical frequency, that is rotational speed. If energised torque ripple is considered it is found that the amplitude increases proportionally with the applied phase currents. The ripple frequencies are multiples of 6 times the electrical frequency. Here the electrical frequency is the mechanical frequency times the number of pole pairs. Also torque ripple induced by current measurement errors is considered. Offset errors of the current transducers lead to torque ripple with a constant amplitude. The frequency is equal to the electrical frequency. Finally torque ripple introduced through gain errors of the current transducers is proportional to the amplitude of the phase currents. The frequency is 2 times the electrical frequency. To reduce cogging torque it is suggested to utilise a cogging torque estimator. The cogging torque estimator determines the cogging torque during an acquisition period. Desired currents are than derived to cancel the cogging torque. Energised torque is described as a product of back emf waveforms and phase current harmonics. Back emf harmonics up to order 7 are taken into account. The resulting torque harmonics of order 6 and 12 can then be cancelled through appropriate choice of the phase currents of order 5 and 7. The proposed torque ripple reduction is implemented for two experimental motors. A DSP is used to execute the required control algorithm. Feedback is provided through a 16-bit resolution resolver. A switching frequency of 10kHz is realised using IGBTs as switching elements. The speed and position control work at 2 kHz. Experimental results for one motor with sinusoidal back emf waveshapes and one motor with trapezoidal waveshapes are presented. First the cogging torque is removed. In a second step the energised torque ripple is reduced. The experimental results show a visible reduction of torque ripple. Unfortunately a quantitative evaluation is not possible as no

48

resolutions are given for the final set of experimental results. Problems occur in the cogging torque estimation, which introduces errors depending on deviation between model parameters and system parameters. As far as the energised torque ripple is concerned only the first two torque harmonics are cancelled as only back emf harmonics up to order seven are considered. The proposed cancellation scheme would not be able to accommodate a higher number of back emf harmonics. Therefore remaining torque ripple is apparent in experimental results.

Clenet, Lefevre, Sadowski, Astier and Lajoie-Mazenc [76] utilise finite element analysis to address the problem of cogging and energised torque ripple. A finite element simulation of the experimental motor is undertaken. First cogging torque is simulated. Then back emf waveforms at a particular current level are determined to calculate energised torque. A formula is derived to calculate desired phase currents from the knowledge of cogging torque and back emf waveforms. This formula takes the same form as Park's transform. The proposed current waveshapes are implemented for an experimental motor. A significant reduction in torque ripple can be observed. It can therefore be concluded that the proposed torque control strategy operates successfully. The major drawback however is the use of finite element modelling to derive the desired phase currents. Considerable modelling and computational effort is required for this.

Kamiya, Shigyo, Makino and Matsui [77] examine cogging torque and energised torque ripple. First the subject of current control is examined. As the conventional three-phase motor is operated in star point connection it follows that the three phase currents are not independent of each other. To establish a desired current profile it is therefore necessary to take into account, which switching combination results in the lowest overall error for all

three phases. To do this it is necessary to calculate the expected currents at the next switching event and to choose the switching vector which results in the lowest overall current deviation. Cogging torque is measured for the test motors. A reference for the i_q current is then derived to cancel cogging torque. To cancel the energised torque ripple Park's transform is used to determine current references for i_q and i_d. i_d is chosen to be zero. i_q is controlled in order to cancel the energised torque ripple. A knowledge of the back emf waveforms is required. Therefore two components of i_q current are necessary to cancel both cogging torque and energised torque ripple. Also offset and gain error of the current transducers are taken into account. A model of the current transducers is developed and the compensation is implemented using calculated values for the terminal voltages, the measured phase currents and the motor parameters R (phase resistance), L (phase inductance) and Ke (torque constant). The proposed control scheme is implemented using a DSP board. A TMS32010 from Texas Instruments is used to realise the control algorithms. It was found that the execution time of the current control is 20 μs, of the torque control 12 μs and of the current sensor correction 26 μs. Therefore a control period between 60 μs and 100 μs can be achieved. The experimental results show a clear reduction in torque ripple. The work undertaken considers all aspects of the torque control. Firstly current control problems are addressed, secondly the actual torque control structure for both cogging torque and energised torque is clearly laid out. Thirdly the problem of current transducer errors is discussed. The authors claim that the remaining torque ripple is as small as 0.3% of rated torque.

Hanselman [78] expands on the problem of torque control. Additionally restrictions imposed by the drive and the electrical time constant of the motor are taken into account. Energised torque ripple for both sinusoidal and trapezoidal motors is considered.

Hanselman also discusses the restrictions on the available current. The maximum available current is limited by the available d.c. link voltage and equally the maximum current rise time is limited through the combination of available d.c. link voltage and phase inductance. These conditions additionally complicate the torque control problem. Three operating regions are discerned. For the first region no torque ripple and minimum ohmic losses are required. Region two demands no torque ripple and minimum losses as well. However here the machine requires the maximum available supply voltage, that is the d.c. link voltage, at least for part of the operating cycle. Finally region 3 is characterised through a combination of minimum torque ripple and minimum ohmic losses. Zero torque ripple is not achievable because the d.c. link voltage is not large enough to supply the machine sufficiently to guarantee zero torque ripple. For region 1 a set of linear equations can be found to describe the problem. A computer optimisation process is required to find the solution to this system of equations. The resulting optimal waveform is found to be independent of speed and universally applicable. For region 2 a constraint optimisation algorithm is necessary because the problem can not be expressed using linear equations. The solution becomes a function of speed and required output torque. For region 3 it is possible to find different formulations for the problem depending on whether the emphasis is on minimum torque ripple or minimum ohmic losses. Again the solution is a function of both speed and required output torque. If additionally the motor is driven in a star-connection, as most brushless ac motors are, further constraints on the solutions for regions 1 to 3 come into play. It is therefore more difficult to find a solution. It seems to be impossible to take armature reaction into account as this greatly increases the complexity of the required computations. Solutions for regions 1 to 3 are calculated based on a motor with trapezoidal back emf waveform, taking harmonics of up to order 13 only into account. The required current waveforms and duty cycles are given for motors of a particular speed range. These

currents are claimed to achieve zero ripple torque for regions 1 and 2. It is not possible to verify this statement as no results for the output torque are given. The solution found is motor-specific as it will depend on parameters and speed range. This prevents it from being universally applicable. Further the required computations are highly complex and time consuming. They also do not yield a systematic understanding of the problem. It can therefore be concluded that the proposed control method is not very practical.

4.3.4 Direct Torque Control

So far measurements of phase currents, voltages, flux, MMF distribution and position feedback have been utilised to calculate the desired supply currents. Either pre-recorded motor parameters or torque observers in one form or the other have been used to predict the expected torque outcome. Finally a method is presented which tries to employ direct torque control to derive the desired supply currents. Here a torque feedback device with a high bandwidth is used to give instantaneous control over the actual torque output. This method can still be classified as current profiling as it makes use of supply side measures to improve the torque ripple characteristic of the motor.

Lonsdale and Schofield [79] present a novel torque transducer. This transducer utilises surface acoustic waves (SAW) to measure strain and subsequently torque. The new device is compact because of the small wavelength of the required acoustic waves. It is therefore suited for use of integrated circuit technology, which makes it a potentially low cost device. It further exhibits a high bandwidth. This makes it ideally suited for motor applications where the use of direct torque transducers has not been very common because conventional torque transducers are bulky, high cost and low bandwidth devices. Energised torque ripple and ripple introduced by position sensor error are addressed. The desired

52

current profile is calculated from the torque feedback signal, which is compared to the reference torque signal. It is found that the system resonance frequency is well within the excitation frequency range. The measured torque signal experiences therefore distortions of magnitude and phase, which lead to wrong control outputs for the currents. It is therefore not possible to employ instantaneous torque control. Instead an average torque control is implemented. This results in a considerable remaining torque ripple as the new control bandwidth does not allow to correct instantaneous torque distortions. It can be concluded that is not possible for direct torque control to utilise the proposed feedback method because of system resonance problems. It can be expected that the system resonance for most systems will be within the range of excitation frequencies. Furthermore a large phase shift of the torque transducer can result in the control system becoming unstable. It can therefore be said that at the moment direct torque control does not offer an acceptable solution for the problem of torque ripple reduction.

Chapter 5 gives a theoretical analysis of torque ripple production in brushless motors. Both cogging and energised torque ripple are investigated in depth.

Chapter 5   Theoretical Analysis of Torque Ripple Production

As already discussed there are two dominant sources for torque ripple production in brushless machines. These are cogging and energised torque ripple. They are caused by separate mechanisms and will therefore be treated individually in the following. A theoretical description of their production will be given first. Then the influence of parameters like speed and current loading on their appearance will be discussed. Also typical numerical values as a percentage of load torque will be stated and measurement methods will be briefly highlighted.

5.1   Cogging Torque

Cogging torque is a phenomenon caused by the machine geometry. The vast majority of brushless motors use stator slots made from iron to hold the armature windings. The presence of these stator slots is the cause for the occurrence of cogging torque.

The individual rotor magnets set up a trapezoidal flux distribution as described in chapter 2. The exact shape depends on the magnet geometry. The rotor flux relies on the iron parts of the armature to close the flux paths. Figure 5.1 illustrates the situation. Parts of the magnet, which are aligned with the stator tooth, can easily close the flux path via the stator yoke. However parts of the magnet, which are opposite the stator slot, can not easily find a flux path because of the high magnetic reluctance of the air in the stator slot opening. The flux paths around the stator slot opening will therefore be distorted towards the iron parts

of the stator teeth. This results in a decreased flux density at the stator slot opening. The dip in airgap flux density can clearly be seen in figure 5.1.
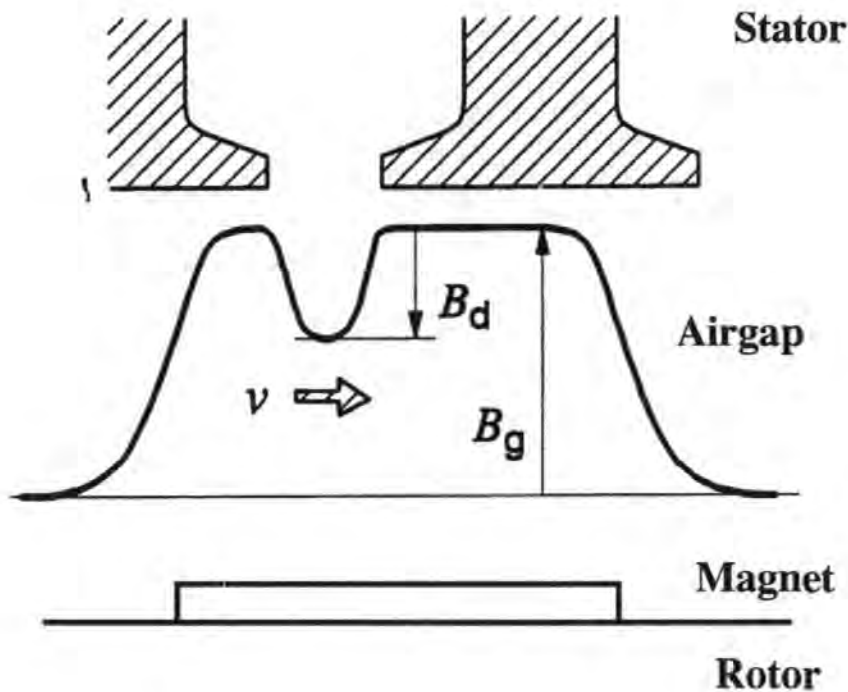
Figure 5.1 Modification of airgap flux distribution due to slot opening from [18]

B_g represents the radial component of flux density in the airgap set up by one magnet on the rotor. B_d is the reduction of the radial component of airgap flux density at the position of the stator slot. v finally stands for the velocity of the rotor magnet relative to the stator.

Recalling the fundamental equation for torque production from chapter 2, we consider the three terms.

$$T = \frac{1}{2} * i^2 * \frac{dL}{d\theta} - \frac{1}{2} * \phi_m^2 * \frac{dR}{d\theta} + N * i * \frac{d\phi_m}{d\theta} \quad (5.1)$$

As before T describes the output torque of the machine. i is the armature current. L stands for the self-inductance of the armature coils. θ denotes the rotational angle of the rotor. ϕ_m

represents the magnet flux. R is the magnetic reluctance of the flux path and finally N gives the number of turns on the armature.

The first term represents the production of reluctance torque if the self-inductance of the armature coils changes with rotational position. In surface mount brushless motors, being considered here, this effect is negligible. The second term describes the production of torque due to changes of reluctance in the magnetic flux path with rotor position. The third term considers changes of the flux linkage between armature coils and rotor magnets. At the moment we only discuss the motor in the unenergised state. The alignment torque from the third term is therefore not present. The only remaining source for torque production is therefore the occurrence of reluctance torque due to term 2. Equation 5.1 can now be simplified as follows.

$$T_R = -\frac{1}{2} * \phi_m^2 * \frac{dR}{d\theta} \quad (5.2)$$

Here T_R is the reluctance torque produced. Again ϕ_m stands for the magnet flux. R denotes the magnetic reluctance of the flux path and θ stands for the rotational angle of the rotor.

Going back to figure 5.1 we can now understand that a change of reluctance in the magnetic path leads to the production of reluctance torque.

Figure 5.2 enables a closer look at the rotational position where changes in the reluctance occur.
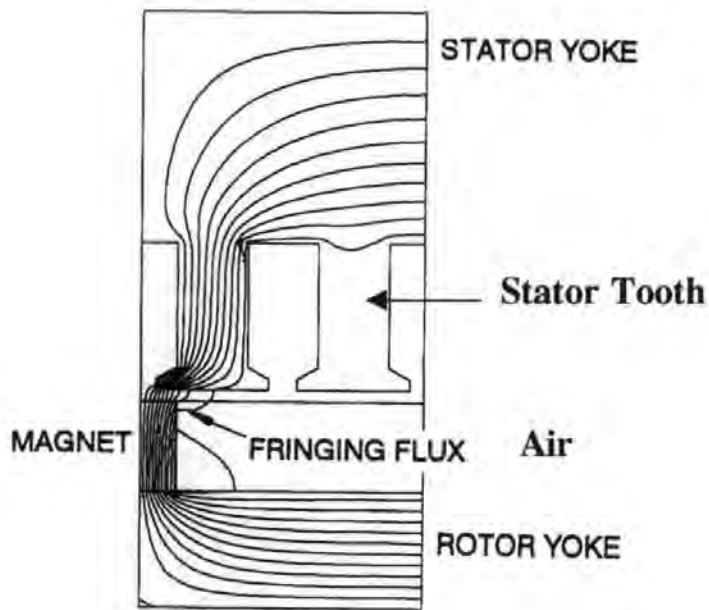
Figure 5.2 Magnet edge aligned with stator tooth to preserve lower reluctance path from [18]

The magnet is shown on the left and carries most of the flux. The air to the right of the magnet allows some fringing flux.

The reluctance of the magnetic path changes when a magnet moves from covering a stator tooth (lower reluctance path) to covering the slot opening (higher reluctance path). The position of the magnet edge is critical here. The magnets will therefore always try to align with the stator teeth as can be seen in Figure 5.2 to minimise reluctance. When the shaft of a brushless motor is turned by hand in the unenergised condition, the rotor positions, where the magnets align with the stator teeth, can normally be felt.

As the reluctance changes occur whenever a magnet edge aligns with a stator tooth the cogging frequency can now be determined. It is simply the number of slots times the rotational frequency.

$$f_c = N * f_m \quad (5.3)$$

Here f_c is the frequency of cogging torque, N is the number of stator slots and f_m is the frequency of rotation.

The amplitude of cogging torque depends on the magnitude of the magnet flux and the magnitude of the reluctance change and can not easily be expressed in equational form.

As can be seen from equation 5.3 the cogging frequency is directly proportional to the machine speed. However the magnet-flux set up by the rotor magnets is independent of speed. Similarly the change in reluctance is constant with motor speed. The amplitude and phase of cogging torque is therefore independent of motor speed.

If the energised case is considered matters are slightly different. The presence of armature currents leads to additional distortions for the flux path. The magnetic reluctance therefore also changes. However this represents a second order effect and will normally be below measurement accuracy for well-designed machines. At very high currents even a partial demagnetisation of the rotor magnets can occur resulting in a lower magnet flux level. However again a well-designed brushless motor should not exhibit this behaviour. It can therefore be concluded that the influence of armature currents on cogging torque is a second order phenomenon, which can be neglected.

In the following the magnitude and phase of cogging torque will therefore be considered constant and independent of speed and armature current.

The description of cogging torque derived so far has not taken into account manufacturing tolerances. Factors like rotor eccentricity, differences in the magnet surfaces and machining of the slot openings will result in higher order harmonics becoming present in the cogging torque. It is also possible that the cogging torque for each slot is different. This makes it necessary to record the cogging torque profile over a whole rotational cycle to derive measures for cancellation.

Cogging torque is normally quantified as peak-to-peak ripple torque. The amplitude of cogging torque entirely depends on the motor geometry. It is therefore not possible to quote typical values. However for well-designed brushless motors between 0.5% and 2% of full load torque are common and can be achieved by using some of the design methods described in chapter 4.

It has been highlighted that cogging torque can be interpreted as unenergised torque. Cogging torque is therefore normally recorded in the no-load situation. To accurately record cogging torque the brushless motor can be connected to a second motor. The terminals of the brushless motor are left unconnected. The second motor then drives the brushless motor. The drive speed depends on the frequency characteristic of the torque transducer and the required harmonic accuracy. As mentioned before it is necessary to record a full rotational cycle.

In the following section the energised torque ripple will be analysed. First some equations from the literature will be quoted, giving different descriptions of the phenomenon of energised torque ripple. Then a general equation for energised torque ripple production will be used to undertake simulations highlighting the nature of energised torque ripple.

Conclusions will be drawn from the simulation results and the influence of speed and current loading will be discussed. Finally typical values for energised torque ripple will be given and practical measurement methods will be briefly introduced.

5.2 Energised Torque Ripple

Energised torque ripple is produced through the interaction of magnet flux from the magnets and the magneto-motive force (MMF) set up by the phase currents. It can be interpreted as mutual or alignment torque and is described by the third term of equation 5.1.

$$T_m = N * i * \frac{d\phi_m}{d\theta} \quad (5.4)$$

Here T_m represents the mutual torque. N is the number of turns. i is the current through the coil. ϕ_m stands for the magnet flux. Finally θ again stands for the rotational angle of the rotor.

Two alternative ways exist to express the production of energised torque ripple. Firstly energised torque ripple can be described as the interaction of magnet flux space harmonics with MMF time harmonics from the phase currents. Alternatively torque ripple can be expressed as the result of back emf space harmonics interacting with phase current time harmonics. It can be shown that both ways of describing torque ripple are equivalent.

In the following some analytical descriptions of torque ripple from the literature are given.

5.2.1 Analytical Descriptions of Energised Torque Ripple

Bolton and Ashen [80] published a fundamental paper describing the torque ripple resulting from the interaction between magnet field harmonics caused by motor design and phase current harmonics supplied to the motor. They are the first to assess the potential of current harmonics for torque ripple production and subsequent reduction strategies. Torque production is expressed using MMF distribution and magnet field flux distribution. It is assumed that magnet field flux distribution is symmetrical, in other words no even harmonics are present. Further it is also assumed that MMF distribution is symmetrical so that it does not contain any even harmonics either.

$$
T = 0.5 N\hat{I}\hat{B}mDLP * \begin{bmatrix} \sum_{p=1,3}^{\infty}(K_{Ip}(X(p,1)K_{w1}\cos(p-1)\omega t + X(p,3)K_3 K_{w3}\cos(p-3)\omega t + \\ X(p,5)K_5 K_{w5}\cos(p-5)\omega t +...) - K_{Ip}(Y(p,1)K_{w1}\cos(p+1)\omega t + \\ Y(p,3)K_3 K_{w3}\cos(p+3)\omega t + Y(p,5)K_5 K_{w5}\cos(p+5)\omega t +...)) \end{bmatrix}
$$

(5.5)

Here T is the energised torque, N is the number of phases, $\hat{I}$ is the peak phase current, $\hat{B}$ is the peak airgap flux density, m is the number of turns in series per pole per phase, D is the stator bore diameter, L is the active axial length of the machine, P is the number of pole pairs, K_{Ip} is the peak value relative to fundamental of pth harmonic in current waveform, K_{wn} is the nth harmonic winding factor, K_n is the peak value relative to fundamental of nth harmonic in field flux density distribution.

$X(p,q) = 1$ when $|p-q| = N*k$ for $k = 0,1,2,...$

$\quad\quad = 0$ otherwise

$Y(p,q) = 1$ when $p+q = N*k$ for $k = 1,2,3,...$

$\quad\quad = 0$ otherwise

61

Equation 5.5 describes production of mutual torque in general for machines with any number of phases. The authors show that it is possible to derive the frequencies of torque ripple from equation 5.5. For machines with an even number of phases torque ripple will have frequencies, which are multiples of the phase number times the electrical frequency. For machines containing an odd number of phases torque ripple occurs at frequencies which are multiples of 2 times the phase number times the electrical frequency. For the most commonly used machine, the 3-phase motor, the following equation can be derived from 5.5.

$$T = 1.5\hat{I}\hat{B}mDLPK_{w1}\left[\begin{array}{l} 1 + \dfrac{K_3 K_{w3} K_{I3}}{K_{w1}} + \dfrac{K_5 K_{w5} K_{I5}}{K_{w1}} + \ldots + (K_{I7} - K_{I5} + \dfrac{K_3 K_{w3} K_{I9}}{K_{w1}} \\[2ex] - \dfrac{K_3 K_{w3} K_{I3}}{K_{w1}} + \dfrac{K_5 K_{w5}}{K_{w1}} + \dfrac{K_7 K_{w7}}{K_{w1}} + \dfrac{K_9 K_{w9} K_{I3}}{K_{w1}} + \ldots)\cos 6\omega t + \\[2ex] (K_{I13} - K_{I11} - \dfrac{K_3 K_{w3} K_{I9}}{K_{w1}} - \dfrac{K_5 K_{w5} K_{I7}}{K_{w1}} - \dfrac{K_7 K_{w7} K_{I5}}{K_{w1}} - \\[2ex] \dfrac{K_9 K_{w9} K_{I3}}{K_{w1}} + \ldots)\cos 12\omega t + \ldots \end{array}\right] \qquad (5.6)$$

Here all variables have the same meaning as in equation 5.5.

As can be seen from equation 5.6 torque ripple frequencies are multiples of 6 times the electrical frequency for 3 phase machines as expected from the previous statements. Bolton and Ashen use a computer program to evaluate equation 5.6 for different cases. They examine different supply current waveforms, look at the effects of non-sinusoidal field flux distributions and the effects of practical winding arrangements. For each case torque ripple frequencies and torque ripple amplitudes are compared for machines with the same ratings, that is either same average output torque, same peak currents or same RMS currents. It is therefore possible to identify supply currents, field distributions and winding arrangements,

which lead to lower torque ripple. However no in-depth investigations of the effects of particular field or current harmonics are undertaken. Their aim is not to achieve torque ripple cancellation but to advise on the best machine design for a particular situation. Equation 5.6 requires closer scrutiny to establish a better understanding of torque ripple production. Therefore a further publication is quoted to show a different way to express torque ripple production.

Hanselman, Hung and Keshura [81] use the complex form of the Fourier series to develop a general torque expression for 3-phase machines. Here back emf and phase current expressions are used.

$$T = \sum_{n=-\infty}^{\infty} T_n \exp(jn\theta) \quad (5.7)$$

T is the energised torque again, T_n is the torque contribution of a particular frequency, n is the order of torque frequencies and θ is the rotational angle.

The Fourier series coefficients in equation 5.7 are expressed as follows:

$$T_n = \tau_n [1 + 2\cos(2\pi \frac{n}{3})] \quad (5.8)$$

The Fourier series coefficients in 5.8 are calculated from:

$$\tau_n = \sum_{m=-\infty}^{\infty} K_m I_{n-m} \quad (5.9)$$

Here K_m is the mth back emf harmonic and I_{n-m} is the current harmonic of order n-m.

The authors show that only torque ripple with frequencies, which are multiples of 3 times the electrical frequency can be developed. If it is further assumed that the back emf waveforms exhibit half wave symmetry due to motor design; then no even harmonics are

present. If it is also assumed that the supply currents are chosen in order not to contain even harmonics; then it can be shown that no odd multiples of three times the electrical frequency are present. In other words only multiples of 6 times the electrical frequency can be observed for torque ripple. This is of course the same result as from [80].

Further the authors deduce that each phase current harmonic will contribute to all phase torque harmonics. Also since back emf harmonics and phase current harmonics are multiplied in the given equations, it follows that the harmonics contribute to torque harmonics which are equal to the sum and the difference of the harmonics.

No further conclusions are drawn from the torque equation. Again it can be said that further exploration of the torque equation will be necessary to come to more precise statements concerning the way torque ripple is produced.

So far the results from the literature search have been reviewed. However it is not easy to derive helpful conclusions concerning the nature of torque ripple production from the presented equations. It is especially difficult to assess the influence of individual back emf and current harmonics. Therefore it has been decided to develop computer simulations to establish these relationships. These simulations represent a new approach to the problem of torque ripple.

In the following the results of these simulations are presented. An overview of individual torque contributions by particular back emf and current harmonics is given in table-form to allow a comprehensive analysis. Only 3-phase systems are dealt with, as they are by far the most common motor-type. The considerations can however easily be extended to machines with other phase numbers.

The basic power relation for mutual torque production in a 3-phase machine can be taken as a starting point.

$$T * \omega = emf_1 * i_1 + emf_2 * i_2 + emf_3 * i_3 \quad (5.10)$$

Here T is the mutual torque, ω is the rotational speed, emf_i is the phase back emf and i_i is the phase current.

The three phases are offset by 120 electrical degrees relative to each other. If it is assumed that the machine is running at constant speed it is possible to assess the effect of individual back emf harmonics and current harmonics.

5.2.2 Sinusoidal Excitation

To investigate the production of ripple torque it is first assumed that the machine is supplied with ideal sinusoidal currents. That means no time harmonics of currents are present. Therefore the interaction between the current fundamental and the back emf space harmonics can be illustrated. Simulations have been used to evaluate equation 5.10 for this purpose. Table 5.1 lists back emf harmonics, phase torque frequencies, resulting torque frequencies and resulting torque amplitudes. The back emf harmonics are assumed to have the same amplitude in order to make results comparable.

Back EMF Harmonics	Phase Torque Frequencies	Resulting Torque Frequencies	Amplitude of Resulting Torque
1	2	0	1
2	1,3	3	-1
3	2,4	0	0
4	3,5	3	1
5	4,6	6	-1
6	5,7	0	0
7	6,8	6	1
8	7,9	9	-1
9	8,10	0	0
10	9,11	9	1
11	10,12	12	-1
12	11,13	0	0
13	12,14	12	1
14	13,15	15	-1
15	14,16	0	0
16	15,17	15	1
17	16,18	18	-1

Table 5.1 Torque ripple frequencies and amplitudes through sinusoidal excitation

The first line of table 5.1 shows that the fundamental of the back emf produces useful output torque (frequency 0 and amplitude 1). All other back emf harmonics either produce ripple torque or don't contribute to torque production.

It can be noted, that back emfs, which are multiples of three, do not have any influence on torque production in 3 phase machines, if the machines are excited with sinusoidal phase currents. They neither produce useful output torque nor torque ripple.

Thirdly back emf harmonics which are multiples of 2, unless they are also multiples of 3, produce torque ripple with frequencies which are odd multiples of the phase number; 3,9,15 etc. .

All other back emf harmonics produce torque ripple at even multiples of the phase number or in other words multiples of 6.

Two back emf harmonics always act together to produce torque ripple of a particular frequency. These pairs are: 2 and 4, 5 and 7, 8 and 10, 11 and 13 and so on. In fact if both back emf harmonics show the same amplitude and phase shift, which is unlikely for a real machine, then they will cancel each other out.

5.2.3 Excitation with Multiples of Two

In a further step the machine will be excited with currents which have frequencies that are multiples of two but not multiples of three. That is 2,4,8,10 and so on. As an example the table for an excitation with the current harmonic of order 2 is given. Again back emf harmonics, phase torque frequencies, resulting torque frequencies and resulting torque amplitudes are listed. It is again assumed that the amplitude of each harmonic is the same to make the results comparable.

67

Back EMF Harmonics	Phase Torque Frequencies	Resulting Torque Frequencies	Amplitude of Resulting Torque
1	1,3	3	-1
2	0	0	1
3	1,5	0	0
4	2,6	6	-1
5	3,7	3	1
6	4,8	0	0
7	5,9	9	-1
8	6,10	6	1
9	7,11	0	0
10	8,12	12	-1
11	9,13	9	1
12	10,14	0	0
13	11,15	15	-1
14	12,16	12	1
15	13,17	0	0
16	14,18	18	-1
17	15,19	15	1

Table 5.2 Torque ripple frequencies and amplitudes through excitation by 2nd harmonic

Firstly the second harmonic of the back emf together with the current produces the useful output torque. For an excitation with 4 times the electrical frequency it would be the back

emf harmonic of order 4. Or in other words current and back emf harmonic of the same order work together to produce constant, that is useful, output torque.

Again multiples of 3 in the back emf waveform do not contribute to torque production.

Thirdly multiples of 2 for the back emf, which are not multiples of 3, produce torque ripple with multiples of 6.

Fourthly other multiples for the back emf result in ripple torque of odd multiples of three. Compared to sinusoidal excitation the torque ripple frequencies are reversed. Multiples of 2 in the back emf waveform are responsible for multiples of 6 and not odd multiples of 3. Again two back emf harmonics contribute to torque ripple of one particular frequency. If the two back emf harmonics possess the same amplitude and phase shift they will cancel each other out.

5.2.4 Excitation with Multiples of Three

The next step is the excitation with currents, which are multiples of three. That is 3,6,9,12 and so on. As an example the table for an excitation with the current harmonic of order 3 is given. Again back emf harmonics, phase torque frequencies, resulting torque frequencies and resulting torque amplitudes are listed. It is again assumed that the amplitude of each harmonic is the same to make results comparable.

Back EMF Harmonics	Phase Torque Frequencies	Resulting Torque Frequencies	Amplitude of Resulting Torque
1	2,4	0	0
2	1,5	0	0
3	0,6	0,6	2,-1
4	1,7	0	0
5	2,8	0	0
6	3,9	3,9	1,-1
7	4,10	0	0
8	5,11	0	0
9	6,12	6,12	1,-1
10	7,13	0	0
11	8,14	0	0
12	9,15	9,15	1,-1
13	10,16	0	0
14	11,17	0	0
15	12,18	12,18	1,-1
16	13,19	0	0
17	14,20	0	0

Table 5.3 Torque ripple frequencies and amplitudes through excitation by 3rd harmonic

Again the back emf of the same order as the current, here order 3, 6, 9 and so on, produces the useful output torque. The same statement as before applies; only currents and back emf harmonics of the same order are responsible for constant output torque.

Multiples of 3 in the back emf waveform contribute torque ripple with frequencies, which are multiples of 3. However as opposed to the cases discussed earlier, each order of back emf will produce torque ripple of 2 frequencies and not just one frequency as before.

All the other back emf harmonics will not contribute to torque ripple production in this case.

5.2.5 Excitation with Other Harmonics

Excitation with other current harmonics yields the same results as for sinusoidal excitation. Useful torque is produced for harmonics of the same order of current and back emf. Multiples of 3 in the back emf waveform do not contribute to torque production. Multiples of 2, which are not multiples of 3, result in odd multiples of 3. All other harmonics in the back emf waveform produce torque ripple with multiples of 6.

5.2.6 Conclusions from Simulations

The simulations have highlighted how each space harmonic of back emf interacts with each time harmonic of current to produce torque ripple with different frequencies. In order to simplify the presentation of results the following assumptions are made.

a. Firstly the back emf waveform will exhibit symmetry due to the construction of the machine. That is no even harmonics are present in the back emf waveform.

b. Secondly the supply currents are forced to be free of even harmonics as well, that is symmetrical. An excitation with even current harmonics is not practical.

From previous considerations this will exclude all odd multiples of 3 for the torque ripple. In other words only multiples of 6 will remain as torque ripple frequencies.

The following table shows the resulting pattern of torque production. Torque ripple frequencies are given for combinations of back emf harmonics and current harmonics.

back emf	1	3	5	7	9	11	13	15	17
current									
1	0	0	6	6	0	12	12	0	18
3	0	0,6	0	0	6,12	0	0	12,18	0
5	6	0	0	12	0	6	18	0	12
7	6	0	12	0	0	18	6	0	24
9	0	6,12	0	0	0,18	0	0	6,24	0
11	12	0	6	18	0	0	24	0	6
13	12	0	18	6	0	24	0	0	30
15	0	12,18	0	0	6,24	0	0	0,30	0
17	18	0	12	24	0	6	30	0	0

Table 5.4 Torque ripple frequencies

The following observations can be made.

Firstly it can be seen that each current harmonic produces two torque harmonics of a particular frequency through interaction with two back emf harmonics.

Secondly all current harmonics contribute to the production of torque ripple of a particular frequency.

The torque ripple frequency is determined by adding or subtracting the order of the current harmonic to respectively from the order of the back emf harmonic.

Usually 3 phase motors are operated in a star configuration. Therefore no currents which are multiples of 3 can be present. If this fact is taken into account the following table can be developed to show interaction of back emf harmonics and current harmonics.

	back emf	1	3	5	7	9	11	13	15	17	19	21	23
current													
1		0	0	6	6	0	12	12	0	18	18	0	24
5		6	0	0	12	0	6	18	0	12	24	0	18
7		6	0	12	0	0	18	6	0	24	12	0	30
11		12	0	6	18	0	0	24	0	6	30	0	12
13		12	0	18	6	0	24	0	0	30	6	0	36
17		18	0	12	24	0	6	30	0	0	36	0	6
19		18	0	24	12	0	30	6	0	36	0	0	42
23		24	0	18	30	0	12	36	0	6	42	0	0

Table 5.5 Torque ripple frequencies for star configuration

From table 5.5 it is obvious that multiples of 3 in the back emf waveform do not have any influence on torque production. Therefore for 3 phase brushless motors with star configuration, which is the most common motor type, the following conclusions regarding torque production can be drawn.

Firstly each current harmonic interacts with all back emf harmonics.

Secondly each current harmonic together with 2 (different) back emf harmonics produces torque ripple of a particular frequency.

The frequency is determined through the sum and the subtraction respectively of the current and back emf harmonic.

If the contributions from all current harmonics are added up the resulting torque ripple of that particular frequency will be found.

Finally torque ripple frequencies are multiples of 6 times the electrical frequency.

5.2.7 Influence of Speed and Current Loading on Energised Torque Ripple

The space harmonics of the back emf waveform are determined by the machine geometry. They are therefore independent of speed. Speed therefore has no influence on energised torque ripple production.

The current through the phase windings sets up a magnetic field, which becomes superimposed onto the magnetic field from the rotor magnets. The resulting magnetic field will considerably change the back emf harmonics. This is a first order effect, which needs to be taken into account when describing the resulting torque ripple. Both the amplitude and the phase of back emf harmonics will be altered with increased current loading.

5.2.8 Typical Values and Measurement Method for Energised Torque Ripple

It is of course difficult to quote typical values for energised torque ripple as they vary considerably with machine design. However as a rough guideline values between 2% to 30% peak-to-peak torque ripple as a percentage of output torque can be assumed.

As the name implies, energised torque ripple only occurs if the machine is excited through some current loading. It can therefore only be measured if phase currents are present.

It is not possible to use a second motor to drive the brushless machine to directly determine the torque ripple produced by the brushless motor. This is because the second motor will also produce some form of torque ripple, which will interact with the torque ripple from the brushless machine. There are only indirect methods, which determine the back emf waveform of the brushless motor. The torque ripple is then calculated from the back emf data. The phase leads of the brushless machine are connected with some form of load. The difficulty here is that the load should only allow for ideal sinusoidal phase currents in order to determine individual back emf harmonics. This requires considerable control effort for the load.

A second method would be to drive the brushless motor with well-defined currents, for example sinusoidal or trapezoidal. Here a second motor or a brake can be used as a load for the brushless motor. However it is much easier to determine the influence of individual back emf harmonics as long as full control over the supply current production is retained. This is usually much easier to realise.

Both methods suffer the drawback that the unenergised torque ripple will also unintentionally be recorded. The only way to prevent this is to cancel the unenergised torque ripple before recording the energised torque ripple. Especially for low current loadings it is possible that the unenergised torque ripple is of greater amplitude than the energised torque ripple.

Chapter 6 will identify promising torque ripple reduction methods for both cogging and energised torque ripple. Based on the literature review in chapter 4 and the simulation results from this chapter the most promising strategies will be presented; again using computer simulations and experimental data.

Chapter 6   Conventional Torque Ripple Reduction Strategies

6.1   Reduction Strategies for Cogging Torque

The literature review revealed different strategies to deal with the problem of cogging torque. Basically it can be differentiated between design measures and system approaches.

First design measures will be looked at. The motor design itself is the obvious starting point to deal with the problem of cogging torque. As chapter 5.1 highlighted, cogging torque is caused by changes in magnetic reluctance. The aim for the designer is to reduce or cancel these changes in reluctance. A whole variety of different design measures have been proposed.

Changing the magnet width and consequently the effective overlap angle for the magnets has been suggested [50] and [54]. Skewing of the rotor is a very common approach. Here the different overlap angles between stator slots and magnet edges along the length of the rotor will cancel each other out [52] and [53]. Changes to the shape of the stator teeth or the magnets themselves are also proposed [54] and [55]. Another measure would be to increase the airgap size [55]; leading to reduced cogging at the expense of loosing torque output. Finally using an odd number of slots is suggested to reduce the instances of magnet alignment with the stator slots [55].

All these design measures have some effect to a greater or lesser extent. Skewing for instance is a standard technique used for high performance motors. However these measures require time consuming calculations or even Finite Element Simulations. They are machine specific and will normally not be sufficient to cancel cogging torque completely. Further they neglect the influence of manufacturing tolerances, which will introduce additional cogging torque contributions. Most of these measures also effect the production of energised torque. Either the achievable level of energised torque will be reduced or additional harmonics are introduced into the energised torque ripple. In conclusion it can be said that some of these design measures can be utilised to improve the cogging torque behaviour of a brushless motor; but they are not sufficient to solve the problem completely.

A system's approach leads to different measures. As already discussed the supply currents into the brushless motor can be manipulated. The idea here is to utilise supply current harmonics in order to create a counter torque, which would cancel the existing cogging torque; rather then to eliminate the production of cogging torque in the motor. This counter torque is a component of the energised torque.

Different realisations are described in literature. A torque observer [58], [59], [60] and [61] can be utilised to record torque ripple (the observer would record both cogging and energised torque ripple and therefore the resulting torque ripple). The observer would then serve to calculate correction currents to reduce the ripple. Principally this system is capable of reducing torque ripple. However in practise the time delay between the occurrence of the torque ripple and the application of the correction currents will lead to a considerable remaining amount of torque ripple, which makes the use of a torque observer unsuitable for

cogging torque correction. Further there is no need to utilise a relatively complicated tool like a torque observer to cancel cogging torque. Cogging torque doesn't change with speed and load conditions and can therefore be regarded as constant. It is therefore not necessary to record and correct it in real time causing a considerable computational overhead.

Another method [75] uses a torque estimator to cancel cogging torque. The difficulty here, as the authors state, is the deviation between model and system parameters; leading to wrong correction currents. Again the computational effort is considerable as a real-time estimation needs to be performed.

A different strategy is presented in [76]. The cogging torque for a particular motor is determined from Finite Element Simulations. A formula is developed to cancel both cogging and energised torque ripple. The difficulty here is that the correction can not be separated into cogging and energised torque ripple components. It is therefore not possible to combat cogging torque itself. Further with changes in energised torque ripple due to different current loading, cogging torque will re-emerge.

The most promising approach is described in [77]. The authors use an 8-pole machine with 24 stator slots. If chapter 5.1 one is recalled it is possible to calculate the basic cogging frequency.

$$f_c = N * f_m \quad (6.1)$$

Here f_c represents the cogging frequency, N is the number of stator slots and f_m is the mechanical frequency of rotation.

From equation 6.1 it is obvious that the described motor will have a fundamental cogging frequency of 24 times the frequency of rotation. To utilise correction currents it is desirable to use electrical quantities instead of mechanical quantities. The rotor contains 8 magnets or in other words 4 pole pairs. The rotor can therefore be divided into 4 symmetrical sections. It is now useful to calculate the electrical frequency of rotation.

$$f_e = p * f_m \quad (6.2)$$

Here f_e represents the electrical frequency of rotation, p is the number of pole pairs and f_m is again the mechanical frequency of rotation.

The electrical frequency for the motor of interest is four times the mechanical frequency of rotation, because it contains four symmetrical sections. It is now possible to calculate the electrical cogging frequency. This is the cogging frequency for one section of the rotor.

$$f_{ec} = \frac{N}{p} * f_m \quad (6.3)$$

f_{ec} represents the electrical cogging frequency, N is the number of stator slots, p is the number of pole pairs and f_m stands for the mechanical frequency of rotation.

If equation 6.3 is evaluated it will be found that the electrical cogging frequency comes out as six times the mechanical frequency of rotation. Figure 6.1 shows measurements for the cogging torque from paper [77]. The upper trace represents the cogging torque and the lower trace shows the electrical angle of rotation.
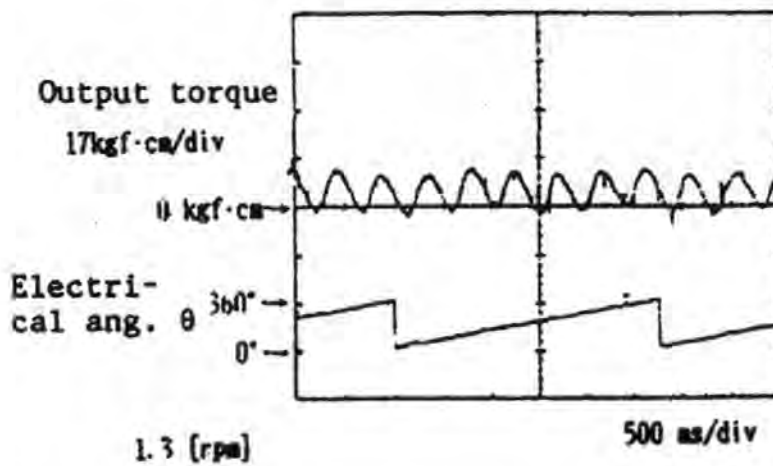
Figure 6.1 Cogging torque from literature [77]

As can be seen from figure 6.1 the basic harmonic of 6 times the rotational frequency is dominant. There are also small contributions from higher harmonics.

The authors use Park's transform to cancel cogging torque. Park's transform will be dealt with in depth in the following subchapter. For now it is sufficient to mention that Park's transform allows the transfer of 3-phase stator quantities into 2-phase rotor quantities and vice versa. The authors suggest a cancellation current in the 2-phase rotor description. This cancellation term can then be transformed into 3-phase stator quantities using Park's transform to determine the required correction currents for the 3 phases. The correction currents will in turn develop a counter torque to cancel the cogging torque. The results from the paper show, that this method works quite well.

However the cancellation current in the 2-phase description has been suggested because of the knowledge of the cogging torque. Here the cancellation current also needs to have a frequency of 6 times the rotational frequency and needs to have a phase shift of 180 degrees to counter the existing cogging torque. For the motor in question it is very easy to

suggest an appropriate cancellation current because of the simple structure of the cogging torque. However if the cogging torque is of a more complicated nature or if manufacturing tolerances distort the cogging torque and result in the appearance of higher harmonics it will not be that easy to suggest appropriate cancellation currents.

Figure 6.2 shows the measured cogging torque for the motor considered in this thesis.

Rotational Angle   200°/div   Torque   86.5mNm/div

Time   50ms/div
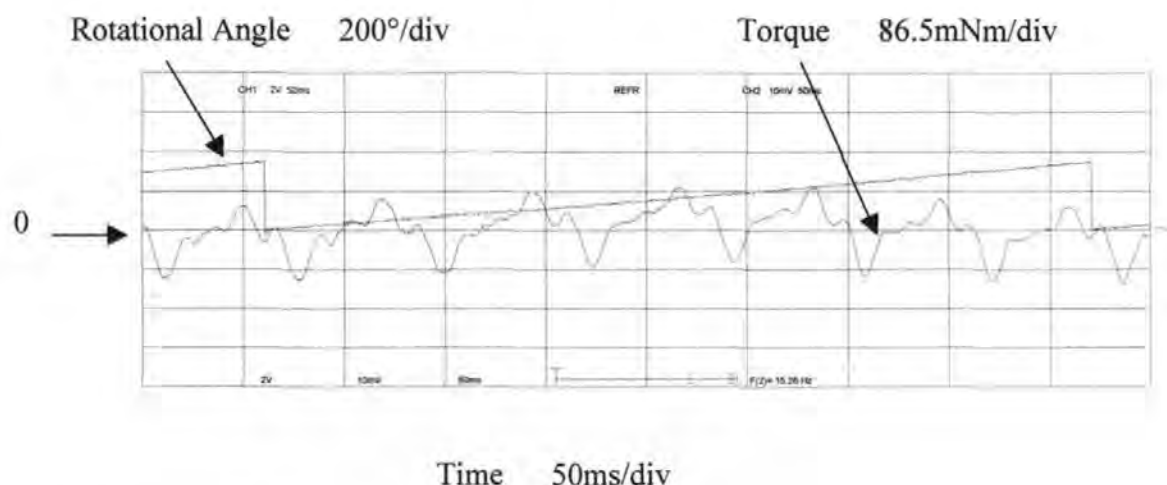
Figure 6.2 Cogging torque with rotational position for sample motor

The first trace in figure 6.2 shows the rotational position in electrical degrees from 0 degrees to 360 degrees. The second trace shows the measured cogging torque from the torque transducer. Over the full rotational cycle of the machine there are 3 sections because the motor in question contains 6 magnet poles. The motor has 18 stator slots.

The motor used here already has a skewed rotor in order to reduce cogging torque. But as can be seen from the measurements some contribution of cogging torque still remains. Further it can be seen that not only the basic frequency of cogging torque is present, but also higher harmonics.

It will be necessary to find some means of calculating the cancellation currents. After calculating the cancellation currents for the 2-phase rotor description, Park's transform will then be used to calculate the 3-phase stator quantities as in [77].

In conclusion it can be said that Park's transform offers a useful tool to cancel cogging torque. However an extension will be necessary to determine the cancellation currents in the 2-phase description. This extension will be described in chapter 8.

6.2 Reduction Strategies for Energised Torque Ripple

The same conclusions as for the cogging torque also apply for the energised torque ripple. Design measures like a particular magnet width [50], a special conductor distribution or a higher number of phases [52] will either cancel individual harmonics, [50] and [51], or decrease the overall amplitude of energised torque ripple [52]. But they are by no means enough to cancel energised torque completely. Design measures can therefore be said to be ineffective for the cancellation of energised torque ripple.

This leaves the system approach to deal with the problem of energised torque ripple. Different strategies have been proposed.

The authors of [72] – [74] develop an expression for torque production based on magnet flux and MMF distribution. This expression is then evaluated to cancel individual torque harmonics. Using an iterative process additional torque harmonics are then cancelled. The proposed method is very computational intensive and leads to a variety of solutions depending on the exact process of iteration.

In [76] Finite Element Analysis is used to develop a common expression to combat cogging and energised torque ripple.

Another publication [78] uses linear differential equations in combination with computer optimisation for the cancellation.

A torque transducer is used in [79] to measure torque ripple in real time. Based on these measurements correction currents are calculated.

Most of these measures are not very systematic [72] – [74] and [78], or they only apply to special cases [76], or they are not practical for a real system [79] because of system resonances.

Most of the other authors however use the technique already mentioned. This technique is called Park's Transform and performs a transition from the 3 phase stator description of the motor to a 2 phase rotor description and vice versa. This transformation will be described in detail below. The main advantage here is that the system description becomes much simpler because only 2 instead of 3 independent variables need to be determined. It is then possible to determine correction currents in the 2-phase description. These correction currents are then transformed into the normal 3-phase stator description of the machine. If the correction currents have been determined properly a counter torque will be developed to cancel energised torque ripple.

There are 2 main difficulties with this method. First it needs to be clarified which quantities are best used for the transformation. Secondly the implementation of the correction factors needs to be done properly. Further none of the authors explains why it would be permissible to use Park's transform and whether any restrictions apply. This also needs to be clarified.

Some authors use flux distribution [58] – [64] as the basic quantity for transformation. Other authors [77] use the current and back emf description of the machine.

In terms of implementation either vector control [62] – [64], current control [77] or some other form of implementation [58] – [61] is used.

In the following Park's transform is explained and it is also discussed whether any restrictions apply to the use of Park's transform. Afterwards it is discussed which quantities are best used for the transformation and how the implementation is done properly. Finally the advantages of using Park's transform compared to alternative methods for torque ripple cancellation are described.

6.2.1 Park's Transform

Park's transform is commonly used in the analysis of conventional synchronous machines. The transformation was described by Park in the 1920ies [82] and [83]. It performs the transformation from a 3-axis description of the motor to a 2-axis description as depicted in figure 6.3.
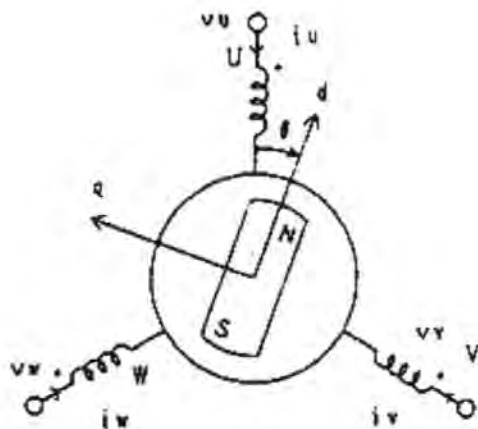
Figure 6.3 Stator and rotor reference frames for brushless motor

84

Here the 3 stator phases are labelled u,v,w, commonly they are referred to as a,b,c. θ is the rotational angle. The rotor phases are called d and q. The transformation is shown for a machine with one pole pair. It is however easily possible to expand it to any number of pole pairs.

The 3-axis description, also referred to as abc-plane description, is associated with the stator phases and remains fixed to the stator frame. The 2-axis or dq-plane description of the machine operates with rotor quantities; in other words the dq-axes are fixed to the rotor frame. In the following Park's transform is shown for back emf waveforms.

$$emf_d(\theta) = \frac{2}{3} * \left(emf_a(\theta) * \cos(\theta) + emf_b(\theta) * \cos(\theta - 120°) + emf_c(\theta) * \cos(\theta - 240°) \right)$$

$$emf_q(\theta) = \frac{2}{3} * \left(emf_a(\theta) * \sin(\theta) + emf_b(\theta) * \sin(\theta - 120°) + emf_c(\theta) * \sin(\theta - 240°) \right)$$

(6.4)

Here $emf_{a,b,c}$ are the phase back emfs, $emf_{d,q}$ are the resulting back emfs in the dq-plane and θ is the rotational angle again.

The stator quantities are mutually coupled as they are at 120 degrees relative to each other. By performing Park's transform a system results, which decouples these quantities, as the resulting two axes are orthogonal to each other; they will therefore not influence each other. This is an important advantage of Park's transform. The two axes system can be interpreted as follows: the d-axis stands for the direct axis. The direct axis is the axis of the magnet field. The other axis, the q-axis or quadrature axis, is the axis for the field produced by the phase currents. It is in quadrature to the direct axis and will produce maximum output torque as magnet and electrical field are at 90 degrees.

6.2.2 Park's Transform for Ideal Sinusoidal Machines

It is helpful to perform Park's transform for an ideal sinusoidal machine to show the significance of direct and quadrature axis. As already discussed in chapter 5.2, the ideal sinusoidal machine has sinusoidal back emfs for all 3 phases. It is then also supplied by ideal sinusoidal phase currents, which are in phase with the back emfs. Equation 5.10 is repeated here to illustrate the consequences for torque production.

$$T * \omega = emf_1 * i_1 + emf_2 * i_2 + emf_3 * i_3 \quad (6.5)$$

T stands for the output torque, ω is the machine speed, $emf_{1,2,3}$ are the phase back emfs and $i_{1,2,3}$ are the phase currents.

If sinusoidal back emfs and currents are assumed the following situation will result.

$$T * \omega = A * \sin(\theta) * \sin(\theta) + A * \sin(\theta - 120°) * \sin(\theta - 120°) + A * \sin(\theta - 240°) * \sin(\theta - 240°) \quad (6.6)$$

A is an assumed amplitude for the product of back emf and current, θ is the rotational angle.

Evaluating the individual components in equation 6.6 leads to.

$$T * \omega = A * \sin^2(\theta) + A * \sin^2(\theta - 120°) + A * \sin^2(\theta - 240°) = A \quad (6.7)$$

This means that an ideal sinusoidal machine, which is supplied with sinusoidal currents, will produce a constant torque output. This is of course desirable for many applications.

However as already discussed it is impossible to build a machine with ideal sinusoidal back emfs.

Now Park's transform will be used for an ideal sinusoidal machine to illustrate the transformation of stator quantities into rotor quantities and to explain the meaning of direct and quadrature axis.

Using equation 6.4 the ideal sinusoidal back emfs for all 3 stator phases are transformed into dq-quantities. Equation 6.8 shows the result.

$$emf_d = 0$$
$$emf_q = 1 \quad (6.8)$$

The resulting back emf on the direct axis equals zero. In other words no contribution from the back emfs will be seen on the magnet axis. A constant contribution is made on the quadrature axis. This is the axis for the torque-producing field under 90 degrees to the magnet axis. Because a constant back emf will be obtained on the quadrature axis the back emf will become independent of the rotational angle. Park's transform is therefore often interpreted as a transformation, which transforms rotationally dependent stator quantities into rotationally independent rotor quantities. This interpretation is only true for sinusoidal quantities. This will become clear in the following. A common misconception assumes that Park's transform only works for sinusoidal quantities. This is not correct as will be shown in the following.

The same transformation can be performed on the stator currents, which are also assumed to be ideally sinusoidal.

$$i_d = 0$$
$$i_q = 1 \quad (6.9)$$

The result is analogues to the result from the transformation of the back emfs. Again the direct axis current is zero and the quadrature axis yields a constant current contribution, which of course is independent of the rotational position.

Finally the torque production in the dq-plane can be calculated as follows.

$$T * \omega = \frac{3}{2}\left(i_d * emf_d + i_q * emf_q\right) \quad (6.10)$$

Similar to the torque production in the abc reference frame torque production in the dq description of the machine is composed of individual torque contributions. The direct axis current and the direct axis back emf form one component of torque. The other contribution is given by the product of quadrature axis current and quadrature axis back emf. If this is compared to the formula for torque production in the stator description from equation 6.5 the same structure is found. In the abc-frame it is necessary to multiply the phase contributions of current and back emf with each other and to sum the products. The same holds true for the dq interpretation of the machine.

The main difference is the reduction from three to two contributions, which makes it easier to interpret the individual torque contributions. In the stator description the individual contributions are caused by the individual stator phases. As these are phase-shifted by a particular angle, for instance 120 degrees in the case of a three phase machine, these contributions are spatially distributed around the machine, or to be more precise around the

airgap. The output torque of the machine is the summation over these spatial contributions for every instance of time.

In the dq interpretation of the machine these contributions are still spatially distributed and the resulting output torque is still the summation of the individual spatial contributions. However these contributions are 90 degrees relative to each other. It therefore becomes possible to interpret these contributions. Rather than representing stator quantities they now become linked with the magnetic field in the machine. The torque contribution on the direct axis is in phase with the magnetic axis of the machine. It is a well-known fact from machine theory that this contribution decreases the useful output torque of the machine and is unwanted. The contribution on the quadrature axis however is under 90 degrees to the magnetic field. This contribution is the useful output torque and represents the maximum torque output of the machine at the same time.

For a classical synchronous machine for instance it is normally not possible to control the torque output in a manner to reduce the contribution from the direct axis completely. The synchronous machine therefore almost always operates with less than maximum torque output.

For a brushless machine it is possible to control the machine so that the contribution from the direct axis remains zero. How this is achieved will be explained later on.

This is also the reason why a brushless machine exhibits the same control characteristics as a conventional dc motor. If the direct axis contribution is controlled to be zero, only the quadrature axis contribution will determine the torque output of the machine. A linear increase in quadrature axis current, the back emf contribution remaining constant with assumed constant machine speed, will result in a linear increase in torque output.

89

Park's transform not only works to transfer stator into rotor quantities but also works the other way. Rotor quantities in the dq-description of the machine can be back-transformed into stator quantities in the abc-description.

The formula for the back-transformation is given in the following.

$$emf_a = emf_d * \cos(\theta) + emf_q * \sin(\theta)$$
$$emf_b = emf_d * \cos(\theta - 120°) + emf_q * \sin(\theta - 120°) \quad (6.11)$$
$$emf_c = emf_d * \cos(\theta - 240°) + emf_q * \sin(\theta - 240°)$$

To complete the application of Park's transform to the machine with sinusoidal back emfs formula 6.11 will be used to back transform back emfs and currents.

From equation 6.8 it is possible to take the back emf contributions in the dq-plane. The direct axis contribution was zero and the quadrature axis contribution was 1 for an ideal sinusoidal machine with back emfs of amplitude 1. Application of equation 6.11 yields the following results.

$$emf_a = \sin(\theta)$$
$$emf_b = \sin(\theta - 120°) \quad (6.12)$$
$$emf_c = \sin(\theta - 240°)$$

This result of course describes the ideal sinusoidal machine with sinusoidal back emfs and shows that Park's transform is fully reversible for sinusoidal quantities. It can also be shown that a contribution from the direct axis of the machine would result in non-sinusoidal back emfs.

90

The same considerations hold true for the current. Equation 6.11 can be used to back-transform the dq-currents if back emf terms in 6.11 are replaced by current terms.

$$i_a = \sin(\theta)$$
$$i_b = \sin(\theta - 120°) \quad (6.13)$$
$$i_c = \sin(\theta - 240°)$$

It can therefore be said that Park's transform works well for machines with sinusoidal quantities, like conventional synchronous machines. In the following the application of Park's transform to machines with non-sinusoidal quantities, both back emfs and currents, will be examined.

6.2.3 Park's Transform for Machines with Non-Sinusoidal Back Emfs

In the following a test motor with non-sinusoidal back emfs is considered. The back emf contains additional harmonics on top of the fundamental, as for any real machine.

For the no load case the phase to star point voltages of the machine are measured at a fixed machine speed. Equation 6.14 describes the relationship between back emf and phase voltage.

$$emf = V + i * R + L * \frac{di}{dt} \quad (6.14)$$

Here V represents the phase to star point voltage, i is the phase current, R stands for the phase resistance and L is the phase inductance.

For the no load case, i.e. open circuit, no current is present. Therefore terms two and three in equation 6.14 will not be present and equation 6.14 simplifies as follows.

$$emf = V \quad (6.15)$$

The resulting phase back emf is therefore equal to the phase to star point voltage. If this voltage is recorded for all three phases it is possible to describe the phase back emfs for the no load case.

The measurements are taken at a fixed machine speed. As already explained in chapter 5.2, machine speed does not have any influence on the shape of the back emfs in the brushless machine.

Figure 6.4 shows the resulting back emfs.
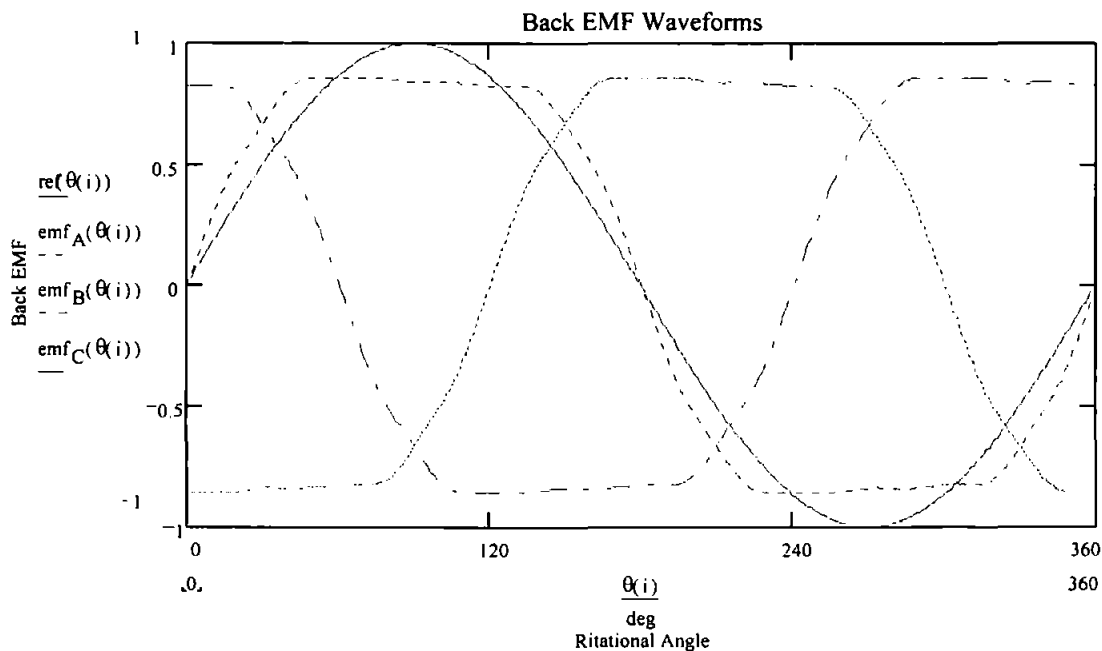
Figure 6.4 Measured back emf waveforms from test motor

The back emfs in figure 6.4 have been scaled to enable comparison with further back emf measurements. The amplitude of the fundamental has been scaled to assume the value of 1. It can already be seen that the recorded back emf waveforms deviate from the ideal sinusoidal form given in form of the solid line. Figure 6.5 shows the result from a Fourier analysis of the back emfs.
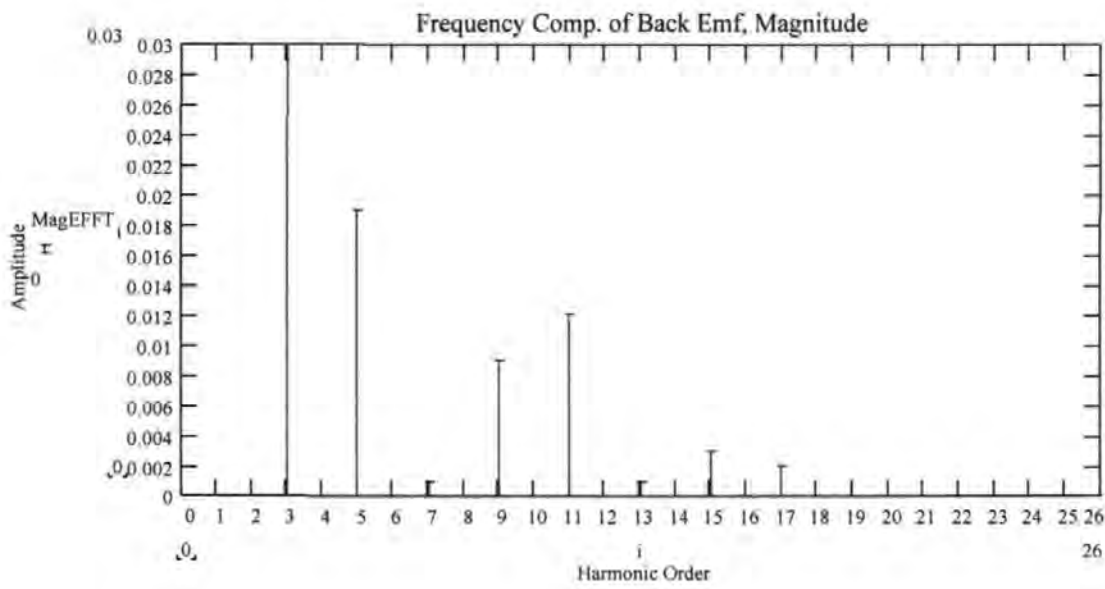
Figure 6.5 Harmonic components of back emf waveform

Harmonics up to the order of 26 have been considered. The amplitude of the fundamental is 1 as already explained. The third harmonic shows an amplitude of 0.178, not visible in figure 6.5, and therefore represents the dominant harmonic. The third harmonic is clearly visible in the flat plateau of the phase back emfs in figure 6.4. The next most important harmonic, the 5th harmonic, already only shows an amplitude of less than 2%. The other harmonics are between 0.2% and 1.2%. Harmonics higher than order 17 are too small to be precisely measured. It can be said that the amplitude of harmonics will tend to decrease

towards higher orders. Only odd harmonics are visible because the back emf waveforms are symmetric as already discussed in chapter 5.2.

As before it is now assumed that the machine is supplied with ideal sinusoidal phase currents. The evaluation of equation 6.5 allows calculation of the resulting torque ripple for this operation of the machine, which could be labelled the normal operation of the machine. Figure 6.6 shows the calculation results for the test motor.
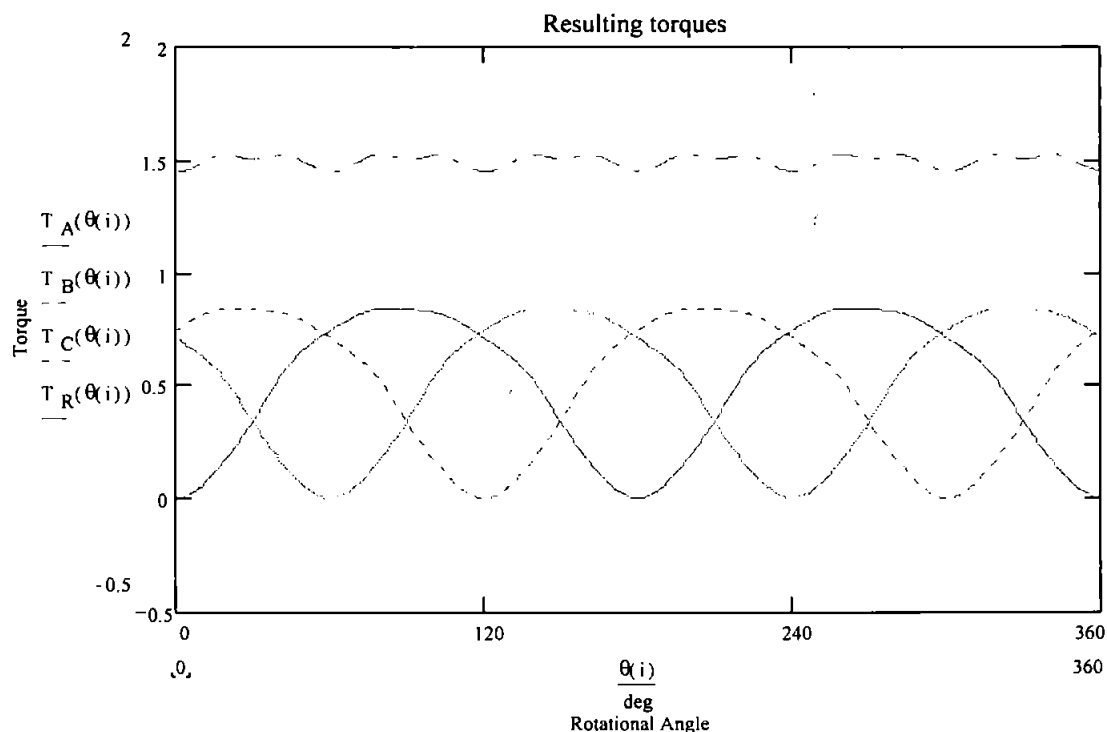
Figure 6.6 Resulting torque ripple for machine with non-sinusoidal back emfs fed with ideal sinusoidal phase currents

Figure 6.6 shows the phase torque contributions and the resulting output torque with the ripple. The torque ripple is clearly visible because the higher harmonics of the back emf will set up torque ripple contributions as explained in chapter 5.2. A look at the spectral components reveals the order of torque ripple harmonics.
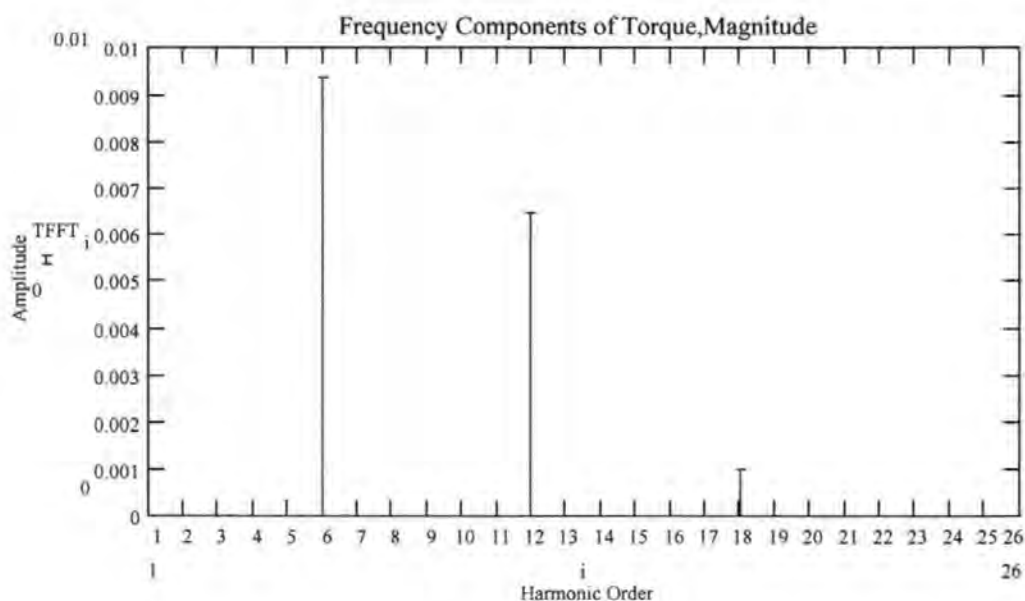
Figure 6.7 Torque ripple harmonics for machine with non-sinusoidal back emfs supplied with sinusoidal phase currents

The order of the resulting torque ripple harmonics in figure 6.7 represents multiples of six times the supply frequency as explained in chapter 5.2.

In the following Park's transform will be used to analyse the machine with non-sinusoidal back emfs. First the measured phase back emfs will be transformed into dq back emfs using equation 6.4. Figure 6.8 shows the transformed back emf waveforms.
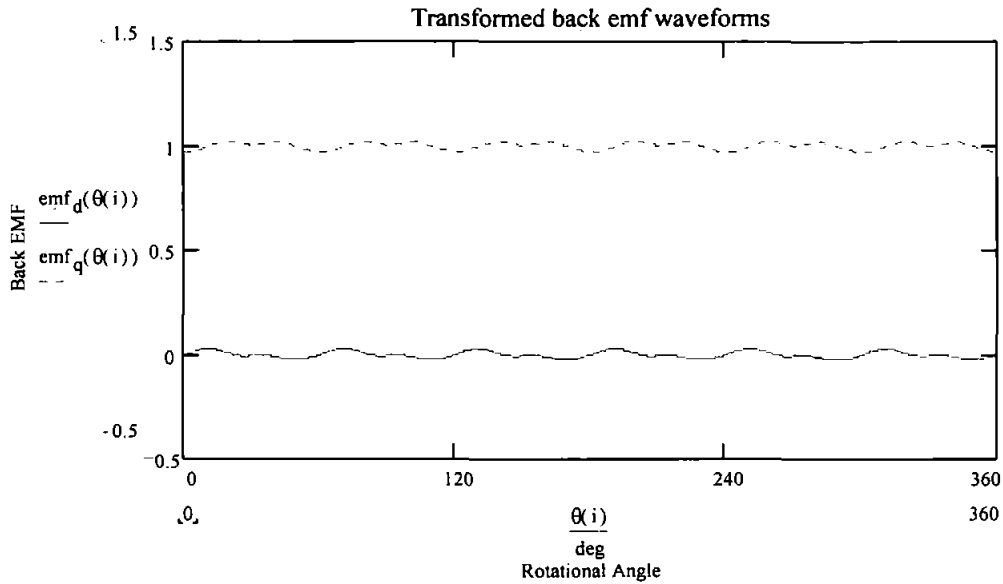
Figure 6.8 Transformed non-sinusoidal back emf waveforms in dq-plane

It can be seen that the quadrature axis contribution is the main contribution with an average amplitude of 1. However a certain ripple is visible around this average. The direct axis component is comparatively small, indicating that the amplitude of the resulting output torque is small compared to the output torque from the quadrature axis. However the ripple on the direct axis would result in output torque ripple if a contribution from the direct axis currents is present according to equation 6.10 as both contributions are additive.

Figure 6.8 shows that the amplitude of the resulting back emfs in the dq-plane will depend on the rotational angle. They are not constant and therefore are not independent of the rotor position. It is very important to calculate the instantaneous value of the back emfs. Otherwise only a constant average value will be calculated, which does not allow cancellation of instantaneous torque ripple.

If the ideal sinusoidal supply currents are transformed into the dq-plane, the evaluation of equation 6.9 will of course yield the same result as before. No contribution is made on the direct axis and a constant current contribution is seen on the quadrature axis.

Now equation 6.10 can be used again to calculate the resulting torque ripple in the dq-plane. The resulting torque ripple is equal to the upper trace in figure 6.8 as the contribution from the direct axis will be zero (i_d was zero). This is of course the same result as shown in figure 6.6. Or in other words the torque ripple can either be calculated in the abc-plane using stator quantities or in the dq-plane using rotor quantities. Exactly the same result will be found indicating that Park's transform can be used for non-sinusoidal quantities.

So far ideal sinusoidal supply currents have been considered. They will result in output torque ripple. It will therefore be necessary to use currents, which deviate from the ideal sinusoidal form. Non-sinusoidal currents could make an additional contribution on the direct axis. From what was explained earlier it is clear that no contribution from the direct axis is wanted, as this contribution only acts to diminish the available output torque level. The direct axis current is therefore chosen to be zero.

$$i_d = 0 \quad (6.16)$$

If i_d is controlled to be zero, a simple form for the torque equation in the dq-plane, 6.10 results.

$$T * \omega = \frac{3}{2} * i_q * emf_q \quad (6.17)$$

97

The only remaining torque contribution now results from the quadrature axis components, back emf and current.

The quadrature axis contribution of the back emf is known because Park's transform was used on the phase back emfs of the real machine. The output torque is demanded to be constant. Rearranging equation 6.17 it will become possible to determine the required current contribution on the quadrature axis.

$$i_q = \frac{2}{3} * \frac{T*\omega}{emf_q} = \frac{2}{3} * \frac{A}{emf_q} \quad (6.18)$$

Here A is the desired value of output torque at a certain speed.

This is an astonishingly simple formula to determine the desired i_q current. The formula will automatically take all back emf harmonics into account and describe the necessary q-axis contribution for torque ripple cancellation.

Equation 6.18 represents the closed form solution to the torque ripple problem. It is not necessary to consider individual back emf and current components and their interaction as proposed in [72] – [74] and [78]. The transformed q-axis back emf contains the description of all phase harmonics of the back emf. It is also not necessary for the phase back emfs to be symmetric, meaning phase shifted by 120 degrees relative to each other, as stated by some authors. Amplitude and phasing of harmonics can differ between the individual phases. Park's transform can therefore also be used for machines with manufacturing tolerances, where individual phase contributions can vary considerably. It is however not possible to back-transform the q-axis back emf and to obtain the original phase back emfs, if these phase back emfs vary in amplitude or phase. Park's transform will always result in symmetric phase quantities. This is presumably the reason why some authors are mistaken

about the conditions of use for Park's transform. Park's transform is therefore not reversible if non-symmetric quantities are considered.

Figure 6.9 shows the required i_q current from equation 6.18.

Required dq-currents
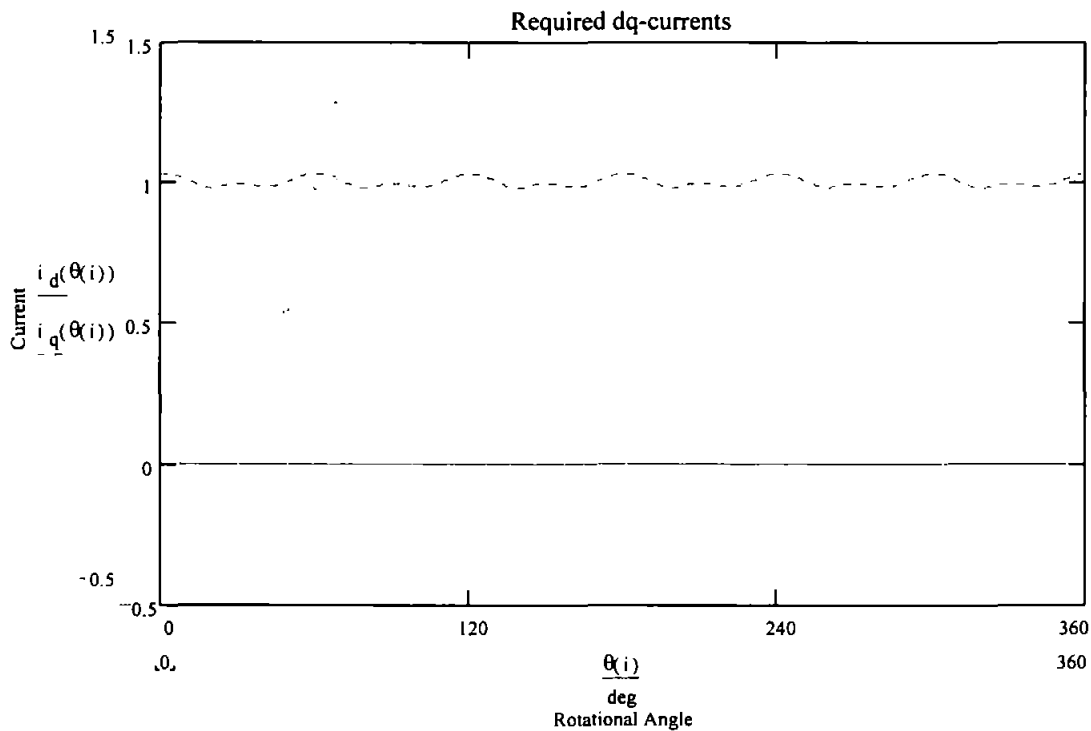
Figure 6.9 Required i_q current for torque ripple compensation

The i_q current in figure 6.9 contains all necessary harmonics including amplitude and phase information in order to cancel torque ripple completely. The remaining step is the back transformation of this i_q current into phase currents, which can then be implemented in the abc-plane. Equation 6.11 can be used in its form for the currents. Figure 6.10 shows the resulting phase currents.
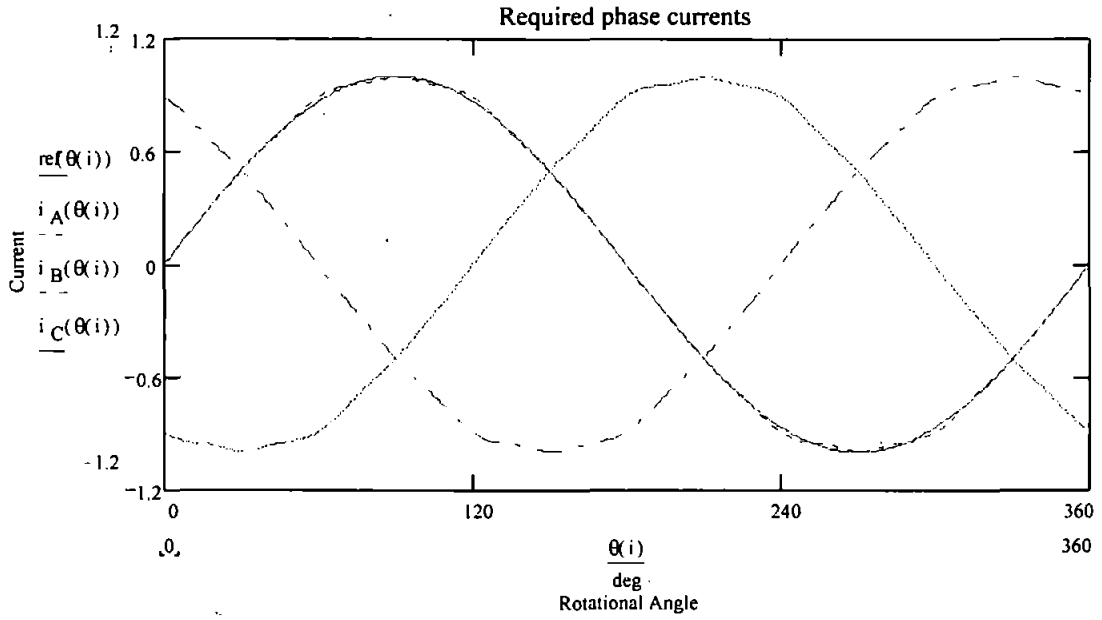
Figure 6.10 Required phase currents for torque ripple cancellation

A closer look at figure 6.10 reveals that all phase currents are symmetric, that is phase shifted by 120 degrees. It is also clear that the depicted currents are easily reproducible. This is a big advantage compared to the scheme suggested in [72] – [74], where the required phase currents are difficult to implement. A look at the spectral components reveals the required order of current harmonics for the cancellation.

100
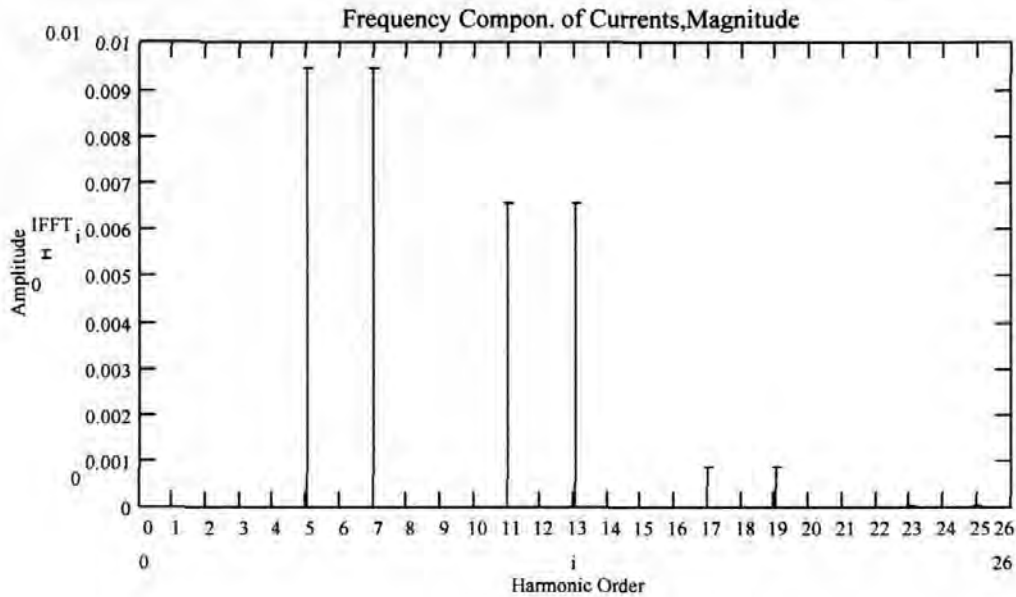
Figure 6.11 Harmonics of required phase currents for torque ripple compensation

The fundamental is again of amplitude 1 to allow comparison with further results. Harmonics of order 5,7,11,13,17 and 19 are required. The harmonics of order 23 and 25 are already too small to be implemented. An in-depth analysis of the back transformation shows that all current harmonics are present in the required phase currents. However the amplitude of these harmonics decreases exponentially. This is of course desirable from an implementation point of view. It is much easier to realise harmonics of lower order than of higher order because of the limited bandwidth of the current control.

The required harmonics are of moderate amplitude; 5 and 7 ca. 1% and 11 and 13 ca. 0.65%.

Finally the resulting torque output using the corrected phase currents can be calculated using equation 6.5 again. Figure 6.12 shows the phase torques and the overall output torque.
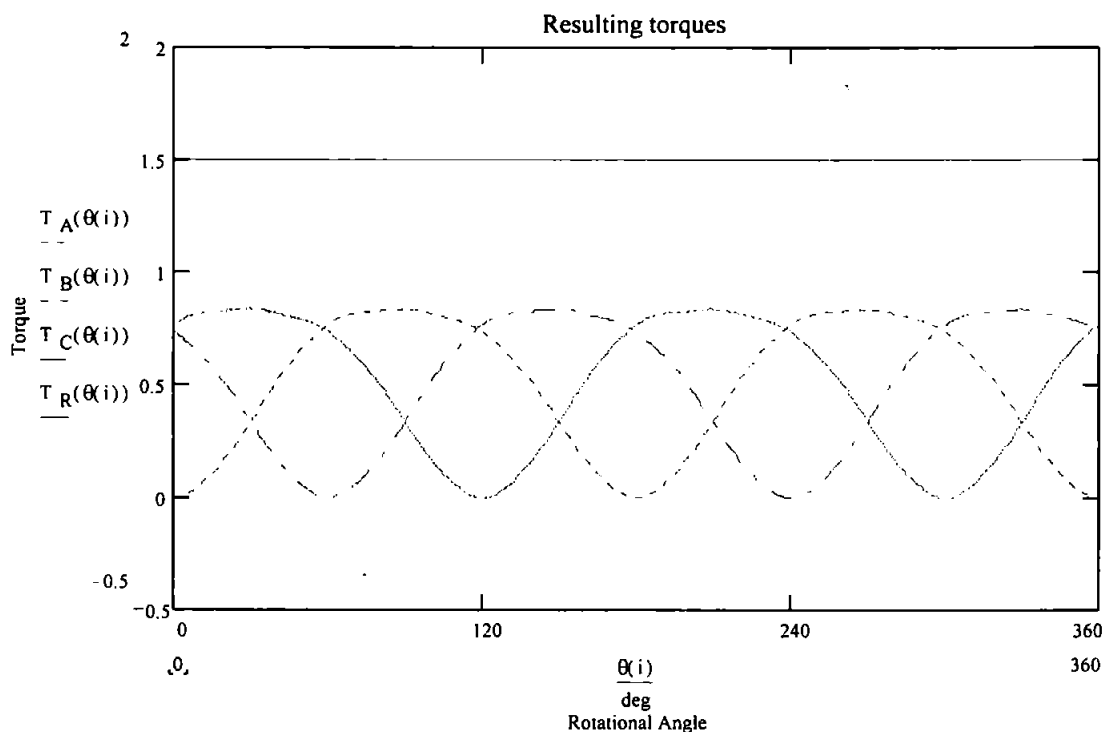
Figure 6.12 Phase torques and resulting torque for proposed phase currents

The resulting output torque is constant as expected. The individual phase torque contributions differ from the ideal $\sin^2$ terms for the ideal sinusoidal machine. The calculated phase currents are therefore effective to cancel to torque ripple.

Basically the same analysis as for the ideal sinusoidal machine has been used. The first difference is the occurrence of a contribution on the direct axis for the back emf. This contribution can be neutralised by forcing the i_d current to be zero. The second difference is the resulting ripple on the quadrature axis of the back emf. This ripple on the back emf is responsible for the occurrence of torque ripple, if the machine is supplied by ideal sinusoidal currents. This torque ripple can be cancelled by selecting an appropriate current contribution on the quadrature axis.

In the following a step by step description is given how Park's transform is used to cancel torque ripple in brushless machines.

Use of Park's transform for torque ripple cancellation

1. The back emf waveforms are measured under no load conditions.

2. The measured back emf waveforms are transformed to the dq-plane using Park's transform.

3. The direct axis current is selected to be zero. The quadrature axis current is determined using equation 6.18.

4. The quadrature axis current is back transformed to the abc-plane using Park's transform.

5. The resulting phase currents are applied to the machine.

As an example a real machine has been measured and the measured quantities have been utilised to demonstrate the use of Park's transform. Any brushless machine can be used without changing the validity of the discussed equations. In particular there is no difference whether a so-called brushless dc or brushless ac motor is used. It is possible to transform back emfs, which are basically sinusoidal or basically trapezoidal. Park's transform is therefore a powerful tool for torque ripple cancellation for all brushless machines.

It is also possible to extend Park's transform to two or four phase machines for example. But as already discussed this thesis will deal with three phase machines because of their popularity.

6.2.4 Validity, Restrictions and Implementation Quantities for Park's Transform

Park's transform has been extensively used in the analysis of conventional synchronous machines. It has proved to be an extremely useful tool to describe the machine behaviour and to devise control strategies. However for the brushless machine it is not immediately clear whether it is permissible to use Park's transform. Although the brushless ac machine can be interpreted as a close relative to the conventional synchronous machine with permanent magnets, there are distinct differences. Even a brushless ac machine with nearly sinusoidal back emfs will still contain some additional harmonics. Also the process of commutation is different because the electronic commutation of the brushless ac machine depends on the rotor position whereas the commutation of the conventional synchronous machine depends on the supply voltages and the load situation. If the brushless dc machine is considered the differences become even more pronounced. The trapezoidal back emfs of the brushless dc machine contain a high number of harmonics. The commutation is often realised as a so-called block commutation whereby each phase is supplied with a dc current for a fixed segment of the rotor rotation. It is therefore not easily possible to apply Park's transform to brushless machines arguing that they are very similar to conventional synchronous machines.

Therefore the general or unified machine theory has been reviewed using several theoretical and text books [84], [85], [86], [87] and [88].

Some authors [85], [88] do not state the conditions under which Park's transform applies. Others [86], [87] assume only fundamental space harmonics. Adkins and Harley [84] concede that Park's transform is justified for some quantities, which contain harmonics, but they don't explicitly describe these quantities. To find out which quantities will fall into that class a further publication has been consulted [89]. It becomes clear that the

transformation is permitted as long as the instantaneous field distribution set up by the resulting rotor quantities is the same as for the stator quantities. Park's transform can therefore be used for all quantities, which fulfil this condition. Or in other words Park's transform can be used for sinusoidal and non-sinusoidal quantities as long as the instantaneous field distribution stays the same. It is therefore possible to use Park's transform to analyse any brushless machine.

Relevant machine quantities have been examined to find out whether they can be used in conjunction with Park's transform. It has been found that it is possible to use currents and voltages respectively back emfs with Park's transform. It is also possible to use flux distribution and MMF distributions. All these quantities must be instantaneous quantities. The use of rms or other average values is not permissible because they will set up the wrong field distribution. It is also not possible to transform composed or calculated quantities like torque or power. The transformation is only reversible for symmetric quantities.

After it has been clarified, which quantities can be used it is now possible to select suitable quantities to implement torque ripple reduction strategies. It is recommendable to use direct quantities, which can be measured. These are for instance currents and voltages. Other quantities can not be directly measured like MMF distribution or are difficult to measure like flux distribution and inductances. Many authors base their torque ripple cancellation on models for the phase inductance of the machine for instance. This is very problematic because they need to make assumption about the behaviour of the phase inductance depending on rotor rotation. Also they neglect machine tolerances. These models are therefore inherently inaccurate. After careful consideration it is recommended

to use the phase back emf measurements in conjunction with the phase currents for torque ripple cancellation.

The correct implementation is as described in subchapter 6.2.3. First the phase back emfs are recorded. These are transformed into the dq-plane. Here it is possible to determine the required i_q current for constant torque output. This i_q current can then be back-transformed to the abc-plane to give the required phase currents. The implementation of these phase currents will then result in constant output torque within the limitations of measurement accuracies and implementation inaccuracies.

Some authors don't control the i_d current to be zero. This will lead to a much more complicated solution for the required currents both in the dq-plane and the abc-plane, because both dq-currents need determining. Also the back emf and current contributions are not any longer controlled to be 90 degrees phase shifted to each other resulting in a phase lag or phase advance compared to the ideal position. This will also result in a reduced torque output. It can therefore be said that any control method, which controls the i_d current to be different from zero, will lead to a sub-optimal solution.

6.2.5 Torque Ripple Reduction using Park's Transform versus other Torque Ripple Reduction Strategies

Finally the advantages of using Park's transform for torque ripple reduction compared to other torque ripple reduction strategies will be discussed.

To reduce torque ripple it is necessary to determine phase currents in the abc-plane, which will result in constant or near constant output torque. These phase currents need to be matched to the phase back emfs of the machine.

Equation 6.5 is recalled to illustrate the mathematical problem.

$$T * \omega = emf_1 * i_1 + emf_2 * i_2 + emf_3 * i_3 \quad (6.5)$$

The phase back emfs are measured at constant machine speed. So they are known and the speed is known as well. Therefore 3 independent phase currents need to be determined if T is chosen to be constant.

For 3-phase machine the star point of the machine is normally connected to all 3 phases. Therefore the following condition applies:

$$i_r = i_a + i_b + i_c = 0 \quad (6.19)$$

Here i_r is the resulting current in the star point and $i_{a,b,c}$ are the phase currents as before.

This condition is called the star point condition.

Using this condition the number of independent variables reduces to two. However there is no other applicable condition to reduce this number down to just one independent variable. This system is therefore undetermined and any number of possible solutions exists.

For instance following the example of the ideal brushless ac machine with non sinusoidal phase back emfs an additional condition could be introduced. The contributions of the first two phase currents could be forced to create $\sin^2$ contributions in conjunction with the first two phase back emfs as in equation 6.7. The remaining third phase current will then follow from equation 6.19 because of the star point condition. The problem here is that the third phase current will take a very different shape from the other two phase currents, which would be difficult to implement. Further even for a small number of harmonics in the phase back emfs this third current could have poles with a steepness near 1, which are

impossible to implement. But even if poles don't occur, the resulting solution will be sub-optimal because there is no physical justification to impose such arbitrary conditions on the phase currents.

Using Park's transform results in a different situation. The number of phase variables is reduced from 3 to 2 by performing the transformation of stator into rotor quantities. This number is further reduced down to just one independent variable by choosing the i_d current contribution to be zero. The physical reason for this choice is the fact that only contributions from the quadrature axis of current are useful. All other contributions will reduce torque output. Now it is possible to find a unique solution for the phase current on the quadrature axis. The back-transformation of this phase current will then give the required phase currents in the abc-plane. Further this solution will also create symmetric phase current contributions, which are easy to implement.

The dq-description of the brushless machine allows the separation of rotor quantities. The quadrature current contribution can be isolated from the direct axis contribution. This is exactly the same process as in the conventional brushed dc motor. In the brushed dc motor this separation is done by the mechanical commutation. For the brushless machine this separation needs to be performed by the electronic commutation, that is fixing the commutation angle of the currents relative to the back emfs. However the brushless machine also allows shifting the commutation. This would be comparable to shifting the commutator elements in the brushed motor.

The use of Park's transform for torque ripple reduction is therefore shown to be superior to other forms of torque ripple reduction strategies. It will therefore be used in the following.

The use of Park's transform for the reduction of both cogging torque ripple and energised torque ripple has been described. It has been discussed whether Park's transform can be used for brushless machines and which restrictions apply to the use of Park's transform. Also permissible quantities for its use have been named. The most suitable quantities have been identified and the best form of implementation has been discussed in detail. Finally the use of Park's transform has been compared to alternative torque ripple reduction strategies.

Here the measurement of the no-load phase back emfs has been used as a quantity for torque ripple reduction. It has been discussed before that the back emf waveforms are independent of motor speed. The proposed control scheme is therefore applicable for any machine speed without modifications. However the effect of the current loading of the machine has not been considered. With increased current loading the effect of armature reaction will start to distort the magnet flux distribution. The resulting phase back emfs will therefore be modified compared to the no load back emfs. This is a non-linear effect, which will result in the reappearance of torque ripple. This effect and its reduction by the use of a new adaptive torque control scheme will be described in the following chapter.

Chapter 7   New Adaptive Torque Ripple Reduction Strategy

The conventional torque ripple reduction strategy using Park's transform as discussed in chapter 6 works well for light loads. However if the current loading is increased this strategy starts to become ineffective. This is caused by the so-called armature reaction of the brushless machine.

7.1   Armature Reaction and its Effect on Torque Ripple

For the no load situation only the flux created by the rotor magnets will be present. Together with the spatial distribution of the stator windings this flux distribution will result in a particular back emf waveform. However if the machine is electrically loaded an additional flux generated by the phase currents will appear. This additional flux will be superimposed onto the magnet flux and will act to disturb the flux distribution set up by the magnets. This effect is called the armature reaction.

FEM calculations have been undertaken to simulate armature reaction for a test motor. Figure 7.1 shows the undisturbed flux distribution from the magnets as a dotted line. For 50% current loading the resulting flux distribution from the magnets and the phase current has been calculated and is described by the solid line in figure 7.1.
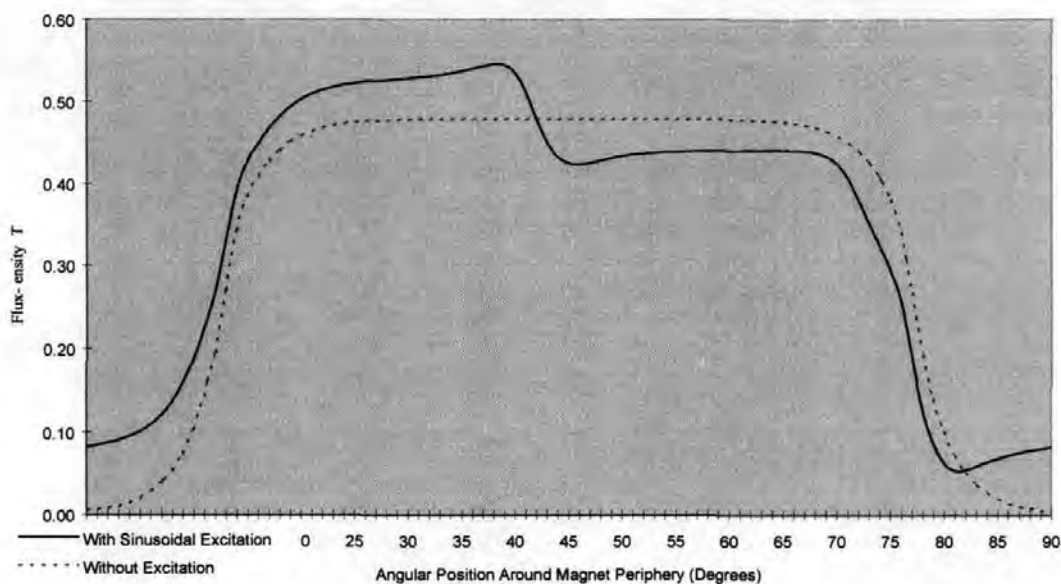
Figure 7.1 Flux distribution without (dotted) and with excitation currents (solid)

The distortion of the flux distribution will become more pronounced with increased current amplitude. The distorted flux distribution will result in modified back emf waveforms. The back emf waveform therefore becomes a function of the excitation currents. The modified back emf waveform finally results in a different torque ripple as a function of current loading.

The torque ripple reduction strategy described in chapter 6 uses the no load measurements of the back emf waveform. It becomes clear, that this is not acceptable for higher current loads. It is therefore necessary to take the variation of back emf waveforms with current loading into account. Subchapter 7.2 describes a new adaptive torque ripple strategy based on the variation of back emf waveforms with current.

The particular problem of the conventional torque ripple reduction strategy is the fact, that it only uses the no load measurement of the back emf waveform or equivalent quantities. It doesn't take into account changes of the back emf waveform.

In the following the effect of armature reaction on the back emf waveforms will be demonstrated for the test motor. The differences between no load and full load back emfs will be discussed. The resulting torque ripple for the no load and the full load case will be compared. Finally the ineffectiveness of the conventional torque ripple reduction strategy will be demonstrated.

For the test motor a set of back emf measurements has been obtained. Here the current loading of the machine has been increased in discrete steps. A three-phase balanced load has been connected to the machine phases and the machine has been back-driven by another motor via a fixed coupling. The driving motor was controlled in order to maintain constant speed for the documentation of the back emf waveforms.

Figure 7.2 repeats the measurement for the no load back emfs.
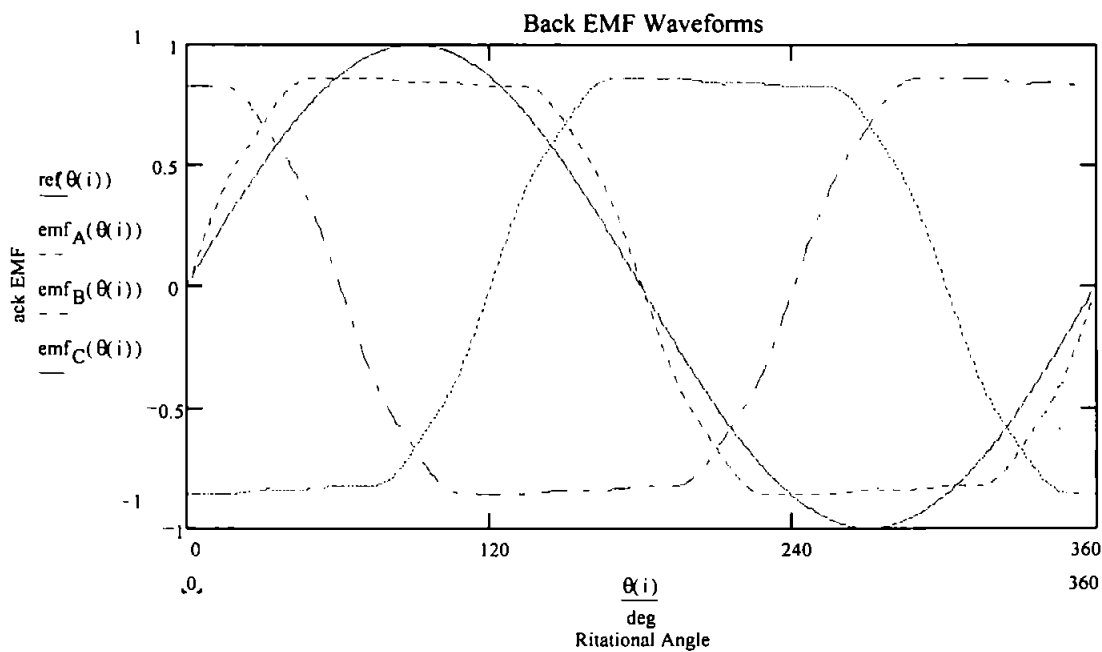
Figure 7.2 No load back emf waveforms for test motor

112

As explained in chapter 6 only the no load back emfs can be measured directly. Back emfs under load cannot be determined directly. This is presumably the reason why many authors only use no load back emf measurements. For the load back emfs it is necessary to measure the phase voltages and to calculate the back emfs.

The phase voltages have been measured for increased current loads. Here the measurement for maximum current loading is shown, figure 7.3.
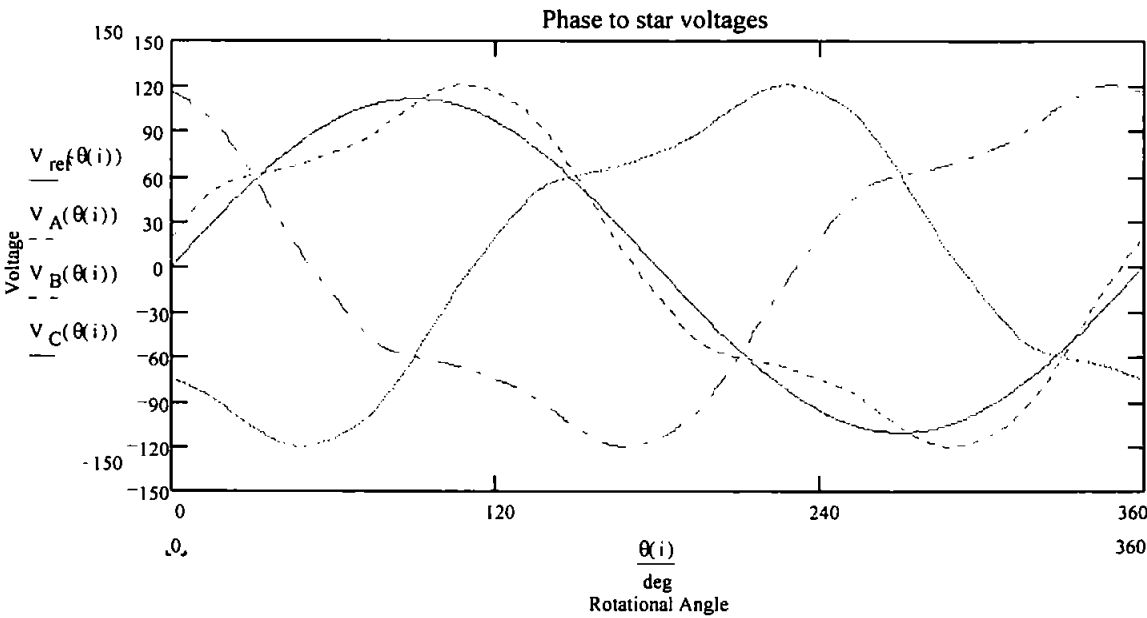
Figure 7.3 Phase to star voltages for maximum current load

To determine the back emf waveform equation 7.1 will be evaluated.

$$emf = V + i * R + L * \frac{di}{dt} \quad (7.1)$$

Here emf is the back emf waveform to be calculated, V is the phase to star point voltage, R is phase resistance, L is phase inductance and i is the phase current.

113

The phase to star point voltage for each phase has been recorded. The phase current is determined by the load and can be measured. The phase resistance can be determined by measurement and is also known from the manufacturer's data. Similarly the phase inductance can be measured and is also known from the motor data.

For a precise analysis it is possible to calculate each phase back emf individually using accurate data for the phase parameters. Here the individual phase waveforms have been assumed to be equal with a phase shift of 120 degrees to each other.

Figure 7.4 shows the result from the calculations. Again the waveforms have been scaled and phase shifted to allow comparison with the no load case.
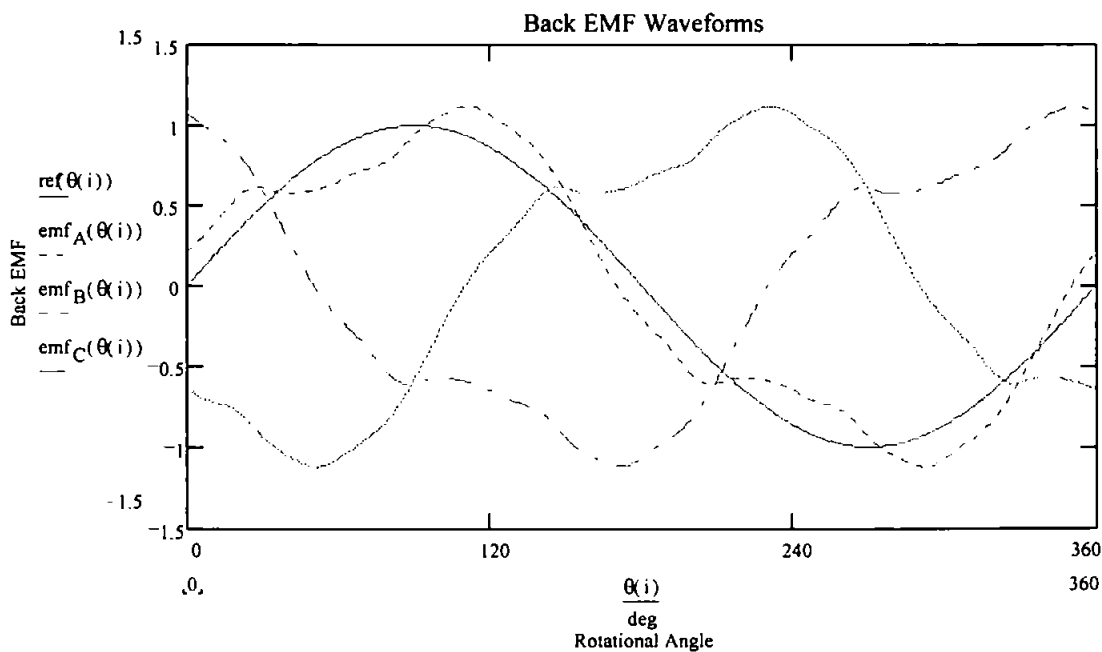
Figure 7.4 Full load back emf waveforms after scaling and phase shifting

If figures 7.2 and 7.4 are compared clear differences become visible. The flat top plateau of the phase back emfs has been distorted by the armature reaction. A look at the reference waveform reveals the deviation of the phase back emfs from the ideal sinusoidal form.

114

To allow further comparison the spectral components of the back emf waveforms for the no load and the full load case will be presented.

The spectral analysis for the no load case is repeated here from chapter 6.
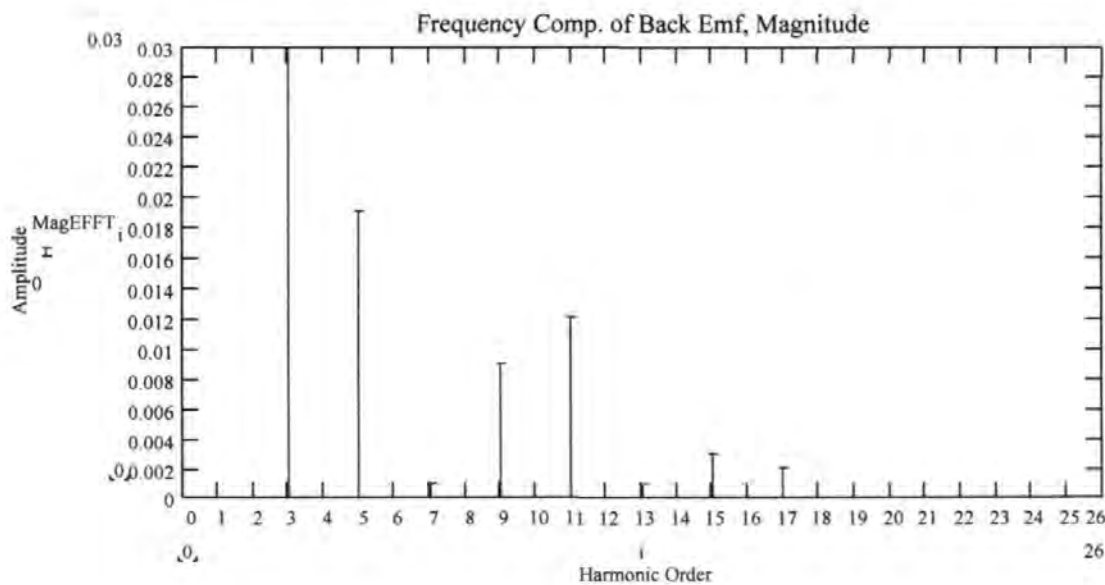
Figure 7.5 Harmonic components of back emf waveform for no load case

Figure 7.6 shows the calculated spectral values for the full load case.
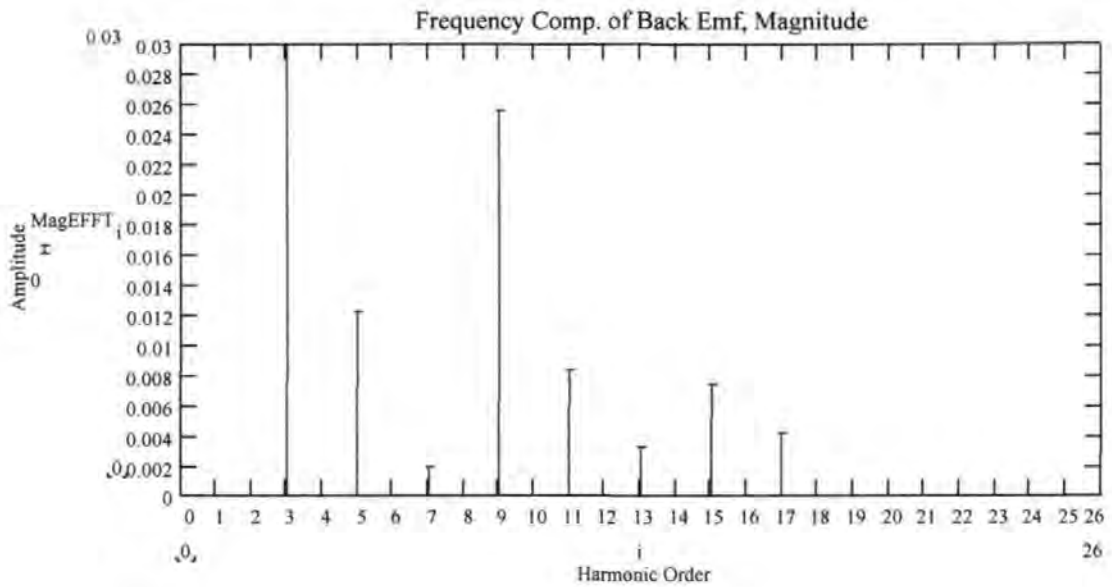
Figure 7.6 Harmonic components of back emf for full load

For both the no load and the full load case the third harmonic represents the dominant harmonic with the full amplitude not shown in both diagrams. However as explained in chapter 5 this harmonic does not cause torque ripple in 3-phase systems. The same argument holds true for the ninth harmonic and the 15th harmonic.

All harmonics show pronounced differences in amplitude. This statement is also true for the phase relationship of the harmonics.

A good way to visualise the differences is the calculation of the expected torque ripple for sinusoidal current excitation for both the no load (respectively light load) case and the full load case.

The resulting output torque with sinusoidal currents for the no load case is repeated from chapter 6.

116
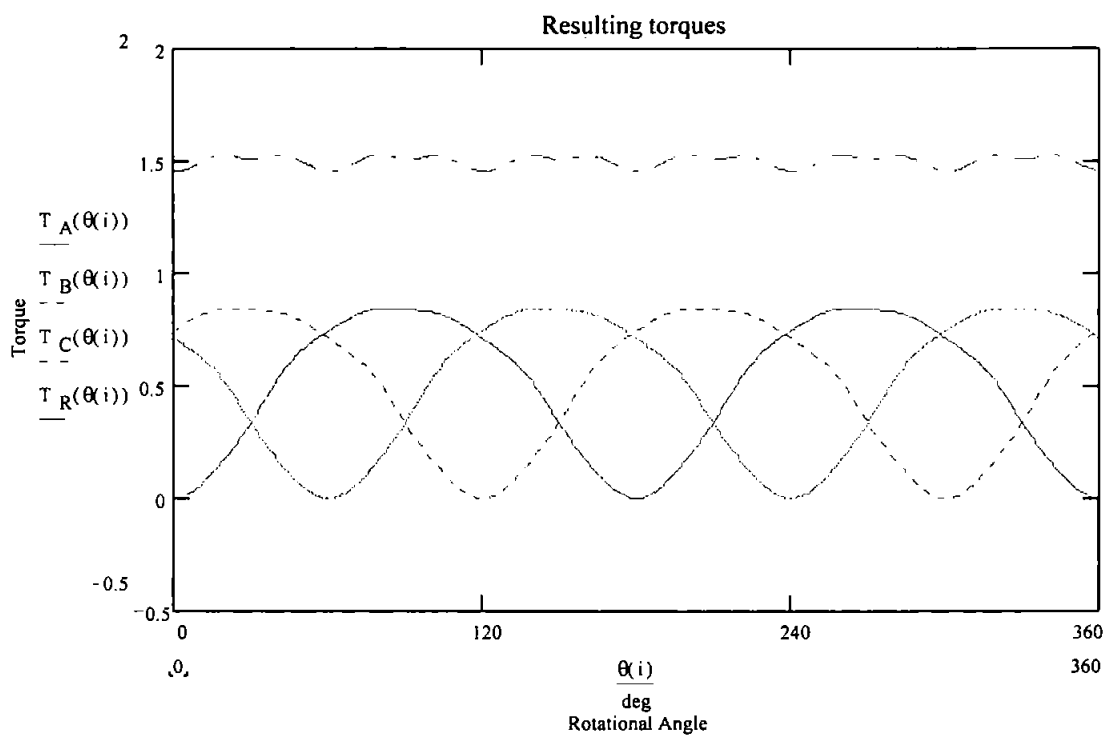
Figure 7.7 Phase torque and resulting torque for no load (light load) case. Excitation with sinusoidal currents.

The resulting torque ripple for the full load case is presented in figure 7.8.
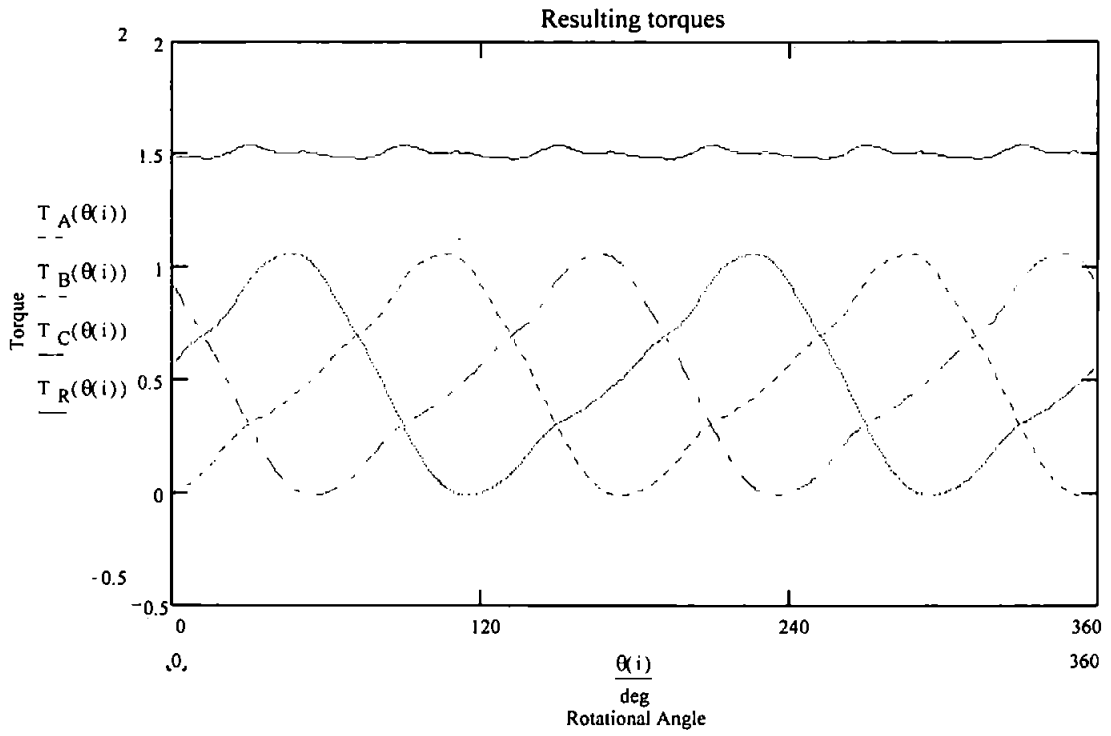
Figure 7.8 Phase torque and resulting torque for load case. Excitation with sinusoidal currents.

Comparison of the individual phase currents already reveals distinct differences. The resulting output torques are also clearly different from each other. A look at the spectral components of the output torques allows a quantitative analysis of the output torques.

First the no load case is shown.
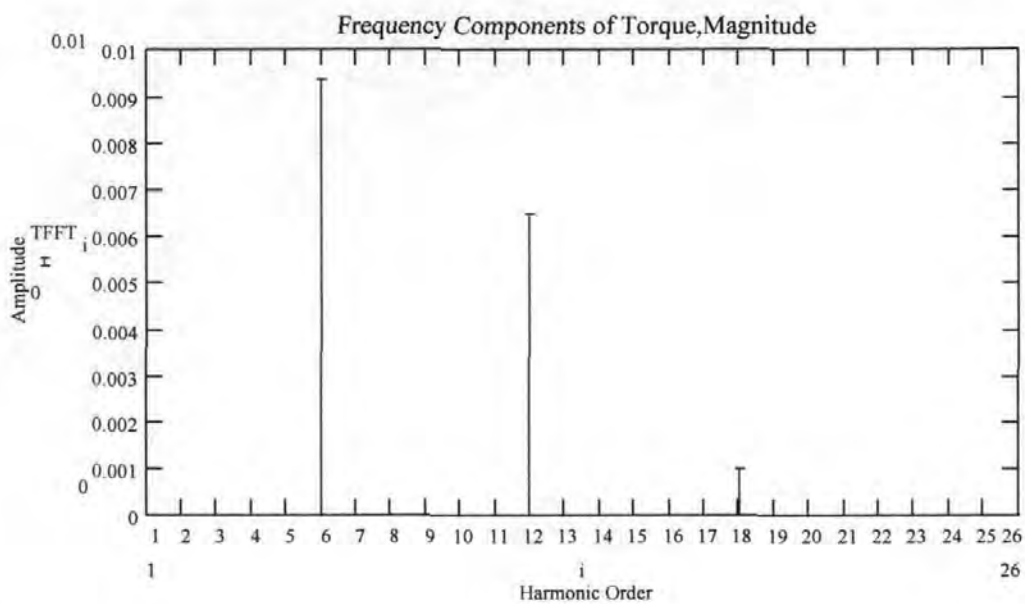
Figure 7.9 Torque ripple harmonics for no load case

Figure 7.10 shows the torque ripple harmonics for the load case in comparison.
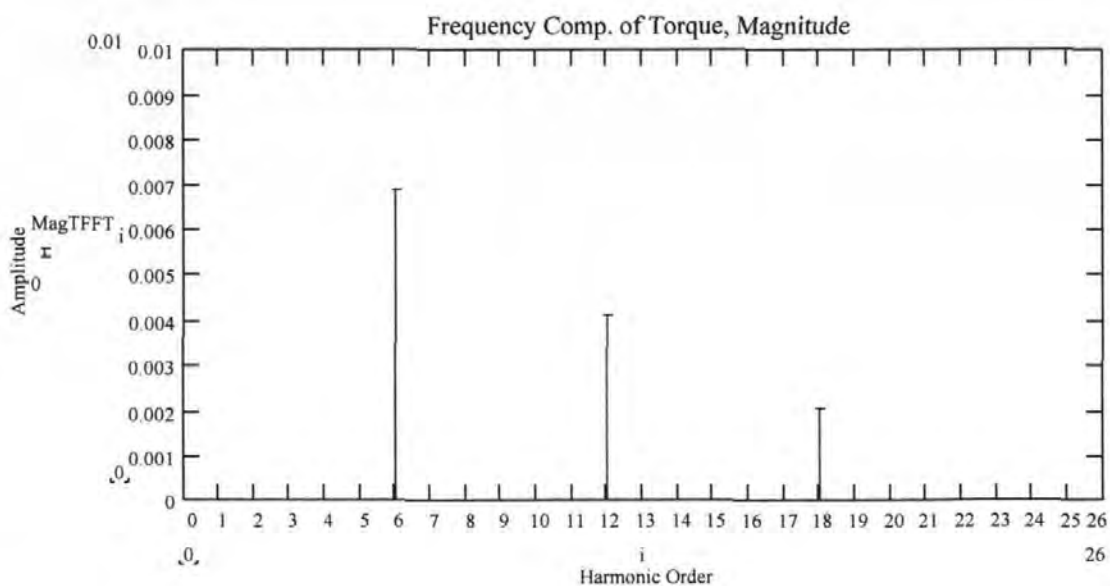
Figure 7.10 Torque ripple harmonics for full load case

119

Again only the 6th, 12th and 18th torque harmonic are visible as torque ripple. Higher torque ripple harmonics have a much reduced amplitude below the measurement accuracy. If figures 7.9 and 7.10 are compared it becomes clear that the resulting output torque ripple changes substantially with load. Table 7.1 lists the differences in amplitude for the no load and the load case.

	no load case %	load case %
harmonic order		
6	0.93	0.69
12	0.65	0.41
18	0.10	0.21

Table 7.1 Amplitude of torque ripple harmonics in percent for no load and load case

Table 7.1 reveals big differences in torque ripple amplitude. Analysis of the phase relationship of the torque ripple harmonics also shows distinct differences. It can therefore be concluded that the torque ripple will change substantially with load. The no load back emf waveforms can therefore not be used to calculate correction currents for the cancellation of torque ripple.

Correction currents calculated from the no load back emfs will prove insufficient for the cancellation of torque ripple if they are used for higher current loads. This will be demonstrated for the full load case.

Figure 7.11 shows the calculated output torque for the full load case if the correction currents from the no load case are used.
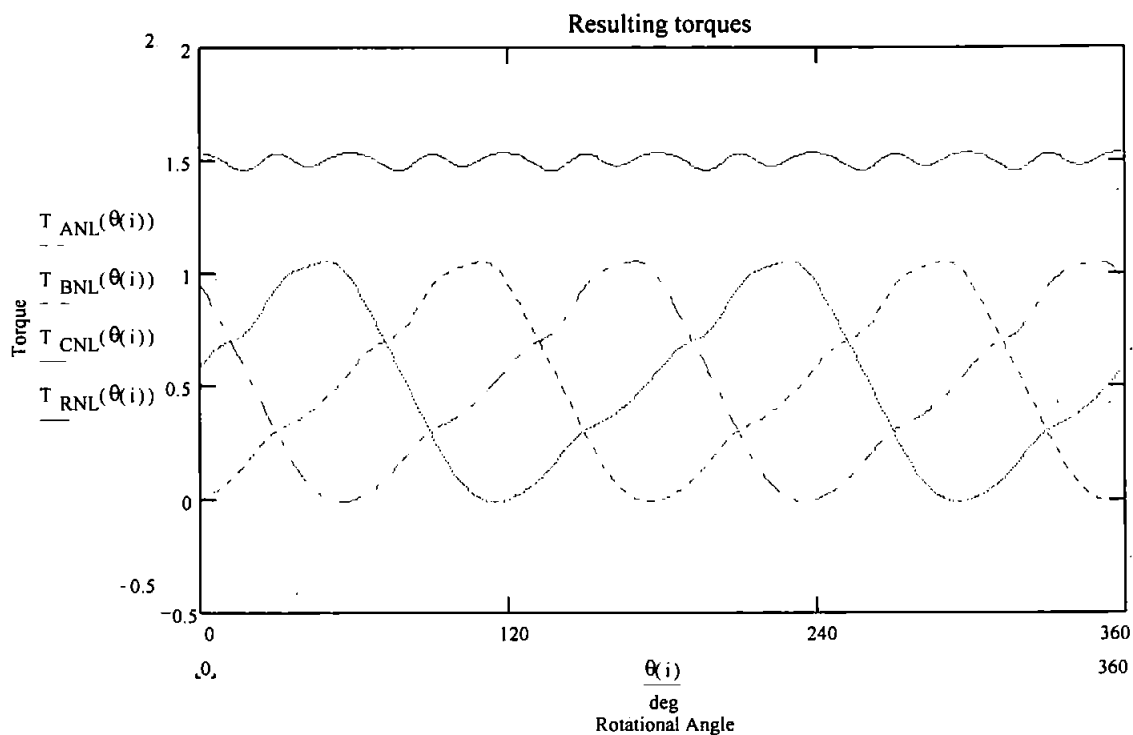
Figure 7.11 Phase torque and resulting torque for full load case. Excitation with corrections currents derived from no load case.

The resulting torque ripple is clearly visible. A look at the spectral components reveals the magnitude of the resulting torque ripple.
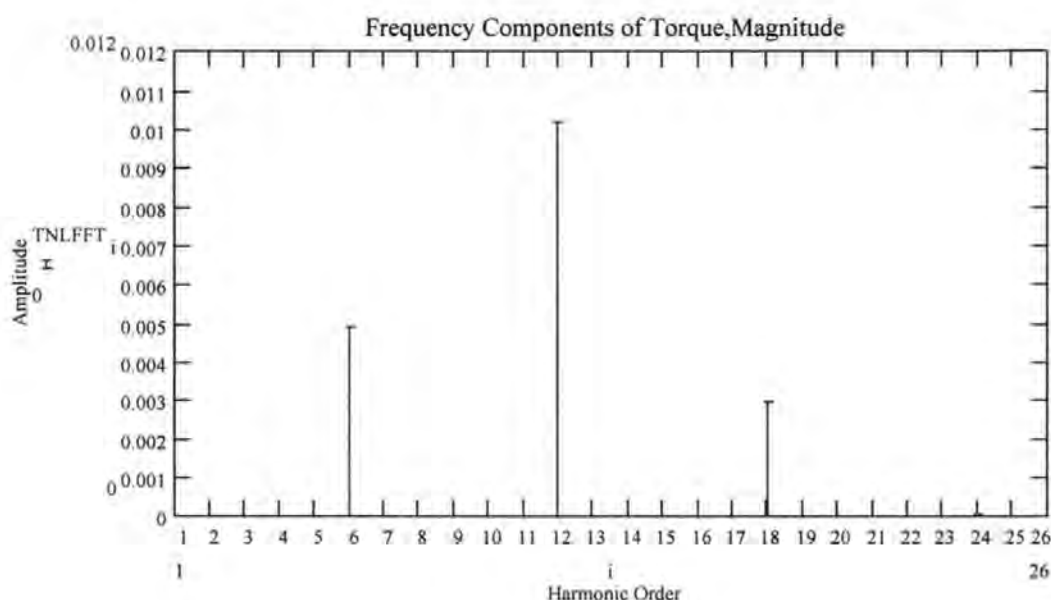
Figure 7.12 Torque ripple harmonics for full load case. Excitation with correction currents derived from no load case.

Figure 7.12 shows, that the resulting torque ripple is substantial.

Table 7.1 will now be extended to include the resulting torque ripple for the full load case if excitation currents derived from the no load case are used.

	No load case in % Sinusoidal excitation	Full load case in % Sinusoidal excitation	Full load case in % Excitation from no load case
Harmonic order			
6	0.93	0.69	0.49
12	0.65	0.41	1.02
18	0.10	0.21	0.29

Table 7.2 Amplitude of torque ripple harmonics in percent for no load and load case for different excitation

122

Table 7.2 shows the resulting torque ripple for the full load case to be of the same order for sinusoidal excitation and excitation with correction currents derived from no load back emfs. A torque ripple correction based on no load quantities, as described by the authors in chapter 6, will therefore be ineffective. For light loads only small deviations from the desired constant output torque will result. However with increased current loading the whole correction procedure becomes ineffective. For full load there will be no difference whether correction currents or sinusoidal currents are applied.

It is therefore necessary to develop a new correction procedure, which takes into account changes of the back emf waveforms with armature reaction. A novel adaptive torque ripple reduction strategy, as first presented in [90], will be suggested in the following.

7.2   Novel Adaptive Torque Ripple Reduction Strategy. Implementation and Advantages

A novel torque ripple reduction strategy uses measurements of no load and load back emf waveforms for torque ripple reduction. The effectiveness of the new reduction strategy will be demonstrated for the full load case.

As already discussed the back emf waveforms for the full load case have been determined from phase voltage measurements and subsequent calculation using equation 7.1. Using Park's transform these waveforms will be transferred to the dq-plane. The dq back emfs will then be used to calculate the correction currents in the dq-plane. Finally the correction currents will be transformed to the stator description of the machine. This is exactly the

123

same procedure as described in chapter 6. The only difference is the use of load instead of

no load back emf waveforms.

The resulting new correction currents will be compared to the correction currents derived

from the no load quantities to highlight the differences.

Figure 7.13 repeats the correction currents calculated in chapter 6.
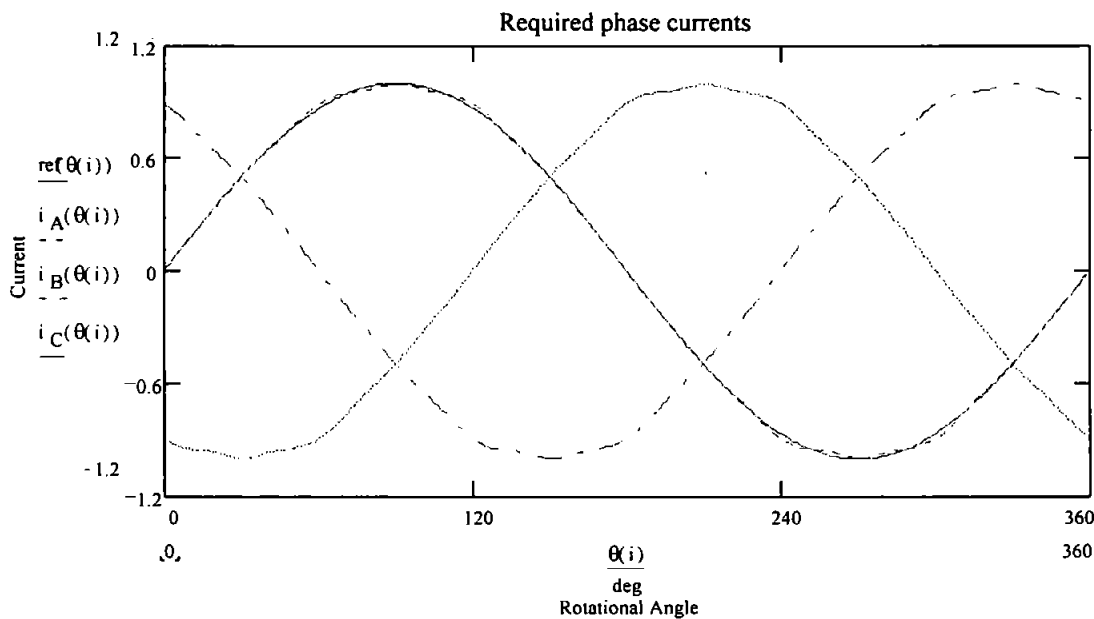
Figure 7.13 Correction currents derived from no load quantities

Figure 7.14 presents the new correction currents calculated from full load quantities.
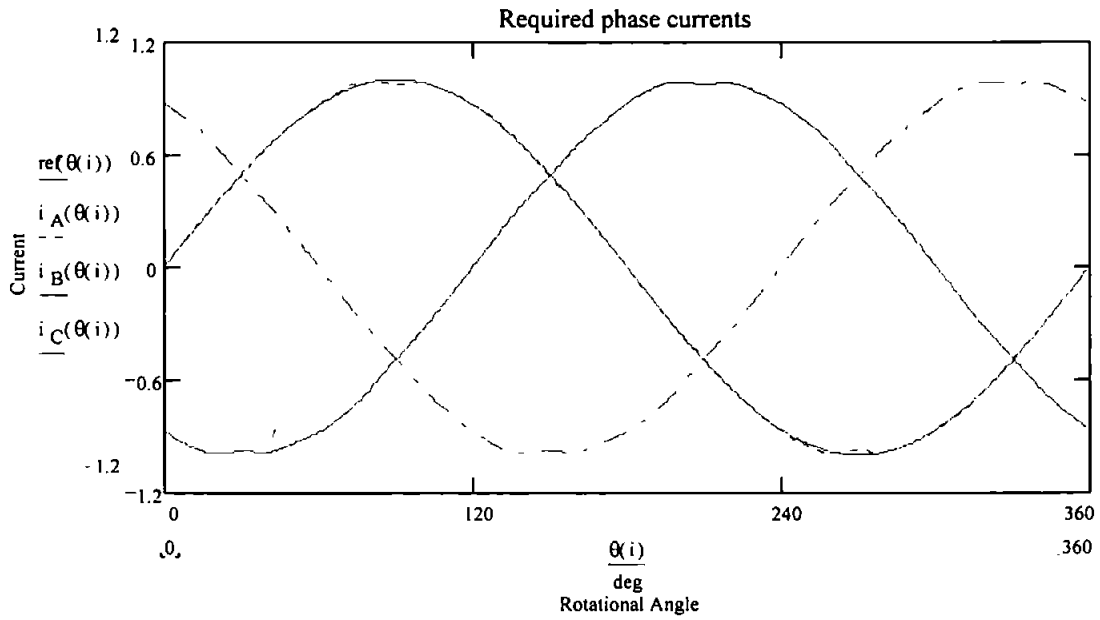
Figure 7.14 Correction currents derived from full load quantities

Comparison between figure 7.13 and 7.14 already reveals visible differences. To allow quantitative analysis the spectral components of the correction currents are calculated.

Figure 7.15 shows the current harmonics for the correction currents derived from no load quantities.

125
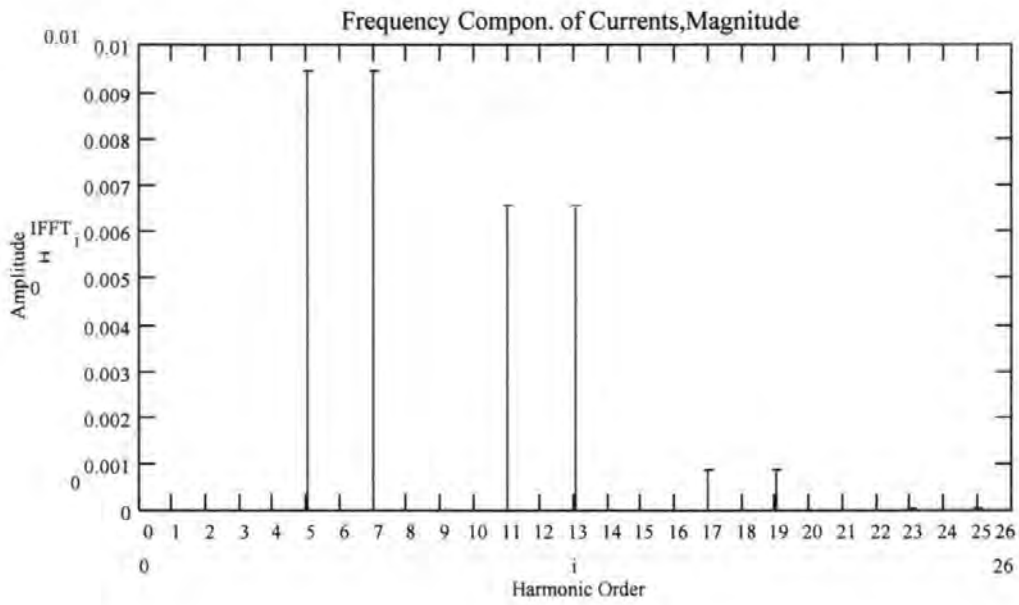
Figure 7.15 Spectral components of correction currents derived from no load quantities

Figure 7.16 gives the current harmonics for the new correction currents derived from load quantities.
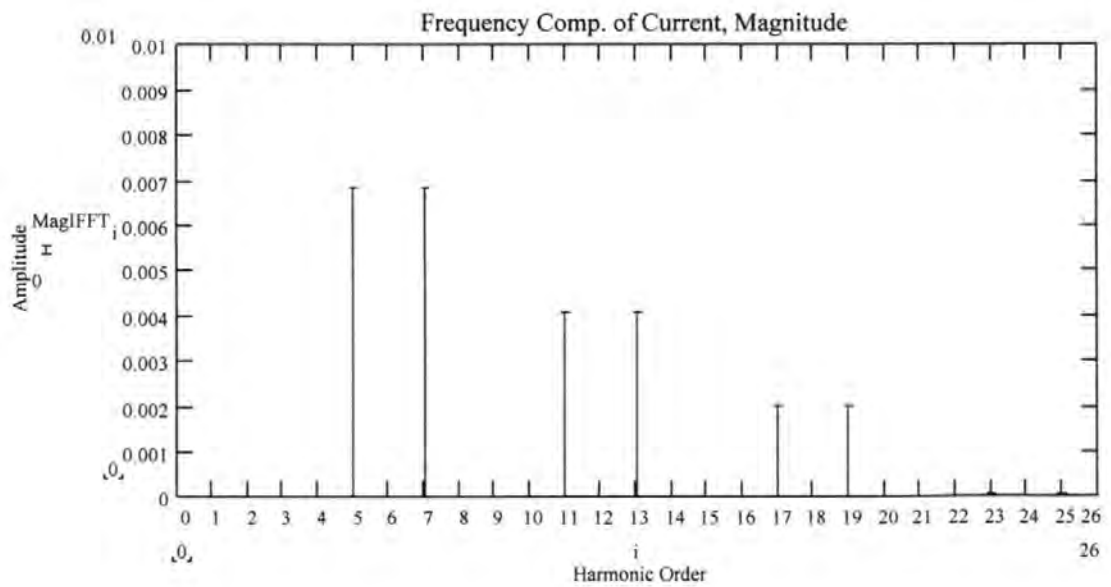
Figure 7.16 Spectral components of new correction currents derived from load quantities

126

Figures 7.15 and 7.16 only show the relevant correction harmonics. The fundamentals are scaled to be of amplitude 1 to allow comparison. Higher harmonics are too small in amplitude to be of any relevance.

Table 7.3 allows a quantitative comparison of current harmonics.

	no load case %	load case %
harmonic order		
5	0.944	0.684
7	0.944	0.684
11	0.656	0.408
13	0.656	0.408
17	0.088	0.201
19	0.088	0.201

Table 7.3 Phase current harmonics in percent derived from no load and load case quantities

Clear differences in amplitude become evident. It can therefore be concluded that the new correction currents are fundamentally different from the original correction currents derived from no load quantities.

Finally the effectiveness of the new correction currents will be demonstrated. Figure 7.17 shows the individual phase torques and the resulting output torque using the new correction currents.
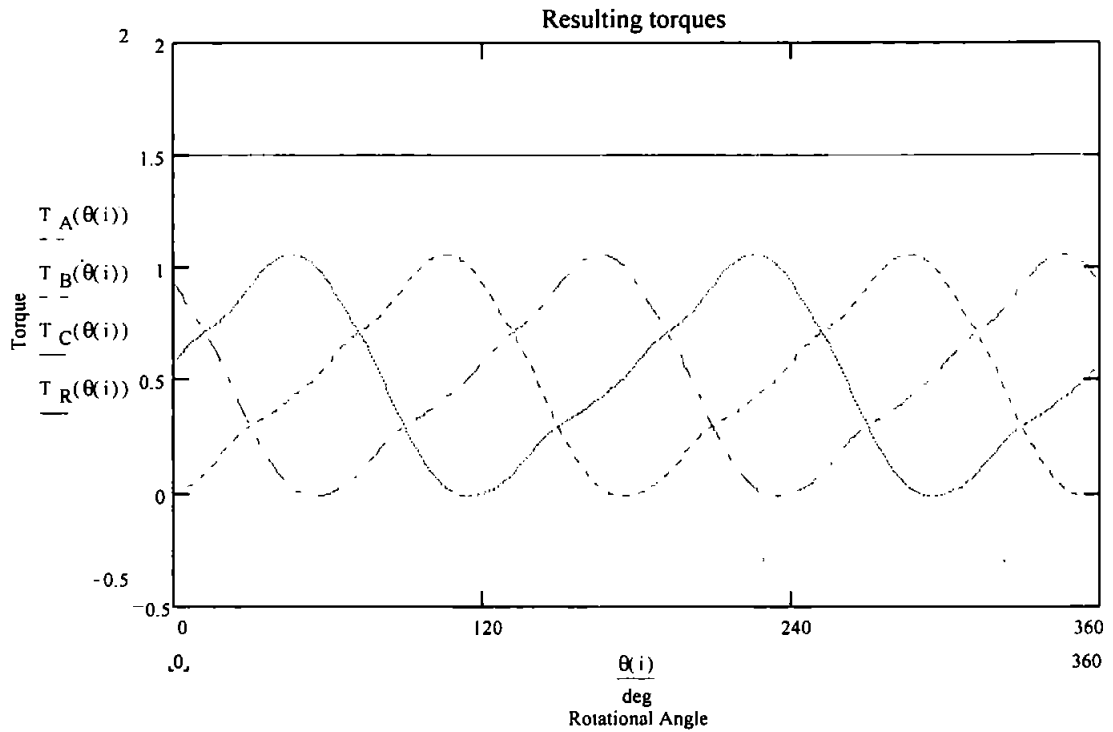
Figure 7.17 Phase torques and resulting torque for currents derived from full load quantities

As expected a constant output torque results. It is therefore possible to find new excitation currents, which eliminate torque ripple in the case of varying load currents.

The conventional torque ripple reduction approach uses measurements of the no load back emf waveforms, which can be taken off line. This means the machine is not connected to any load. The novel adaptive torque ripple reduction scheme requires measurements of the load back emfs. As explained before the direct measurement of load back emfs is not possible. It is therefore necessary to connect a three-phase balanced load across the machine phases, with the machine being back-driven by a second machine. This enables measurement of the phase voltages. It is then possible to calculate the phase back emfs. A set of load measurements can be taken first. Secondly the phase back emfs for different load levels will be calculated. Finally correction currents for various load levels will be

128

derived. These correction currents will then be implemented into the reduction algorithm. This maintains the advantage of the conventional torque ripple reduction strategy, that no on-line calculations and transformations need performing. In other words the reduction algorithm can be pre-prepared, thus reducing the computational overhead.

Depending on the required accuracy a larger or smaller number of back emf measurements needs taking. The reduction algorithm will evaluate the actual load level and will apply the nearest correction current. This correction current will be an approximation of the correct correction current. However the change of correction currents is relatively small if a sufficient number of load points is taken into account. The resulting output error will be small compared to applying the correction currents derived from no load quantities.

Some of the methods discussed in chapter 6 propose the use of a torque observer. This torque observer would be capable of sensing changes in back emf waveforms. However there are two problems associated with this method. The model for the torque observer would need to be quite complicated to allow modelling of back emf changes and therefore very computational intensive. Also the fine-tuning of the model parameters would be difficult and the resulting accuracy might be quite low. Finally the time delay of the observer doesn't allow the use of the controller for real-time dynamic applications.

One author suggested the use of a torque sensor. If the torque sensor is assumed to have a high enough bandwidth it would of course be capable of sensing changes of output torque with current loading. However as discussed before system resonances prevent the effective use of this torque sensor.

The advantage of the novel torque ripple reduction scheme, proposed here, is the fact, that it can be used in real time. All relevant calculations are done beforehand, therefore

allowing for fast response times. Further accurate torque ripple reduction can be achieved, because model inaccuracy and resonance problems are not present.

The following chapter describes a new improved torque ripple reduction strategy. The torque ripple reduction strategy described in this chapter has been developed further to allow higher correction accuracies and easier implementation.

Chapter 8 New Improved Torque Ripple Reduction Strategy

The torque ripple reduction strategies described in chapter 6 and 7 have been based on the measurement of back emf waveforms. There are two problems associated with the measurement and use of the back emf waveforms.

Firstly it is difficult to measure the back emf waveforms with a high accuracy. For instance if a second motor is used to back-drive the brushless motor as described in chapters 5 and 7 it is necessary to provide a load, which guarantees sinusoidal phase currents. This cannot be achieved by using a simple passive load. It is therefore necessary to use an electronic load, which is capable of varying the load resistance in order to maintain sinusoidal phase currents. This constitutes a very high demand because the control of the electronic load needs to be fast enough to react to current deviations in real time. Particularly it is desired to measure the back emf waveforms at higher speeds in order to profit from the inertia effect to keep torque variations introduced by the driving machine down. This effectively requires a very high control bandwidth of the electronic load. Further it needs to be ensured that the control of the electronic load does not interact with the control of the driving machine. Also it is possible that the control of the individual phase loads starts to interact with each other. Another problem associated with the measurement of back emf waveforms is the fact that the back emf waveforms cannot be measured directly as already discussed earlier. It is only possible to measure the phase voltages and it is then necessary to calculate the back emf waveforms. The relevant equation is repeated here from chapter 7.

$$emf = V + i * R + L * \frac{di}{dt} \quad (8.1)$$

131

Here emf is the back emf waveform to be calculated, V is the phase to star point voltage, R is phase resistance, L is phase inductance and i is the phase current.

It is necessary to measure the phase voltage with a high accuracy for all three phases. Further it is necessary to know the phase current, either from the current control or from measurement of the phase current. Again this is necessary for all three phases. Knowledge of the phase currents is particularly relevant as this affects the second and the third factor in equation 8.1. Further a good knowledge of the phase resistance is required. For a very precise measurement it would be necessary to determine the phase resistance at the relevant harmonic frequency of the phase current. The knowledge of the phase inductance is even required at all relevant harmonic frequencies of the phase current. It can be concluded that it requires considerable effort to obtain highly accurate data for the back emf waveforms.

Secondly the back emf waveform is only an indirect quantity. The quantity of interest is the torque ripple, which needs to be derived from the back emf waveforms. It would therefore be desirable to use the measurement of the torque ripple directly as the base quantity for the torque ripple reduction strategy.

In the following a new torque ripple reduction strategy is described, which directly uses measurements of the torque ripple at different current loads instead of data for the back emf waveforms. The theory behind the new torque ripple reduction strategy is described. Further the advantages and implementation of the new method are explained.

First the power relationship for torque production in the three-phase machine is recalled.

$$T(\theta) * \omega(\theta) = emf_a(\theta) * i_a(\theta) + emf_b(\theta) * i_b(\theta) + emf_c(\theta) * i_c(\theta) \quad (8.2)$$

T is the output torque, ω represents the machine speed, $emf_{a,b \text{ and } c}$ are the phase back emfs and $i_{a,b \text{ and } c}$ are the phase currents and θ is the rotational angle of the machine.

The brushless machine is now supplied with ideal sinusoidal phase currents. This results in the following situation for the torque production described by the power relationship.

$$T(\theta) * \omega(\theta) = (emf_a(\theta) * \sin(\theta) + emf_b(\theta) * \sin(\theta - 120°) + emf_c(\theta) * \sin(\theta - 240°)) * \mathit{factor1}$$
(8.3)

All variables are as above. Factor1 is an amplitude factor to reflect the amplitude of the supply currents.

If constant machine speed is assumed equation 8.3 can be rewritten as follows.

$$T(\theta) = (emf_a(\theta) * \sin(\theta) + emf_b(\theta) * \sin(\theta - 120°) + emf_c(\theta) * \sin(\theta - 240°)) * \mathit{factor2}$$
(8.4)

Here factor2 is a constant multiplication factor to account for the machine speed and the amplitude of the supply currents.

The torque ripple reduction strategies described in chapters 6 and 7 require the measurement of the phase back emf waveforms. Once these waveforms have been determined Park's transform is used to transfer the phase back emfs to the dq-description of the machine. The equation for Park's transform is recalled here.

$$emf_d(\theta) = \frac{2}{3} * \left(emf_a(\theta) * \cos(\theta) + emf_b(\theta) * \cos(\theta - 120°) + emf_c(\theta) * \cos(\theta - 240°)\right)$$

$$emf_q(\theta) = \frac{2}{3} * \left(emf_a(\theta) * \sin(\theta) + emf_b(\theta) * \sin(\theta - 120°) + emf_c(\theta) * \sin(\theta - 240°)\right)$$

(8.5)

$emf_{d\ and\ q}$ are the two-phase back emf waveforms.

Only emf_q is needed to determine the correction current i_q in the dq-description of the machine as can be seen from equation 8.6.

$$i_q = \frac{2}{3} * \frac{T * \omega}{emf_q} = \frac{2}{3} * \frac{A}{emf_q} \quad (8.6)$$

Here i_q is the required correction current to be calculated, T is the output torque, ω is the speed, emf_q is the back emf description for the quadrature component and A is the desired value of output torque at a certain speed.

It is therefore only necessary to determine emf_q and not emf_d. Equation 8.5 can be simplified to the following expression.

$$emf_q(\theta) = \frac{2}{3} * \left(emf_a(\theta) * \sin(\theta) + emf_b(\theta) * \sin(\theta - 120°) + emf_c(\theta) * \sin(\theta - 240°)\right) \quad (8.7)$$

Equation 8.7 can now be compared to equation 8.4. A detailed analysis reveals that both equations are of the same structure except for a constant multiplication factor if constant machine speed is assumed. In other words the recorded output torque for ideal sinusoidal supply currents corresponds to the quadrature component of the back emf waveform.

Instead of measuring the phase back emfs and transferring them to the dq-description of the machine it is also possible to record the torque output for ideal sinusoidal phase currents.

There are a few advantages associated with this new strategy for torque ripple reduction. Firstly the output torque can be recorded with a much higher accuracy than the phase back emf waveforms. It is possible to separate the output torque into a constant dc level of torque output and a superimposed ac level of torque ripple. Once the dc level is determined it is only necessary to accurately record the torque ripple itself. As the torque ripple is only a percentage of the complete output torque the full sampling accuracy can be used for this part of the torque output signal. For the test motor the torque ripple is in the order of 5% of torque output. The signal accuracy can therefore be improved by a factor of 20 compared to having to record the full phase back emf waveform.

Secondly it is only necessary to record one signal for the output torque and not three signals as in the case of the phase back emf waveforms.

Thirdly it is not necessary to perform Park's transform to transfer the phase back emf waveforms to the dq-description of the machine. This transformation is automatically performed through supplying the machine with ideal sinusoidal phase currents.

Further it is possible to record the output torque at low machine speed because it is not necessary to use the inertia effect as in the case of the measurement of the back emf waveforms. This allows for higher sampling accuracy.

Further it is not necessary to calculate the back emf waveforms from the phase voltage measurements. This is time consuming and will introduce calculation errors as the phase quantities like phase resistance and phase inductance are not accurately known.

135

The implementation of the new torque ripple reduction strategy is easier than the implementation of the strategies described in chapters 6 and 7. This is because the measurement required to determine emf_q is simpler and no subsequent calculations are necessary. Once emf_q is measured using equation 8.4 the implementation follows exactly the same implementation procedure as for the torque ripple reduction strategies described in chapters 6 and 7. The correction current i_q is calculated from emf_q. This correction current is then transferred to the abc-description of the machine using Park's transform. The phase currents are then implemented as correction currents in the usual way. This represents a further advantage of the new method. It is not necessary to alter the implementation of the phase currents. The same software and hardware can be used.

Further the adaptive torque ripple reduction strategy described in chapter 7 can also be implemented. The amplitude of the sinusoidal supply currents is adjusted and a set of output torque measurements is taken for different amplitudes. This set of measurements is used to replace the measurement and calculation of the back emf waveforms at different current loadings.

The following chapter deals with the experimental system used to implement the torque ripple reduction strategies. System requirements, hardware and software implementation are described in detail.

Chapter 9 Experimental System

9.1 System Requirements

Previous chapters have developed an adaptive torque ripple reduction strategy and a new improved torque ripple reduction strategy. These strategies have been developed based on theoretical considerations and computer simulations. It is desirable to validate these proposals using an experimental set-up. The experimental system has to fulfil different requirements.

First the system should allow accurate measurements of the torque ripple. This is necessary to determine the level and character of torque ripple for the original system. Further this allows evaluation of improvements in torque ripple reduction. Therefore there is a high demand on the accuracy of the torque sensing instrument and the processing of the torque signal.

Secondly the system should accommodate various supply current waveforms. Especially the implementation of small magnitudes and phase shifts of harmonics requires a high accuracy of the current sensing and the current control of the system. Further the switching devices on the drive need to have a high switching frequency to allow accurate current control across the speed range of the motor.

Thirdly the system should allow real-time implementation of different control strategies. This means that a high processing power is necessary to implement measurement, evaluation of measurements and the calculation of control values.

9.2   Hardware

The hardware of the experimental system consists of four main parts, the motor itself, the drive, the control unit and the load. These components are described in detail in the following.

9.2.1 Motor

Principally it is possible to either utilise a brushless dc or a brushless ac motor for the demonstration of the torque ripple reduction strategies. However brushless dc motors suffer a distinctive disadvantage. Because of the sudden change between states it is necessary to generate a high di/dt during switching instances. The steepness of the current increase is however limited by the motor phase inductance. Brushless ac motors provide a much better dynamic because the sinusoidal supply currents avoid these sharp transitions. It has therefore been decided to use a brushless ac motor to demonstrate the torque ripple reduction strategies. These motors not only guarantee potentially higher dynamics but also allow for higher accuracies for the torque control.

The motor considered here has been designed as a high performance motor. Especially the low rotor inertia facilitates a high dynamic performance. Here the torque ripple can adversely affect the dynamic performance. Further a high torque to weight ratio is realised. So the motor can be used in applications, where space is at a premium. This also means, that the armature effect will become more pronounced, demanding an adaptive control strategy. The rotor has been skewed in order to lower the cogging torque. No other design measures have been taken to reduce torque ripple.

The motor parameters are given in the following.

- Sinusoidal brushless motor

- 6-pole surface mount high energy Samarium Cobalt magnets

- 18 stator slots

- Continuous stall torque: 17 Nm

- Rated torque: 15.3 Nm

- Continuous stall current: 10.7 A

- Rated power: 4.9 kW

- Rated speed: 3000 rpm

- Torque constant: $K_t = 1.6$ Nm/A$_{rms}$

- Voltage constant: $K_e = 98$ V/1000 rpm

Motor data sheets with performance charts are given in the appendix, see A1.

9.2.2 Drive

For the drive a standard inverter has been chosen as could also be used for supplying induction motors. The advantage here is the use of standard, off-the-shelf technology. No special drive stage is required to implement the torque ripple reduction strategies. The inverter converts the incoming ac supply voltage from the mains into a dc link voltage via a standard rectifier element. This dc link voltage is then connected to the individual motor phases via 6 IGBT switches. The control over the IGBT switches was formerly performed by an ASIC. This ASIC has been removed and the inverter has been interfaced to the DSP control board. This allows direct switching control of the inverter. The IGBTs allow switching times in excess of 20 kHz, thus permitting high-speed power control of the motor.

9.2.3 Control

The control is the most complicated part of the system. Only a high-speed control unit with high accuracy allows the correct implementation of the torque reduction strategies.

A general-purpose control board has been designed around a DSP-controller. This hardware was readily available for the current work. The DSP used is a TMS320C25 from Texas Instruments. It is a 16-bit, fixed-point device with an instruction time of 100ns. The control board contains additional data and program memory as RAM memory for the execution of programs. Also EPROM memory can be used to store different programs. By simply changing the EPROM different control algorithms can be tested. The control board also contains A/D and D/A-converters and a 16-bit digital input and a 16-bit digital output port.

The control board has three main functions. It contains the program software (EPROM). It executes the control algorithm (DSP and RAM). It reads the signals from various measurement devices, processes the input data and generates output data to the inverter drive. Figure 9.1 gives an overview over the complete system, illustrating the function of the control board.
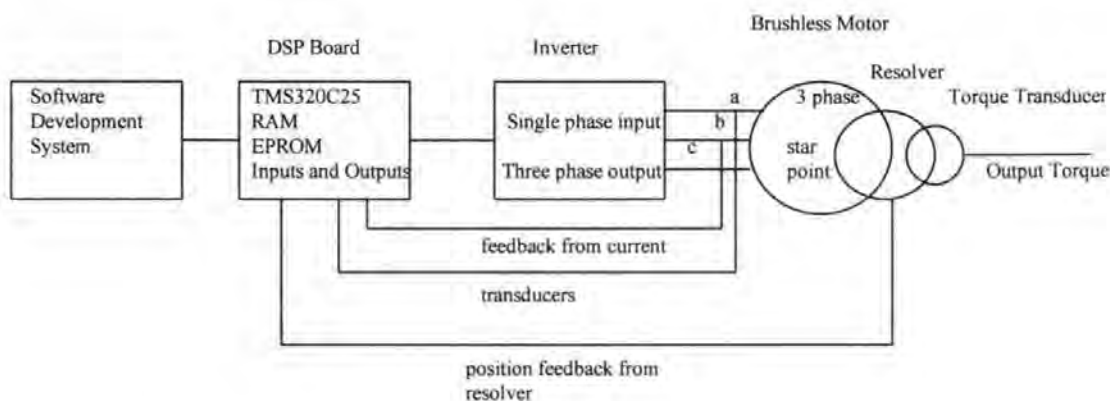
Figure 9.1 Complete system

Apart from the control board itself some measuring devices and adequate interfacing logic is required to feed input data to the control board.

Two current transducers are used to measure 2 of the 3 phase currents. The third phase current will be calculated by the control algorithm. The current transducers allow isolated dynamic measurement of the phase currents up to 200kHz, which is sufficient for high-speed control. The two transducers have been specified by extensive calibration measurements. From these measurements offset and gain factors have been determined. These factors allow software correction of the measured values to achieve high measurement accuracy for the currents. Some interfacing logic has been designed to provide current input signals to the control board.

A resolver is used to measure the rotor position of the brushless motor. The resolver is a high-precision tool to determine the rotor position with a high accuracy. It will produce sinusoidal and cosinusoidal position information modulated by the excitation frequency of the resolver. It is necessary to employ a sophisticated interfacing logic to convert these

signals into a digital position information for the control board. For this purpose a resolver-to-digital converter from Analog Devices has been used, which allows fast and accurate conversion of the position information. The converter produces a 14-bit digital position signal for the control. Further the necessary excitation and conditioning logic has been designed for the converter. The circuit logic can be found in appendix A2.

9.2.4 Load

For loading the brushless motor a second motor has been used acting as a dynamometer. This second motor, a standard brushed dc motor, is also capable of driving the brushless motor. This allows the acquisition of back emf data by measuring the terminal voltages of the brushless motor. During experiments it has been found that the dc motor is not well suited for loading the brushed motor. The system brushless motor, coupling, brushed motor and test rig exhibits resonances, which disturb measurements. Further the shaft run out of the brushed motor will negatively influence the torque output of the brushless motor.

It has therefore been decided to utilise a friction brake to load the brushless motor. In this case a simple belt brake has been used for applying the load torque to the machine. This belt brake reaches thermal limits at higher torque loadings. The experiments have therefore been restricted to a maximum of 75% of continuous load torque. Otherwise the belt brake has been found to allow accurate and constant, i.e. ripple-free, loading of the brushless motor. For this reason is has been decided not to use an eddy current brake, as those brakes would distort the original torque ripple of the brushless motor.

To allow accurate measurement of the torque output a precision torque transducer was used. The torque transducer is mounted to the test rig and is connected to the motor via a load arm. This load arm is mounted to the motor housing and serves to pre-load the strain

gauge in the torque transducer. The strain gauge allows measurement of positive and negative torque loadings. It is therefore possible to measure the torque output of the motor for clockwise and counter-clockwise rotation. The torque transducer provides an analog output signal. The output signal is then amplified and filtered by specially designed logic. The description of the torque transducer and the logic circuit is given in appendix A3.

9.3 Software

9.3.1 Software System and Language

A software system for the C25 provided by Texas Instruments has been used for program development. The, PC-based, software system allows editing, compiling and debugging of programs. It is possible to control program execution and to do program corrections. It is also possible to compile executable programs, which can then be downloaded to the EPROMs via an EPROM burner. This mode allows stand-alone execution of programs on the control board without being controlled by the software system. This form of program execution was preferred due to safety considerations. Synchronisation problems and interrupt handling could otherwise endanger the real-time execution of the control leading to malfunctions in the power stage.

The programming language used for the C25 is assembler. This allows real time implementation of signal read-ins and signal generation for the power stage.

9.3.2 Software Strategy

Type of Control

Here a torque control is implemented. No speed control is realised. The output torque should follow the demand torque. The main task of the control algorithm is to produce proper switching signals for the power stage in real-time depending on the actual motor speed and the desired torque output. It is therefore necessary to detect the speed of the machine. This is done by evaluating the position information from the resolver. Switching of the power devices is synchronised to the detected rotor position. The torque control is essentially a current control. It is therefore necessary to measure the phase currents. The actual values are compared to the desired current values calculated for the demand torque. Depending on the detected deviation the switching signals are given.

Control Bandwidth

The current measurement and current control constitutes an inner control loop with a control frequency of 20kHz. This allows the accurate implementation of desired current waveforms, which can substantially deviate from sinusoidal currents, even for high motor speeds. The outer position loop is slower because of the resolver-to-digital converter and allows a control bandwidth of 2kHz for the synchronisation of the rotor position signal.

Implementation

The output torque of the test motor is known and has been measured with sinusoidal currents applied. The results are presented in chapter 10. The measurements have been done for a number of load levels. It is now possible to calculate appropriate supply currents for each load level off-line using the algorithm described in chapter 8. The values for these supply currents can then be stored in program memory and can be utilised for real time

correction of the torque ripple. This allows the fast response time of 50μs for the ripple correction.

Modularity

The correction algorithm has been split in three parts. The first part implements sinusoidal current waveforms with variable current amplitude. The second part realises the cogging torque correction, which constitutes a fixed waveform. The third part allows the load dependent correction of the electromagnetic torque ripple. The modular approach makes it possible to test the motor with sinusoidal excitation and to evaluate the effectiveness of the cogging torque and electromagnetic torque ripple correction separately.

Adaptive Torque Ripple Correction

The supply currents are only correct for the measured load levels. If a different load level is required some torque ripple will reappear because of the armature reaction effect as described in chapter 7. Here the nearest two load levels are used to reduce this effect. Their demand values are weighted to achieve a good approximation of the required correction currents for the desired load level. However a small error will still occur. Chapter 11 describes a new technique to avoid this problem.

Speed Control

A speed control could easily be added to the control algorithm as only half of the control time and only a third of the available memory is used.

145

Chapter 10 presents the experimental results in detail. Measurements of the original torque ripple, the remaining torque ripple after correction and the required phase currents are given.

Chapter 10   Experimental Results

10.1   Measurements

The rotational angle of the brushless motor is measured by the resolver described in chapter 9. The resolver-to-digital chip is then used to convert the analogue output signals of the resolver into a 14-bit digital signal for the DSP. This 14-bit signal is an accurate representation of the rotational angle within 10 arcminutes. The 14-bit value is used internally to provide position information to the reduction algorithm. The digital value is then converted into an analogue output signal via the 12-bit D/A-converter of the DSP-board to be displayed and recorded on a digital storage oscilloscope.

For recording the torque output of the brushless motor the torque transducer described in chapter 9 has been used. This transducer works on the strain gauge principle and produces an analogue output signal. This analogue output signal is accurate within 0.01 Nm. The system torque transducer-motor-rig displays a resonance frequency at 300 Hz. It is therefore necessary to record the torque output at frequencies below this resonance frequency. This restriction does however not apply to the torque ripple reduction algorithm, which is capable of working at normal machine speed. The analog output signal of the torque transducer can again be displayed and stored on the digital storage oscilloscope.

To correct for friction and windage torque the cogging torque has been recorded in clockwise and counter-clockwise direction. The level of friction and windage torque has

147

been calculated from these recordings and subsequently been subtracted by adjusting the offset of the analog output signal of the torque transducer.

The phase current is recorded using the current transducers described in chapter 9. The analogue output signals of the current transducers have been calibrated and are accurate within +/- 10 mA. These analog signals are converted via the 12-bit A/D converter on the control board and the 12-bit representation is used for the control algorithm. As before the output signals of the current transducers can also be displayed and recorded on the digital storage oscilloscope.

The digital storage oscilloscope provides 8 bits of display resolution. The displayed signals are therefore displayed within 0.4% of the full-scale value. The input signals can be stored in data memory and can then be transferred to a PC for further processing.

10.2   Cogging Torque

The cogging torque has been recorded with no load connected to the brushless motor and the motor being driven by a second motor. This is the measurement method described in chapter 5.

The first trace shows the output of the resolver indicating the angle of rotation. Here only the electrical angle of rotation is displayed between 0 and 360 degrees. 0 degrees is to be found half way on the y-axis as indicated by the marker to the right of the grid.

The second trace shows the output of the torque transducer after amplification. The recorded signal of the torque transducer x in Volts can be interpreted as output torque as follows.

$$
\begin{aligned}
T(in \quad Nm) &= \frac{x(in \quad V)}{3.544V} * 25kg * 0.125m * 9.81\frac{m}{s^2} = \\
&= x(in \quad V) * \frac{8.65Nm}{V}
\end{aligned}
\qquad (10.1)
$$

Here T is the output torque measured by the torque transducer and x in Volts is the recorded signal from the torque transducer.

The time scale is recorded on the x-axis with units of 50ms. The recording is performed at constant machine speed. The recordings show slightly more than one electrical revolution of the machine.

The figure 10.1 shows the output torque of the brushless machine on a scale, which allows to display up to the full load torque of the machine. 0 Nm is to be found at the bottom of the y-axis as indicated by the marker to the right of the grid.
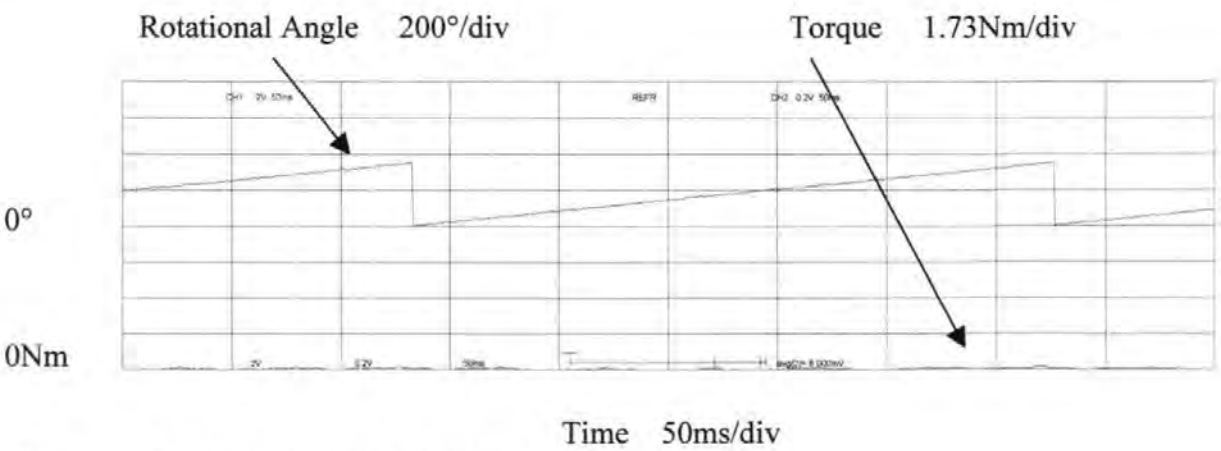
Figure 10.1 Cogging torque for test motor

The cogging torque oscillates around the zero line of the grid depending on the rotational position. This can be explained by the attraction and repulsion the rotor experiences when aligned with the relevant sections of the stator magnets, as explained in chapter 5.1.

Figure 10.2 shows a zoomed-in view of the cogging torque. The scale is enlarged by a factor of 20 to allow a detailed look at the cogging torque ripple. The 0 Nm point is now shifted to the middle of the y-axis as indicated by the marker.
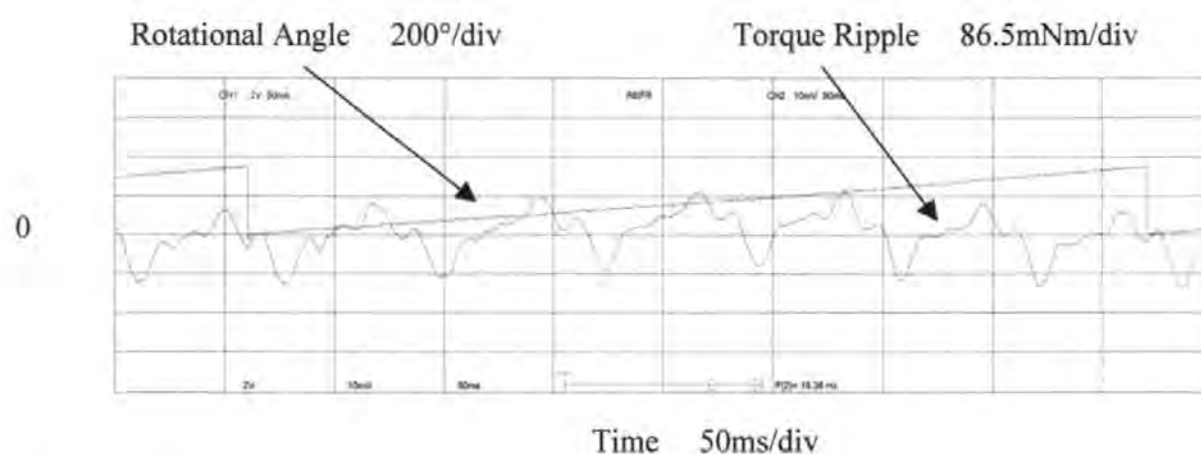
Figure 10.2 Cogging torque ripple for test motor

As can be seen from figure 10.2 the cogging torque contains the basic harmonic of 6 times the electrical frequency of the motor and higher harmonics of the order 12, 18 and 24. The cogging torque therefore has quite a complicated structure, which can be explained by the skewed design of the rotor and the special shaping of the magnets.

A counter torque in order to cancel the cogging torque has been calculated using the algorithm described in chapter 8. This counter torque will be implemented by the current control of the machine. The resulting output torque from the cogging torque and this counter torque should be nearly constant and be zero in amplitude. In order to be able to

record the effectiveness of the correction algorithm it is necessary to add a very small positive torque contribution to the counter torque. This small positive torque contribution provides enough torque to overcome friction losses and to turn the machine. It will however act as a small offset.

Figure 10.3 shows the resulting output torque with the cogging correction implemented. First the output torque is shown for the same scaling as in figure 10.1. The 0 Nm point is again found on the bottom of the y-axis as indicated.
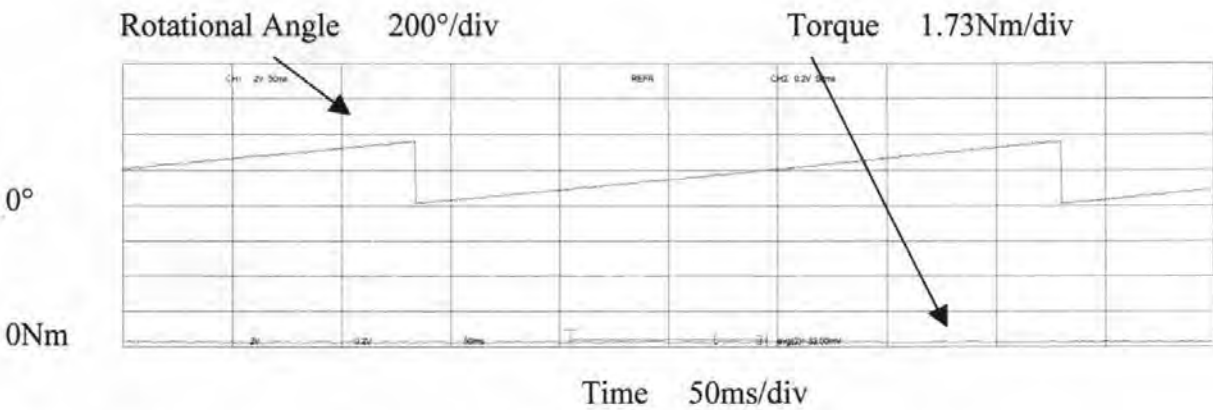
Figure 10.3 Resulting output torque after cogging torque correction

The small offset to allow rotation of the machine is clearly visible.

Further a zoomed-in view of the remaining cogging torque ripple is provided. The scale is again enlarged as in figure 10.2. Only the ac-component is shown and the 0 Nm point is positioned in the middle of the y-axis as indicated.

Rotational Angle   200°/div   Torque Ripple   86.5mNm/div

Time   50ms/div
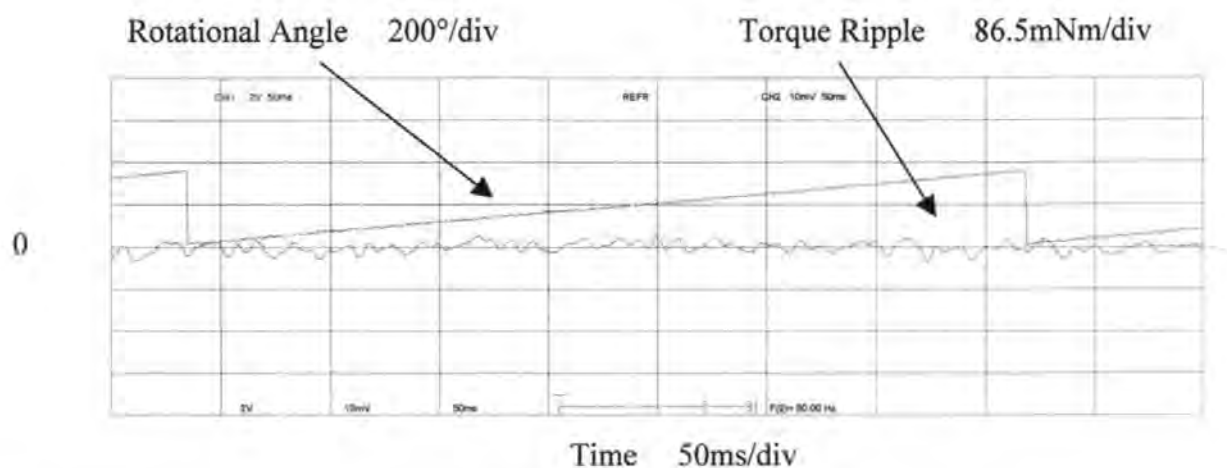
Figure 10.4 Resulting cogging torque ripple after cogging torque correction

If figures 10.2 and 10.4 are compared a clear reduction of cogging torque is visible. The peak-to-peak cogging torque is about 0.175 Nm. This corresponds to 1% of full load torque. This value has been reduced to 0.045 Nm or 0.25% of full load torque.

The cogging torque has only been recorded over one electrical rotation. In order to take manufacturing tolerances into account it would be necessary to record cogging torque over the full cycle of mechanical rotation. This would improve the accuracy of the correction algorithm and allow for lower remaining cogging torque ripple. Here however the achieved reduction in cogging torque ripple has been judged to be sufficient.

Finally one phase current has been recorded to illustrate the effectiveness of the current control. The current waveform shows the correction content plus the sinusoidal element to overcome machine friction and ensure rotation.

The second trace shows the output of the current transducer. The recorded signal of the current transducer y in Volts can be interpreted as phase current in Amperes as follows.

152

$$I(in \quad A) = \frac{y(in \quad V) * 1000}{4.5 * 75\Omega} =$$

$$= \frac{y(in \quad V) * 2.96}{\Omega} \qquad (10.2)$$

Here I is the phase current measured by the current transducer and y in Volts is the recorded signal from the current transducer.

The 0 A point is found in the middle of the y-axis as indicated. The first trace again shows the electrical angle of rotation.
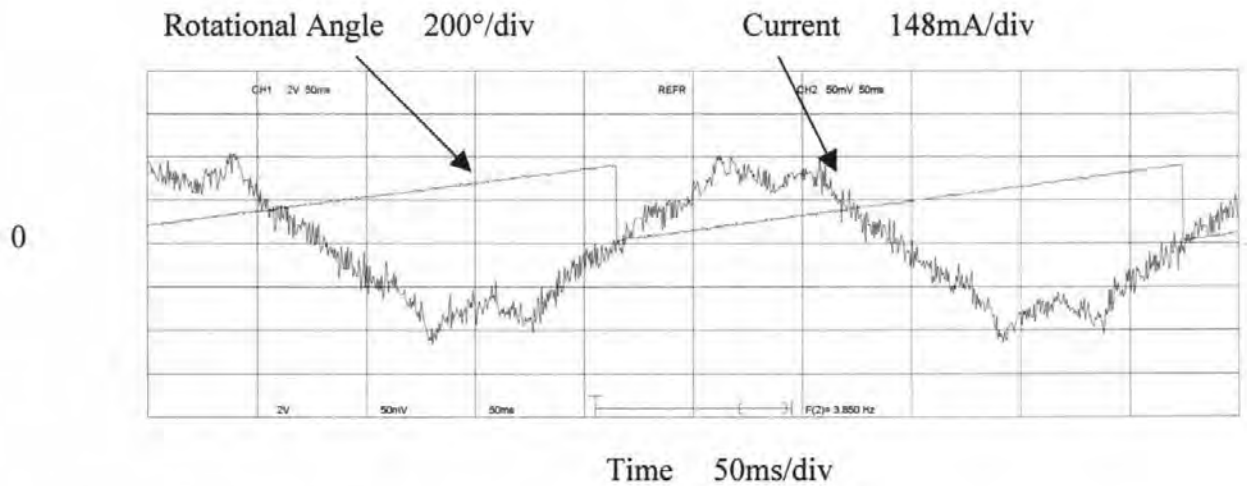
Figure 10.5 Phase current for correction of cogging torque

The required correction current contains a high number of harmonics in order to cancel the higher harmonics of the cogging torque. The peak amplitude of the correction current including the sinusoidal contribution is roughly 300mA.

153

10.3 Electromagnetic Torque Ripple

The next step after the reduction of the cogging torque is the reduction of the electromagnetic torque ripple. This represents a bigger problem because the electromagnetic torque ripple will be dominant and of a larger scale towards higher current loads.

To illustrate the effectiveness of the proposed torque ripple reduction strategy the torque output of the brushless machine will be shown for light load, medium and full load. Significant differences in torque ripple will be obvious.

First the machine is supplied by ideal sinusoidal phase currents. Here the resulting torque ripple is composed of the cogging torque and the electromagnetic torque ripple. Then the cogging torque reduction algorithm described in the previous subchapter is implemented. This removes most of the cogging torque and only the electromagnetic torque ripple remains. Finally the electromagnetic torque ripple is reduced using the algorithm described in chapter 8. The remaining torque ripple and the required correction currents are shown.

Two different forms of illustration are chosen. First the resulting output torque of the machine is represented on a scale, which allows comparison between all load situation up to full load. Here the ac and dc components of the output torque are given. The 0 Nm point is located at the bottom of the y-axis. The conversion according to equation 10.1 applies for the torque level. Secondly a zoomed-in view on the resulting torque ripple is given. The scale is chosen in order to achieve the highest resolution on the torque ripple. Therefore the scale varies between the individual load cases. Here only the ac component of the output

torque is pictured. The 0 Nm point is to be found in the middle of the y-axis. The same conversion according to equation 10.1 as before applies.

Finally one phase current is shown to illustrate the required correction currents. Both dc and ac components of the current waveform are pictured. The 0 Amperes point is located in the middle of the y-axis. The conversion of the voltage signal from the current transducer given in equation 10.2 applies. Again the scale varies between the individual load cases to allow for maximum resolution.

For all diagrams the first trace shows the electrical angle of rotation between 0 and 360 degrees. With 0 degrees located at the middle of the y-axis. The unit for the time scale is 50ms. Slightly more than one electrical cycle of rotation is recorded.

10.3.1 Torque Ripple Reduction at Light Loads

First the machine is excited with a low load current of 1.12 Arms. This represents roughly 10% of full load torque.

Figures 10.6 and 10.7 show the resulting output torque and the resulting torque ripple respectively for sinusoidal excitation of the machine.
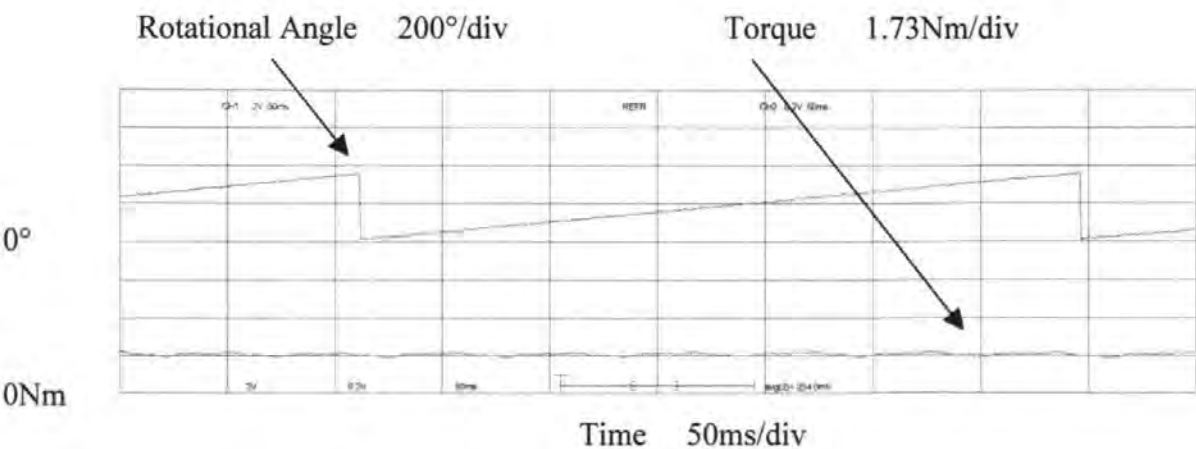
Figure 10.6 Resulting output torque at light load with sinusoidal excitation
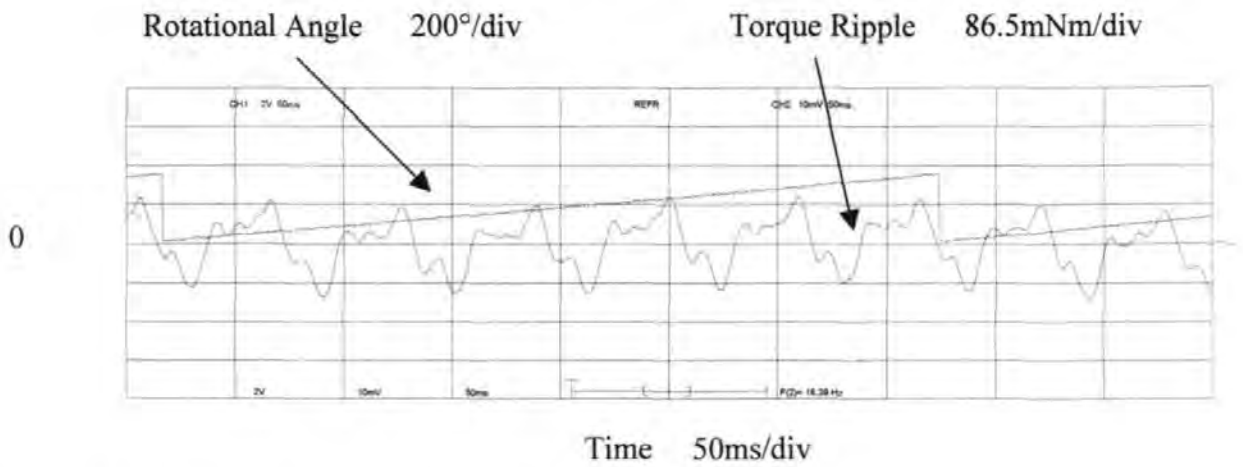
Figure 10.7 Resulting torque ripple at light load with sinusoidal excitation

The dc level of the output torque can be determined to be roughly 1.8 Nm. The peak-to-peak torque ripple, this is cogging plus electromagnetic torque ripple, is about 0.19 Nm or in other words 10% of the output torque level or 1% of the full load torque.

Figure 10.8 shows the remaining electromagnetic torque ripple after the cogging torque reduction has been implemented. Only the torque ripple is shown.
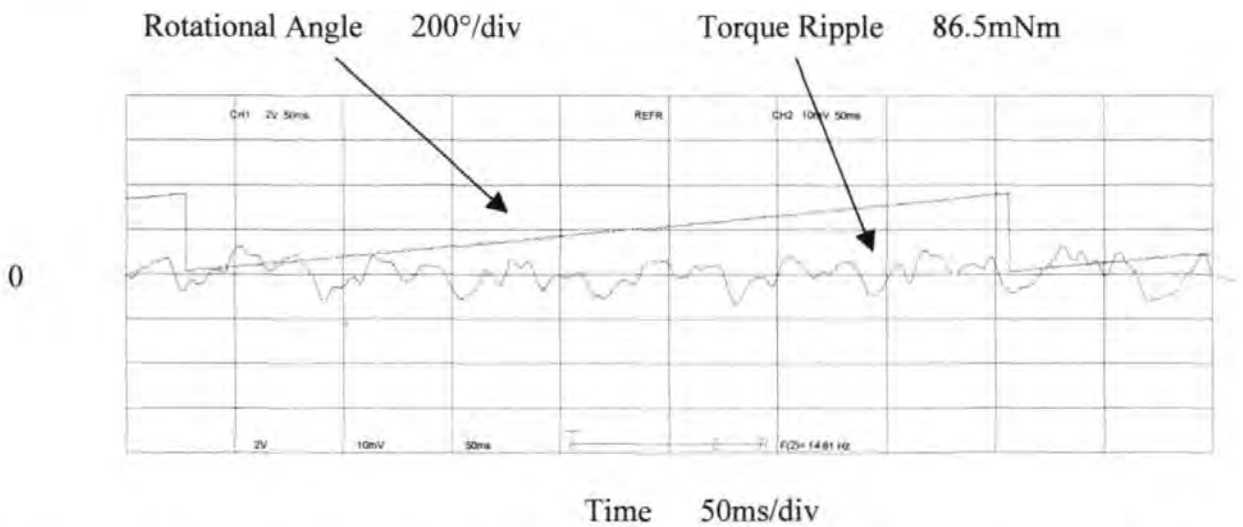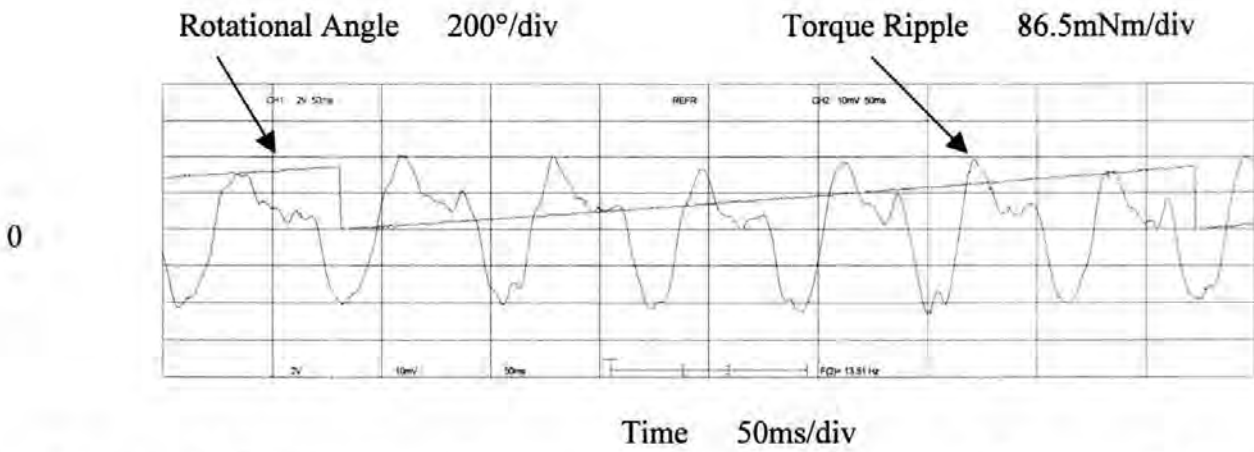

Figure 10.8 Remaining electromagnetic torque ripple at light load after implementation of cogging torque reduction

The electromagnetic torque ripple has a peak-to-peak amplitude of about 0.085 Nm. This corresponds to about 5% of the output torque or 0.5% of full load torque. It becomes clear that the electromagnetic torque has been masked by the cogging torque, which is dominant for light loads.

Figures 10.9 and 10.10 show the remaining output torque and torque ripple after the implementation of the reduction algorithm for the electromagnetic torque ripple.

Rotational Angle   200°/div   Torque   1.73Nm/div
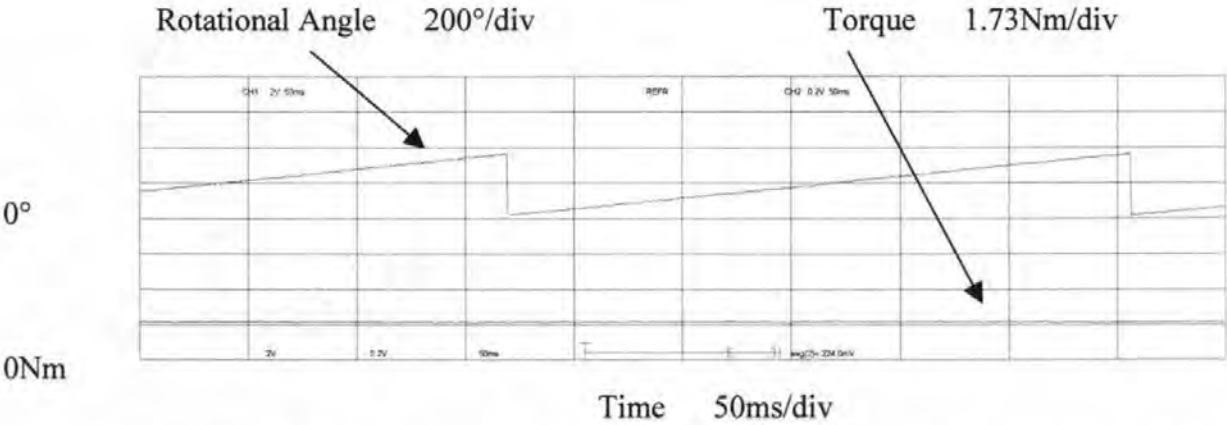
Figure 10.9 Resulting output torque at light load after cogging torque and electromagnetic torque ripple reduction

Rotational Angle   200°/div   Torque Ripple   86.5mNm/div
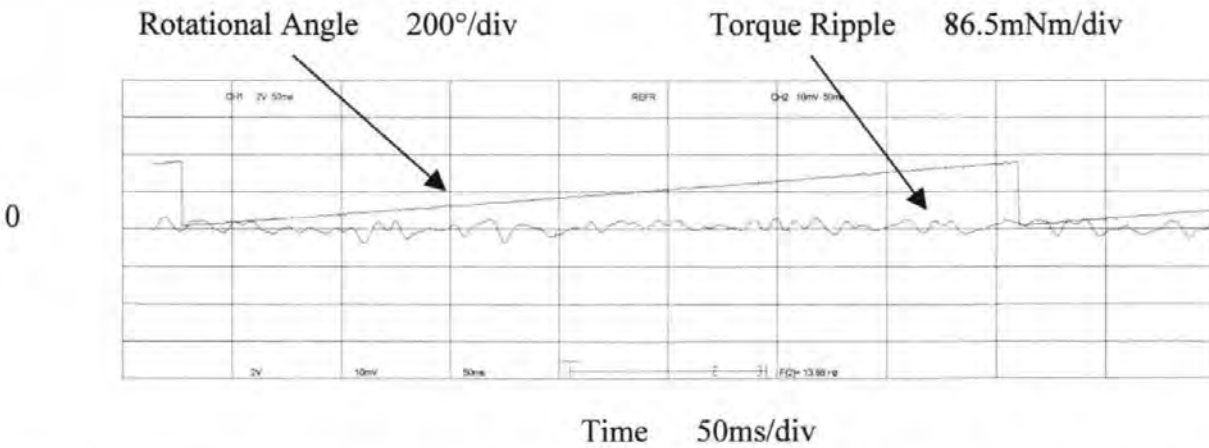
Figure 10.10 Remaining torque ripple at light load after cogging torque and electromagnetic torque ripple reduction

If figures 10.6 and 10.9 are compared the clear improvement using the reduction algorithm becomes visible. A further comparison between figures 10.7 and 10.10 reveals the magnitude of the reduction. The remaining peak-to-peak torque ripple is about 0.04 Nm. This represents about 2% of the output torque or 0.2% of the full load torque. In other words the torque ripple has been reduced by a factor of 5.

Finally the required phase current is shown.

Rotational Angle   200°/div   Current   592mA/div

0

Time   50ms/div
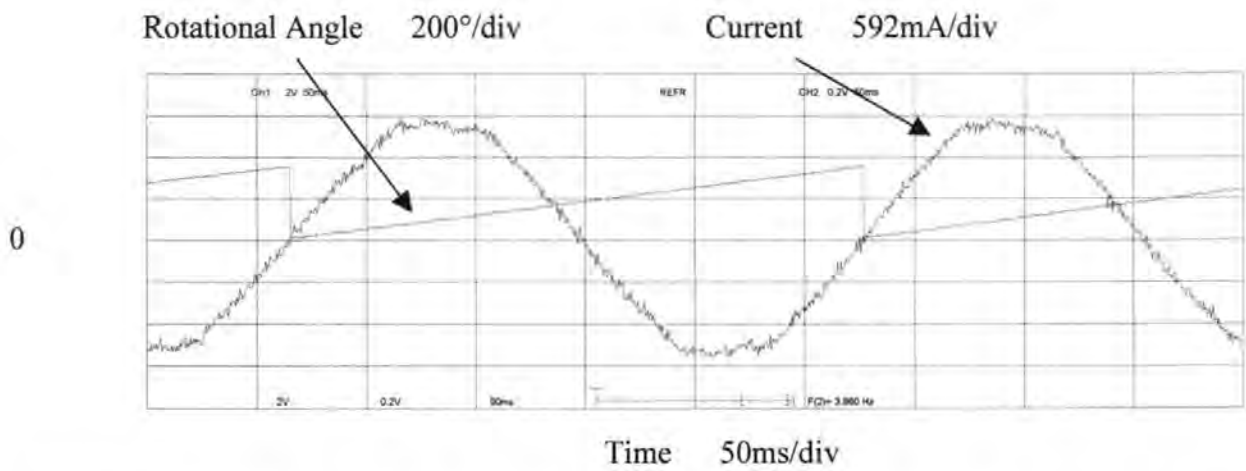
Figure 10.11 Required phase current for cogging and electromagnetic torque ripple reduction at light loads

Clear deviations from the ideal sinusoidal shape are visible. The peak amplitude of the phase current corresponds to 1.6 A or 1.13 Arms.

10.3.2 Torque Ripple Reduction at Medium Loads

Now the machine is excited with a medium load current of 4.17 Arms. This represents roughly 40% of full load torque.

Figures 10.12 and 10.13 show the resulting output torque and the resulting torque ripple respectively for sinusoidal excitation of the machine.

Rotational Angle   200°/div   Torque   1.73Nm/div

Time   50ms/div
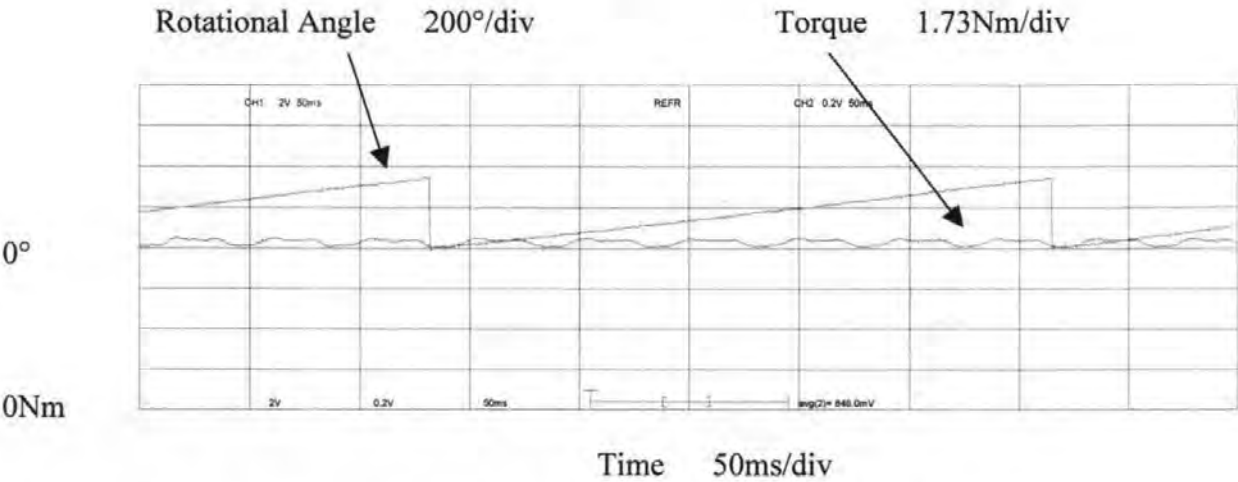
Figure 10.12 Resulting output torque at medium load with sinusoidal excitation

Rotational Angle   200°/div   Torque Ripple   86.5mNm/div

Time   50ms/div
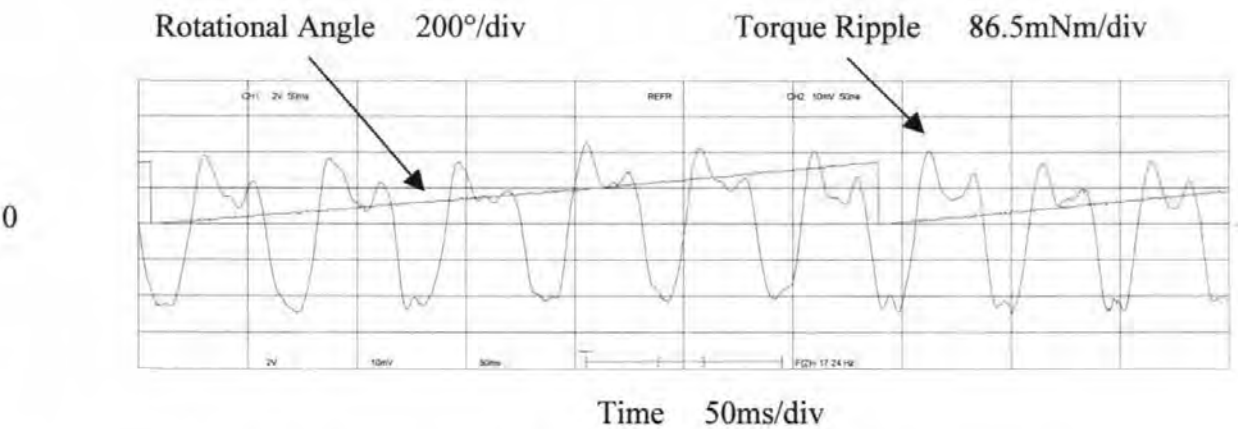
Figure 10.13 Resulting torque ripple at medium load with sinusoidal excitation

The dc level of the output torque can be determined to be roughly 7.2 Nm. The peak-to-peak torque ripple, this is cogging plus electromagnetic torque ripple, is about 0.36 Nm or in other words 5% of the output torque level or 2% of the full load torque. The percentage of torque ripple referred to the full load torque has therefore doubled.

Figure 10.14 shows the remaining electromagnetic torque ripple after the cogging torque reduction has been implemented. Only the torque ripple is shown.
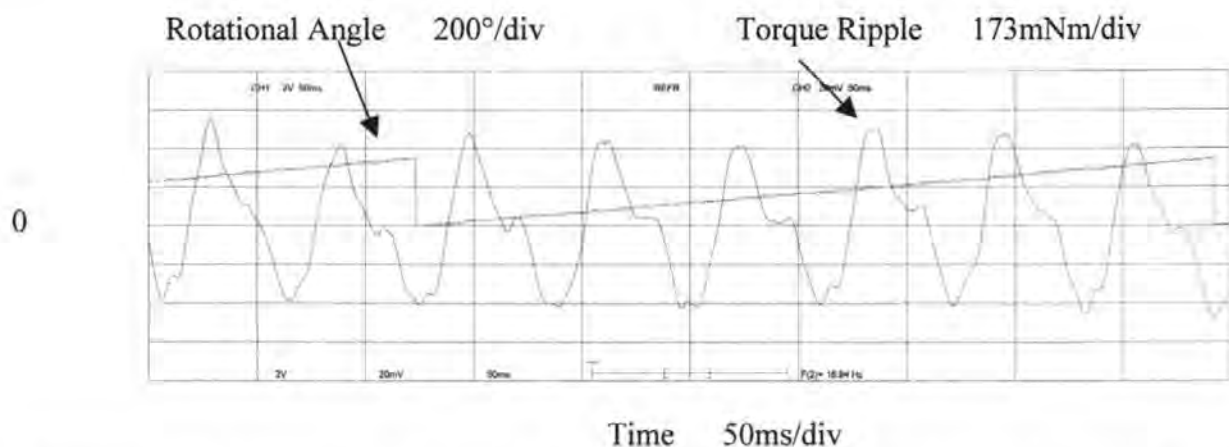
Rotational Angle   200°/div   Torque Ripple   86.5mNm/div

Time   50ms/div

Figure 10.14 Remaining electromagnetic torque ripple at medium load after implementation of cogging torque reduction

The electromagnetic torque ripple has a peak-to-peak amplitude of about 0.35 Nm. This corresponds to about 5% of the output torque. The cogging torque has virtually no influence at this load level and will be fully masked by the electromagnetic torque ripple. The level of electromagnetic torque ripple is comparable to the situation at light loads with roughly 5% of the output torque. However the absolute level has increased and now represents 2% of full load torque as opposed to 0.5% before. This is consistent with a load increase by a factor of 4 from light to medium loads. If figures 10.8 and 10.14 are compared clear differences in the shape of the electromagnetic torque ripple are visible as predicted before. A quantitative analysis is undertaken in chapter 11.

Figures 10.15 and 10.16 show the remaining output torque and torque ripple after the implementation of the reduction algorithm for the electromagnetic torque ripple.

Rotational Angle   200°/div   Torque   1.73Nm/div

0°

0Nm

Time   50ms/div
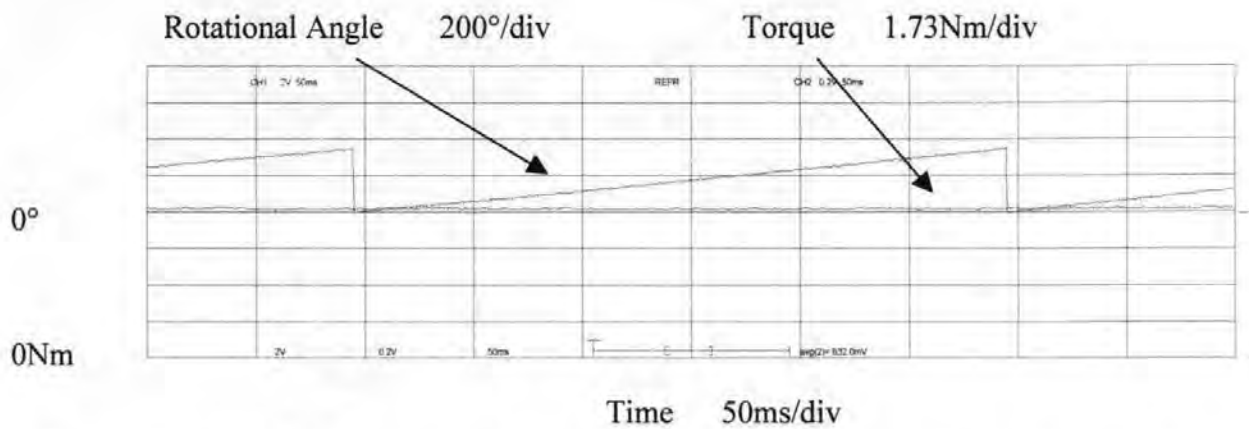
Figure 10.15 Resulting output torque at medium load after cogging torque and electromagnetic torque ripple reduction

Rotational Angle   200°/div   Torque Ripple   86.5mNm/div

0

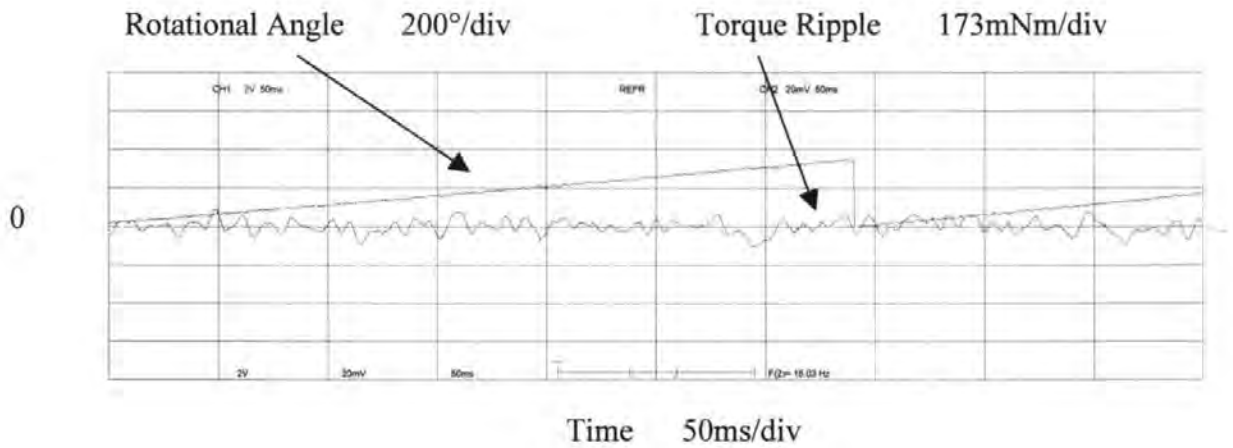Time   50ms/div
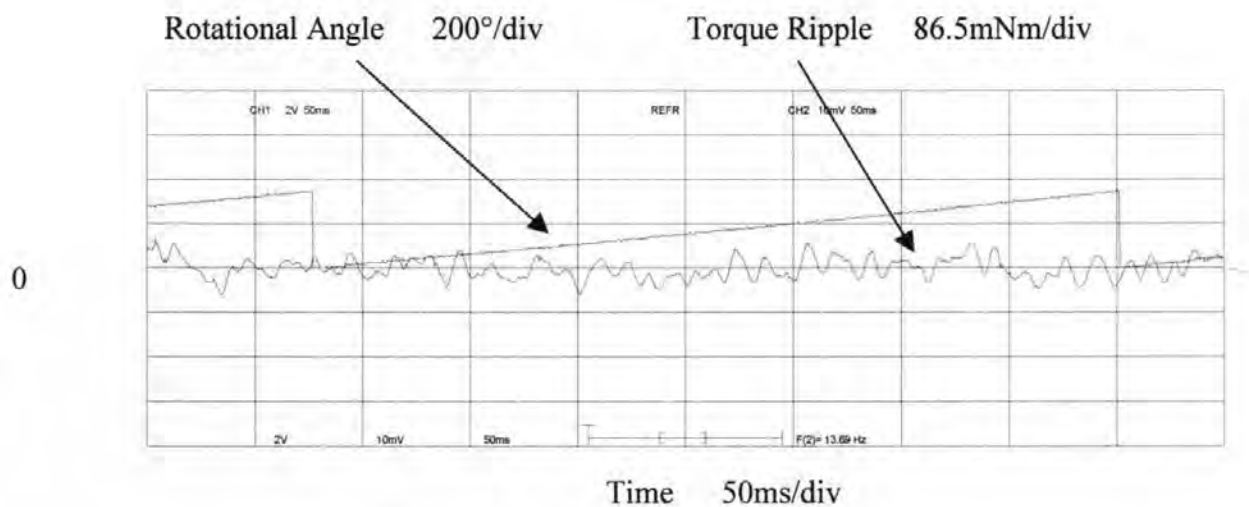
Figure 10.16 Remaining torque ripple at medium load after cogging torque and electromagnetic torque ripple reduction

If figures 10.12 and 10.15 are compared the clear improvement using the reduction algorithm again becomes visible. A further comparison between figures 10.13 and 10.16 reveals the magnitude of the reduction. The remaining peak-to-peak torque ripple is about 0.06 Nm. This represents about 0.8% of the output torque or 0.35% of the full load torque. In other words the torque ripple has been reduced by a factor of 6.

Finally the required phase current is shown.

161

Rotational Angle   200°/div   Current   2.96A/div

Time   50ms/div
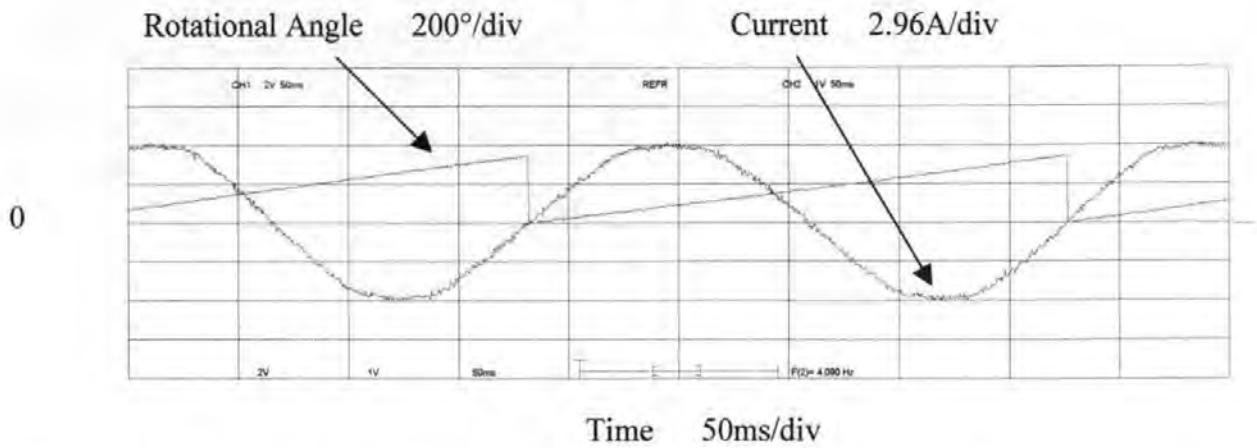
Figure 10.17 Required phase current for cogging and electromagnetic torque ripple reduction at medium loads

Clear deviations from the ideal sinusoidal shape are visible. The peak amplitude of the phase current corresponds to 5.9 A or 4.18 Arms. If figures 10.11 and 10.17 are compared clear differences are obvious. In other words the required correction current is load dependent and changes from light to medium loads.

10.3.3 Torque Ripple Reduction at Full Load

Now the machine is excited with a near full load current of 7.8 Arms. This represents roughly 75% of full load torque. The brake used does not facilitate higher torque levels.

Figures 10.18 and 10.19 show the resulting output torque and the resulting torque ripple respectively for sinusoidal excitation of the machine.

162

Rotational Angle   200°/div   Torque   1.73Nm/div

0°

0Nm

Time   50ms/div
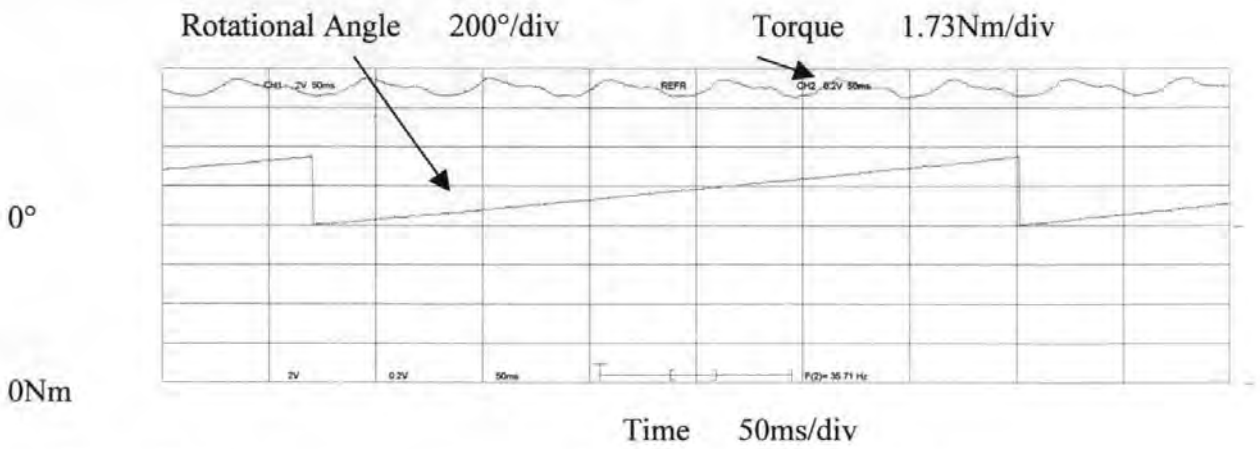
Figure 10.18 Resulting output torque at full load with sinusoidal excitation

Rotational Angle   200°/div   Torque Ripple   173mNm/div

0

Time   50ms/div
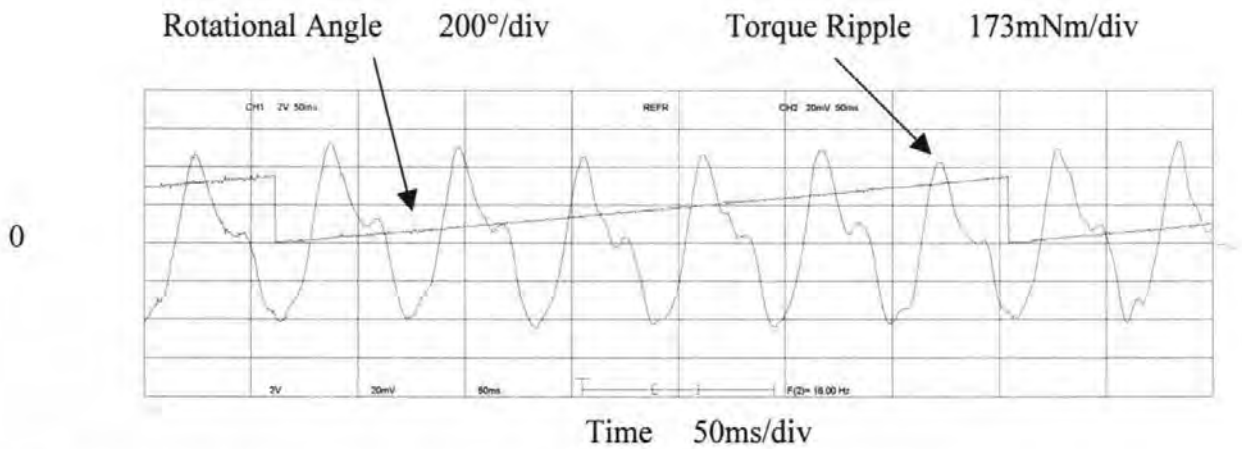
Figure 10.19 Resulting torque ripple at full load with sinusoidal excitation

The dc level of the output torque can be determined to be roughly 13.2 Nm. The peak-to-peak torque ripple, this is cogging plus electromagnetic torque ripple, is about 0.78 Nm or in other words 6% of the output torque level or 4.5% of the full load torque. The percentage of torque ripple referred to the full load torque has therefore more than doubled.

Figure 10.20 shows the remaining electromagnetic torque ripple after the cogging torque reduction has been implemented. Only the torque ripple is shown.

163

Figure 10.20 Remaining electromagnetic torque ripple at full load after implementation of cogging torque reduction

The electromagnetic torque ripple has a peak-to-peak amplitude of about 0.78 Nm. This corresponds to about 6% of the output torque. The cogging torque has no influence any more at this load level and will be fully masked by the electromagnetic torque ripple. The level of electromagnetic torque ripple is comparable to the situation at light loads with roughly 5% of the output torque. However the absolute level has increased and now represents 4.5% of full load torque as opposed to 0.5% before. This is consistent with a load increase by a factor of 8 from light to full loads. If figures 10.8 and 10.14 and 10.20 are compared clear differences in the shape of the electromagnetic torque ripple are visible as predicted before. The scale of figure 10.20 is changed compared to figures 10.8 and 10.14 to allow the recording of the complete torque ripple. The quantitative analysis is undertaken in chapter 11 as mentioned already.

Figures 10.21 and 10.22 show the remaining output torque and torque ripple after the implementation of the reduction algorithm for the electromagnetic torque ripple.

Rotational Angle   200°/div   Torque   1.73Nm/div

0°

0Nm

Time   50ms/div
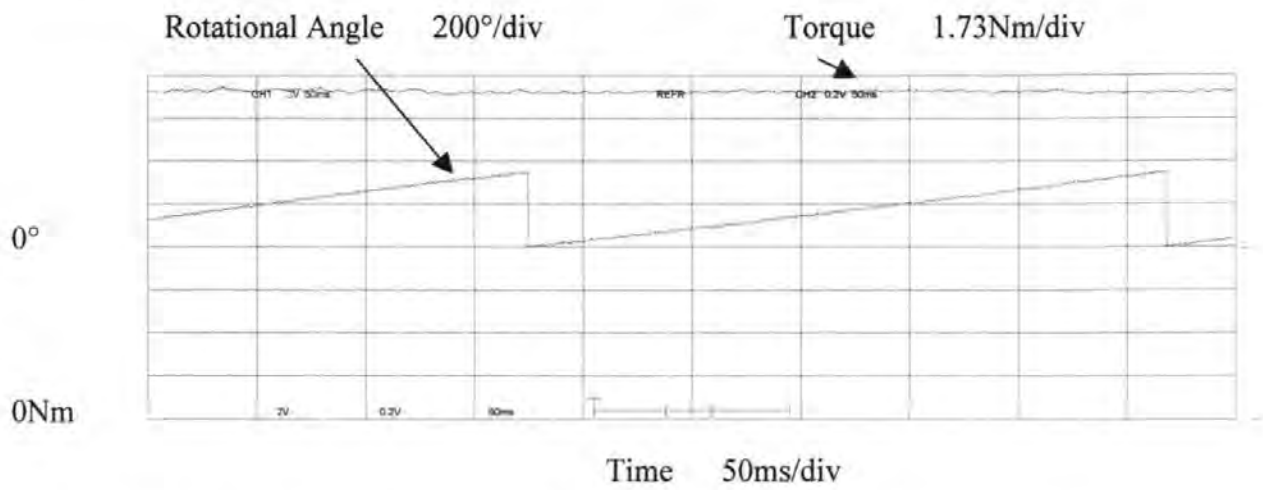
Figure 10.21 Resulting output torque at full load after cogging torque and electromagnetic torque ripple reduction

Rotational Angle   200°/div   Torque Ripple   173mNm/div

0

Time   50ms/div

Figure 10.22 Remaining torque ripple at full load after cogging torque and electromagnetic torque ripple reduction

If figures 10.18 and 10.21 are compared the clear improvement using the reduction algorithm again becomes visible. A further comparison between figures 10.19 and 10.22 reveals the magnitude of the reduction. The remaining peak-to-peak torque ripple is about 0.09 Nm. This represents about 0.65% of the output torque or 0.5% of the full load torque. In other words the torque ripple has been reduced by a factor of 9.

Finally the required phase current is again shown.

165

Rotational Angle   200°/div   Current   5.92A/div

Time   50ms/div
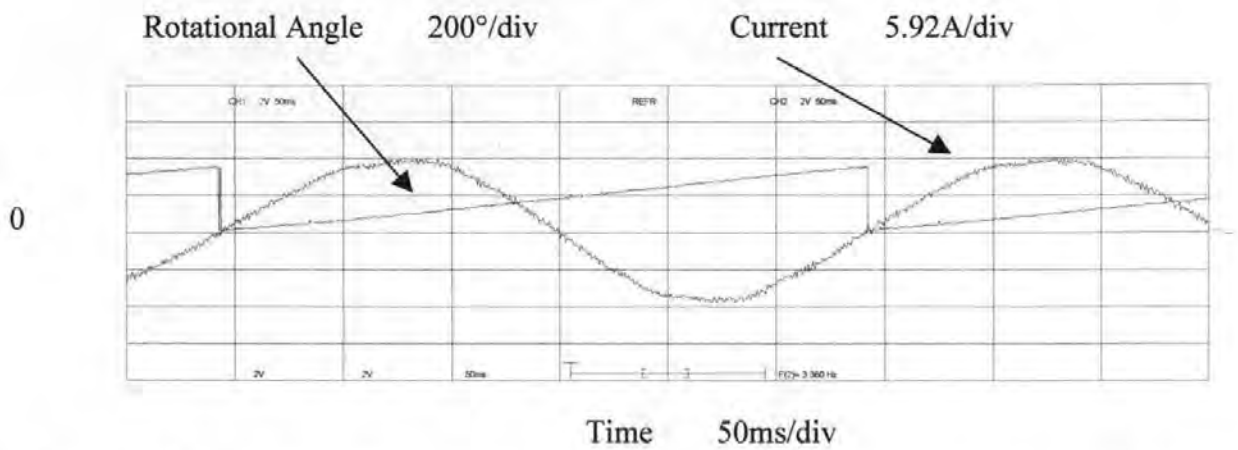
Figure 10.23 Required phase current for cogging and electromagnetic torque ripple reduction at full load

Clear deviations from the ideal sinusoidal shape are again visible. The peak amplitude of the phase current corresponds to 11.1 A or 7.85 Arms. If figures 10.11 and 10.17 and 10.23 are compared clear differences are again obvious. In other words the required correction current is load dependent and has further changed from medium to full loads.

The full set of experimental results is given in appendix A4.

10.3.4 Torque Ripple Reduction Using the Conventional Torque Ripple Reduction Strategy

Finally it is demonstrated that the conventional torque ripple reduction strategy will prove ineffective for the test motor. The correction current derived for the no load situation is used and applied in the full load situation.

Figure 10.24 shows the resulting output torque for this reduction algorithm.

166

Rotational Angle   200°/div   Torque   1.73Nm/div

0°

0Nm

Time   50ms/div
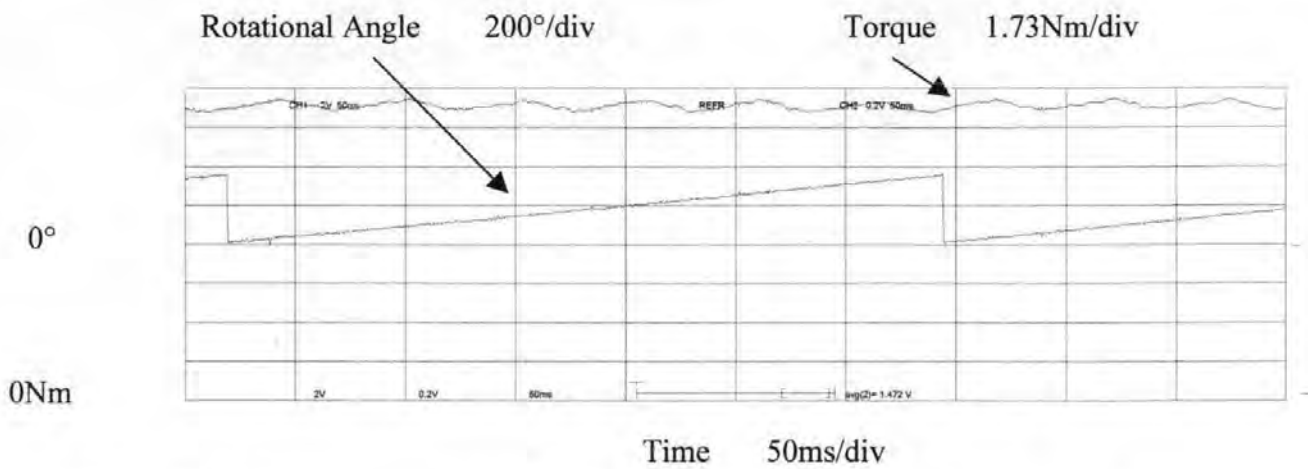
Figure 10.24 Output torque at full load for conventional torque ripple reduction strategy

Figure 10.25 reveals the remaining torque ripple.

Rotational Angle   200°/div   Torque Ripple   173mNm/div

0

Time   50ms/div
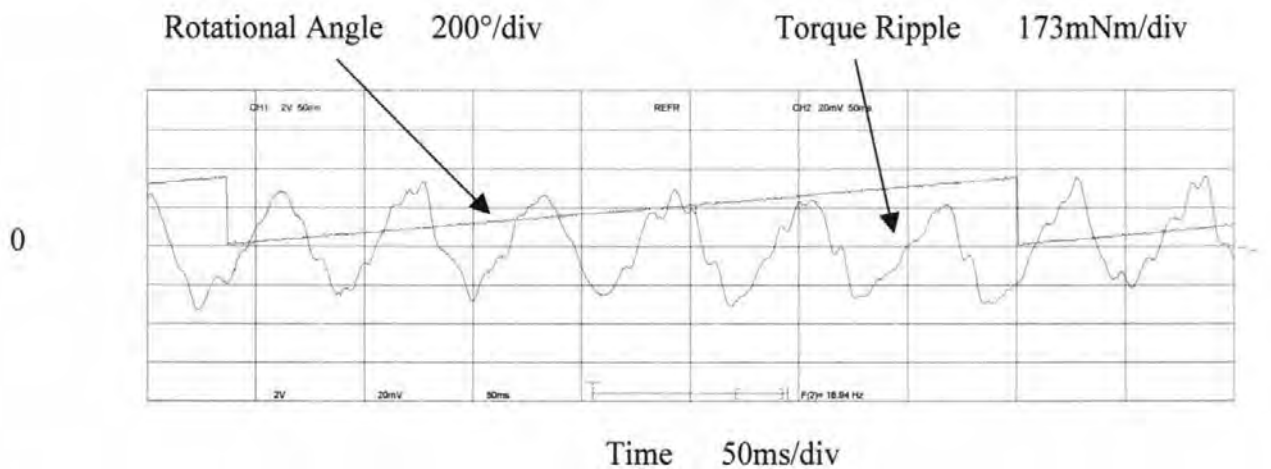
Figure 10.25 Remaining torque ripple at full load for conventional torque ripple reduction strategy

The remaining torque ripple is about 0.52 Nm compared to 0.78 Nm torque ripple with sinusoidal excitation. The torque ripple has been reduced from 6% to 4% of output torque. The conventional torque ripple reduction strategy can therefore be said to be ineffective at high loads. Hardly no reduction in torque ripple is achievable.

Chapter 11 presents a quantitative analysis of the experimental results. The torque ripple is analysed and the load dependence is quantified. Finally a correction formula is derived to allow continuous correction of the torque ripple over the full load range.

Chapter 11   Formula for Reduction of Electromagnetic Torque Ripple

The output torque of the test motor has been measured at discrete load points and not continuously. The recorded torque ripple is strictly speaking only valid for the particular load current. If a very high accuracy over the total load range is required, it would be necessary to record the torque ripple for a high number of different load currents.

This is not desirable as the necessary measurement time will increase. Further each measurement requires analysis in order to determine the correction current. Finally the reduction algorithm would incorporate a large number of data sets.

The recorded set of torque measurements has been analysed in order to find any systematic change with load variation. This would allow derivation of a formula describing the variation of torque ripple over the load range.

The torque ripple has been scaled and the peak-to-peak torque ripple has been calculated for each torque ripple harmonic over the load range. The following matrix shows the individual torque harmonics on the left, the top row shows the average output torque in Nm in ascending order. The torque ripple is shown referred to the output torque level to enable comparison.

$$
T = \begin{vmatrix}
0 & 1.904 & 3.808 & 5.627 & 7.089 & 8.738 & 10.591 & 11.9 & 13.26 \\
6 & 0.026 & 0.032 & 0.036 & 0.036 & 0.04 & 0.044 & 0.046 & 0.05 \\
12 & 0.028 & 0.022 & 0.022 & 0.02 & 0.02 & 0.018 & 0.018 & 0.018 \\
18 & 0.002 & 0.004 & 0.002 & 0.002 & 0.002 & 0.004 & 0.004 & 0.004
\end{vmatrix}
$$

Table 11.1 Matrix T, Torque ripple over output torque level

Figure 11.1 gives a graphical representation of torque ripple over the load range.
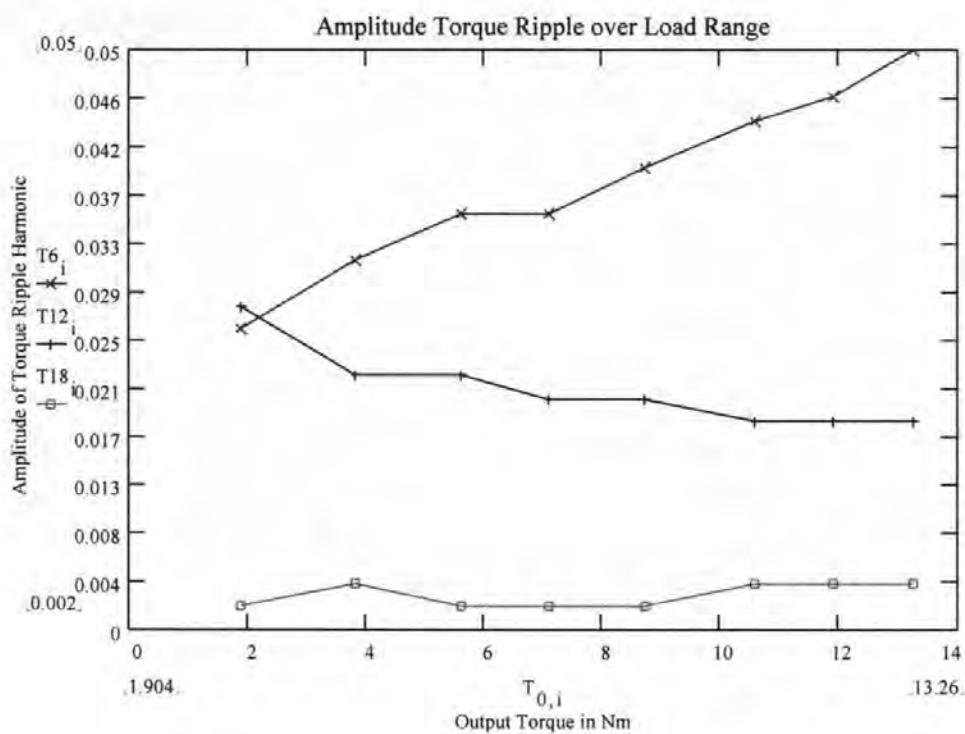
Figure 11.1 Amplitude of peak-to-peak torque ripple for individual torque ripple harmonics over load range

The x-axis denotes the output torque in Nm. The y-axis shows the contribution for individual torque harmonics, peak-to-peak value, referred to the output torque level.

Only relevant torque ripple harmonics are considered. It is clearly visible that the torque harmonic of order 6 is dominant and increases in a linear fashion with load current. The 12th harmonic reduces slightly to a constant value and the harmonic of order 18 remains constant, although being very small, over the load range.

The required correction currents have also been analysed for any systematic variation. The following matrix shows the order of the current harmonics on the left and the rms-value of current on the top row. The current values are scaled to allow comparison.

$$
A = \begin{bmatrix}
0 & 1.12 & 2.24 & 3.31 & 4.17 & 5.14 & 6.23 & 7.00 & 7.80 \\
5 & 0.0075 & 0.0085 & 0.0096 & 0.0108 & 0.0116 & 0.0124 & 0.0124 & 0.0137 \\
7 & 0.0075 & 0.0085 & 0.0096 & 0.0108 & 0.0116 & 0.0124 & 0.0124 & 0.0137 \\
11 & 0.0066 & 0.0067 & 0.0066 & 0.0068 & 0.007 & 0.0067 & 0.0063 & 0.0063 \\
13 & 0.0066 & 0.0067 & 0.0066 & 0.0068 & 0.007 & 0.0067 & 0.0063 & 0.0063 \\
17 & 0.0005 & 0.0004 & 0.0003 & 0.0003 & 0.0008 & 0.0006 & 0.0005 & 0.0004 \\
19 & 0.0005 & 0.0004 & 0.0003 & 0.0003 & 0.0008 & 0.0006 & 0.0005 & 0.0004 \\
23 & 0.0011 & 0.0011 & 0.0011 & 0.0007 & 0.0011 & 0.0012 & 0.0012 & 0.0011 \\
25 & 0.0011 & 0.0011 & 0.0011 & 0.0007 & 0.0011 & 0.0012 & 0.0012 & 0.0011
\end{bmatrix}
$$

Table 11.2 Matrix A, Correction current harmonics over load range

Figure 11.2 depicts a graphical representation of the current harmonics over load.
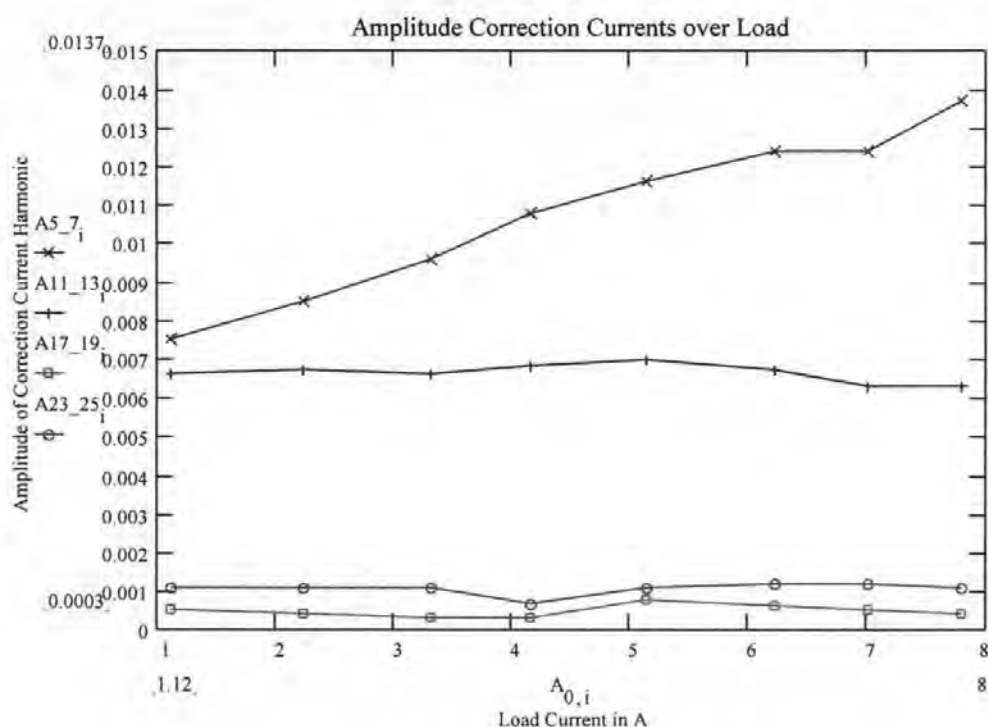
Figure 11.2 Amplitude of correction current harmonics over load range

The x-axis represents the load current (rms-value) in A. The y-axis shows the amplitude value of the individual current harmonics referred to the load current.

The current harmonics form pairs of the order 5 and 7, 11 and 13, 17 and 19, 23 and 25 and so on. The amplitude of these current harmonics is equal as a result of the way Park's transform determines the correction current.

The harmonics of order 5 and 7 show a linear increase, whereas the other harmonics remain constant. Harmonics of order 5 and 7 are mainly responsible for the correction of torque ripple of the order 6. This corresponds to the linear increase of the torque harmonic of order 6 in figure 11.1.

Similarly harmonics of order 11 and 13 mainly influence torque ripple of order 12. These harmonics are therefore constant over the load range.

172

Harmonics of the orders 17 and 19 are responsible for correction of torque harmonics with the order 18. They also remain constant over the load range and are very small in amplitude compared with harmonics of the orders 5 and 7.

Finally harmonics of the orders 23 and 25 correct the remaining torque ripple of higher order. They are again even smaller.

This is only a rough classification concerning the effectiveness of correction current harmonics. As explained in chapter 5, each current harmonic will interact with each back emf harmonic. Each current harmonic will therefore influence more than one torque harmonic. The proper correction current therefore only results if all the mutual influences are taken into account. Park's transform automatically insures that this is the case.

Matrix A and figure 11.2 allow derivation of a formula for the reduction of electromagnetic torque ripple. This formula adds the individual contributions of the correction current harmonics.

$$
\begin{aligned}
I_{correction} = {} & \sin(\theta) + I_5 * \sin(5*\theta + P_5) + I_7 * \sin(7*\theta + P_7) + \\
& I_{11} * \sin(11*\theta + P_{11}) + I_{13} * \sin(13*\theta + P_{13}) + \\
& I_{17} * \sin(17*\theta + P_{17}) + I_{19} * \sin(19*\theta + P_{19}) + \\
& I_{23} * \sin(23*\theta + P_{23}) + I_{25} * \sin(25*\theta + P_{25})
\end{aligned}
\qquad (11.1)
$$

$I_{correction}$ is the required correction current, I_n depicts the magnitude of individual current harmonics, P_n stands for the individual phase contributions and θ represents the angle of rotation.

All contributions remain constant except the contributions made by the 5th and 7th current harmonic. They are determined as follows.

$$I_5 = I * 0.000928 + 0.0065$$
$$= I_7 \qquad (11.2)$$

Here I_5 and I_7 are the magnitude of the current harmonics and I is the rms value of the load current.

$$P_5 = I * 6.51 + 92.7 \qquad (11.3)$$

$$P_7 = I * 6.51 - 87.3 \qquad (11.4)$$

P_5 and P_7 are the phase value of the current harmonics in degrees. I is again the rms value of the load current.

To prove the effectiveness of the derived formula for electromagnetic torque ripple reduction a value between the two measured current loads has been selected. For this value the required correction current has been calculated and tested. The value selected is 4.5 Arms for a typical medium load situation.

Figure 11.3 shows the resulting torque output for sinusoidal excitation.
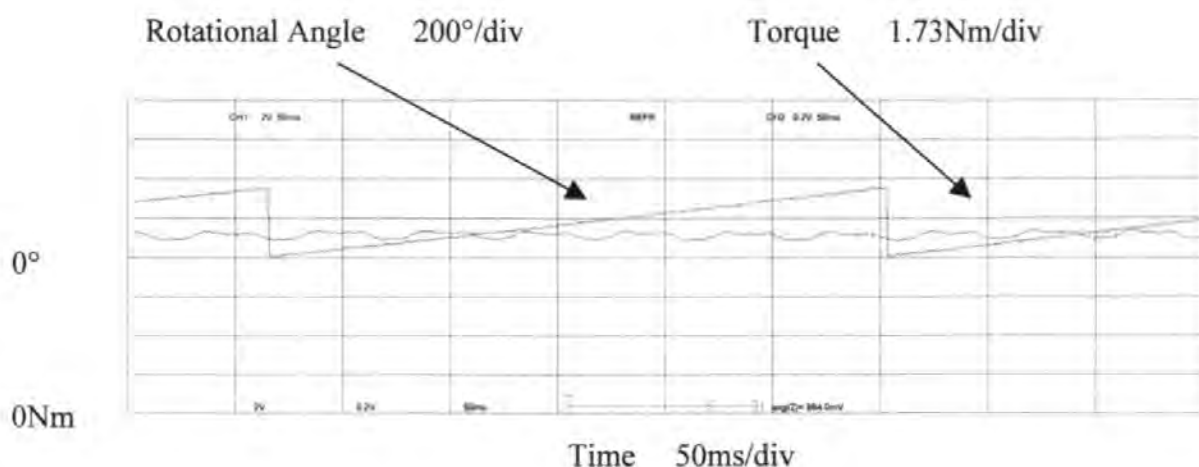
Figure 11.3 Torque output with sinusoidal excitation for load current of 4.5 Arms

Figure 11.4 is the resulting torque ripple after cogging torque correction.

Rotational Angle   200°/div   Torque Ripple   86.5mNm/div

Time   50ms/div
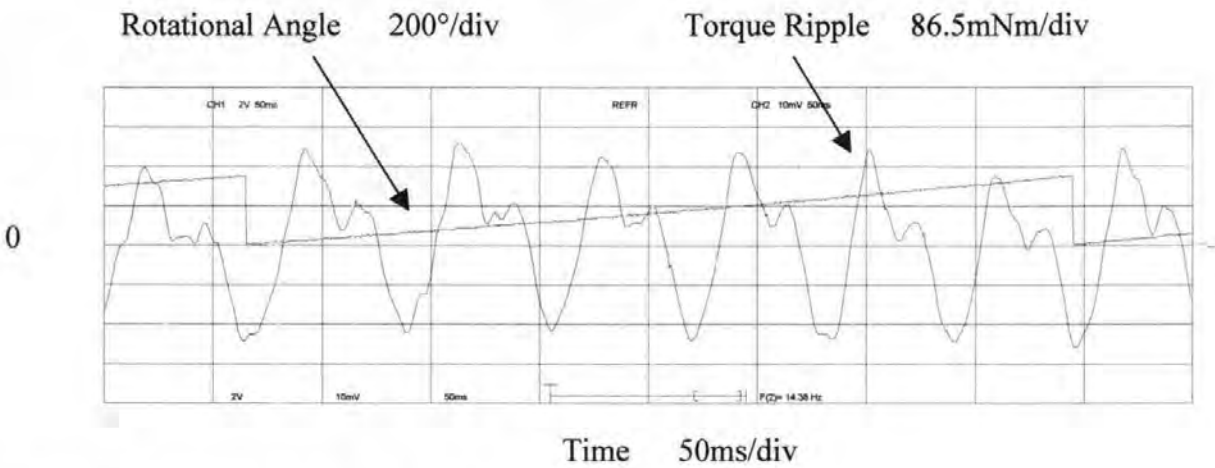
Figure 11.4 Torque ripple after cogging torque correction for 4.5 Arms

Figure 11.5 shows the resulting output torque with the new formula applied.

Rotational Angle   200°/div   Torque   1.73Nm/div

Time   50ms/div
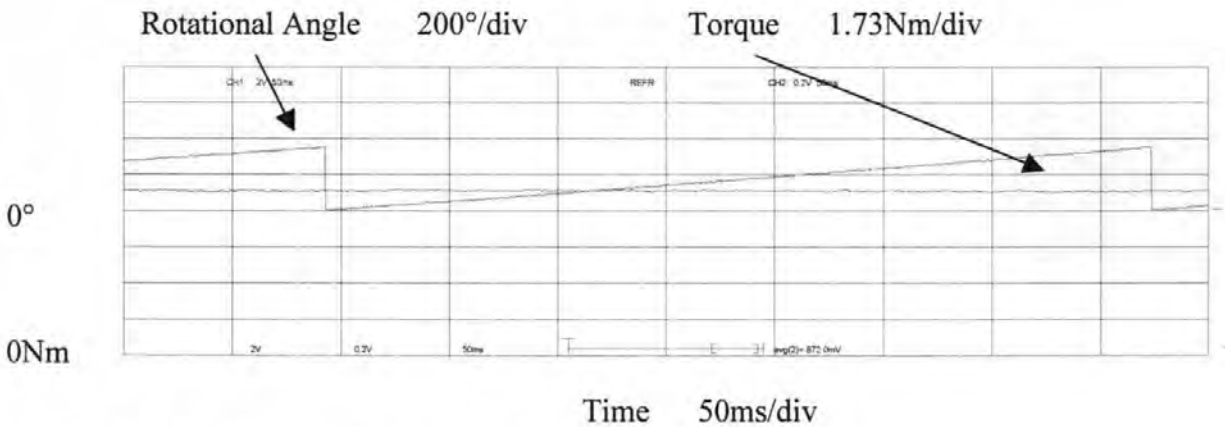
Figure 11.5 Resulting output torque with new formula for 4.5 Arms

Finally figure 11.6 gives the remaining torque ripple after reduction.

175

Rotational Angle   200°/div   Torque Ripple   86.5mNm/div

0

Time   50ms/div
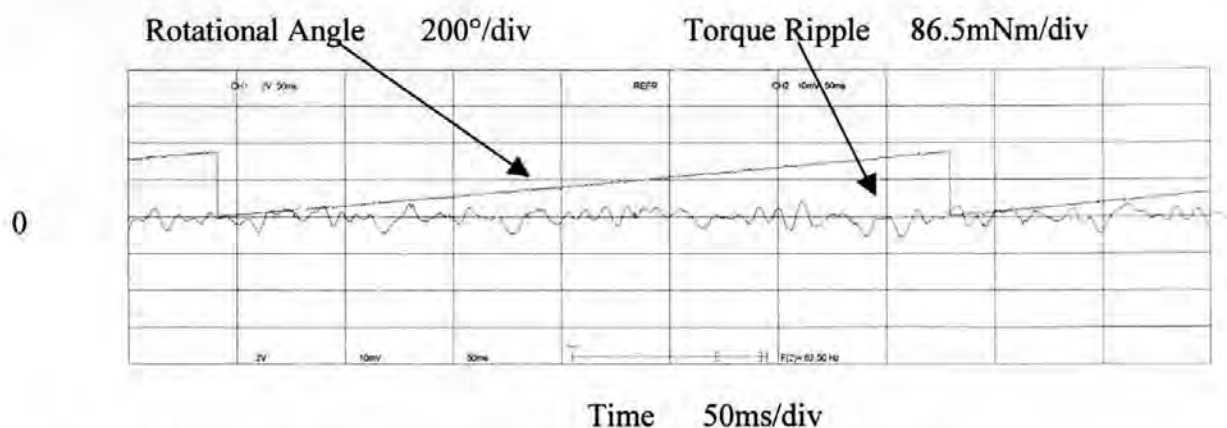
Figure 11.6 Remaining torque ripple after reduction with new formula

If figures 11.4 and 11.6 are compared the clear reduction on torque ripple becomes visible. The torque ripple has been reduced by a factor of 9. This is even better than the reduction achieved previously from the measurement of torque ripple. The formula can therefore be said to be effective in reducing electromagnetic torque ripple.

There are also additional advantages attached to the use of the new formula. The formula allows online calculation of correction currents if the correct load current is sensed. This results in higher correction accuracies over the load range and reduces the required memory otherwise used for storing correction data.

The correction formula also allows a first, preliminary insight into the structure of torque ripple for the test motor. The torque characteristic for low load currents is determined by the winding arrangement on the stator and the flux shaping of the magnets on the rotor. It is therefore given by geometric factors. However for medium and high load currents the armature reaction will act to superimpose flux alterations onto this geometric arrangement. As already discussed the 6th harmonic of torque increases in a linear fashion, whereas all higher harmonics remain more or less constant over the load range. This can be explained

176

by the fact that at any given time 6 stator teeth will be covered by one pole pair on the rotor. The currents through the 6 stator slots will produce a torque disturbance of order 6, which will increase in magnitude with increasing current level. Higher torque harmonics will remain uninfluenced by these flux changes.

Chapter 12 lists the achievements of this work, and highlights areas of possible future research.

Chapter 12   Conclusions

12.1   Achievements

An extensive literature review has been undertaken, which covers both fundamental papers dealing with the production of torque ripple and first proposals for torque ripple reduction and more recent papers, which suggest a variety of different torque ripple reduction strategies.

Based on the literature review the production of torque ripple, both cogging and electromagnetic torque ripple, has been investigated in depth. Computer simulations have been used to highlight the structure of torque ripple and to illustrate the interaction of the individual components, which lead to the production of torque ripple. The complexity of the torque ripple phenomenon has been demonstrated.

Different torque ripple reduction strategies have been described and usefulness, ease of implementation and validity of assumptions have been assessed. A torque ripple reduction strategy using Park's transform has been identified as the most promising reduction strategy. The unified machine theory has been checked to clarify the theory behind Park's transform; in particular assumptions made and general validity of the theory. It has been found that Park's transform can be applied to both brushless dc and brushless ac machines without any limitations, as long as the instantaneous description of quantities is used. Further the best implementation for this reduction strategy has been identified to allow the development of effective reduction algorithms.

The torque ripple reduction strategy based on Park's transform has been extended to include the effect of armature reaction. A novel adaptive torque ripple reduction algorithm has been designed. The ineffectiveness of the conventional approach, using no load back emf values, has been demonstrated.

A novel torque ripple reduction strategy has been suggested, which uses measurements of the torque ripple directly instead of measurements of back emf waveforms. The new strategy reduces implementation time and allows higher accuracies for torque ripple reduction.

An experimental system consisting of the drive and a control-logic has been designed and implemented. The hardware allows high measurement resolution, quick response times and provides sufficient capacity for extended control strategies. The software allows great flexibility for implementing new control strategies. The system has been tested and was found to provide very accurate results.

Extensive measurements from the experimental system show the validity of the novel torque ripple reduction strategy. They also show the effectiveness of the adaptive torque ripple reduction strategy.

The experimental results have allowed derivation of a formula to cover all load situations. This formula makes it possible to increase the reduction accuracy further and enables improved real time implementation of the torque ripple reduction algorithm. Further it allows reduction of the required memory consumption of the reduction algorithm, thus freeing this memory for future applications like dynamic compensation.

12.2 Further Work

The torque ripple reduction method presented here can be used to overcome manufacturing imperfections in brushless machines thus removing the cost for precise manufacturing tools.

Future designs of controllers could "build" their own correction formula during set-up runs, providing a motor specific torque ripple correction.

The work presented here also forms the basis for the development of intelligent dynamometers for motor test beds. Conventional dynamometers allow static load control with limited accuracy. A dynamometer using the proposed torque ripple reduction strategy could provide much better torque control accuracies.

An almost torque ripple free torque production is also required for dynamometers with dynamic load profiles, which could allow positive and negative torque production. This makes it possible to do intensive in-house testing of motors before they are installed on site. Thus speeding up the commissioning process and reducing set-up costs.

The new improved torque ripple reduction strategy using direct measurements of the torque ripple is universally applicable for any kind of brushless machine. Similarly the adaptive torque ripple reduction strategy is also universally applicable. However is has been developed using measurements from the test motor. Measurements for further brushless machines should be taken and the adaptive torque ripple reduction strategy should be applied to these machines. This would allow a closer examination of the effect of armature reaction on brushless machines. Are there pronounced differences between standard brushless motors? Perhaps it would be possible to find a general solution to account for the armature effect.

Further saturation in the armature requires a thorough analysis. Could saturation become a dominant effect on the torque ripple for higher current loads or is it not very pronounced for other machine designs? If the latter is the case some designs could be identified to avoid the effect of saturation on torque ripple.

On a more general level the torque ripple of a higher number of different brushless machines should be recorded and analysed. The analysis might lead to new knowledge concerning the production of torque ripple with emphasis on individual torque harmonics as opposed to older investigations, which mainly highlight the quantitative aspect. This analysis could lead to design recommendations.

The torque ripple reduction strategies developed here are designed for reducing torque ripple for the static load case. They work well if the machine has reached a steady state condition. This is of course the normal operating condition for most motors. It would however be interesting to investigate the dynamic behaviour of the machines. What happens to the torque output if sudden load changes occur? Does the torque ripple increase during these dynamic transitions or remain at the static level? How does the transition speed affect the torque ripple? Perhaps it would be possible to find an optimum between transition speed and torque ripple level. These questions require detailed investigations.

Appendices

A1   Motor Data Sheets

Motor used is: 142DSC170300

MOTOR DATA
Brushless Servo

		75DSA013300	*75DSB023300	75DSC031300	*75DSD040300	95DSA025300	95DSB043300	*95DSC060300	95DSD076300	*95DSE092300	115DSA045300	115DSB074300	*115DSC105300	*115DSD13...
Continuous Stall Torque	Lb Ins	11.5	20.4	27.4	35.4	22.1	38.1	53.1	67.3	81.4	38.9	65.5	92.9	
	Nm	1.3	2.3	3.1	4.0	2.5	4.3	6.0	7.6	9.2	4.5	7.4	10.5	
Rated Torque	Lb Ins	10.6	18.6	24.8	31.9	20.4	34.5	47.8	61.1	73.5	36.3	59.3	84.1	
	Nm	1.2	2.1	2.8	3.6	2.3	3.9	5.4	6.9	8.3	4.1	6.7	9.5	
Peak Torque	Lb Ins	34.5	61.1	82.3	106.2	66.4	114.2	159.3	201.8	244.3	119.5	196.5	278.8	
	Nm	3.9	6.9	9.3	12.0	7.5	12.9	18.0	22.8	27.6	13.5	22.2	31.5	
Rated Power	kW	.4	.7	.9	1.2	.8	1.3	1.7	2.2	2.6	1.3	2.1	3.0	
Continuous Stall Current	Arms	.9	1.5	2.0	2.5	1.6	2.7	3.8	4.8	5.8	2.9	4.7	6.6	
Phase to Phase Resistance	Ohms	96	30	16.5	12.1	36	11.5	6.5	4.1	3.0	18.9	5.9	3.0	
Phase to Phase Inductance	mH	144	70.3	48.7	36.5	88.6	44.3	30	22	16.3	56.5	28.7	19.3	
Thermal Time Constant	Sec	1315	1500	1431	1587	1422	1618	1800	1997	2178	1436	1614	1792	
Rotor Inertia (J)	Lb Ins Sec²	.00053	.00097	.00142	.00177	.00133	.00230	.00327	.00434	.00531	.00372	.00628	.00876	.0
	Kgm² x 10⁻³	.06	.11	.16	.2	.15	.26	.37	.49	.6	.42	.71	.99	
Weight	Lbs	6.6	8.1	9.7	11.2	11.0	13.4	15.8	18.3	20.9	14.3	18.0	21.8	
	Kgms	3.0	3.7	4.4	5.1	5.0	6.1	7.2	8.3	9.5	6.5	8.2	9.9	
Recommended Servo Amplifier	Cont.	DB140	DB140	DB140	DB140	DB140	DB140	DB220	DB420	DB420	DB140	DB420	DB420	D
	Peak	DB140	DB140	DB220	DB220	DB140	DB220	DB420	DB420	DB420	DB220	DB420	DB600	D

ADDITIONAL MOTOR DATA (All Models)

Rated Speed: 3000 RPM (2000 and 6000 RPM windings available)
Torque Constant: (K_t) 14.2 Lb Ins/A_{rms} (1.6 Nm/A_{rms})

Ambient Temperature: 25°C
Voltage Constant: (K_e) 98V/1000 RPM

CONTINUOUS STALL TORQUE
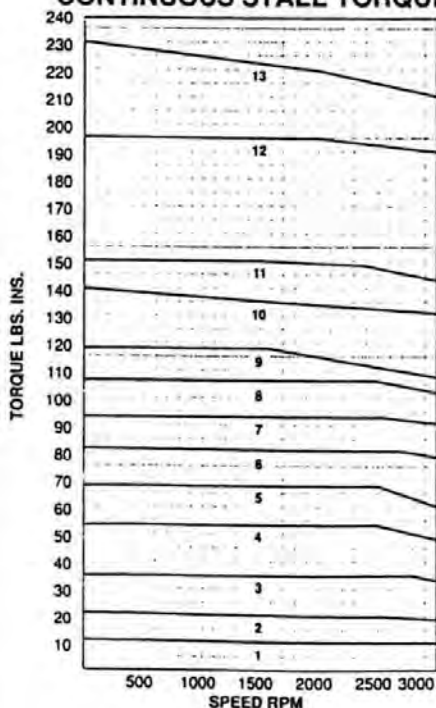
RATED CONTINUOUS STALL TORQUE

	MOTOR	SERVO AMPLIFIER	
13	*142DSE260300	DB750	
12	*142DSD220300	DB750	
11	*142DSC170300	DB600	
10	115DSE157300	DB600	
9	*115DSD133300	DB420	
8	142DSB120300	DB420	
7	*115DSC105300	DB420	
6	*95DSE092300	DB420	
5	95DSD076300 115DSB074300 142DSA070300	DB220 DB420 DB220	} SIMILAR CURVES
4	*95DSC060300	DB220	
3	*75DSD040300 95DSB043300 115DSA045300	DB140 DB140 DB141	} SIMILAR CURVES
2	*75DSB023300 95DSA025300 75DSC031300	DB140 DB140 DB140	} SIMILAR CURVES
1	75DSA013300	DB140	
	* denotes preferred sizes		

ISO 9002 APPROVAL

	*142DSB120300	*142DSC170300	*142DSD220300	*142DSE260300
62.0	106.2	150.5	194.7	230.1
7.0	12.0	17.0	22.0	26.0
55.8	95.6	135.4	175.2	205.3
6.3	10.8	15.3	19.8	23.2
85.9	318.6	451.4	584.1	690.3
21.0	36.0	51.0	66.0	78.0
2.0	3.4	4.9	6.3	7.4
4.4	7.5	10.7	13.8	16.3
8.4	2.42	1.2	.87	.63
42.2	20.8	13.3	10.4	8.0
2093	2313	2548	2700	3003
0752	.01292	.01832	.02372	.02921
.85	1.46	2.07	2.68	3.3
24.0	29.0	34.1	39.2	45.1
10.9	13.2	15.5	17.8	20.5
B220	DB420	DB600	DB750	DB750
B420	DB600	DB750	DB750	DB750

* denotes preferred sizes

MOTORS

The *DutymAx DS Series Servo Motors* have excellent shaft power to size ratio for dynamic response. This is achieved by:

- *Superior design of motor magnetic circuit.*
- *Use of high energy Samarium Cobalt magnets.*
- *Use of low inertia laminated rotor.*
- *Specially constructed high slot filled stator.*

A Control Techniques resolver is used for brushless electronic commutation. This ensures high reliability. The resolver is mounted directly onto the motor shaft, giving an accurate measurement of velocity and position for the DigitAx drive system. DS Series Servo motors are available in four frame sizes: 75, 95, 115 and 142 with a torque range of 11.5 Lb. Ins. (1.3 Nm) to 230 Lb. Ins. (26 Nm). Rated speed is 3000 RPM. Optional 2000 and 6000 RPM windings are available.

MAIN FEATURES

- High energy Samarium Cobalt magnets.
- Low inertia laminated rotor.
- Modular rotor design — modules keyed to shaft.
- Class H insulation.
- High thermal dissipation.
- Thermal overload protection.
- Rugged preloaded bearing system.

- Rotor assembly balanced to ISO 1940 grade 6.3.
- Rear shaft extension for additional feedback devices.
- Resolver commutation.
- Front shaft lip seal for windings up to 3000 RPM.
- Tach and Encoder options.
- Optional holding brake.

DESIGN BENEFITS

- High output for size and weight.
- IP65 standard up to 3000 RPM.
- Mating connectors standard.
- Parking brake retrofittable.
- Modular construction for cost effective range.
- Four position orientation Terminal Box.
- Electrical characteristics optimized to DigitAx Drives.
- Flexibility to add additional feedback devices.
- Thermal protector as standard.
- Ease of assembly to precision gearboxes.

BRAKE SPECIFICATIONS				
MOTOR FRAME SIZE	75DS	95DS	115DS	142DS
Holding Torque Lb.Ins.	17.7	44.3	106.2	177.0
Current (Amps)	.58	1.25	1.25	1.25
Inertia Lb.In.Sec.^{2}	.000028	.000133	.000454	.004288
Weight Lbs.	.66	1.76	1.98	5.50

Note: 24 VDC Brake

PEAK TORQUE
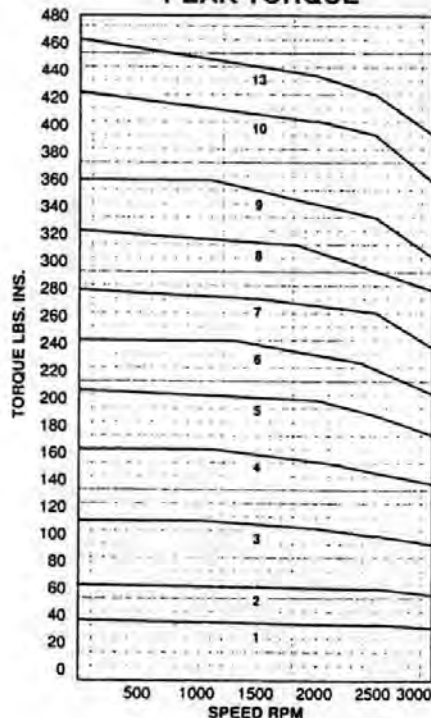
PEAK TORQUE		
	MOTOR	SERVO AMPLIFIER
13	*142DSE260300	DB750
12	*142DSD220300	DB750 } SIMILAR CURVES
11	*142DSC170300	DB750
10	115DSE157300	DB750
9	*115DSD133300	DB600
8	142DSB120300	DB600
7	*115DSC105300	DB600
6	*95DSE092300	DB420
5	95DSD076300	DB420 } SIMILAR CURVES
	115DSB074300	DB420
	142DSA070300	DB420
4	*95DSC060300	DB420
3	*75DSD040300	DB220 } SIMILAR CURVES
	95DSB043300	DB220
	115DSA045300	DB220
2	*75DSB023300	DB140 } SIMILAR CURVES
	95DSA025300	DB140
	75DSC031300	DB220
1	75DSA013300	DB140
	* denotes preferred sizes	

A2 Resolver Circuit

A3 Torque Transducer

A3.1 Calibration Certificate for Torque Transducer

CALIBRATION CERTIFICATE

Calibration of Transducer

Date: 18 November 1996

Customer:
Norcroft Dynamics Limited
Fellows House
Royce Close
West Portway Industrial Estate
Andover
Hants SP10 3TS

Customer Order Ref: RDAUTO/11518   AML Order Ref: S151096E
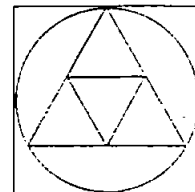
APPLIED MEASUREMENTS LIMITED
6 VULCAN HOUSE
CALLEVA PARK
ALDERMASTON
BERKS
RG7 8PA
UK
Tel: (+44) 0118 981 7339
Fax: (+44) 0118 981 9121
e-mail: info@appmeas.co.uk
Internet: www.appmeas.co.uk

<u>Calibration Results:</u>

Transducer Type:	Act Load Junior-25kg
Serial No:	13833
Load Rating:	25kg
Proof Rating:	150%
Ultimate Rating:	200%
Sensitivity:	1.772mV/V
Zero Balance:	-0.079mV @ 10V
Non-linearity:	0.022%FS
Hysteresis:	0.011%FS
Thermal Sensitivity Shift:	<0.01%/°C
Thermal Zero Shift:	<0.01%/°C
Compensated Temp Range:	0°C to +60°C
Operating Temp Range:	-20°C to +65°C
Supply Voltage:	10.00Vdc
Bridge Resistance Input:	350Ω nominal
Output:	350Ω nominal
Insulation Resistance:	>10000 megohms at 50Vdc

Electrical Connections:

Red	+ve excitation
Green	+ve signal
Yellow	-ve signal
Blue	-ve excitation

Applied Measurements Limited hereby certifies that the above item has been inspected, tested and calibrated in all respects with the requirements of the customer's order.

Directors:
P.A.LEWIS
S.C.GOTELEE

A3.2 Torque Transducer Circuit
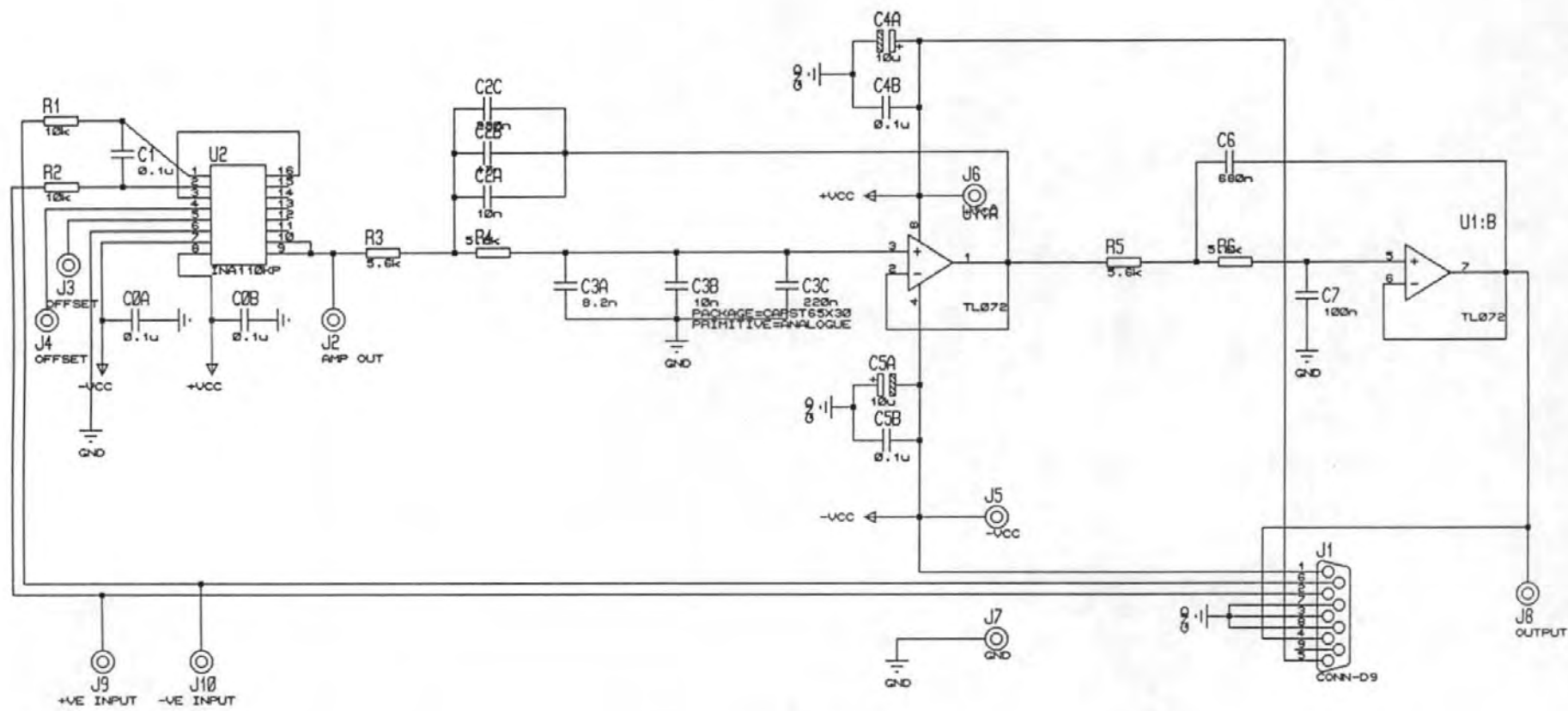
A4   Full Set of Experimental Results
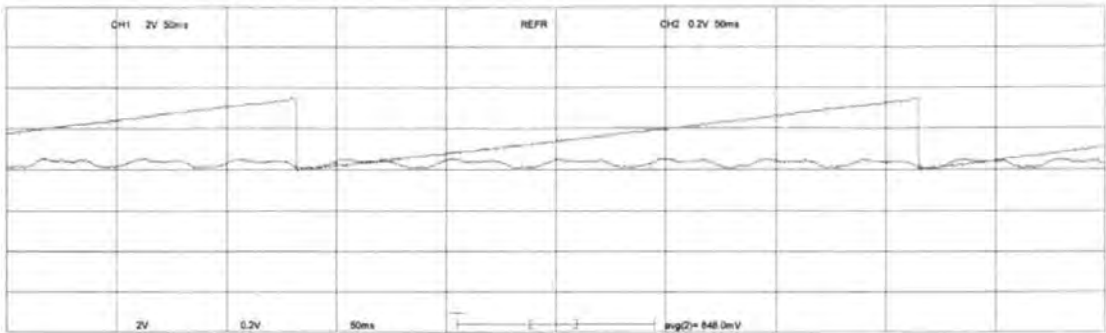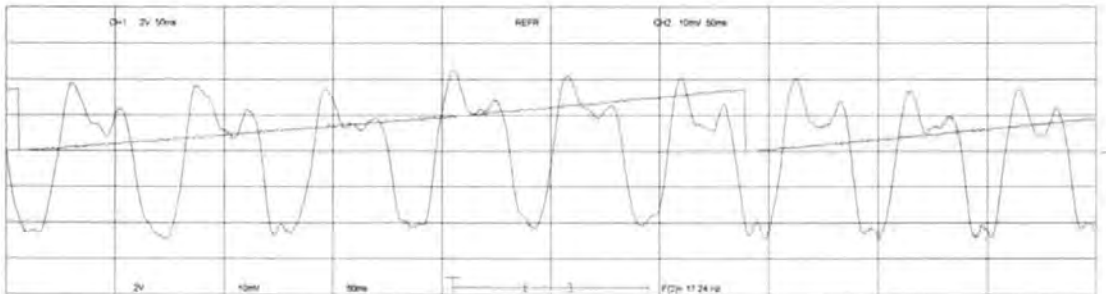
Experimental Results

Excitation : 0.1 Arms
Clockwise Rotation
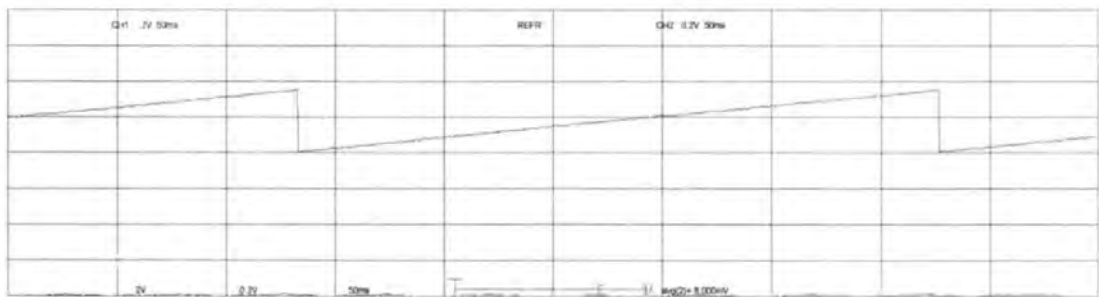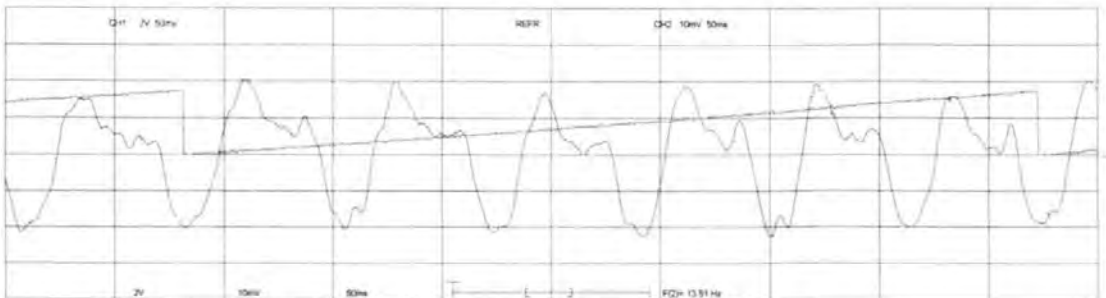
1. Sinusoidal Excitation
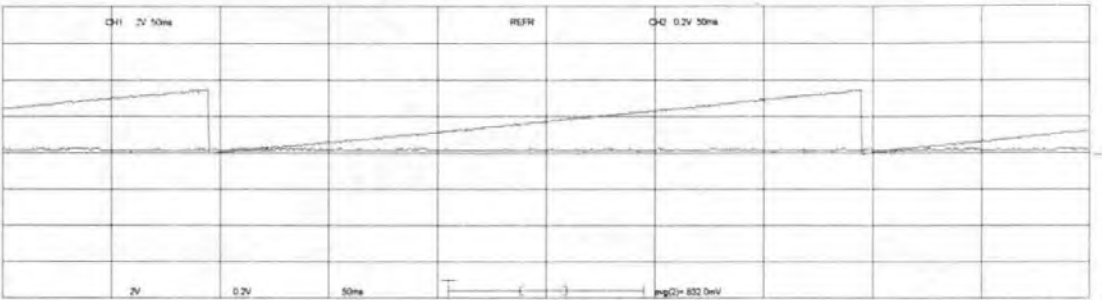
a. Resulting Output Torque

b. Resulting Torque Ripple
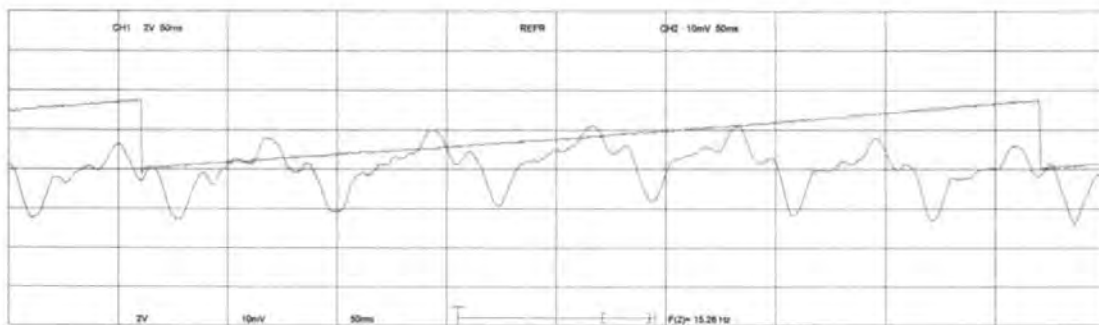
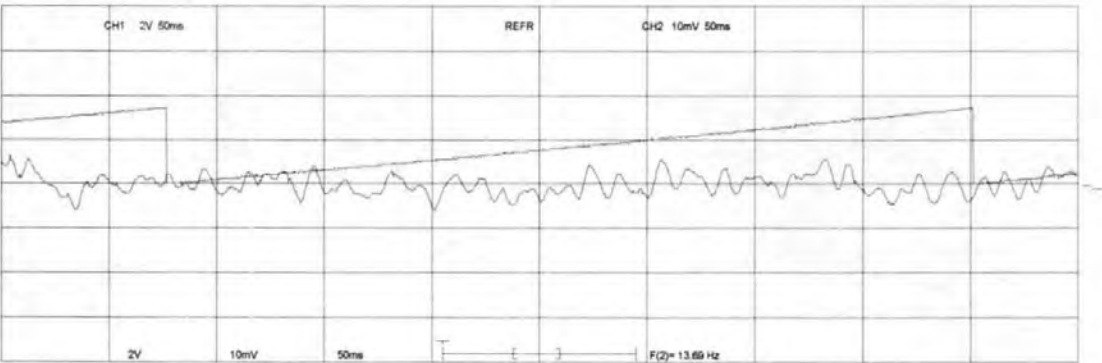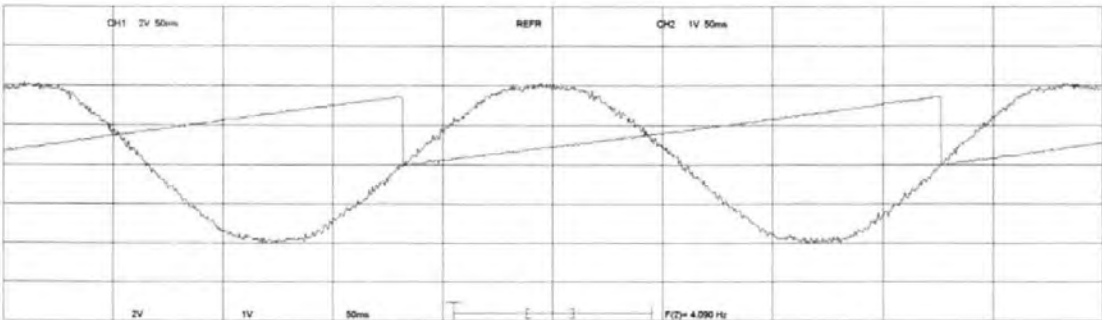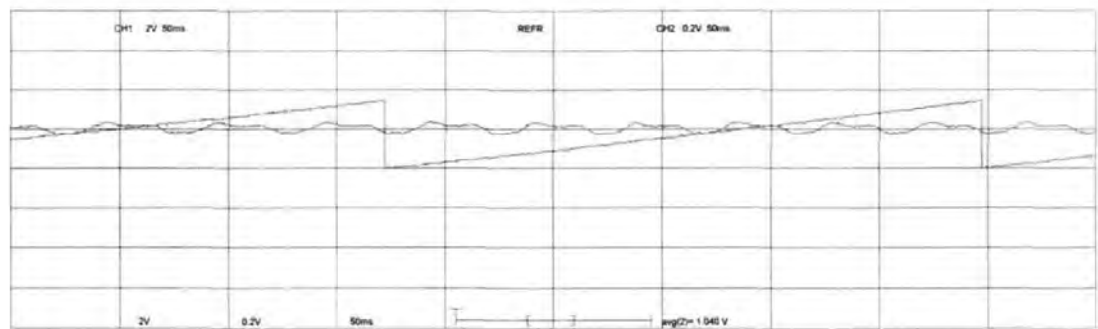## 2. Sinusoidal Excitation with Cogging Torque Correction

a. Resulting Output Torque
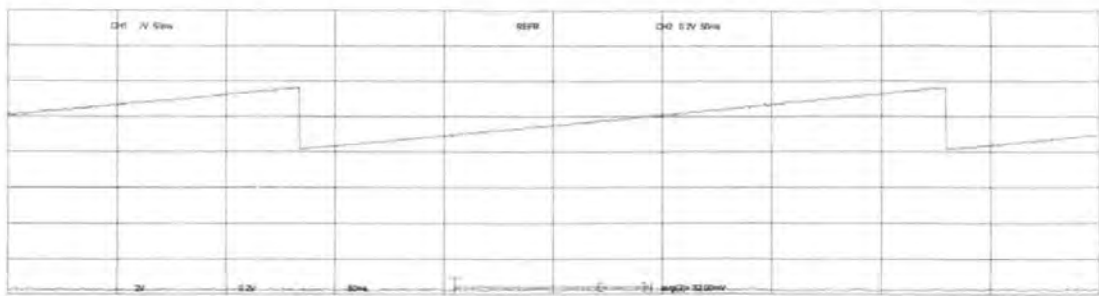
b. Resulting Torque Ripple
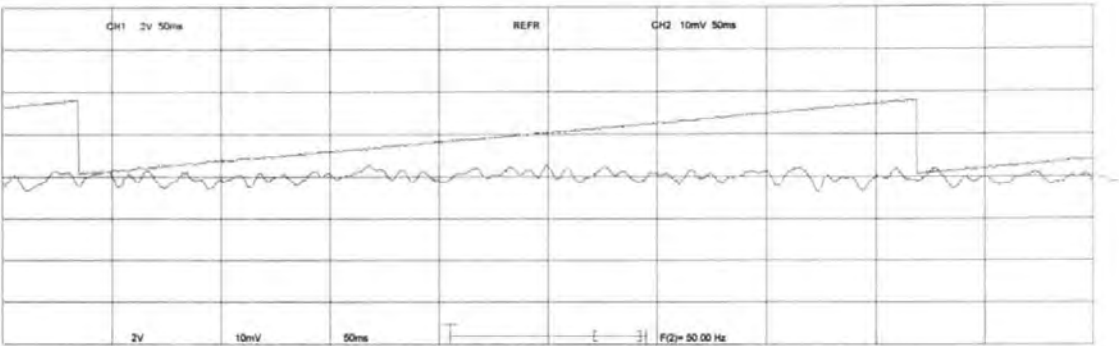
c. Current Waveform Phase A
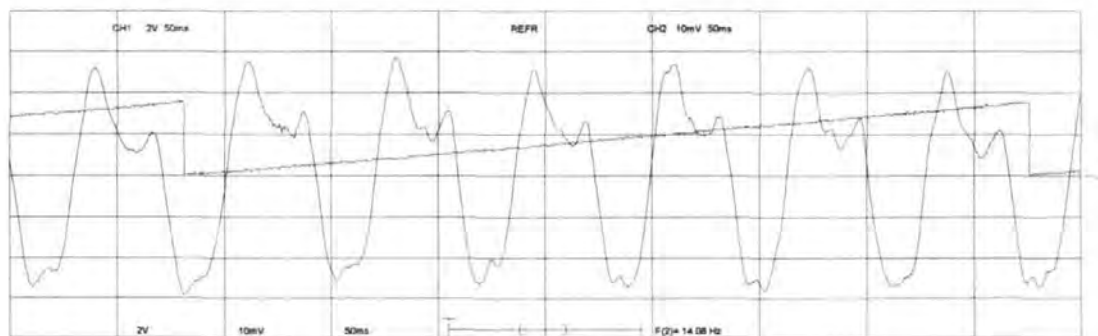
Experimental Results

Excitation : 1.12 Arms
Clockwise Rotation
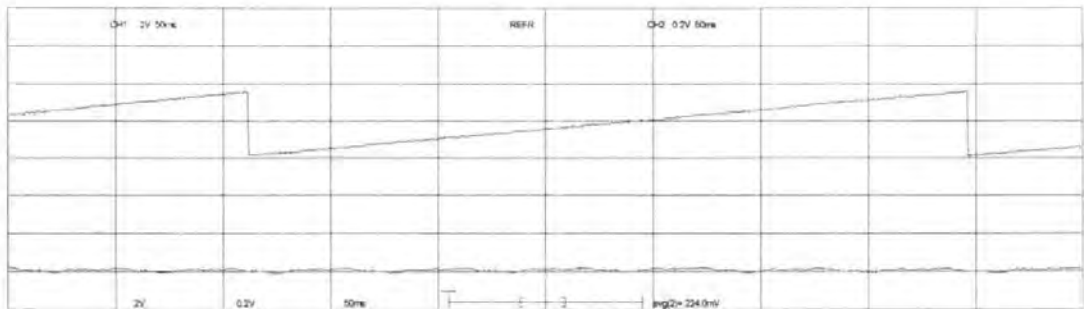
1. Sinusoidal Excitation
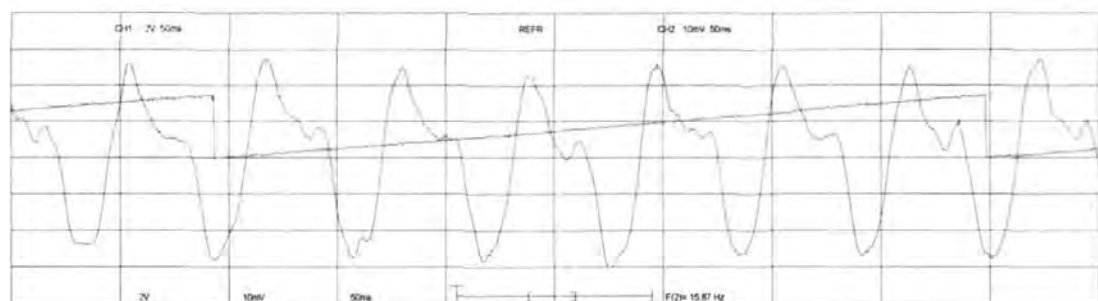
a. Resulting Output Torque
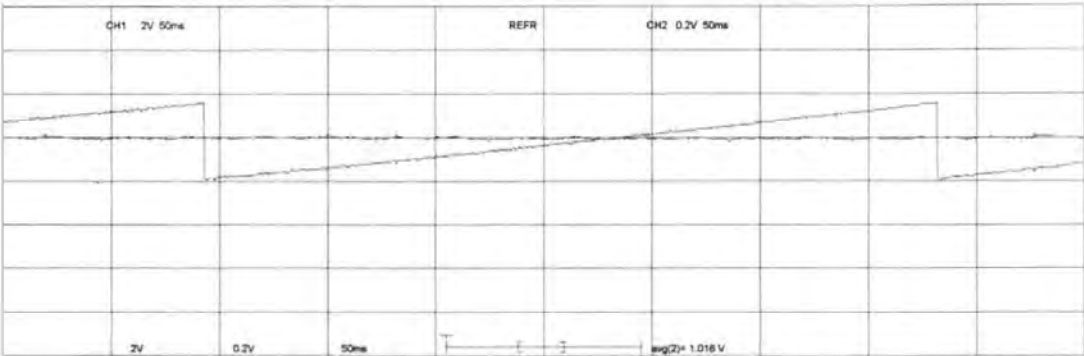

b. Resulting Torque Ripple

2. Sinusoidal Excitation with Cogging Torque Correction
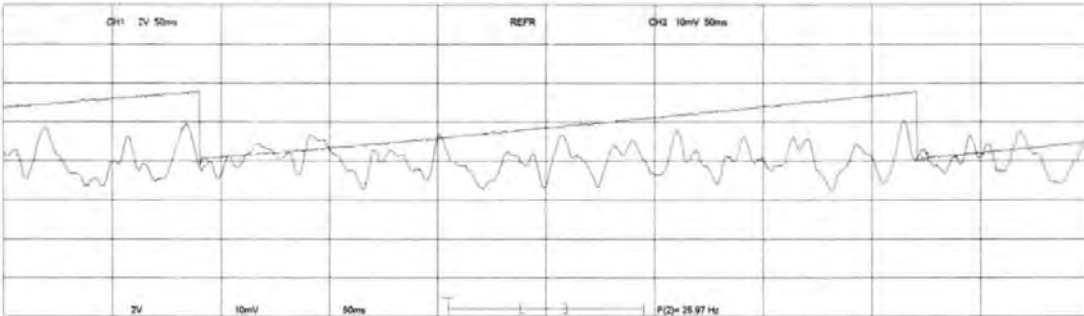
Resulting Torque Ripple

197
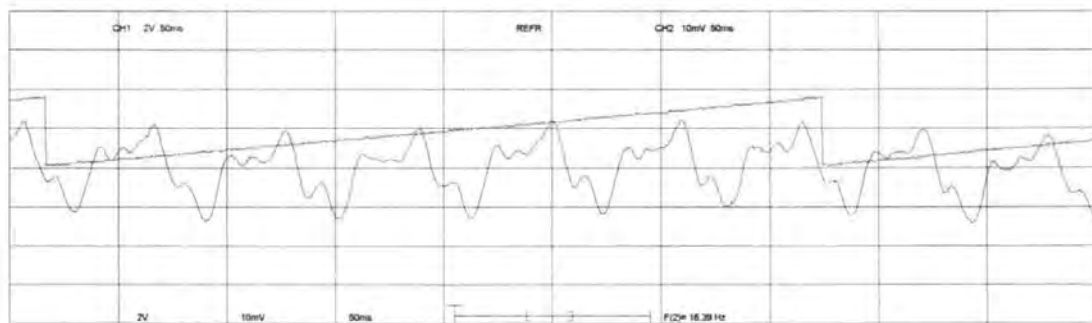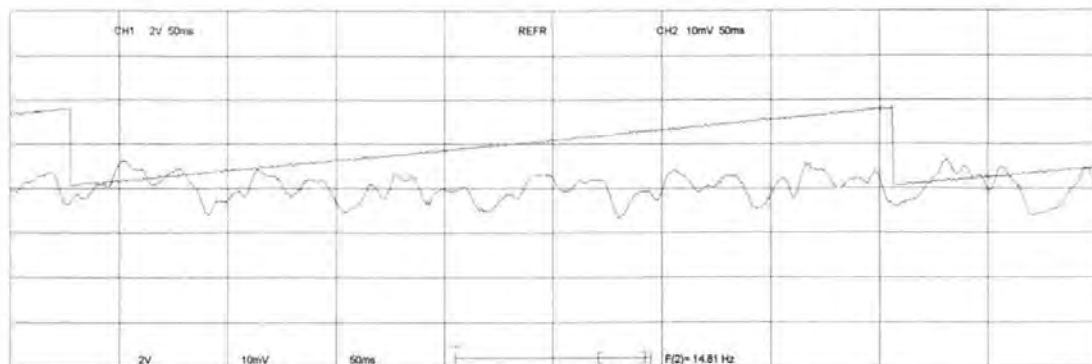
3. Sinusoidal Excitation with Cogging Torque and Electromagnetic Torque Correction

a. Resulting Output Torque
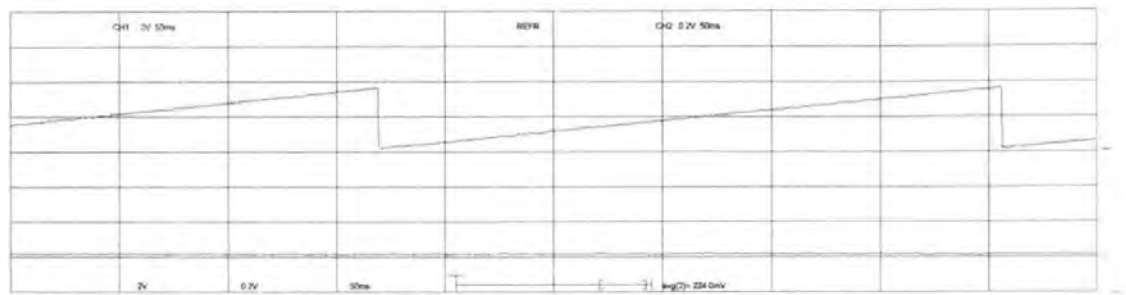
b. Resulting Torque Ripple
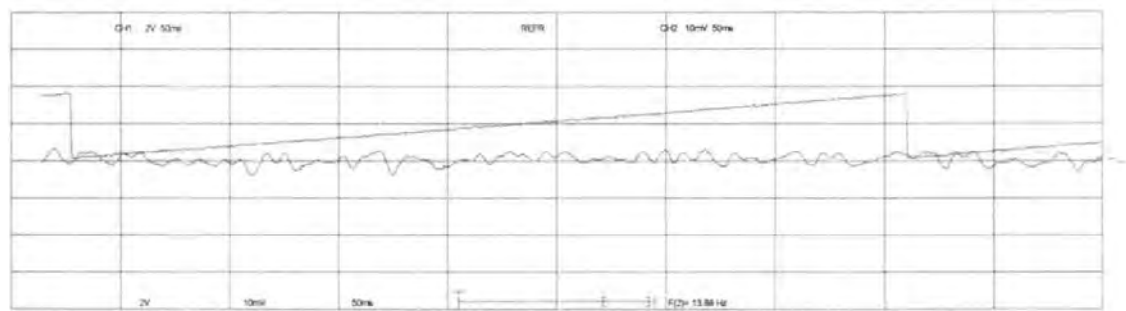
c. Current Waveform Phase A
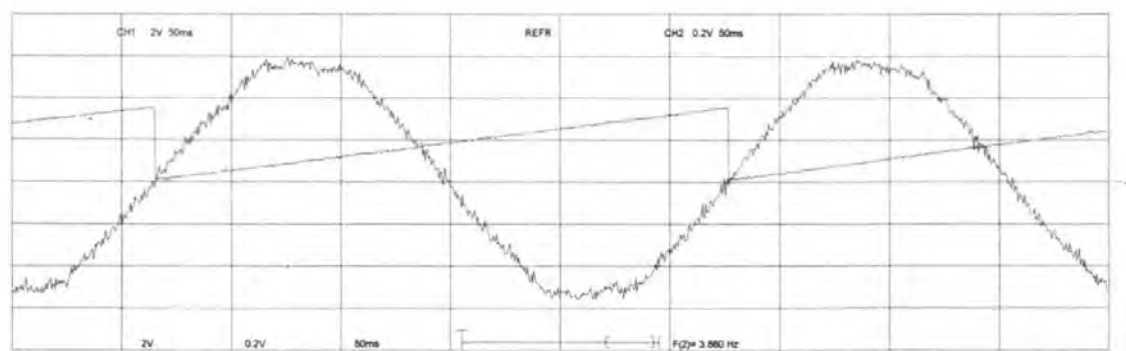
Experimental Results

Excitation : 2.24 Arms
Clockwise Rotation
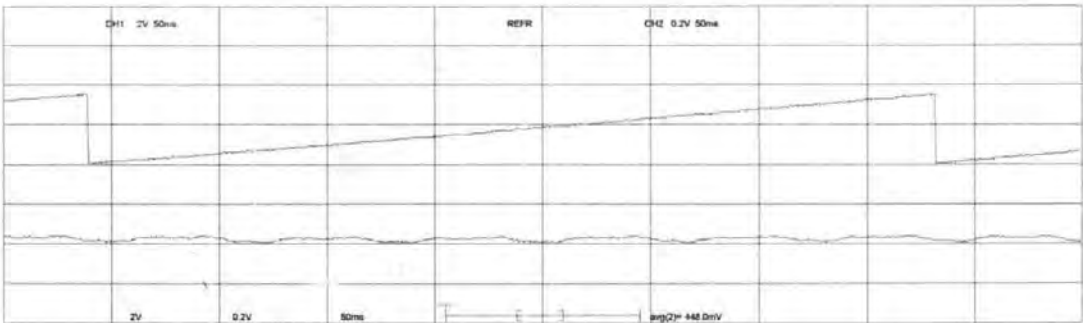
1. Sinusoidal Excitation

a. Resulting Output Torque

b. Resulting Torque Ripple

2. Sinusoidal Excitation with Cogging Torque Correction

Resulting Torque Ripple

3. Sinusoidal Excitation with Cogging Torque and Electromagnetic Torque Correction
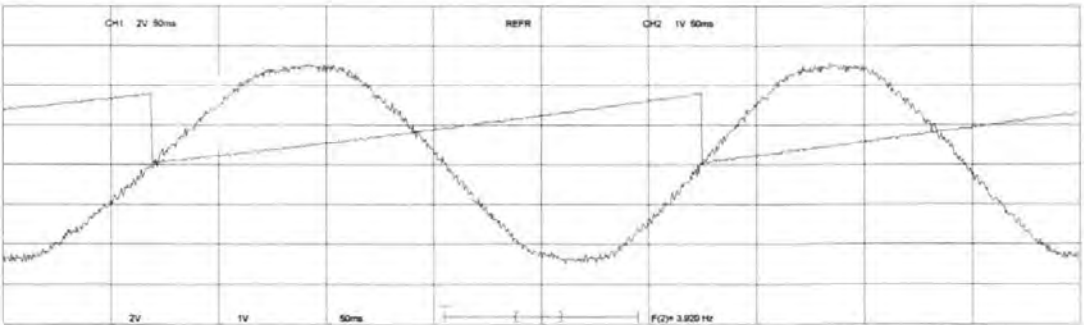
a. Resulting Output Torque

b. Resulting Torque Ripple

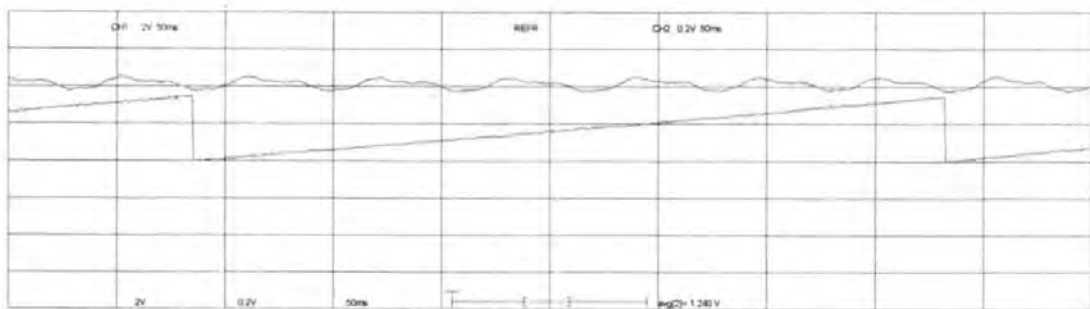### c. Current Waveform Phase A
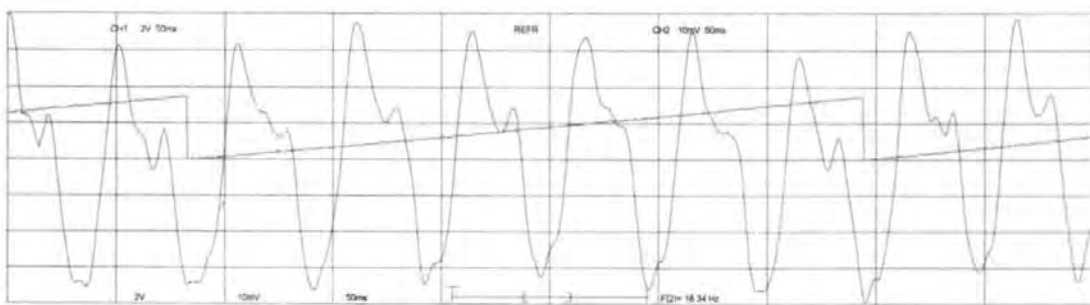

200
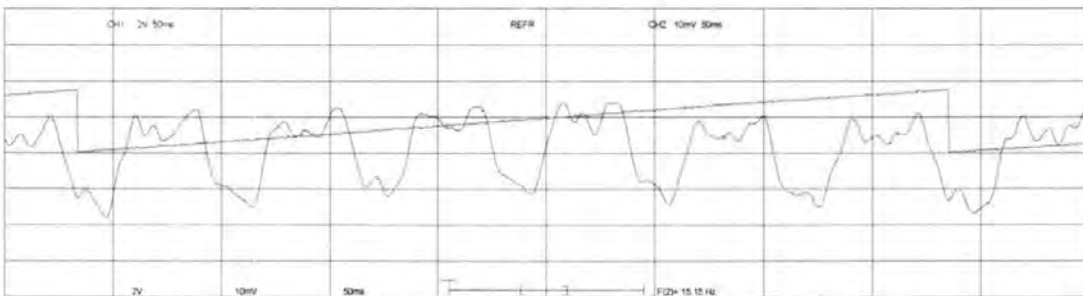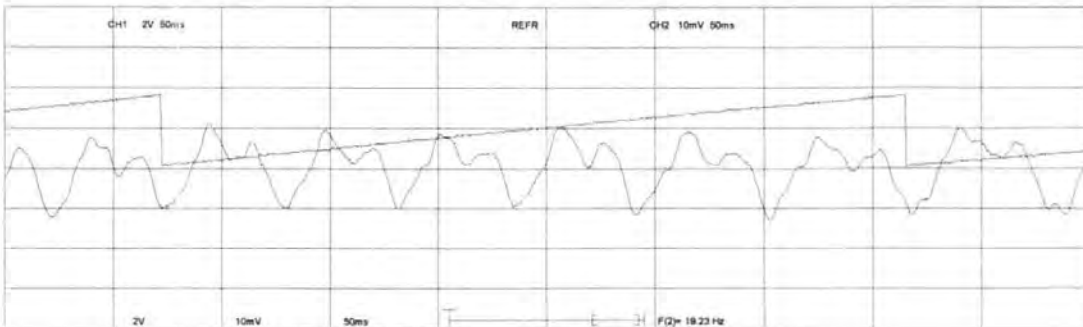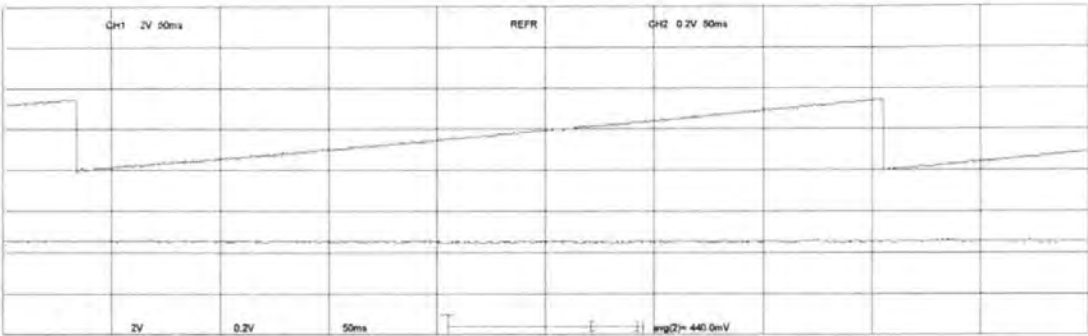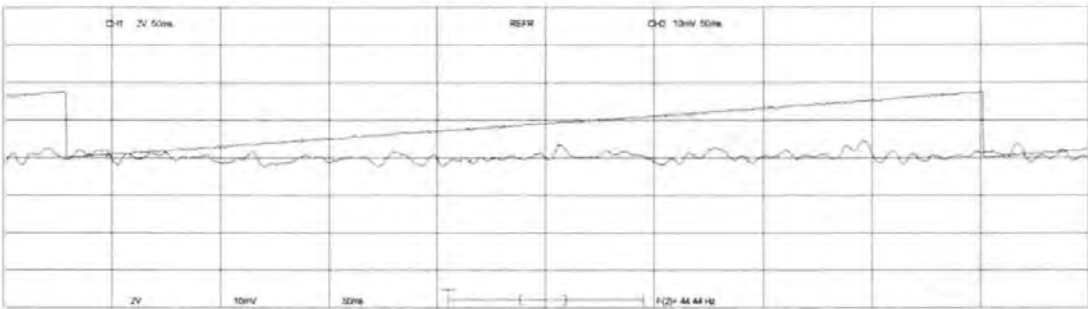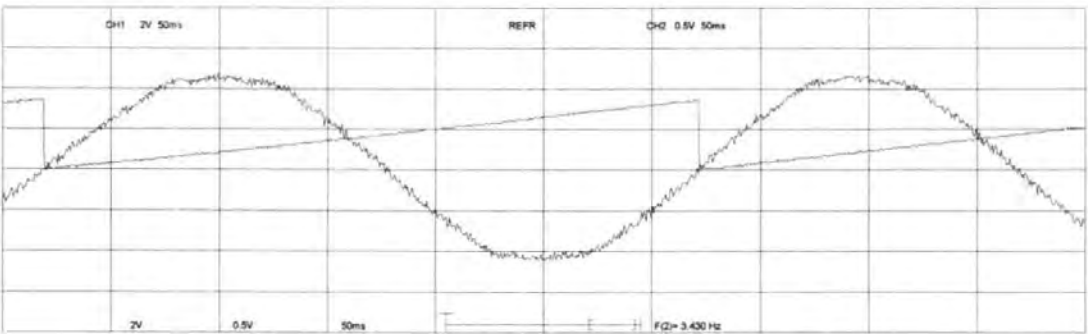
Experimental Results

Excitation : 3.31 Arms
Clockwise Rotation
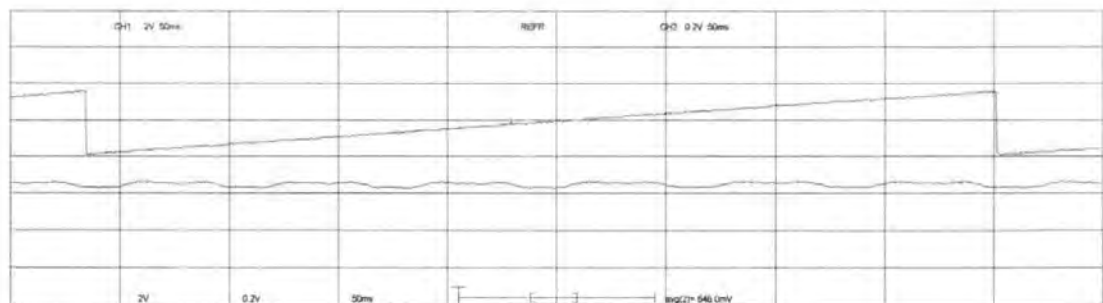
1. Sinusoidal Excitation

a. Resulting Output Torque

b. Resulting Torque Ripple
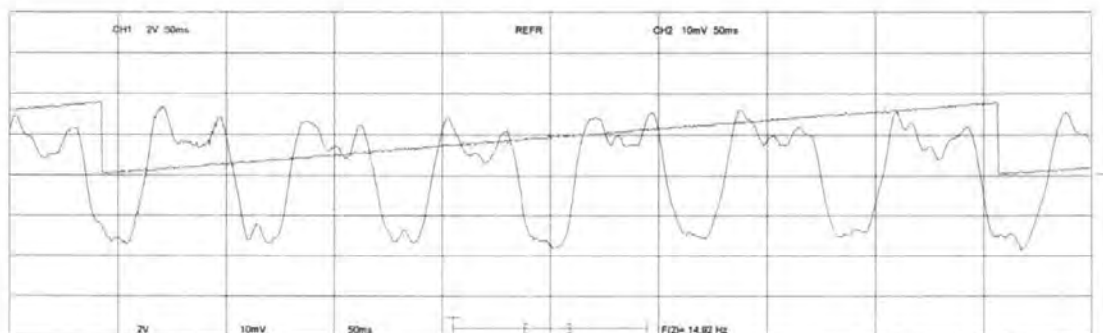
2. Sinusoidal Excitation with Cogging Torque Correction

Resulting Torque Ripple
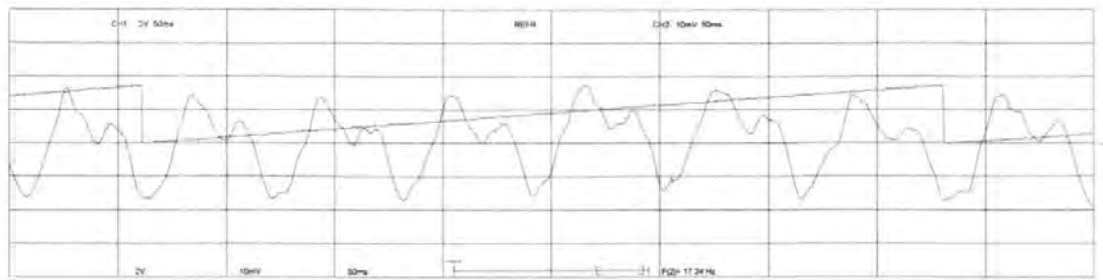
3. Sinusoidal Excitation with Cogging Torque and Electromagnetic Torque Correction

a. Resulting Output Torque
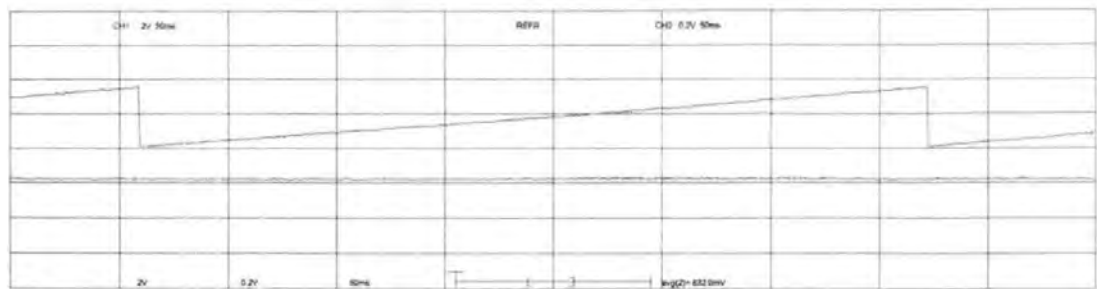
b. Resulting Torque Ripple
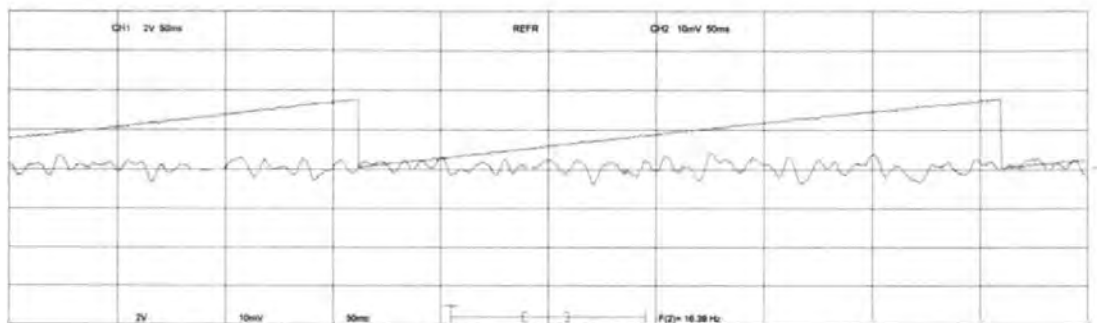
c. Current Waveform Phase A
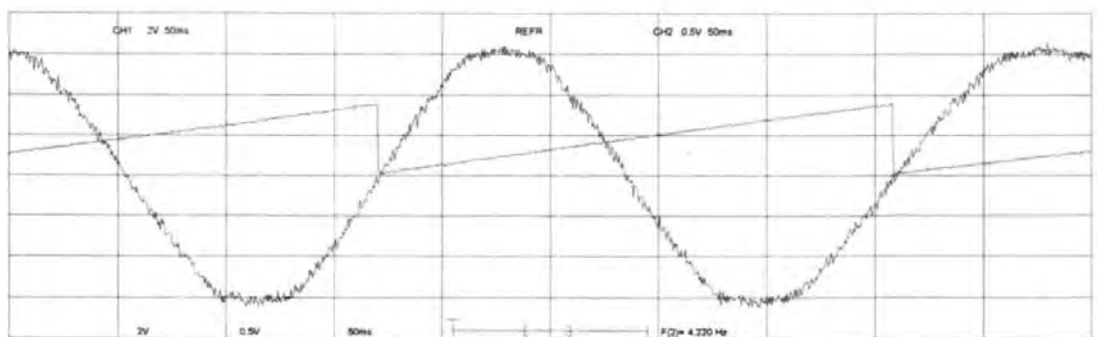
Experimental Results

Excitation : 4.17 Arms
Clockwise Rotation

1. Sinusoidal Excitation

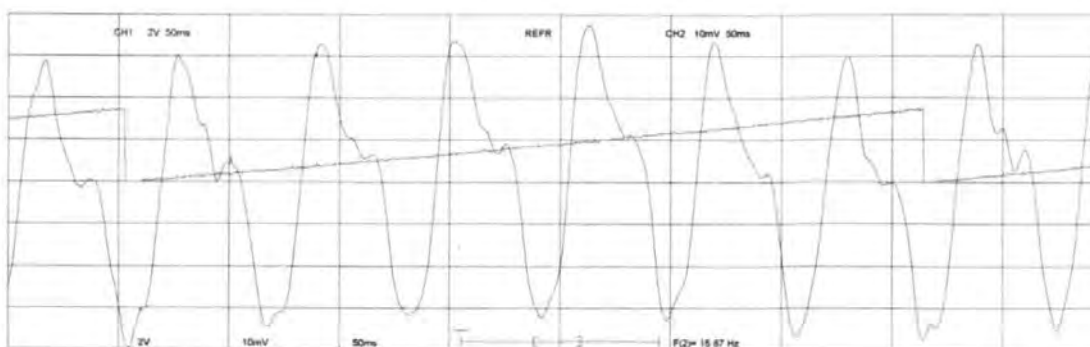### a. Resulting Output Torque
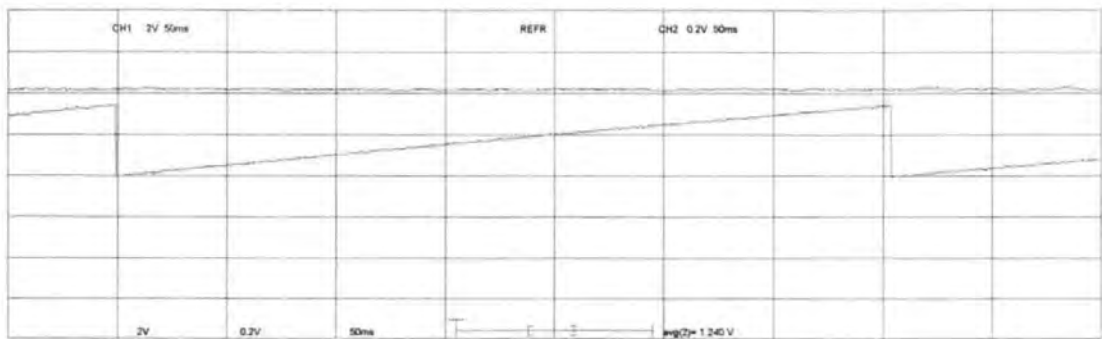

b. Resulting Torque Ripple

2. Sinusoidal Excitation with Cogging Torque Correction

Resulting Torque Ripple

203

3. Sinusoidal Excitation with Cogging Torque and Electromagnetic Torque Correction

a. Resulting Output Torque

b. Resulting Torque Ripple

c. Current Waveform Phase A

Experimental Results

Excitation : 5.14 Arms
Clockwise Rotation

1. Sinusoidal Excitation

a. Resulting Output Torque

b. Resulting Torque Ripple

2. Sinusoidal Excitation with Cogging Torque Correction

Resulting Torque Ripple

205

3. Sinusoidal Excitation with Cogging Torque and Electromagnetic Torque Correction

a. Resulting Output Torque

b. Resulting Torque Ripple

c. Current Waveform Phase A

Experimental Results

Excitation : 6.23 Arms
Clockwise Rotation

1. Sinusoidal Excitation

a. Resulting Output Torque

b. Resulting Torque Ripple

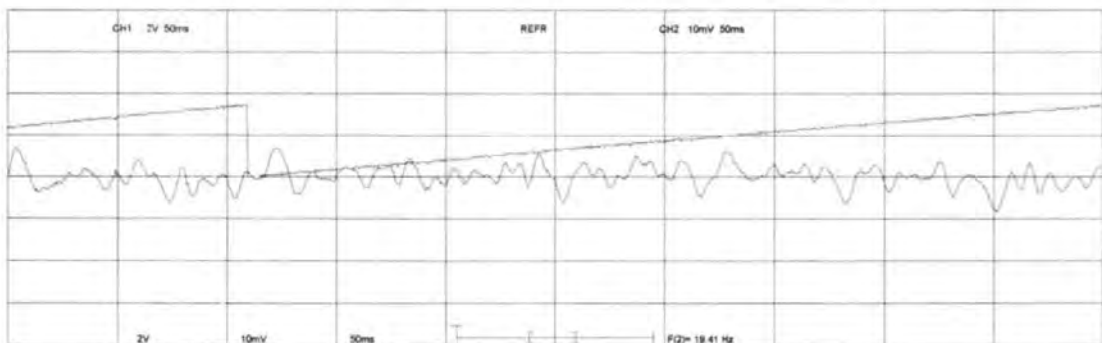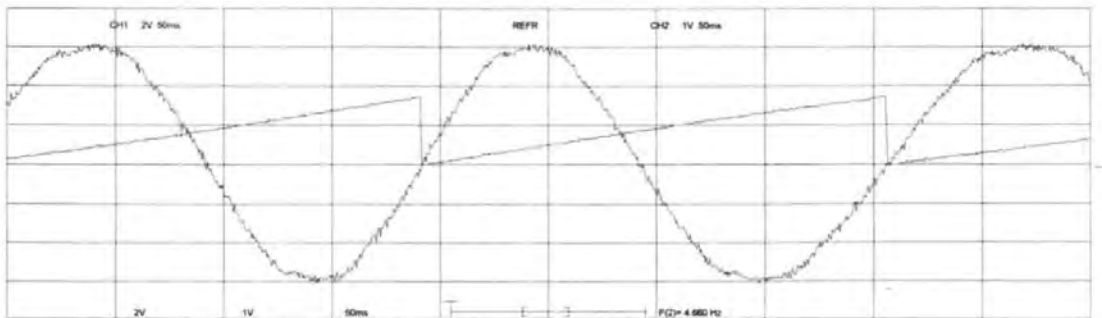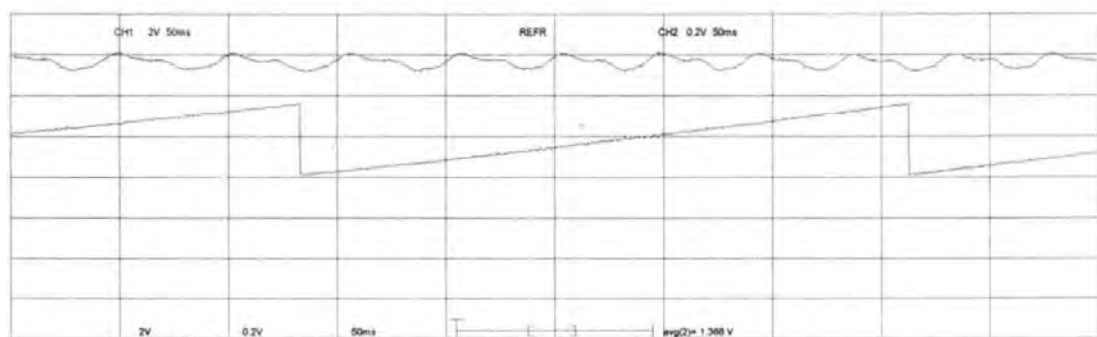## 2. Sinusoidal Excitation with Cogging Torque Correction

Resulting Torque Ripple

3. Sinusoidal Excitation with Cogging Torque and Electromagnetic Torque Correction

a. Resulting Output Torque

b. Resulting Torque Ripple

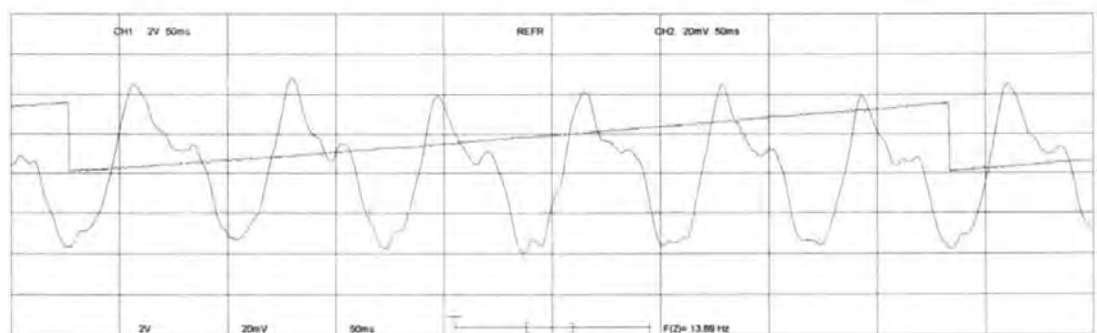### c. Current Waveform Phase A

Experimental Results

Excitation : 7.00 Arms
Clockwise Rotation

1. Sinusoidal Excitation
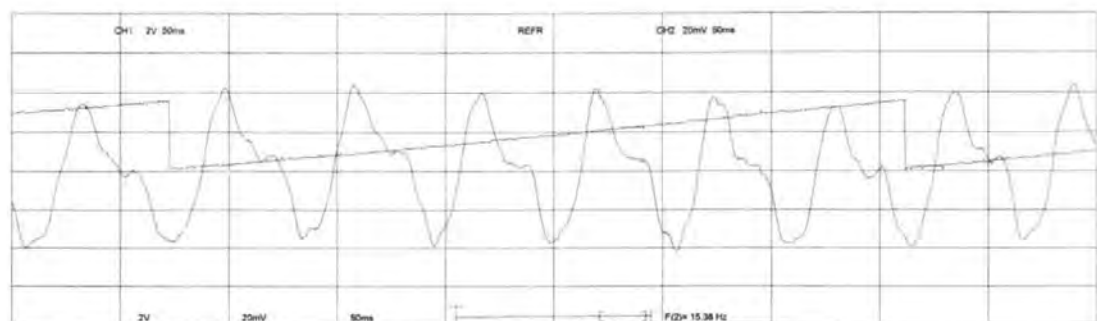
a. Resulting Output Torque
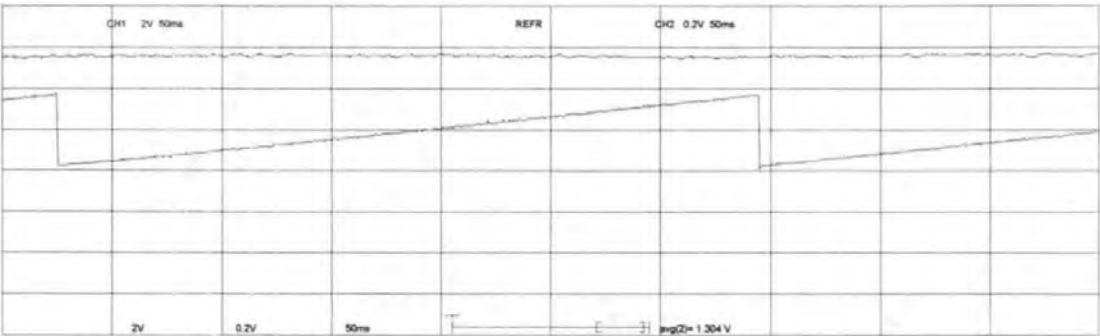

b. Resulting Torque Ripple

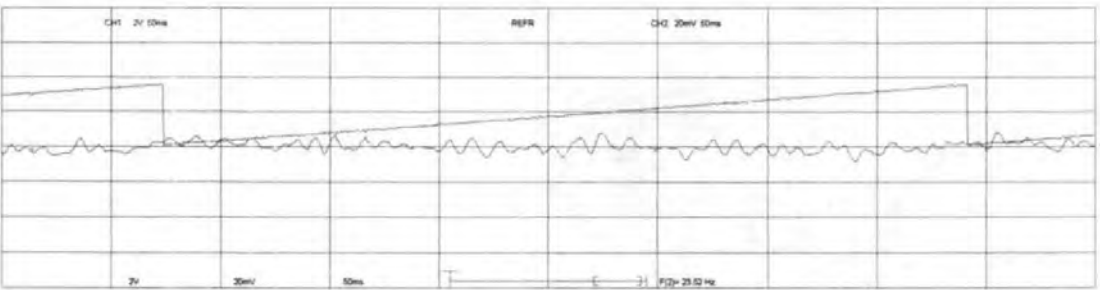## 2. Sinusoidal Excitation with Cogging Torque Correction

Resulting Torque Ripple

3. Sinusoidal Excitation with Cogging Torque and Electromagnetic Torque Correction

a. Resulting Output Torque

b. Resulting Torque Ripple

c. Current Waveform Phase A

210

Experimental Results

Excitation : 7.8 Arms
Clockwise Rotation

1. Sinusoidal Excitation

a. Resulting Output Torque

b. Resulting Torque Ripple

2. Sinusoidal Excitation with Cogging Torque Correction

Resulting Torque Ripple

3. Sinusoidal Excitation with Cogging Torque and Electromagnetic Torque Correction
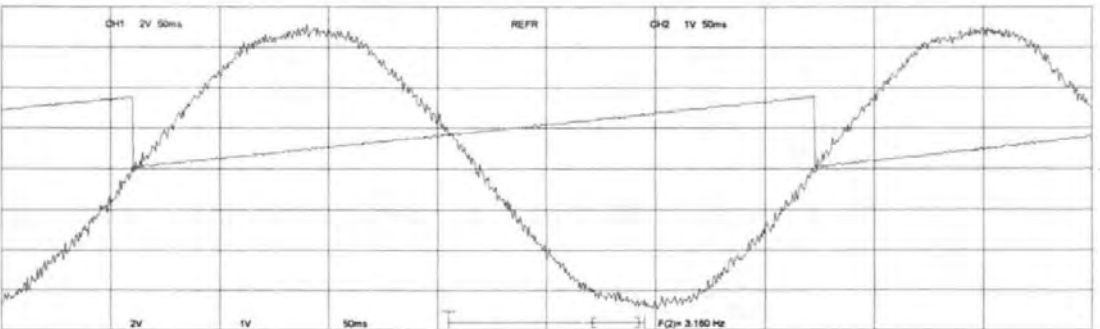
a. Resulting Output Torque

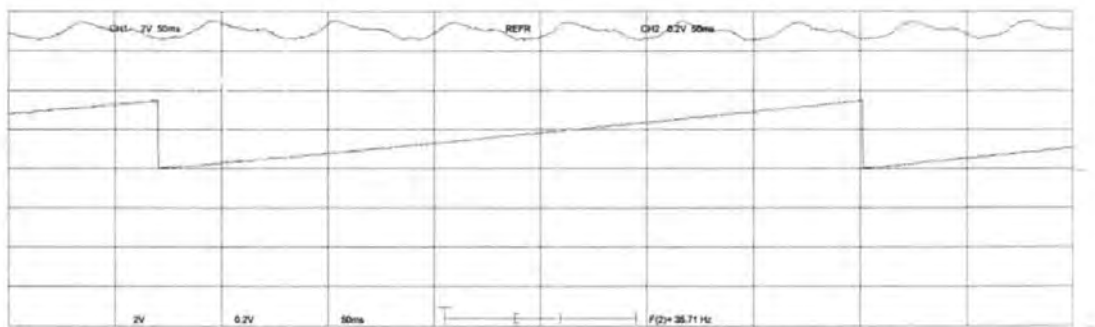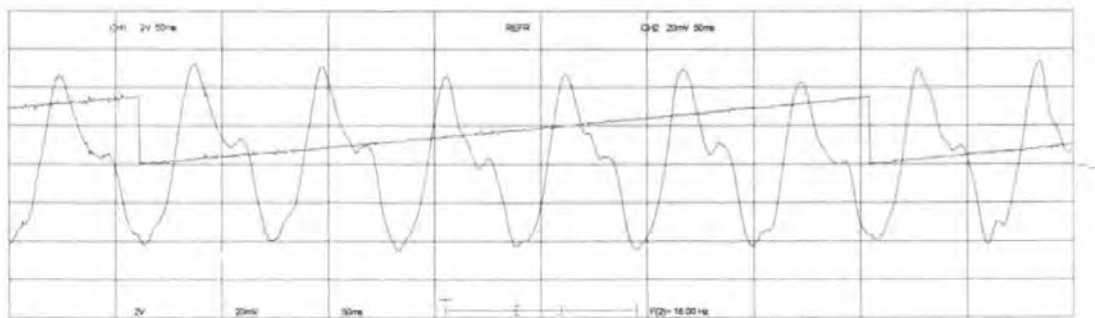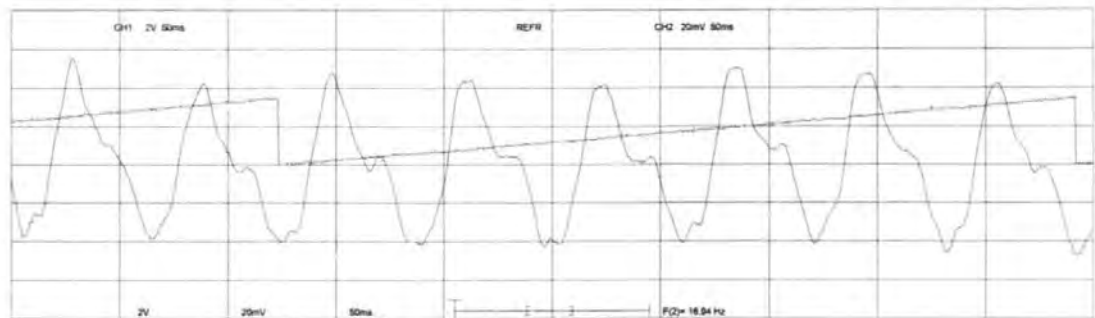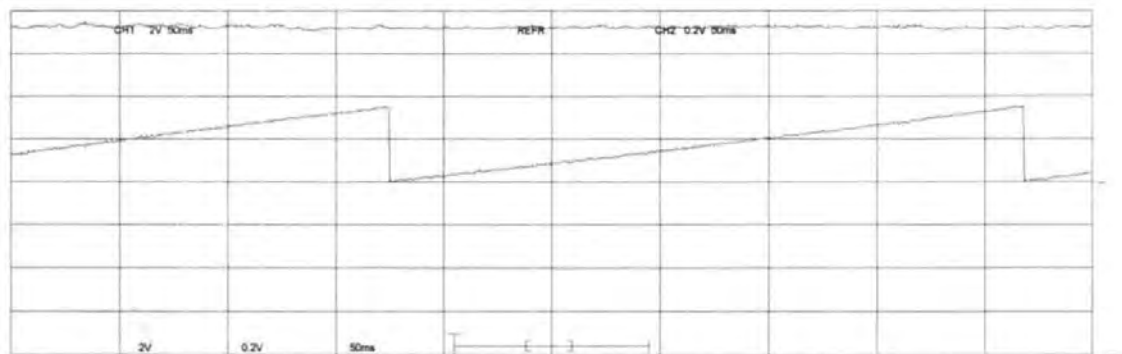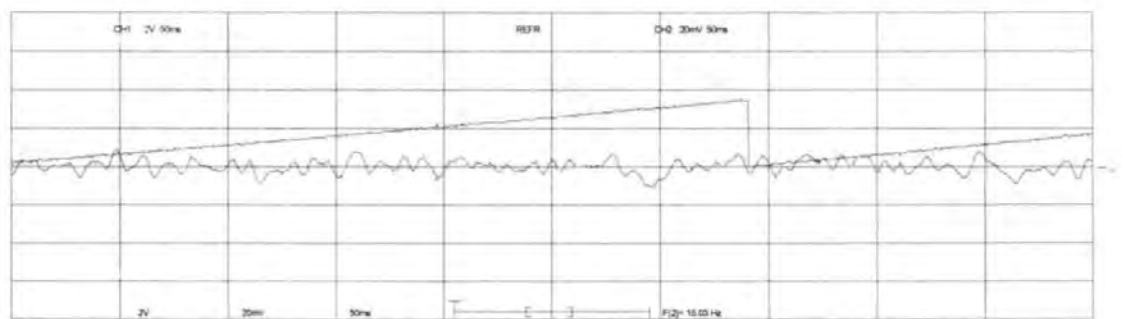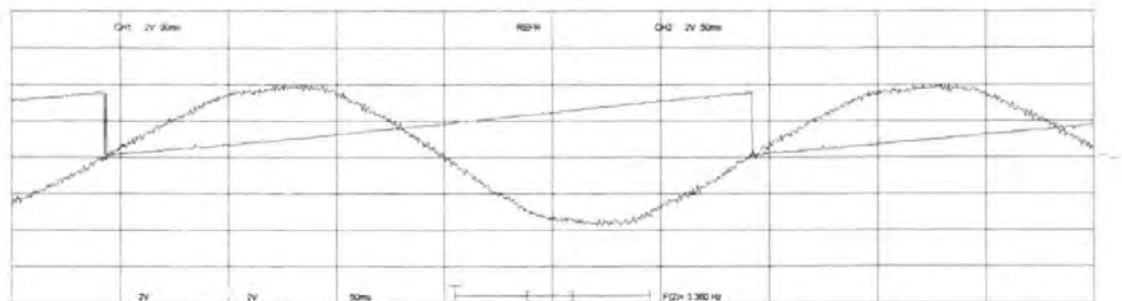### b. Resulting Torque Ripple

c. Current Waveform Phase A

212

References

[1] B. Bose, "Power Electronics and AC Drives", Prentice-Hall N. J., 1987

[2] P. Sen, "Principles of Electrical Machines and Power Electronics", John Wiley and Sons, New York, 1989

[3] J. Kassakian, M. Schlecht and G. Verghese, "Principles of Power Electronics", Addison-Wesley Publishing Company, 1991

[4] B. Bose, "Microcomputer Control of Power Electronics and Drives", IEEE Press, 1987

[5] A. Hughes, "Electric Motors and Drives: Fundamentals, Types and Applications", Heinemann Newnes, Oxford, 1993

[6] D. O'Kelly, "Performance and Control of Electrical Machines", McGraw-Hill, London, 1991

[7] J. Edwards, "Electrical Machines and Drives: An Introduction to Principles and Characteristics", Macmillan, 1991

[8] G. Henneberger, "Servo Drives: A Status Review", Intelligent Motion, June 1993, p. 1-14

[9] H. Huffman, "Introduction To Solid-State Adjustable Speed Drives", IEEE Industry Applications Society Meeting, 1989, p. 1761-1768

[10] P. Pillay and P. Freere, "Literature Survey Of Permanent Magnet AC Motors and Drives", IEEE Industry Applications Society Meeting, 1989, p. 74-84

[11] C. Cabrita, "Comparison Between Three-Phase Asynchronous And Brushless DC Motors", ICEMA 1993, Adelaide, p. 331-336

[12] R. Green, "A Comparison Of AC And DC Extruder Drives", IEEE Industry Applications Society Meeting, 1989, p. 1663-1666

[13] E. Lee, "Brushless D.C., A Modern Approach To Variable Speed Drives", IEEE Industry Applications Society Meeting, 1990, p. 1484-1488

[14] T. Miller, "Brushless Permanent-Magnet and Reluctance Motor Drives", Clarendon Press, Oxford, 1989

[15] Y. Dote and S. Kinoshita, "Brushless Servomotors: Fundamentals and Applications", Clarendon Press, Oxford, 1990

[16] T. Kenjo and S. Nagamori, "Permanent-Magnet and Brushless DC Motors", Clarendon Press, Oxford, 1985

[17] D. Hanselman, "Brushless Permanent-Magnet Motor Design", McGraw-Hill, London, 1994

[18] J. Hendershot and T. Miller, "Design of Brushless P.M. Motors", Oxford University Press, Oxford, 1995

[19] S. Nasar, I. Boldea and L. Unnewehr, "Permanent Magnet, Reluctance and Self-Synchronous Motors, CRC Press, London, 1993

[20] J. Hendershot, "Design of Brushless Permanent-Magnet Motors", Magna Physics Corporation, Hillsboro, 1994

[21] T. Sokira and W. Jaffe, "Brushless DC Motors, Electronics Commutation and Controls", Tab Books Inc, Blue Ridge Summit PA, 1990

[22] B. Bose, "Power Electronics and Motion Control-Technology Status and Recent Trends", IEEE Transactions on Industry Applications, Vol. 29, No. 5, September/October 1993, p. 902-909

[23] E. Tez, "Application Experience With Intelligent Power Modules For A.C. Drives", 5th European Conference on Power Electronics and Applications 1993, Brighton, p. 215-219

[24] R. Locher and O. Zschieschang, "IGBT Module Eases Inverter Design", PCIM Europe, May/June 1994, p. 128-133

[25] B. Taylor, "Cost of Three-Phase Bridges", PCIM Europe, July/August 1994, p. 186-187

[26] M. Allan, I. Kemp, T. Westwood and B. Pitches, "Hardware/Software Strategies In DC Brushless Motor Development", APEC 1990, p. 401-405

[27] A. Jack, "Drives and Control Strategies for Permanent Magnet Machines", Colloquium on Permanent Magnet Machines and Drives, 1993, p. 3/1-3/13

[28] D. Hanselman, "Effect of skew, pole count and slot count on brushless motor radial force, cogging torque and back EMF", IEE Proceedings Electrical Power Applications, Vol. 144, No. 5, September 1997, p. 325-330

[29] N. Hemati and M. Leu, "A Complete Model Characterization of Brushless DC Motors", IEEE Industry Applications Society Meeting, 1990, p. 169-177

[30] A. Renfrew and J. Karunadasa, "Simulation Of A Brushless DC Motor Control Scheme With Sliding Mode Control", 5th International Conference on Electrical Machines and Drives, London, 1991, p. 213-217

[31] I. Ha and C. Kang, "Explicit Characterization Of All Feedback-Linearizing Controllers For A General Type Brushless DC Motor", IEEE Transactions on Automatic Control, Vol. 39, No. 3, March 1994, p. 673-677

[32] Y. Baudon, D. Jouve and J. Ferrieux, "Current Control Of Permanent Magnet Synchronous Machines Experimental And Simulation Study", PESC 1990, Vol. 1, p. 443-450

[33] T. Rekioua, F. Tabar, J. Caron and R. Doeuff, "Study And Comparison Of Two Different Methods Of Current Control Of A Permanent Magnet Synchronous Motor", Modelling and Control of Electrical Machines, 1991, p. 145-151

[34] J. Hung and Z. Ding, "Design of currents to reduce torque ripple in brushless permanent magnet motors", IEE Proceesings, Part B, Vol. 140, No. 4, July 1993, p. 260-266

[35] C. Lee and N. Kwok, "Torque Ripple Reduction in Brushless DC Motor Velocity Systems Using a Cascade Modified Model Reference Compensator", PESC 1993, p. 458-464

[36] J. Dente and J. Esteves, "Improved Hysteresis Controlled Inverter For A Three Phase Brushless Servo Motor", 3rd European Conference on Power Electronics and Applications, Aachen, 1989, p. 257-260

[37] J. Kempkes and P. Sattler, "Comparison Of True Running At Different Concepts Of Controlling Brushless DC-Motors", 5th European Conference on Power Electronics and Applications, Brighton, 1993, p. 15-20

[38] M. Rahman, K. Low and K. Lim, "Software Controllers For Permanent Magnet Synchronous Motor Drive", 5th European Conference on Power Electronics and Applications, Brighton, 1993, p. 249-254

[39] C. Kang and I. Ha, "An Efficient Torque Control Algorithm for BLDCM with a General Shape of Back EMF", PESC 1993, p. 451-457

[40] T. Low, T. Lee, K. Tseng and K. Lock, "Servo Performance of a BLDC Drive with Instantaneous Torque Control", IEEE Transactions on Industry Applications, Vol. 28, No. 2, March/April 1992, p. 455-462

[41] H. Buyse, F. Labrique, B. Robyns and P. Sente, "Digital Field Oriented Control Of A PM Synchronous Actuator Using A Simplified Strategy For Controlling The Park Components Of The Stator Currents", Modelling and Control of Electrical Machines, 1991, p. 203-207

[42] B. Robyns, H. Buyse, F. Labrique and P. Sente, "PM Synchronous Actuator Digital Control Based On Field Orientation And Decoupling State Feedback", ICEM 1992, Manchester, Vol. 3, p. 878-882

[43] T. Rekioua, F. Tabar and R. Doeuff, "A New Appoach For The Field-Oriented Control Of Brushless, Synchronous, Permanent Magnet Machines, 4th International Conference on Power Electronics and Variable Speed Drives, London, 1990, p. 46-50

216

[44] B. Pioufle, G. Georgiou, J. Louis and C. Bergmann, "Application Of A Decoupling Controller And Non-Linear Methods For The Control Of Self-Controlled Synchronous Motors", Modelling and Control of Electrical Machines, 1991, p. 185-190

[45] H. Le-Huy, K. Slimani and P. Viarouge, "Analysis and Implementation Of A Real-Time Predictive Current Controller For Permanent-Magnet Synchronous Servo Drives", IEEE Industry Applications Society Meeting, 1991, Vol. 1, p. 996-1002

[46] P. Pillay, "Vector Control Of AC Permanent Magnet Machines", 4th International Conference on Electrical Machines And Drives, London, 1991, p. 293-297

[47] A. Renfrew and A. Al-Naamany, "Control of a Brushless DC Motor using a Torque Vector Method and Modulated Conduction", Colloquium on Advances In Control Systems For Electric Drives", London, 1995, p. 10/1-10/4

[48] J. Karundasa and A. Renfrew, "A Flexible Fast Digital Controller For A Brushless DC Motor", 4th International Conference on Power Electronics and Variable Speed Drives, London, 1990, p. 429-434

[49] C. Rossi and A. Tonielli, "Sliding Mode Control Of AC Motor Drives: Analysis Of Mapping Functions Properties", IEEE International Workshop on Intelligent Motion Control, Istanbul, 1990, p. 749-756

[50] T. Ishikawa and G. Slemon, "A Method of Reducing Ripple Torque in Permanent Magnet Motors without Skewing", IEEE Transactions on Magnetics, Vol. 29, No. 2, March 1993, p. 2028-2031

[51] B. Nogarede and M. Lajoie-Mazenc, "Torque Ripple Minimisation Methods In Sinusoidal Fed Synchronous Permanent Magnet Machines", 5th International Conference on Electrical Machines and Drives, London, 1991, p. 41-45

[52] M. Lajoie-Mazenc, B. Nogarede and J. Fagundes, "Analysis Of Torque Ripple In Electronically Commutated Magnet Machines And Minimization Methods", 4th International Conference on Electrical Machines and Drives, London, 1989, p. 85-89

217

[53] K. Kim, D. Sim and J. Won, "Analysis of Skew Effects on Cogging Torque and BEMF for BLDCM", IEEE Industry Applications Society Meeting, 1991, Vol. 1, p. 191-197

[54] Y. Kawashima and Y. Mizuno, "Reduction Of Detent Torque For Permanent Magnet Synchronous Motor By Magnetic Field Anlysis", 11th International Vehicle Symposium, Florence, 1992, p. 8.10, 1-11

[55] A. Murray, "Torque And EMF Ripple Reduction In Brushless Machines", IEE Colloquium on Permanent Magnet Machines and Drives, London, 1993, p. 8/1-8/4

[56] M. Benkhoris, F. Meibody, J. Caron and R Le Doeuff, "Study Of The SCSM Behaviour, Digital Estimation Of The Damper Losses And Torque Pulsations", International Conference on Electrical Machines 1992, Vol. 1, p. 230-234

[57] I. Cihen, G. Cohen, D. Berg and H. Petsch, "Digital Concept For Brushless AC Motors Servo Amplifier", PCIM Intelligent Motion, 1993, p. 74-81

[58] N. Matsui, T. Makino and H. Satoh, "Auto-Compensation of Torque Ripple of DD Motor by Torque Observer", IEEE Industry Applications Society Meeting, 1991, Vol. 1, p. 305-311

[59] N. Matsui, T. Makino and H. Satoh, "Autocompensation of Torque Ripple of Direct Drive Motor by Torque Observer", IEEE Transactions on Industry Applications, Vol. 29, No. 1, January / February 1993, p. 187-194

[60] N. Matsui, "Autonomous Torque Ripple Compensation of DD Motor by Torque Observer", IEEE Asia-Pacific Workshop on Advances in Motion Control, Singapore, 1993, p. 19-24

[61] H. Satoh, T. Makino and N. Matsui, "An Automatic Torque Ripple Compensation System for Direct Drive Motors", Electrical Engineering in Japan, Vol. 113, No. 6, 1993, p. 141-148

[62] S. Bogosyan, M. Goekasan, F. Guerleyen and T. Kutman, "Adaptive Torque Ripple Minimization In Permanent Magnet Synchronous Motor", IEEE International Workshop on Intelligent Motion Control, 1990, p. 669-674

[63] T. Low, K. Tseng, K. Lock and K. Lim, "Instantaneous Torque Control", 4th International Conference on Electrical Machines and Drives, London, 1989, p. 100-105

[64] T. Low, K. Tseng, T. Lee, K. Lim and K. Lock, "Strategy for the instantaneous torque control of permanent-magnet brushless DC drives", IEE Proceedings, Vol. 137, Part B, No. 6, November 1990, p. 355-363

[65] T. Low, Y. Ding and K. Lock, "Analysis and control of torque ripples in inverter-fed permanent-magnet synchronous motors using the electromechanical spring-stiffness coefficient $\partial T_e/\partial \theta$", IEE Proceedings on Electrical Power Applications, Vol. 141, No. 3, May 1994, p. 169-176

[66] J. Kettleborough, I. Smith, K. Al-Hadithi and V. Vadher, "Current Profiling For Torque Pulsation Minimisation In Brushless DC Motor Drives", 11th International Vehicle Symposium, Florence, 1992, p. 8.09, 1-12

[67] J. Hung and Z. Ding, "Minimization of Torque Ripple in Permanent Magnet Motors: A Closed Form Solution" ,IECON 1992, Vol. 1, p. 459-463

[68] K. Cho, J. Bae, S. Chung and M. Youn, "Torque harmonics minimisation in permanent magnet synchronous motor with back EMF estimation", IEE Proceedings on Electrical Power Applications, Vol. 141, No. 6, November 1994, p.323-330

[69] J. Karunadasa and A. Renfrew, "Analysis Of Torque Production In Brushless DC And AC Motor Drives", 4th International Conference on Power Electronics and Variable Speed Drives, London, 1990, p. 451-456

[70] K. Cho, J. Bae, S. Chung and M. Youn, "Torque harmonics minimisation in permanent magnet synchronous motor with back EMF estimation", IEE Proceedings, Vol. 141, Part B, No. 6, November 1994, p. 323-330

[71] N. Wavre, "Design Of Brushless Torque Motor Without Detent Torque And Very Low Ripple", Total Solutions in Drives / Motors / Controls, Birmingham, 1990

[72] E. Favre and M. Jufer, "Current Shapes Leading To A Constant Torque", Modelling and Control of Electrical Machines, 1991, p. 47-52

[73] E. Favre, L. Cardoletti and M. Jufer, "Permanent Magnets Synchronous Motors : a General Approach for Cogging Torque Suppression", IEEE Industry Applications Society Meeting, 1991, Vol. 1, p. 204-210

[74] E. Favre, L. Cardoletti, E von Siebenthal and M. Jufer, "Speed Control of a Constant Torque Brushless Motor", International Conference on Electrical Machines 1992, Vol. 2, p. 828-832

[75] D. Jouve and D. Bui, "Torque Ripple Compensation In DSP Based Brushless Servo Drive", PCIM Intelligent Motion, 1993, p. 28-37

[76] S. Clenet, Y. Lefevre, N. Sadowski, S. Astier and M. Lajoie-Mazenc, "Compensation of Permanent Magnet Motors Torque Ripple by Means of Current Supply Waveshapes Control Determined by Finite Element Method", IEEE Transactions on Magnetics, Vol. 29, No. 2, March 1993, p. 2019-2023

[77] S. Kamiya, M. Shigyo, T. Makino and N. Matsui, "DSP-Based High-Precision Torque Control of Permanent Magnet DD (Direct Drive) Motor", Electrical Engineering in Japan, Vol. 110, No. 4, 1990, p. 51-58

[78] D. Hanselman, "Minimum Torque Ripple, Maximum Efficiency Excitation of Brushless Permanent Magnet Motors", IEEE Transactions on Industrial Electronics, Vol. 41, No. 3, June 1994, p. 292-300

[79] A. Lonsdale and N. Schofield, "An Integrated Low Cost Sensor For The Direct Torque Control Of Brushless DC Motors", IEE Colloquium on Machines for Automotive Applications, London, 1996, p. 6/1-6/7

[80] H. Bolton and R. Ashen, "Influence of motor design on torque ripple in brushless DC drives", IEE Proceedings, Vol. 131, Part B, No. 3, May 1984, p. 82-90

[81] D. Hanselman, J. Hung and M. Keshura, "Torque Ripple Analysis in Brushless Permanent Magnet Motor Drives", International Conference on Electrical Machines 1992, Vol. 2, p. 823-827

[82] R. Park, "Definition of An Ideal Synchronous Machine and Formula for the Armature Flux Linkages", General Electric Review, Vol. 31, No. 6, June 1928, p. 332-334

[83] R. Park, "Two-Reaction Theory of Synchronous Machines, Generalized Method of Analysis-Part I", Winter Convention of the American Institute of Electrical Engineers, New York, Vol. 48, 1929, p. 716-730

[84] B. Adkins and R. Harley, "The General Theory of Alternating Current Machines", Chapman and Hall, London, 1975

[85] N. Hancock, "Matrix Analysis of Electrical Machines", Pergamon Press, Oxford, 1974

[86] M. Say, "Introduction to the unified theory of electromagnetic machines", Sir Isaac Pitman and Sons, London, 1971

[87] D. O'Kelly and S. Simmons, "Introduction to Generalized Electrical Machine Theory", McGraw-Hill, London, 1968

[88] C. Jones, "The Unified Theory of Electrical Machines", Butterworths, London, 1967

[89] A Randell, "Performance of Electrical Machines using Generalised Theory and Including Air-Gap Flux Harmonics", University of London, PhD Thesis, 1965

[90] P. Kocybik and P. White, "Influence of Armature Reaction on Torque Ripple in Permanent Magnet Machines", PCIM 1997, Nürnberg, p. 149-156

Influence of Armature Reaction on Torque Ripple in Permanent Magnet Machines

P. Kocybik and P. White
University of Plymouth, UK

Abstract - The paper demonstrates the use of Park's Transform for torque ripple cancellation in permanent magnet machines. It is shown that it is possible to derive optimum phase currents from the no load back emf waveforms. Further it is shown that under load conditions a substantial amount of torque ripple remains if the machine is fed with the optimum phase currents, due to the armature reaction of the machine. Therefore it is necessary to calculate new optimum phase currents from the load measurements of back emf to cancel the remaining torque ripple.

1. Introduction

Recent advances in magnet technology and power electronics have increased the popularity of the permanent magnet machine for a wide range of applications. Due to its high power density, large torque to inertia ratio and high efficiency it is often used as a direct replacement for dc and other machines. The permanent magnet synchronous motor, sometimes called brushless motor, requires a higher control precision than the brushed dc motor. For that reason Digital Signal Processors (DSPs) are used which provide powerful and relatively cheap processing power. The use of DSPs allows the system designer to implement more sophisticated control approaches.

A major problem for direct drive applications like robot arms, machine tools or aerospace applications is the occurrence of torque ripple at low speeds. This torque ripple is caused by the interaction of machine parameters and phase currents. Through the use of Park's Transform it is possible to predict the optimum current waveforms which will cancel the torque ripple.

Implementations using this technique have shown that an effective reduction of torque ripple is possible [1], [2] and [3]. However these cancellation techniques were based on the no load machine parameters.

In the following it will be shown in detail how Park's transform can be used to determine optimum phase currents. Further it is shown that the use of no load parameters for torque ripple cancellation under load leads to a reappearance of torque ripple. A strategy will be described to determine new sets of phase currents which lead to the cancellation of torque ripple under load conditions.

2. Torque Ripple Cancellation

In the following three phase permanent magnet machines are considered, as they are by far the most popular type of permanent magnet machines. The power relationship for these machines can be expressed as follows :

$$T(\theta) * \omega = emf_A(\theta) * i_A(\theta) + \\ emf_B(\theta) * i_B(\theta) + emf_C(\theta) * i_C(\theta) \qquad (1)$$

T : instantaneous output torque
θ : rotor position in electrical degrees
ω : rotational speed of machine
$emf_{A,B,C}$: back emf waveforms for phase A, B and C
$i_{A,B,C}$: phase currents

The left hand side represents the mechanical output power and the right hand side the electrical input power after internal losses. At constant speed the instantaneous output torque will be determined through the product of back emf waveforms and phase currents summed up over all machine phases. This relationship holds true for machines with back emf waveforms of any kind.

If an ideal sinusoidal permanent magnet machine is considered the back emf waveforms are assumed to be ideally sinusoidal. To achieve a constant torque output the machine has to be supplied by ideal sinusoidal phase currents. If equation 1 is evaluated for this case the resulting output torque will be found to be :

$$T = \frac{1}{\omega} * (E * \sin(\theta) * I * \sin(\theta) + E * \sin(\theta - 120°) * I * \sin(\theta - 120°) \\ + E * \sin(\theta - 240°) * I * \sin(\theta - 240°) \\ = \frac{1.5 * E * I}{\omega} \qquad (2)$$

arrive at a solution for the phase currents, for instance [6]. Apart from requiring high computing power these schemes also exhibit the disadvantage of arriving at suboptimal solutions to the problem. Depending on the iteration strategy the solution will be weighted in a particular direction, often by introducing an additional condition.

If the first condition, the star point condition is dropped, the number of possible solutions further increases. It becomes therefore even more unlikely for an algorithm to produce the optimal solution to the constant torque problem.

It is however possible to use a completely different strategy if the attempt to solve the problem in the three phase domain (phases A, B and C) is abandoned. Park's transform allows the problem to be redefined in a two phase description (phases d and q).

Equation 5 shows the required transformation for the back emf waveforms.

$$emf_d = \frac{2}{3} * (\cos(0) * emf_A +$$
$$\cos(0 - 120^0) * emf_B + \cos(0 - 120^0) * emf_C) \quad (5)$$

$$emf_q = \frac{2}{3} * (\sin(0) * emf_A +$$
$$\sin(0 - 120^0) * emf_B + \sin(0 - 120^0) * emf_C)$$

The subscript d denotes the so called direct axis of the machine. The direct axis is in alignment with the magnetic axis produced by the permanent magnets. Any current on the direct axis will therefore not contribute to useful torque production as it is aligned with the magnetic field.

The subscript q denotes the quadrature axis of the machine. The quadrature axis has an offset of 90 degrees relative to the magnetic axis. Current on the quadrature axis will therefore fully contribute to useful torque production.

Torque production in the dq-plane can be expressed as follows :

$$T = \frac{1}{\omega} * \frac{3}{2} * (i_d * emf_d + i_q * emf_q) \quad (6)$$

Equation 6 already simplifies equation 1. Only two currents need to be determined as opposed to three phase currents before.

From previous discussions it follows that the current on the direct axis should be chosen to be zero. This guarantees that the quadrature current makes the sole contribution to torque production therefore eliminating undesired contributions on the direct axis.

This will further simplify the torque equation :

$$i_d = 0$$
$$T = \frac{1}{\omega} * \frac{3}{2} * i_q * emf_q \quad (7)$$

The remaining problem now is to find the current i_q in such a manner that it matches the back emf waveform on the q axis. This simply requires rearrangement of equation 7.

$$i_q = \frac{2}{3} * \frac{T}{emf_q} * \omega \quad (8)$$
$$T = const$$

As can be seen from equation 8 a simple division and some scaling is required to describe the required currents in the dq-plane. Equation 8 represents the closed form solution to the torque ripple problem.

Finally back transformation of the calculated currents in the dq-plane to the three phase description is necessary. The back transformation takes a similar form to equation 5.

Park's transform has been used to find the required phase currents for the test motor with no external load. Figure 3 shows the result of the calculations.
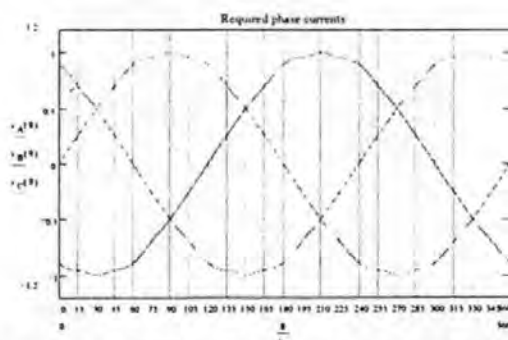

Figure 3: Required phase currents (no load back emf)

As can be seen from figure 3 all phase currents are symmetric with a phase shift of 120 and 240 degrees respectively. Park's transform automatically fulfils the star point condition by making the currents symmetric.

E : amplitude of back emf waveforms
I : amplitude of phase currents

If constant machine speed is assumed it can be seen that the instantaneous output torque will be constant regardless of rotor position. Similar considerations apply to machines with ideal rectangular back emf waveforms.

For a real permanent magnet machine the back emf waveform will always deviate from the ideal sinusoidal or rectangular form due to practical design limitations. If a real machine is supplied with sinusoidal currents it can therefore be expected that the instantaneous output torque will not remain constant for all rotor positions.

Knowledge of the back emf waveform allows calculation of the expected torque ripple in this case.

The no load back emf waveforms have been measured on a test motor. Motor parameters are given in the appendix. The back emf waveforms have been scaled so that the fundamental is of magnitude 1 in order to make results comparable with other measurements. Figure 1 shows the measured no load waveforms after scaling : k_A, k_B and k_C.
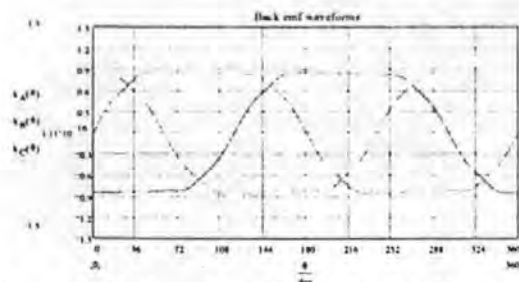

Figure 1 : Back emf waveforms (no load back emf)

It can clearly be seen that the actual back emf waveforms differ significantly from the ideal sinusoidal waveforms. Especially 3rd and 5th order harmonics feature prominently.

As explained above it can be expected that a significant torque ripple will result if the motor is supplied with ideal sinusoidal phase currents. Simulations have been used to predict the expected torque ripple. Figure 2 shows the instantaneous output torque against rotor position.
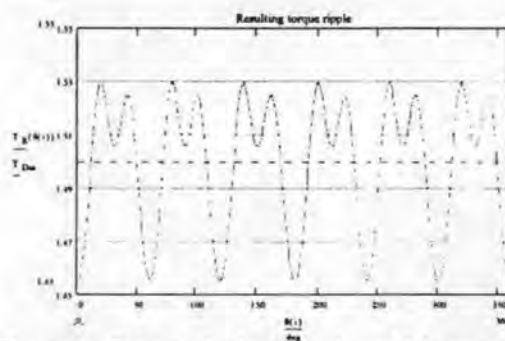

Figure 2 : Torque ripple with sinusoidal currents (no load back emf)
T_{des} : Desired torque (1.5)

The scaled back emf waveforms depicted in figure 1 have been used. The desired output torque is therefore 1.5, see dashed line. Figure 2 reveals that the actual output torque differs markedly from the desired output torque. The magnitude of the torque ripple is 5% of the desired output torque. A Fourier analysis of the expected torque ripple shows that 6th and 12th order harmonics are predominant as can be seen from figure 2.

This is in accordance with the theory. Bolton and Ashen [4] came to the conclusion that only multiples of 6 times the electrical frequency can be present as torque ripple in three phase machines. Hanselman, Hung and Keshura [5] came to the same result after evaluating the torque expressions in complex form.

To achieve a constant output torque it is possible to manipulate the phase currents in a way that they match with the measured back emf profile. If equation 1 is considered, two conditions need to be met, to arrive at a constant output torque.

1. The star' point condition must be fulfilled; i.e. the sum of all three phase currents needs to equal zero.
$$0 = i_A + i_B + i_C \quad (3)$$
2. The sum of the products of back emf waveforms and phase currents must be constant.
$$const = \sum_i emf_i * i_i \quad (4)$$
$$i = A, B, C$$

These two conditions must be fulfilled in order to eliminate torque ripple. However three phase currents need to be calculated. The system is therefore undetermined and does not have a unique analytical solution. Schemes have been suggested where intensive computer simulations perform multiple iterations to

If equation 1 is used the resulting phase torques and the output torque can be calculated. This has been done using the calculated phase currents and the scaled back emf waveforms from figure 1.
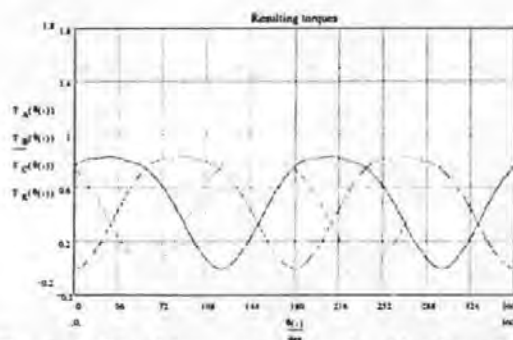

Figure 4 : Resulting torques (no load back emf)

Figure 4 shows the result of these calculations. As can be seen all three phases make an equal contribution and the output torque coincides with the desired output torque of magnitude 1.5, see dashed line in figure 4.

Further it is relatively easy to produce the required phase currents as they do not exhibit awkward slopes or high magnitudes as some of the iterative solutions do.

It can be concluded that Park's transform presents a simple and effective way to arrive at a solution for the torque ripple problem. It can be shown that the presented solution is superior to solutions found using iterative strategies. The method has been successfully used by different authors to minimise torque ripple in permanent magnet machines.

Authors reporting the use of this method utilise back emf waveforms derived from the no load case. In the following it will be shown that this results in considerable remaining torque ripple if the machine is progressively loaded. It will be suggested to use back emf waveforms derived under load instead to arrive at a constant torque output.

3. Torque Ripple Cancellation for Loaded Machine

The back emf waveform describes the voltage over the conductors induced by the magnetic field. In the no load case the magnetic field is set up by the permanent magnets only. If the machine becomes electrically loaded the conductors are supplied by currents. These currents set up their own magnetic field which will be superimposed on the magnetic field from the permanent magnets. For part of the slot the two magnetic fields will have the same direction. For the other part they will oppose each other. The resulting magnetic field will consequently be distorted compared to the no load field. This distortion is initially small and becomes more important when the machine approaches full load. At higher currents the distortion will be very significant. This effect is called the armature reaction.

The magnitude and the shape of the armature reaction will depend on machine design. For instance special machines designed with a large airgap do not usually show a significant armature reaction. However most permanent magnet machines will exhibit considerable armature reaction since a smaller airgap results in a more efficient machine.

Because of the non-linear nature of the material characteristics it is not easily possible to calculate the changes to the magnetic field or the back emf waveforms respectively. However the use of a Finite Element package (FE) allows to determination of new back emf waveforms. Alternatively, it is possible to use measurements to determine the new back emf waveforms under load.

Finite element modelling requires an accurate modelling of the machine which is time consuming and demands high computing powers. It has therefore been decided to use measurements to arrive more quickly at a solution to the torque ripple problem.

Measurements have been taken by progressively loading the motor up to nominal output torque. To illustrate the effect of the armature reaction on torque ripple the full load case will be considered. Figure 5 shows the phase to star point voltages for full load current.
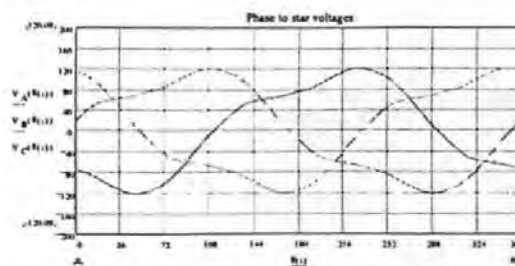

Figure 5 : Phase to star voltages (load back emf)

Waveforms in figure 5 are not scaled but represent the actual magnitudes of voltage waveforms. It is now

necessary to calculate the back emf waveforms from these voltages. Equation 9 describes the relation ship between back emfs, voltages and currents.

$$emf = V + i * R + L * \frac{di}{dt} \quad (9)$$

emf : back emf voltage
V : measured phase to star voltage
i : phase current
R : phase resistance
L : phase inductance

The calculated back emf waveforms are scaled to make them comparable to the no load case, k_A, k_B and k_C. They are given in figure 6.
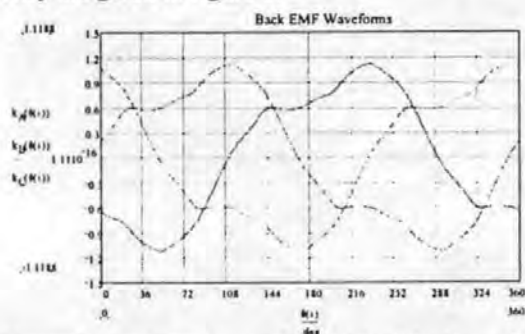

Figure 6 : Back emf waveforms (load back emf)

It can clearly be seen that the waveforms are distorted compared to the no load waveforms, figure 1. A Fourier analysis reveals that 3rd, 5th and 9th order harmonics feature prominently. The actual magnitude of the harmonics is different to the magnitude of the harmonics in the no load case.

Following the same line of argument as in section 2 the machine will be supplied by sinusoidal currents. This will again result in a significant torque ripple. Simulation results calculating this torque ripple are shown in figure 7.
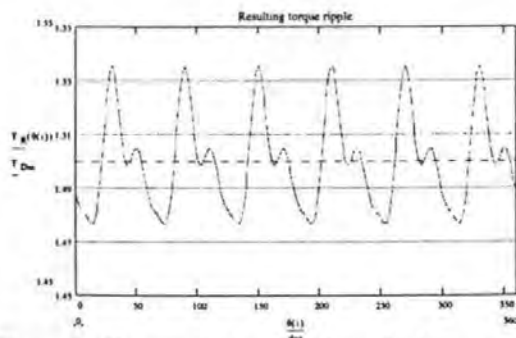

Figure 7 : Torque ripple with sinusoidal currents (load back emf)

The magnitude of torque ripple is down to about 4% from 5% in the no load case. A comparison with figure 2 clearly shows the differences in torque ripple. The Fourier analysis reveals that again 6th and 12th order harmonics are predominant. However magnitude and phase are different compared to the no load case. Supplying the machine under load conditions with ideal sinusoidal currents therefore leads to a different but still significant torque ripple.

Using Park's transform to calculate the required optimum phase currents as above leads to a new set of currents for the load case. Figure 8 shows the new optimum currents.
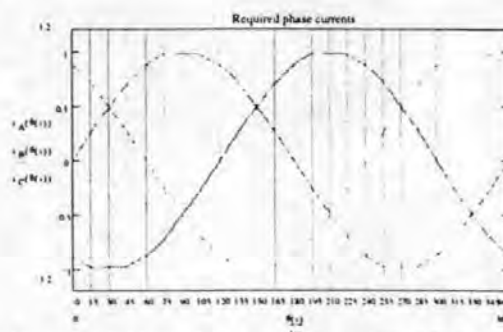

Figure 8 : Required phase currents (load back emf)

If figure 8 is compared to figure 3 the differences become clear. The currents are again symmetric and fulfil the star point condition because Park's transform has been used. However a flat top is required for the full load case. Again Park's transform yields currents which are easily reproducible.

If equation 1 is used again the resulting phase torques and the output torque of the machine can be determined, see figure 9.
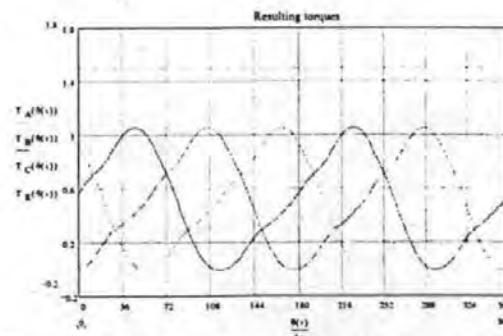

Figure 9 : Resulting torques (load back emf)

Again the phase contributions are equal to each other and just offset by a 120 and 240 degrees phase shift. The resulting torque is 1.5 as requested, see dashed

line. The phase contributions are clearly different from the no load case depicted in figure 4.

It can therefore be concluded that the permanent magnet machine under load conditions requires different supply currents to the no load case because of the effect of the armature reaction. This also becomes clear as the torque ripple for sinusoidal supply currents differs from the no load to the load case.

Finally it is assumed that only no load measurements are used. This is the standard practice widely used so far. The phase currents are then calculated from the no load back emf waveforms. These currents have been determined in chapter 2. It is now assumed that the loaded machine will be supplied with these currents.

It can be anticipated that these currents will not match the back emf profile of the machine under load and subsequently lead to the reappearance of torque ripple. If equation 1 is used with the load back emf waveforms and the currents derived in the no load case the resulting torque ripple will be as follows, see figure 10.
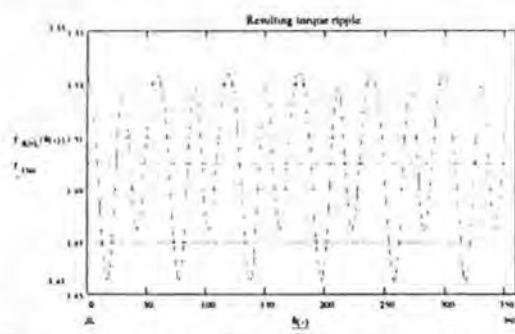

Figure 10 : Torque ripple with currents from no load back emf (load back emf)

The reappearance of torque ripple is clearly visible. The magnitude of torque ripple is again around 5%. Fourier analysis reveals the dominant harmonic to be of order 12. It therefore becomes clear that supplying the machine with currents derived for the no load case will result in significant torque ripple for the machine under load. Here it does not make any difference whether the machine is supplied with ideal sinusoidal currents or through currents derived from the no load case. Both sets of supply currents will lead to significant torque ripple of similar magnitude.

It therefore becomes clear that load measurements need to be used to eliminate the torque ripple in the load case.

Results here are presented for the full load case. At lower load currents the distortion of the back emf waveforms will be less pronounced. It is therefore more critical to correct the supply currents for higher load levels.

A practical scheme comprises measurements at a discrete number of load situation and calculation of sets of required phase currents. Depending on the actual operating point of the machine the nearest set of currents will then be selected to supply the machine. The number of required sets depends on the desired accuracy of the torque ripple minimisation. Load measurements of the back emf waveform are easily obtainable and can therefore be used to calculate the required phase currents. This allows a fast and efficient implementation of the torque ripple minimisation.

4. Conclusions

It has been demonstrated that optimal phase currents obtained from the no load parameters using Park's transform lead to a constant torque output of the permanent magnet machine for the no load case. However when the machine is electrically loaded the armature reaction becomes effective and starts to distort the magnetic field. This will result in the reappearance of torque ripple. The resulting torque ripple can be of the same order as the torque ripple for sinusoidal excitation. It is therefore not useful to apply the torque minimisation strategy based on no load parameters under load conditions.

It has been described how new sets of optimum supply currents can be derived from load measurements. These new supply currents will lead to the cancellation of torque ripple under load conditions.

A practical scheme has been proposed to minimise torque ripple under load conditions using a discrete number of load measurements.

The use of new optimum phase currents, leading to the cancellation of torque ripple, enables the permanent magnet machine to be used for high precision applications, like robot arms, machine tools and aerospace applications. Furthermore the accurate torque control allows cancellation of undesired speed deviations introduced by torque ripple.

5. Further Work

Further work is currently being undertaken to extend the findings from the measured data using a finite element package. It is desired to visualise the field distortion and to confirm back emf and torque results under different load conditions.

A test rig is under construction to implement the proposed supply currents on the test motor. The experimental results will then be compared to the findings from the calculations.

Acknowledgement

References

[1] N. Matsui, T. Makino, H. Satoh, "Auto-Compensation of Torque Ripple of DD Motor by Torque Observer", IEEE Industry Applications Society Meeting, 1991, vol.1, p. 305-311

[2] T. Low, K. Tseng, K. Lock, K. Lim, "Instantaneous Torque Control", Fourth International Conference on Electrical Machines and Drives, 1989, p.100-105

[3] S. Kamiya, M. Shigyo, T. Makino, N. Matsui, "DSP-Based High-Precision Torque Control of Permanent Magnet DD (Direct Drive) Motor", Electrical Engineering in Japan, Vol. 110, No.4, 1990, p. 51-58

[4] H. Bolton and R. Ashen, "Influence of motor design and feed-current waveform on torque ripple in brushless DC drives", IEE Proceedings, Vol. 131, Pt. B, No. 3, May 1984, p. 82-90

[5] D. Hanselman, J. Hung and M. Keshura, "Torque Ripple Analysis in Brushless Permanent Magnet Motor Drives", International Conference on Electrical Machines 1992, Vol. 2, p. 823-827

[6] E. Favre, L Cardoletti and M. Jufer, "Permanent Magnets Synchronous Motors : a General Approach for Cogging Torque Suppression", IEEE Industry Applications Society Meeting, 1991, Vol. 1, p. 204-210 .

Appendix

Motor Data :
Three phase permanent magnet motor
Rated output power : 3.4 kW
Rated torque : 10.8 Nm
Rated speed : 3000 rpm
Number of poles : 6
Torque constant : 1.6 Nm / A_{rms}
Voltage constant : 98V / 1000 RPM

i